Bond and Flexural Behaviour of Self Consolidating Concrete Beams Reinforced and Prestressed with FRP Bars

by

Slamah Krem

A thesis
presented to the University of Waterloo
in fulfillment of the
thesis requirement for the degree of
Doctor of Philosophy
in
Civil Engineering

Waterloo, Ontario, Canada, 2013

AUTHOR'S DECLARATION

I hereby declare that I am the sole author of this thesis. This is a true copy of the thesis, including any required final revisions, as accepted by my examiners.

I understand that my thesis may be made electronically available to the public.

Abstract

Self consolidating concrete (SCC) is widely used in the construction industry. SCC is a high performance concrete with high workability and consistency allowing it to flow under its own weight without vibration and making the construction of heavily congested structural elements and narrow sections easier. Fiber reinforced polymer (FRP) reinforcement, with its excellent mechanical properties and non-corrosive characteristic, is being used as a replacement for conventional steel reinforcement. In spite of the wide spread of SCC applications, bond and flexural behaviour of SCC beams reinforced or prestressed with FRP bars has not been fully studied. Furthermore, the ACI 440.1R-06 equation for determining the development length of FRP bars is based on Glass FRP (GFRP) bars and may not be applicable for Carbon FRP (CFRP) bars.

This research program included an experimental and analytical study to investigate the flexural and bond behaviour of SCC beams reinforced with FRP bars and SCC beams prestressed with CFRP bars. In the experimental phase, fifty-six beams were fabricated and tested. Sixteen of these beams were prestressed with CFRP bars and forty beams were reinforced with non-prestressed GFRP or CFRP bars. Four concrete batches were used to fabricate all the specimens. Three mixes were of self consolidating concrete (SCC) and one mix was of normal vibrated concrete (NVC). The test parameters for the non-prestressed beams were the concrete type, bar type and bar diameter, concrete cover thickness and embedment length while the test parameters for the prestressed beams were the concrete type and the prestressing level (30%, 45% and 60%). The transfer length of the prestressed CFRP bars was determined by means of longitudinal concrete strain profile and draw-in methods. All beams were tested in four-point bending to failure. Measurements of load, midspan deflection, bar slip if any at the beam ends, strain in reinforcing FRP bar at various locations, and strain in concrete at the beam midspan were collected during the flexural test.

The concrete compressive strength at flexural tests of SCC mix-1, mix-2, and mix-3 were 62.1MPa, 49.6MPa and 70.9MPa, respectively and for the NVC mix was 64.5MPa. The material test results showed that SCC mixes had lower modulus of elasticity mechanical properties than the NVC mix. The modulus of elasticity of the SCC mixes ranged between 65% and 82% of the NVC mix. The modulus of rupture of the SCC mixes was 86% of the NVC mixes.

The test results for beams prestressed with CFRP bars revealed that the variation of transfer length of CFRP bars in SCC versus their prestressing level was nonlinear. The average measured transfer lengths of 12.7mm diameter CFRP bars prestressed to 30%, 45% and 60% was found to be $25d_b$, $40d_b$, $54d_b$, respectively. Measured transfer lengths of the 12.7mm diameter CFRP bar prestressed to 30% in SCC met the ACI440.4 prediction. However, as the prestressing level increased, the predicted transfer length became unconservative. At a 60% prestress level, the measured/prediction ratio was 1.25. Beams prestressed with CFRP bars and subjected to flexural testing with shear spans less than the minimum development length had local bar slippage within the transmission zone. Beams that experienced local bond slip, their stiffness was significantly decreased. A modification to the existing model used to calculate the transfer and development lengths of CFRP bars in NVC beams was proposed to account for the SCC.

The test results for beams reinforced with FRP bars indicated that the average bond strength of CFRP bars in NVC concrete is about 15% higher than that of GFRP bars in NVC. The ACI 440.1R-06

equation overestimated the development length of the CFRP bars by about 40%, while CAN/CSA-S6-06 equation was unconservative by about 50%. A new factor of (1/1.35) was proposed to estimate the development length of the CFRP bars in NVC when the ACI440.1R-06 equation is used.

Beams made from SCC showed closer flexural crack spacing than similar beams made from NVC at a similar loading. The deflection of beams made from SCC and reinforced with CFRP bars was found to be slightly larger than those made from NVC. The average bond stresses of GFRP and CFRP bars in SCC were comparable to those in NVC. However, FRP bars embedded in SCC beams had higher bond stresses within the uncracked region of the beams than those embedded in NVC beams. In contrast, FRP bars in SCC had lower bond stresses than FRP bars in NVC within the cracked region. The average bond strength of GFRP in SCC was increased by 15% when the concrete cover thickness increased from $1.0d_b$ to $3.0d_b$. Cover thicknesses of $2d_b$ and $3d_b$ were found to be sufficient to prevent bond splitting failure of GFRP and CFRP bars in SCC, respectively. Bond splitting failure was recorded when the cover thickness dropped to $1.5d_b$ for the GRP bars and to $2.0d_b$ for the CFRP bars. An insignificant increase in average bond stress was found when the bar diameter decreased from 12.7mm to 6.3mm for the CFRP bars, and a similar increase occurred in GFRP bars when the bar diameter decreased from 15.9mm to 9.5mm.

New models to calculate the development length of GFRP and CFRP bars embedded in SCC were proposed based on the experimental results. These models capture the average bond stress profile along the embedment length. A good agreement was found between the proposed model and the experimental results.

Analytical modeling of the load-deflection response based on the effective moment of inertia (ISIS Canada M5) was unconservative for SCC beams reinforced with CFRP bars by 25% at ultimate loading. A new model for bond stress versus M_a/M_{cr} (applied moment to cracking moment) ratio was developed for GFRP and CFRP bars in SCC and for CFRP bars in NVC. These bond stress models were incorporated in a new rigorous model to predict the load-deflection response based on the curvature approach. The FRP bar extension and bond stress models were used to calculate the load-deflection response. With these models 90% of the calculated deflections were found to be within ± 15% of the experimental measured results for SCC beams reinforced with FRP bars.

Analytical modeling of the load-deflection for NVC and SCC beams prestressed with CFRP bars are proposed done. The moment resistance was calculated using Sectional Analysis approach. The deflection was calculated using simplified and detailed methods. The simplified method was based on the effective moment of inertia while the detailed method was based on effective moment of inertia and effective centroid. The experimental results correlated well with the detailed method at higher loads range.

This study provided an understanding of the mechanism of bond and flexural behaviour of FRP reinforced and prestressed SCC beams. The information presented in this thesis is valuable for designers using FRP bars as flexural reinforcement and also for the development of design guidelines for SCC structures.

Acknowledgements

I would like to express my sincere thanks to my mother and my wife, who supported me during the completion of this work.

My sincere appreciation goes to my supervisor, Professor Khaled Soudki, who provided me with excellent guidance during this research program and allowed me to do independent work. During this work, I learnt many lessons and insights about academic research. The friendly environment available among our research group in particular and at the Department of Civil and Environmental Engineering at the University of Waterloo is gratefully acknowledged.

I would like to extend my special thanks to Richard Morrison, Douglas Hirst and Robert Sluban, the technicians in the Structural Laboratory at the University of Waterloo, for their assistance and technical support during the specimen fabrication and testing.

I would like to thank to my colleagues Rania Al-hamoud, Rizwan Azam, Adham El-Menoufy, Martin Noel, Abed-Alaziz Alsaker, Mohamed Yakhlaf, and Hisham Elhuni for their assistance in specimen fabrication and casting.

I gratefully acknowledge Tripoli University in Tripoli, Libya for the scholarship provided to me to accomplish this research program. The financial support provided by NSERC for the material and equipment is highly appreciated. A special thanks to Lafarge Canada and Pultrall Inc. for their material donations.

To engineers and contactors in the field of concrete construction

TABLE OF CONTENTS

List of Figures

List of Tables

Chapter 1 - Introduction

1.1 General

Corrosion of steel reinforcement is the main cause of deterioration in reinforced concrete structures. America's 583,000 concrete bridges are of particular concern because they are subject to corrosion. The estimated cost of repair/replacement of corrosion-damaged bridges in the USA is about 8.3 billion annually (Koch et al. 2002). This figure is expected to continue to rise significantly as the bridges become older. It was reported that, with the best corrosion protection programs, only 25% of this cost could be saved (Schmitt et al. 2009).

In the last two decades, fiber reinforced polymer (FRP) reinforcement was introduced as a promising material that can replace conventional reinforcing steel, thus resolving the corrosion problem in many applications. Currently, FRP is used as a primary reinforcement in several concrete structures and bridge decks. The advantages of FRP materials are attributed to their high-strength to weight ratio, non-corroding nature, and high fatigue resistance (ISIS M7 2008, ACI 440.4R-04 2004). This material, however, still represents a relatively new technology in the reinforced and pre-stressed concrete industry. More research is still needed to provide the required confidence through a better understanding of the behavior of FRP reinforced concrete (ACI 440.1-07, 2007).

Self consolidating concrete (SCC) is a new generation of concrete mixture that was developed in the late 1980s. SCC can be defined as a highly workable high performance concrete that can flow and fill the target spaces under its own weight without vibration or any other means of consolidation (ACI-237-07). SCC provides many advantages in both quality and cost reduction over normal vibrated concrete (NVC). Consequently, SCC has become a popular alternative for NVC. Most of the research work done to date on SCC has focused on evaluating material based properties (Burgueno and Haq 2007). The incomplete understanding of its structural behaviour and lack of adoption by the current design codes are the primary reasons for its limited use, especially when FRP bars are used.

1.2 Research Significance

One of the research areas that has not been investigated is the use of FRP reinforcement in SCC construction. The bond behviour of SCC beams reinforced with GFRP and CFRP bars and the bond

behaviour of SCC beams prestressed with CFRP bars are of particular interest. This research study will experimentally determine the transfer and development length of CFRP bars in prestressed SCC beams and the development length of GFRP and CFRP bars in reinforced SCC beams. The flexural behaviour of SCC beams was also investigated in this research. An analytical model of the bond versus applied load was proposed to predict the bond and flexural behviour of SCC beams reinforced or prestressed with FRP bars. The findings of this work provide an understanding of the bond behaviour of FRP bars embedded in SCC and concrete flexural members in general. The information presented in this thesis is valuable for designers using FRP bars as flexural reinforcement and also for the development of design guidelines for SCC structures.

1.3 Research Objective

This research is intended to evaluate the bond and the flexural behaviour of beams made with SCC and reinforced with GFRP and CFRP bars and SCC beams prestressed with CFRP bars. The specific objectives of the study can be summarized as follows:

a) Investigate and validate the currently available equations in design guidelines for the bond stress and development length of GFRP and CFRP bars embedded in NVC
b) Study the flexural behaviour of SCC beams reinforced with GFRP or CFRP bars and compare the results with available design models
c) Investigate the effects of SCC on the bond behaviour of GFRP and CFRP reinforcing bars
d) Investigate the effects of SCC on the transfer and development lengths of 12.7mm diameter sand-coated prestressed CFRP bars
e) Compare the flexural behaviour of SCC beams prestressed with CFRP bars to that of NVC beams prestressed with CFRP bars
f) Examine the validity of current code equations to predict the transfer and development lengths of CFRP bars in reinforced or prestressed SCC and propose modifications for these equations
g) Develop an analytical model to predict the flexural response of FRP reinforced SCC beams that takes into account the different bond behaviour of FRP bars in SCC

1.4 Scope of the study

This research provides a comprehensive investigation of the bond and flexure behaviour of SCC beams reinforced or prestressed with FRP bars. The main parameters considered in this study for the non-prestressed beams were the concrete type (SCC, NVC), concrete compressive strength (49MPa to 71MPa), concrete cover thickness ($1.0d_b$, $1.5d_b$, $2.0d_b$ and $3.0d_b$), bar diameter (6.3mm, 9.5mm,

12.7mm CFRP bars and 9.5, 12.7 and 15.9mm GFRP bars), and the embedment length to bar diameter ratio (10 to 100). For the prestressed beams, the prestressing level was the main variable (30%, 45% and 60% of the guaranteed tensile strength), and type of concrete (NVC, SCC).

The experiments were carried out using 56 beam specimens. The beams were in groups of three beams for the non-prestressed beams based on the bar diameter and in groups of four beams for the prestressed beams based on the prestressing level. Cylindrical specimens were taken from each concrete batch to examine the compression strength, modulus of elasticity and tensile strength of the concrete batch used for beam casting. Prestressed beams were tested for transfer length immediately after prestressing load release. Then, all beams were tested under four point static flexural loads. Measurements of load, midspan deflection, bar slip at beam ends (if any), strain in the FRP bar, and the strain in the concrete were collected.

The analytical modeling phase of the study includes proposing modification of the exiting model to predict the development length of CFRP reinforcement bars in NVC reinforced beams. A modification of the exiting model for predicting the transfer and development length of pretensioned CFRP bars in SCC prestressed beams is provided. A new bond model for GFRP and CFRP reinforcement bars in reinforced SCC beams is proposed. An analytical model is proposed to predict the flexural behviour of FRP reinforced SCC beams. Design recommendations are provided.

1.5 Organization of the study

The present work investigates, experimentally and analytically, the bond and flexural behaviour of SCC beams reinforced with GFRP and CFRP bars. Companion specimens were made from NVC to evaluate the existing design equations and provide a reference comparison to beams made from SCC. The present work also investigates the effect of the prestressing level on the transfer and development length of 12.7mm CFRP bar in SCC. This thesis has eight main chapters and is organized as follows.

Chapter 1 provides an introduction to the problem statement, research objectives and scope of the study.

A literature review on the bond and flexural behaviour of SCC beams reinforced with steel bars is provided in Chapter 2. This chapter also provides a review of the bond behaviour of beams reinforced or prestressed with FRP bars. A summary of the available experimental and analytical work is presented. The gaps in the existing knowledge on the bond behaviour of FRP bars in SCC are highlighted.

Chapter 3 provides a detailed description of the experimental program of this study. Specimen design, instrumentation, fabrication and test procedures are presented. The material properties and concrete test results are also presented in this chapter.

Chapter 4 provides the test results and discussion for FRP reinforced non-prestressed beams. The modes of flexural failure experienced during the testing, results for beams reinforced with GFRP bars and results for beams reinforced with CFRP bars are presented in this chapter.

Chapter 5 presents the test result and discussion of the CFRP prestressed beams. Transfer length measurements and flexural test results are presented and discussed.

Chapter 6 presents the analytical modeling of the non-prestressed SCC beams. Included in this chapter are models for the load-deflection responses and bond stress profiles. Predictions of the load-deflection responses were done based on a simplified model for design guidelines and a rigorous model based on a newly developed local bond stress model of FRP in SCC. The predictions were compared to the experimental results. A proposed design bond equation for SCC beams reinforced with GFRP bars or CFRP bars were developed based on measured data. A modification factor for the ACI equation for CFRP bars in concrete is proposed.

Chapter 7 presents the analytical modeling of CFRP prestressed beams. Transfer and development length results are compared to the available design equations. Modifications to the exiting equations for transfer and development length for CFRP bars in SCC are proposed. A verification of an existing load-deflection prediction model with SCC beams is performed.

Chapter 8 summarizes the current study findings and gives recommendations for future work.

Appendices A and B provide the flexural test results for all non-prestessed beams that are reinforced with GFRP and CFRP bars, respectively. The flexural test results for all prestressed beams are presented in Appendix C.

Chapter 2 - Background and Literature Review

The first part of this chapter presents a brief background on Self Consolidating Concrete (SCC) with emphasis on the available literature related to SCC members. Fiber Reinforced Polymer (FRP) bars is introduced in the second part of this chapter. Key research on the bond behaviour of FRP bars in concrete is presented, and available equations related to the bond behaviour of FRP reinforcement in concrete are reviewed.

2.1 Self Consolidating Concrete (SCC)

2.1.1 Definition of SCC

Self-Consolidating Concrete (SCC) is a high performance concrete with high workability and consistency allowing it to flow under its own weight without vibration and making the construction of heavily congested structural elements and narrow sections easier (ACI 237R-07 2007). In other words, SCC is a new generation of high performance concrete that provides a highly flowable homogeneous and non segregating concrete mixture (Hwang et al. 2006). Basically, SCC provides a better plastic performance with improved in concrete quality and productivity.

SCC was first introduced to the concrete industry in Japan in the late 1980s to address the lack of expert labor in the construction industry. In fact, SCC was invented for the sake of improving concrete construction quality with minimum skilled labor requirements. The first large scale projects using SCC were a building constructed in Japan in 1990 and a tower of a prestressed concrete cable-stayed bridge in Japan in 1991 (Okamura and Ouchi 2003). As the new generation of polycarboxylate superplasticiser was introduced, SCC technology spread to Europe and North America. Goodier (2003) reported that by 2003 about 108,000-135,000 m^3 of SCC were being used at precast plants in North America annually. In 2004, about fifty percent of all precast prestressed concrete manufacturers shifted to SCC technology, except for highway bridge construction. This tremendous growth in SCC application further increases the need for a better understanding of its structural behaviour, and the assessment of the applicability of the current design equations developed for normal vibrated concrete (NVC) for use with SCC members (Schindler et al. 2007, Khayat and Mitchell 2009).

2.1.2 SCC Advantages

SCC offers a wide range of benefits in quality and economy. The major benefits are given below:

a. SCC provides high filling and passing ability. It can fill narrow or complicated dense reinforcement sections without any segregation or honeycombing.
b. SCC allows engineers to improve concrete quality independently of the casting crew skills. A well designed mixture can produce a homogeneous section without bleeding or coarse aggregate settlement. Furthermore, improved concrete quality produces structures with a longer life span without repair requirements.
c. Labor and machinery requirements are less than those in NVC applications. SCC reduces casting noise and enhances the casting environment. Okamura and Ouchi (2003) reported that the number of labourers can be reduced by 30% from those required if NVC is used in large scale projects.
d. Using SCC enables accelerating the casting with more flexibility in the points of concrete placement. This factor reduces the mixer truck movement and pump operations, which decreases the overall construction time. Okamura and Ouchi (2003) indicated that the construction period can be reduced by 20% in large scale projects where SCC is used.
e. SCC produces a high quality smooth surface finish.

When SCC is being considered for an application, several points must be taken into consideration. SCC production requires highly experienced designers to produce a suitable concrete mixture. It needs detailed knowledge of quality control and assurance programs. The increase in cement content for SCC mixtures may increase the potential for shrinkage in the hardened concrete. However, the use of supplementary cementing materials could reduce the shrinkage risk. In some cases, the use of SCC does not reduce the total construction cost (Okamura and Ouchi 2003). However, the necessity of using concrete with high flowability and filling capacity may govern the construction requirements, as in cases of high concentration of reinforcing bars or where the finishing surface is of particular interest. Furthermore, producing durable concrete has positive effects on a structure's cost analysis.

2.1.3 Mix Design Principles for SCC

SCC has the same ingredient components that are found in NVC: cement, aggregate, and water. However, to increase the flowability and reduce segregation, SCC requires a greater content of fine particles, and superplastizer, and possibly a viscosity-modifying admixture as a lubricant for the coarse aggregate. Figure 2.1 shows the average range of SCC mix proportions compared to those of NVC mixture (Holschemacher and Klug 2002). A successful SCC mix must ensure a good balance between two parameters (deformability and stability) and prevent the blockage of concrete flow (Khayat 1999). Deformability can be defined as the ability of the mix to deform and change its shape under its own weight, while stability refers to the ability of the mix to resist segregation during all phases of the construction process.

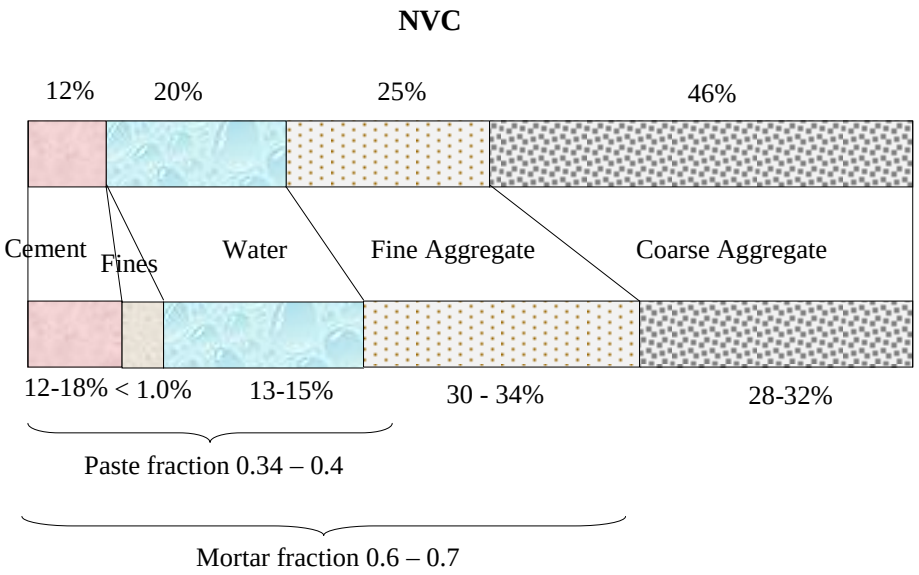

Figure 2.1 Comparison between SCC and NVC ingredient ratio (by volume)

There is no adopted standard mix design methodology for SCC in ACI 237R-07 or any other available standard; however, in general, three mix design approaches are used by researchers and concrete manufacturers. These approaches are as follows (Khayat 1999):

a) SCC can be produced from mixtures with high fines content such as fly ash, blast-furnace slag, or limestone (powder type), a low water to powder ratio (w/p), and a high dosage of high-range-water-reducing agent (HRWRA). The typical range of w/c in this approach is 0.30 to 0.35. The typical range of fines (≤ 80μm) is between 500- 600kg/m^3 (Okamura, 1997).
b) SCC can be produced from mixtures with a low to normal fines content, moderate w/c ratio, low ratio of HRWRA, and a viscosity modifying agent (VMA) to provide mix stability. In this approach, a typical w/c is around 0.40 (Khayat 1998).
c) SCC can be produced using a combination of the above two approaches.

Any mix design approach should consider both the fresh and hardened properties of SCC, and include the characteristics of the cementitious materials and fillers, w/c ratio, coarse aggregate content, and sand to aggregate ratio. Figure 2.2 provides the general principles of SCC mix design (Khayat 1999). These principles produce a concrete that normally contains different ingredient proportions than NVC. These differences are mainly in the low coarse aggregate content, increased paste content, low

water/powder ratio (w/p), and increased admixture dosage such as HRWRA and VMA. Generally, a successful SCC mixture requires the combination of key characteristics that be attained. Guidelines to evaluate such properties are presented below, (Khayat 1999).

a. The fluidity and viscosity of the paste is balanced by careful selection and proportioning of the cement and additives, limiting the w/p ratio, and then by adding HRWRA and (optionally) VMA. The compatibility and interaction of these components is the key for achieving good filling ability, passing ability and segregation resistance.
b. Adding a significant portion of type I or II inorganic mineral material, to keep the cement content at an acceptable level is a successful way to reduce temperature rise and thermal shrinkage cracking.
c. Because the paste in SCC is the transportation vehicle of the aggregate particles, the volume of the paste must be greater than the void volume in the aggregate so that all individual aggregate particles are fully coated and lubricated by a layer of paste. Satisfying this condition increases fluidity and reduces aggregate friction.
d. Increasing the fine-to-coarse aggregate ratio reduces the risk of coarse aggregate interlock in members with narrow spacing. High fine-to-coarse aggregate ratio enhances the passing ability of the SCC.

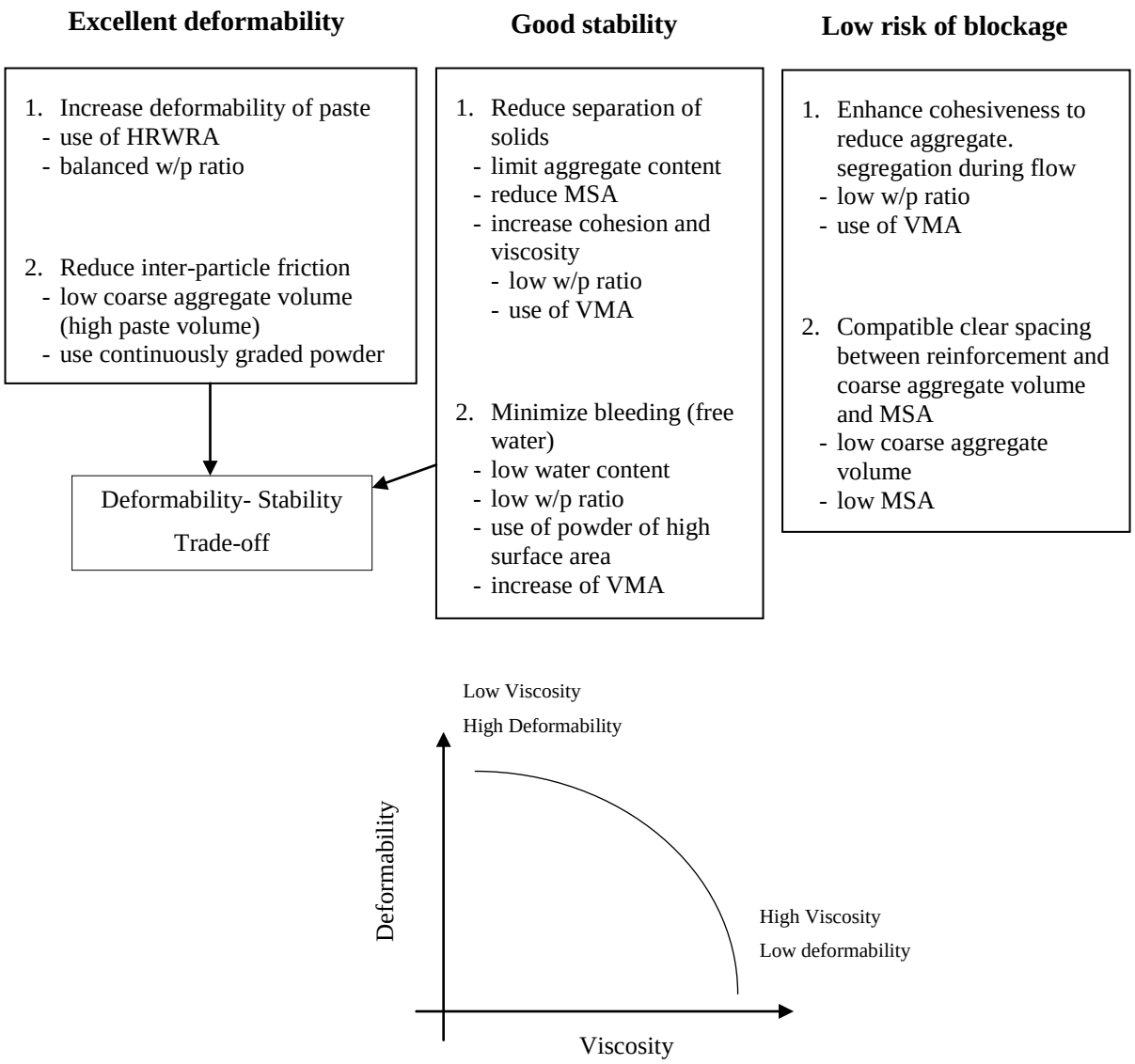

Figure 2.2 Principles of SCC mix design (Khayat 1999)

2.1.4 Fresh Properties of SCC

SCC is defined by ACI committee 237 as "highly flowable, nonsegregating concrete that can spread into place, fill the formwork, and encapsulate the reinforcement without any mechanical consolidation." Therefore, significant differences in fresh properties are expected from SCC in comparison to NVC. Consequently, different tests are required to evaluate SCC fresh properties. Codes have extensive testing requirements to evaluate the SCC mixture characteristics to ensure that it meets the required performance criteria. Table (2.1) lists the most common tests for the SCC fresh properties.

Table 2.1 List of the main available tests for fresh SCC properties

Test name	Category	Characteristic	What test measures
Slump flow	Free flow	Filling ability	Flow distance
Visual stability index (VSI)	Static condition	Resistance to segregation	Visual stability of the mixture
T50	Free flow	Filling ability	Rate of flow
J-ring	Confined flow	Passing ability	Flow rate
L-box	Confined flow	Passing and filling ability	Flow rate and distance
Column segregation test	Confined flow	Resistance to segregation	Segregation of aggregates

ACI 237R-07 (2007) provides a description and interpretation for results of each of the tests given in Table 2.1. It also provides guideline and selection criteria for SCC mix.

2.1.5 Hardened Properties of SCC

The hardened properties of SCC are crucial in designing reinforced and prestressed concrete members. Tests for SCC's concrete compressive strength and modulus of elasticity are discussed below.

2.1.5.1 Compressive strength

Normally, SCC mixtures produce high-strength concrete, above 40MPa, due to SCC's mix proportion requirement to produce high flowable and cohesive mix. These characteristics often require a lower w/c ratio compared to NVC, which is the key component in determining the concrete compressive

strength. The typical W/C range in SCC is between 0.37-0.42 (ACI 237, 2007). Other factors such as the sand-to-total-aggregate ratio (s/a) and type and dosage of chemical admixtures can significantly affect the rate of compressive strength gained by SCC.

Schindler et al. (2008) carried out experiments to evaluate the fresh and hardened properties of 21 mixes of SCC. Their work included the effects of w/c ratio, s/a ratio, and cementitious material combinations (Type III cement, class C and F fly ash, ground-granulated blast-furnace slag, and silica fume). Concrete compressive strength was monitored and tested. The research concluded that the s/a ratio has a small affect on compressive strength. Furthermore, at a given w/c, cement type III with a mineral admixture of class C fly ash or GGBF produced lower compressive strength at early stages than other mixes. Holschemacher and Klug (2002) and Domone (2007) reported a slight delay in SCC's concrete compressive strength development at early ages; however, at 28 days, similar to NVC, SCC reached the target compressive strength.

2.1.5.2 Modulus of Elasticity

The modulus of elasticity (E_c) is a crucial factor in calculating the stiffness of reinforced concrete members. As stiffness of a flexural member is increased the deformation of the member decreases. In prestressed concrete application, the E_c plays an important role in reducing the prestress losses. Modulus of elasticity depends on several factors, including the concrete compressive strength, coarse aggregate characteristics and content. Where a low maximum aggregate size and high fines content are used, SCC is anticipated to have a lower E_c than that of NVC by 10 – 15 % (ACI 237, 2007); however, some studies indicate that for a comparable concrete compressive strength, the E_c of SCC is similar to that of NVC (Person 1999, Schindler et al. 2008). ACI 237 allows using the expression given by ACI 318-08 clause 8.5.1 to calculate the E_c of normal density concrete to estimate the E_c of SCC mixtures.

$$E_c = 4700\sqrt{f_c'} \qquad (2.1)$$

Where

E_c is the concrete modulus of elasticity in MPa; and

f_c' is the concrete compressive strength in MPa.

Schindler et al. (2008) reported that at early ages, and for comparable compressive strength, SCC exhibits a lower E_c than does NVC; however, at later ages, E_c values of SCC mixtures were very similar to those of NVC. A database collected by Holschemacher and Klug (2002) and Domone P. L. (2007) indicated that the modulus of elasticity of SCC can be 20-40% lower that NVC's at low

concrete compressive strength, but the differences decrease to about 5% when the concrete compressive strength approaches 60MPa.

2.1.6 Bond Behaviour of non-prestressed Reinforcement in SCC

The design of reinforced and prestressed concrete flexural members assumes a perfect bond between the reinforcement and the concrete. In other words, the reinforcement and the concrete at the level of reinforcement experience the same strain change. This assumption allows engineers to use the strain compatibility approach in designing reinforced concrete structures.

SCC has the ability to encapsulate reinforced bars or prestressed reinforcement. An SCC mixture reduces the potential of bleed water accumulation under horizontally embedded bars. This phenomenon is known as local w/c increase, and locally reduces the compressive strength and the bond strength of concrete (ACI 237-07, 2007). The following sections present the available literature on the bond strength of steel reinforcement in SCC, in two parts: research related to the bond of reinforced (non-prestressed) SCC members and research related to the bond of prestressed SCC members. All research to date has used steel bars; to the best of the author's knowledge, no data is available in the literature on using FRP reinforced or prestressed SCC members.

2.1.6.1 Bond behaviour of steel reinforcement bars in SCC

Generally, the bond stress between reinforcing bars and concrete depend on three mechanisms: adhesion, friction, and mechanical interlock (Hanson and Kaar 1959). Adhesion has an insignificant effect on the bond strength as it is destroyed immediately when slip between the reinforcing bars and concrete occur. The friction between the reinforcing bars and concrete has significant contribution in bond stresses... Mechanical interlock resistance plays dominant factor in bond stress. Mechanical interlock is a function of the surface configuration of the reinforcing bars. Bar surface patterns can produce surface interlock, especially ribbed and indented surface patterns (Barnes et al. 2003).

When a reinforcing bar in concrete is subjected to a bond pullout test, it experiences bond stress versus slip behaviour, as shown in Figure 2.3. Two main terms are associated with bond strength: "critical bond strength," defined as the average bond strength corresponding to a slippage of 0.25mm, and "ultimate bond strength," defined as the peak level of the bond stress at a slip of 4 to 6mm (Chan et al. 2003). Adoption of the critical bond strength leads to a conservative estimate of the development length of the reinforcement in concrete members (Chan et al. 2003).

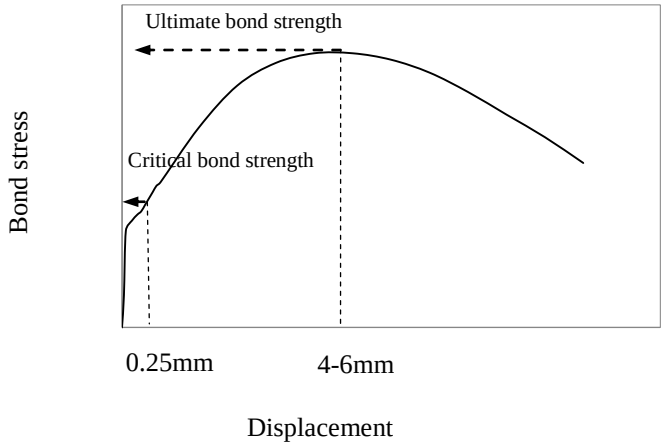

Figure 2.3 Bond stress versus slip in a pullout test (Chan et al., (2003)

Chan et al. (2003) compared the bond strength of steel reinforcement in SCC to that in NVC. One large concrete block, with a depth of 1200mm, was made from each type of concrete. The steel reinforcement was arranged at three levels (200, 500, and 800mm) from the bottom face of the section to evaluate the top bar effect. The embedded length was kept constant at 300mm. A pull out test was performed to evaluate the bond strength at various concrete ages: at 6 hrs for NVC, at 17hrs for SCC and at 28days for NVC and SCC. Figure 2.4 shows the bond strength of the bottom bars (level of 200mm from the top face) in SCC and NVC. The ultimate bond strength of the reinforcing bars in SCC was 9.5 MPa for the bottom bars, 6.98 MPa for the middle bars, and 6.38 MPa for the top bars. For NVC, the ultimate bond strength of the reinforcing bars was 6.38 MPa for the bottom bars, 4.36 MPa for the middle bars, and 3.66 MPa for the top bars. The authors concluded that SCC exhibits a better bond strength with less significant effect of top bars on the bond strength. It was found that the development of concrete compressive strength and bond strengths were slower in SCC than in NVC. However, at 7 days, SCC's properties substantially exceeded those of NVC.

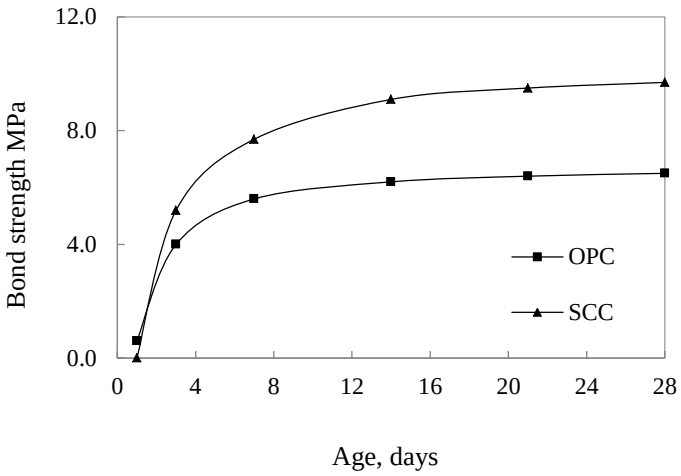

Figure 2.4 Bond strength developments in SCC and NVC (Chan et al., 2003)

Castel et al. (2006) compared the bond behavior of steel bars embedded in SCC to NVC at various concrete compressive strengths. SCC was found to exhibit more bleeding resistance than NVC. Two specimen types were utilized: small prisms (100×100×500mm) and large specimens (100×500×1100mm). The larger specimen type was used for evaluating the top bar effect. A deformed steel bar with 12mm diameter and 60mm (5d) embedded length was used. All bars were debonded for 60mm at the pulling end. The results of this study indicate that the ultimate bond strength of bottom steel bars in SCC was on average 20% more than that in NVC at a given compressive strength. The maximum bond strength reduction due to top bar effect for the 25 MPa concrete specimens was 33.6% in SCC and 52.1% for NVC. However, for the 40 MPa concrete specimens, the bond strength reduction due to top bar effect was 39% in SCC and 35% in NVC.

Esfahani et al. (2007) compared the bond strength and top-bar effect of steel bars in SCC to those in NVC. Two concrete mixes were used for each type of concrete. The compressive strengths of the two SCC mixes were 62 and 68 MPa, and for the two NVC mixes were 58 and 61 MPa. Deformed steel bars with a diameter of 25 mm and an embedded length of 100mm were used. The specimen height was 900mm and the concrete cover ranged from 30 to 60mm. The bond strengths of the steel bars were measured by pullout tests. The results indicate that the bond strength of bottom bars was similar in both types of concrete; however, the bond strength for the top bars in NVC specimens was about 20% higher than that in SCC specimens. To account for using SCC, the authors proposed using a multiplier factor of 1.3 to increase the development length calculated by ACI 318 Code equations.

Hossain and Lachemi (2008) studied the effect of using SCC with different mineral and chemical admixtures on the bond strength of 25M steel bars with an embedded length of 100mm. Three SCC mixtures and one NVC mixture were used. The main variation in the SCC mixtures was the admixtures: fly ash, slag cement, and VMA. The concrete compressive strength for the three SCC mixtures was 62, 39, and 47 MPa, respectively, while for the NVC mixture, it was 53 MPa. Pullout tests were used to determine the bond stress of the reinforcement in concrete. The test findings showed that the variation in bond stresses at different concrete covers was less pronounced in SCC than in NVC. However, in the case of slag cement SCC, the bond stress was lower than that in NVC.

Valcuende and Parra (2008) compared the bond strengths of SCC and NVC using four mixtures from each type. Cube specimens (200×200×200 mm) were used in the pullout tests and column specimens (1500mm in height) were used to study the top bar effect. The cube specimens had a 16mm diameter steel bar with an embedded length of 80mm (5d), and the column specimens had a 12mm diameter bar with an embedded length of 60mm (5d). Figure 2.5 shows the normalized mean and ultimate bond strength of both concrete types. The study found that the bond strength of SCC was greater than that of NVC. The reduction in the mean bond strength ranged from 30% to 10% as the concrete compressive strength increased from 30MPa to 70MPa. The reduction was less pronounced at the ultimate bond strength.

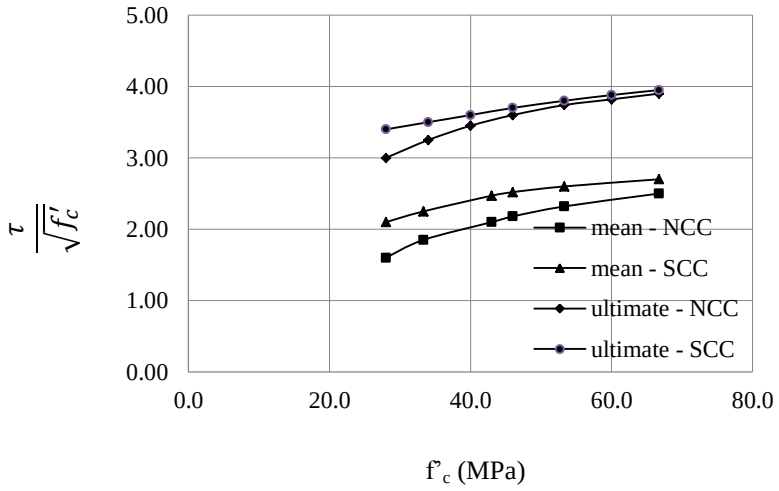

Figure 2.5 Normalized mean and ultimate bond strength (Valcuende and Parra 2008)

2.1.6.2 Bond Behaviour of Prestressing Steel Strand in SCC

Transfer and development lengths of prestressing reinforcement depend on the bond characteristics between the concrete and the prestressing bars. Transfer length is defined as the embedded length from

the free end of a prestressed member to where the stress in the prestressing bar becomes uniform. In other words, the transfer length can be defined as the embedded length of the prestessing strand to develop the full effective prestress. The accurate prediction of transfer length is crucial for stress analysis in the transmission zone for both service and factored load effects. Over estimation of the transfer length leads to un-conservative service stress calculations. Underestimation of the transfer length can lead to un-conservative shear capacity calculations under factored loads since the concrete shear capacity depends on the pre-compression level at a specified section (Barnes et al. 2003, Russell and Burns 1993).

As a prestressed member is loaded in flexure, additional tensile stresses are developed in the prestressing reinforcement to generate an internal moment to counteract the external applied moment. This tensile stress in the prestressing bars is transferred to the concrete by means of bond stresses. The minimum embedment length required for a prestressing bar to develop a tensile stress from the effective prestressing stress to the full tensile strength of this prestressing bar is defined as the flexural bond length. Similar to the transfer length, the flexural bond length depends on the bond strength that can develop between the strand and the concrete during flexural loading. The main difference between these two lengths is the state of the concrete. In the transfer region, concrete is typically in compression; however, during flexural action, the concrete surrounding the prestressing reinforcement could be under tension and flexural cracks may occur. The summation of the transfer length and the flexure bond length is defined as the development length.

In addition to the bond mechanism discussed for non-prestressed concrete members, the bond transfer between the prestressing tendon and concrete, friction resistance is developed due to the existence of radial compressive stress as a result of radial expansion of the tendon (Barnes et al., 2003). This phenomenon is known as the Hoyer effect. The mechanical resistance or wedge effect is a function of several effects. The first is the tendon surface configuration, which can produce a surface interlock, especially for ribbed prestressing bars or multi-wire warped strands (Russell and Burns 1993). The second is the interlock bond at the free ends where the tendon expands in the transverse direction due to the Poisson's ratio of the tendon material. The third is the bearing effect resulting from the confinement action by support reactions.

Girgis et al. (2005) carried out research on the bond strength and transfer length of pretensioned concrete bridge girders made from SCC. Three concrete mixtures were used: two SCC (mixes 1 and 2) and one NVC (mix 3). Each mixture was used for a different bridge construction project. The concrete strengths of theses mixes at transfer were 44.8, 41.2, and 48.1 MPa, and at 28days were 75.2,

55.5, and 65.7 MPa respectively. One girder was selected from each project and tested for transfer length using concrete surface strain measurement. All the steel strands used in these projects were 15mm in diameter. The bond quality of the strands was assessed using pullout tests based on the criteria proposed by Logan (1997). The test results showed that the average pullout load capacity for mix-1 (SCC), mix-2 (SCC), and mix-3 (NVC) was 43.4Kips, 54.3Kips and 48.0Kips, respectively. The average transfer length results were 36", 43", and 20" for mix-1, mix-2, and mix 3, respectively. These results indicate that SCC experienced a longer transfer length than NVC. The authors concluded that this is due to SCC showing lower early bond strength than NVC. At 28 days, SCC exhibits higher bond strength than NVC, which may lead to a shorter development length.

Larson et al. (2005) conducted tests on full scale pre-tensioned concrete girders to determine the effect of using SCC on their bond and flexure behaviour. The main parameters studied were the embedded length: 80% and 100% of the expected development length based on the equations for NVC and the top strand effect. Concrete beams with cross sections of 8" × 12" and 8" × 24" were used to evaluate the top strand effect. Before specimen fabrication, pullout tests were carried out to evaluate the bond quality of the strand according to the criteria proposed by Logan (1997). End-slip measurements were used to determine the transfer lengths. The study found that the bond quality of the strand exceeded the criteria set by Logan (1997). The ultimate pullout capacity was 39.6 kips, which was above the limit of 36 kips set by Logan (1997). The transfer lengths were found to be 21" and 32" for bottom and top strands, respectively. The flexure test results indicated that specimens with 80% and 100% embedded lengths failed by strand rupture with no strand end-slip.

Naito et al. (2005) investigated the behavior of four 35-ft-long bulb-tee girders made of SCC and high early strength concrete (HESC). Low relaxation, 0.5-inch seven-wire steel strands, 270ksi, was used. The girder length was selected to test each end independently. Two girders were fabricated and tested from each type of concrete, resulting in eight flexural tests. The transfer lengths were determined by means of embedded vibrating wire strain gauges bonded to the stressed strand prior to detensioning. Thirty five pullout tests were carried out to examine the bond quality of the prestressing strand according to the method described by Logan (1997). This research found that the ultimate pullout force was 31.5 kips, which was about 84% of the benchmark load set by Logan (1997). The transfer lengths were 15.7" for the SCC girders and 15.8" for the HESC girders. These values were below the predicted transfer length value suggested by the PCI equation. The results indicated that the SCC bond strength was similar to that of HESC. Both SCC and HESC girders exceeded the nominal strength predicted using ACI 318 equations.

Burgueno and Haq (2007) conducted a comprehensive investigation of the transfer and development lengths of steel strands, using three SCC and one NVC mixtures. The compressive strength of SCC1, SCC2, and SCC3 were 28.1, 30.1, and 33.4 MPa at release and 31.2, 39.8, and 35.0MPa at 28 days respectively, while the strength for NVC was 32 MPa at transfer and 35 MPa at 28 days. The main variable in the mixture proportions was the fines to coarse aggregate ratio: SCC1 mix represented high fines content, SCC3 represented minimum fines content, and SCC2 was in-between. The NVC concrete mixture proportions were very close to those of SCC3. Transfer lengths were determined in two way- end-slip and concrete surface strain measurements- and the development lengths were estimated by flexure testing. The results showed that the transfer lengths were about 30 to 39% longer in SCC than in NVC. For all SCC mixes, except the SCC1 mixture, the ACI 318 code requirements were met. Figure 2.6 shows the transfer and development lengths compared to the ACI 318 equations. The results indicate that high fines content plays the main role in reducing the bond performance in SCC. Increased fines in SCC mixture lead to higher paste content and use of chemical admixture which result in modified microstructure, especially the interfacial zone between the strand and concrete. Due to lower coarse aggregate content in SCC mixture, both tensile strength and elastic modulus decreased which might reduce the bond strength of prestressing strand in SCC. Both types of concrete exhibited a similar development length, with only a 3% increase in the case of SCC as compared to NVC. Research on bond and structural behaviour of prestressed SCC members is limited (Girgis and Tuan 2005, Larson et al. 2006, Stanton et al. 2006, Naito et al. 2006, and Burgueno and Haq 2007).

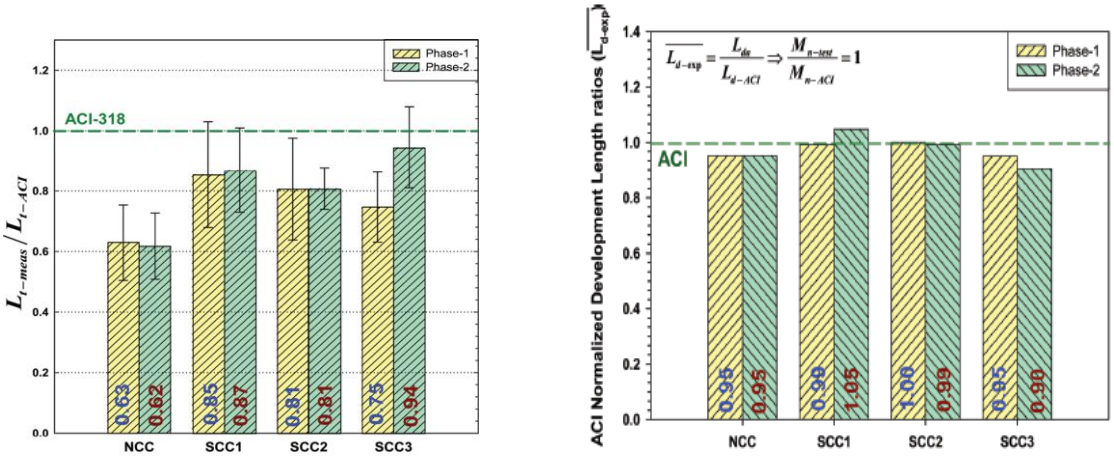

Figure 2.6 Transfer length and (b) development length normalize to ACI 318 predictions (Burgueno and Haq 2007)

2.2 Fibre Reinforced Polymer (FRP)

2.2.1 Definition and Properties of FRP

FRP composites consist of aligned continuous fibres embedded in a resin matrix. The fibres can be Carbon, Aramid, or Glass, and the corresponding composite would be known as CFRP, AFRP, and GFRP, respectively. Commonly used resins are epoxy, polyester, or vinyl ester. Depending on the fibre quality, orientation, length, shape, volumetric ratio, adhesion to matrix, and the manufacturing process, the mechanical performance of the composite will vary. FRP composites can be produced as plates, sheets, ropes or grids. Its high cost and lack of codes prevented the wide use of FRP by the construction industry when it was first introduced; however, with the development and better availability of design guidelines, applications using FRP reinforcement have increased rapidly in recent years (Newman et al., 2007).

The main advantage of FRPs is that they are non corrosive, with high abrasion and chemical resistance. In addition to their non-corroding nature, FRPs much lighter than steel bars (one-sixth to one-fourth the weight of steel), leading to lower transportation cost and greater ease in handling of the bars on project sites. The main drawbacks of FRP are their lack of ductility and low fire resistance. FRP material has a linear elastic stress-strain relationship until failure, without any plastic behaviour. Ductility is an important requirement in reinforced and pre-stressed concrete applications. To avoid sudden structural failure due to FRP rupture, most of the current guidelines recommend a compression failure design approach rather than a tension failure mode (ACI 440.1R-06, ISIS M3 2007).

FRP bars normally have a tensile strength higher than that of conventional steel reinforcing bars. This relatively high tensile strength makes FRP bars particularly attractive for prestressed concrete applications. Typical tensile stress-strain relationships of FRP bars as compared to conventional steel bars and high tensile prestressing steel strands are shown in Figure 2.7. The modulus of elasticity of FRP bars is lower than that of steel bars. In fact, the modulus of elasticity for commercially available GFRP and AFRP bars ranges from 20 to 25 % that of steel, while that of CFRP bars ranges from 60 to 75 % compared to steel.

The bond behaviour of the FRP bar depends on the surface condition and mechanical properties of the bar as well as the environmental conditions. Surface conditions of the FRP bars can be divided into two categories: 1) bearing forming surface and 2) friction forming surface. FRP bars in the second category are coated with a granular material before the bars are completely cured. These granular particles increase the bond transfer through friction between the FRP bars and the concrete. Another

way of increasing the bond strength of the bars is through indentations or deformations on the bar prior to full curing.

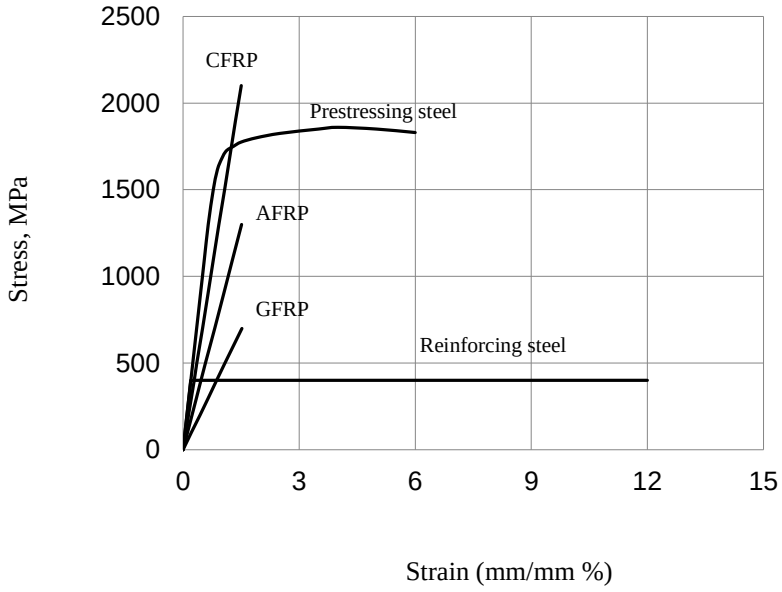

Figure 2.7 Typical tensile stress-strain relationships for FRP and steel

2.2.2 Bond Behaviour of FRP Bars in Concrete

In the following sections, the bond behaviour of FRP-reinforced or prestressed concrete flexural members will be presented and discussed. The presentation is limited to FRP reinforcing (non-prestressed) bars and prestressing tendons in NVC flexural members. To the best of the author's knowledge there is no available work in the literature on the bond or flexural behviour of prestressed FRP bars in SCC.

2.2.2.1 Non-prestressed FRP bars in NVC

FRP bars are available commercially as Aramid, Glass or Carbon FRP reinforcing bars. Due to the high cost of CFRP, most of the previous research and applications focused on GFRP bars (Rafi et al. 2007). This section presents the available information on the bond and development length and design guidelines.

2.2.2.1.1 Previous published work on the bond of FRP bars in NVC

Aly et al. (2006) published a study on the tensile lap splice behaviour of FRP reinforcing bars in concrete. The study investigated the tensile strength of FRP bars of various splice lengths. Twelve beams (250×400×4200mm) were tested in flexure using a four-point bending arrangement. Each beam

was reinforced with two sand coated GFRP or CFRP bars in the longitudinal direction. The bars were spliced within the mid length of the constant moment region. Transverse reinforcement was provided throughout the beam length in the form of 8mm diameter closed steel stirrups spaced at 100mm intervals within the shear span and at 150mm intervals throughout the splice length. The test variables included the bar diameter (9.5mm, 12.7mm, 15.2mm, and 19.1mm) and the splice length (500, 700, 800, 1100, 1400mm). This work concluded that the maximum stress at the ends of spliced FRP bars was proportional to the splice length. The critical bond stresses associated with the critical splice lengths were larger in CFRP bars than in GFRP bars. For both bars, the critical bond stress decreased as the bar diameter increases. The recommended splice length for 9.5mm and 12.7mm diameter CFRP bars were $70d_b$ and $90d_b$, respectively. The recommended splice length for 15.9 and 19.1 mm diameter GFRP bars were $40d_b$ and $50d_b$, respectively. These results confirm ACI 440.1R-06's estimation of shorter development lengths for CFRP bars than for GFRP bars due to the higher stiffness of CFRP bars. However, ACI 440.1R-06 does not provide a correction factor other than 1.0 for using CFRP bars. The authors found that predictions based on pullout failure using the ACI 440.1R-03 equation was conservative for small bar diameters and unconservative for larger bar diameters; however, predictions based on splitting failure using the ACI 440.1R-03 equation was more realistic. Similarly, CAN/CSA-S806-12's equation gave conservative predictions for small bar diameters and un-conservative values for larger bar diameters.

Rafi et al. (2007) compared beams reinforced with CFRP bars to beams reinforced with steel bars. The beams were reinforced with two 9.5mm diameter CFRP bars or two 10M steel bars. All beams were the same size, 120×200×2000mm, and had the same concrete cover of 20mm. Shear reinforcement was provided over the full beam length to prevent any shear failure. The concrete compressive strength was in the range of 42 to 47 MPa. The ultimate strength of the reinforcing bars was 1676 MPa for the CFRP bars and 530 MPa for the steel bars. The beams were subjected to four-point bending with a shear span of 675mm. This study investigated the flexural and bond behavior of CFRP-reinforced beams in comparison to steel-reinforced beams. Both beam types showed similar cracking patterns up to failure. The CFRP-reinforced beams exhibited more deflection than did the steel-reinforced beams; however, the steel-reinforced beams experienced significant deflection after yielding of the steel bars. The maximum deflection was 35.4mm for the CFRP-reinforced beams and 28.4mm for the steel-reinforced beams. Both beam types failed by concrete crushing. In the steel-reinforced beams, the steel bars yielded, and then the concrete crushed under the ultimate load. In the CFRP-reinforced beams, the CFRP bars reached 80 to 90% of their rupture capacity at the beam failure load. No signs of premature bond slip failure were observed for CFRP-reinforced beams. The authors concluded that the CFRP-

reinforced beams had adequate bond characteristics, and that ACI 440.1R-03 equation underestimated the theoretical deflection of CFRP-reinforced beams.

Mosley et al. (2008) studied the bond behaviour of FRP reinforcing bars using the beam splice test. Twelve beams were tested in three sets, including beams reinforced with steel or GRFP or CFRP bars. The shear reinforcement was only provided within the shear spans. There was no transverse reinforcement within the constant moment region. All beams had a splice length within the constant moment region. The splice length of the first set was 457 mm, with a concrete cover of 38 mm and a bar clear spacing of 25mm. The splice length of the second and third sets was 305mm, with a concrete cover of 38mm and a bar clear spacing of 25mm for set 2, and a concrete cover of 38mm and a bar clear spacing of 121mm for set 3. The test results showed that all beams failed by splitting of the concrete cover within the splice length. The results indicated that at the same embedded length, the bond strength of the GFRP and AFRP bars was approximately 50% that of steel bars. This ratio increased to about 65% when the bar spacing increased to 121mm. It was found that the bond strength increased as the modulus of elasticity increased. Furthermore, the bar tensile stress versus the splice length was not linear as assumed by ACI 318 and ACI 440. The bar tensile stress was found to be proportional to the square root of the splice length.

2.2.2.1.2 Design guidelines and available development length equations

The Canadian Highway Bridge Design Code (CAN/CSA-S6-06 2006) and ISIS Canada-M3-07 (2007) provide the same equation for the development length calculation for FRP reinforcement. This equation is based on the splitting failure mode.

$$l_d = 0.45 \frac{k_1 k_4}{d_{cs} + k_{tr} \frac{E_{frp}}{E_s}} \left(\frac{f_{frp}}{f_{cr}} \right) A_{frp} \qquad (2.2)$$

Where

l_d is the development length in mm;

k_1 is the bar location factor;

k_4 is the bar surface factor;

f_{frp} is the stress in the FRP bar to be developed;

f_{cr} is the flexural cracking strength of concrete;

A_{frp} is the cross section area of the FRP bar;

E_{frp} is the modulus of elasticity of the FRP reinforcement;

E_s is the modulus of elasticity of steel;

d_{cs} is the smaller of the distance from the concrete surface to the bar centre and two-thirds of the centre to centre spacing of bars; and

k_{tr} is the transverse reinforcement index, and can be taken as:

$$k_{tr} = \frac{A_{tr}\, f_y}{10.5\, s\, n} \qquad (2.3)$$

Where

A_{tr} is the transverse cross sectional area of the transverse reinforcement;

f_y is the specified yield stress of steel reinforcement stirrups;

n is the number of bars being developed along the plane of splitting; and

s is the centre-to-centre spacing of the transverse reinforcement.;

and the value of the term $(d_{cs} + k_{tr}\frac{E_{frp}}{E_s}) \leq 2.5\, d_b$

The development length equation for reinforcement FRP bars provided by the Canadian Building Code CAN/CSA-S806-12 is as follows:

$$l_d = 1.15\, \frac{k_1 k_2 k_3 k_4 k_5}{d_{cs}}\, \frac{f_{frp}}{\sqrt{f_c'}}\, A_{frp} \qquad (2.4)$$

Where

K_1 is the bar location factor;

k_2 is the concrete density factor;

k_3 is the bar size factor;

k_4 is the bar fibre factor; and

k_5 is the bar surface profile factor;

f_{frp} is the design stress in FRP tension reinforcement at ultimate limit state;

A_{frp} is the cross sectional area of an individual bar;

f_c' is specified compressive strength of concrete; and

The term d_{cs} shall not be taken to be greater than $2.5d_b$; and other terms are as defined in Eqn (2.2).

In 2006, the American Concrete Institute (ACI) Committee 440 published design guidelines for FRP reinforced concrete structures, ACI 440.1R-06. In this guide, a completely new approach was

introduced for calculating the development length for FRP bars in concrete. The approach is based on the equilibrium principles for bars anchored in concrete, Eqn (2.6), and empirically derived formula for normalized average bond stress in terms of normalized cover and normalized embedment length, Eqn (2.7). Equation (2.7) was formulated based on a database collected by Wambeke and Shield (2006). This database was primarily based on beams reinforced with GFRP bars.

$$l_e \, \pi \, d_b \, u \; = \; A_{frp} \, f_{frp} \tag{2.5}$$

$$\frac{u}{0.083 \sqrt{f_c'}} = 4.0 + 0.3 \, \frac{C}{d_b} + \; 100 \, \frac{d_b}{l_e} \tag{2.6}$$

Where

l_e is the embedment length, mm;

d_b is the reinforcement bar diameter, mm;

u is the average bond stress, MPa;

A_{frp} is the cross sectional area of the FRP reinforcement bar, mm^2;

f_{frp} is the tensile stress developed in the FRP bar at the end of the embedment length, MPa;

$f_c^{'}$ is the concrete compressive strength, MPa; and

C is the lesser of the cover to the centre of the bar or one-half of the centre-to-centre spacing of the bars being developed, mm.

Using Eqn. (2.5) and Eqn. (2.6), ACI 440.1R-06 provides an expression for the bar stress at a given embedment length, Eqn. (2.7). By rearranging Eqn (2.7), the required embedment length of FRP bars to develop a given bar stress is given in Eqn (2.8). A factor of safety that satisfies the test-predicted ratio of less than 1.0 of a subset selected from the database collected by Wambeke and Shield (2006) was 22%. Additionally, ACI committee 440 set a limit of 3.5 on the cover-to-bar diameter ratio so that Eqn. (2.8) can be used for either splitting or pullout modes of failure.

$$f_{frp} = \frac{0.083\sqrt{f_c^{'}}}{\alpha} \left(13.6 \, \frac{l_e}{d_b} + \, \frac{c}{d_b} \, \frac{l_e}{d_b} + \, 340 \right) \leq \, f_{fu} \tag{2.7}$$

Where

f_{fu} is the rupture tensile stress of the FRP bar.

$$l_d = \frac{d_b\left(\frac{f_{frp}}{0.083\sqrt{f_c'}} - 340\right) \propto}{13.6 + \frac{c}{d_b}} \quad (2.8)$$

Where

$\propto$ is the top bar location factor.

The ACI 440.1R-06 equation for determining the development length of FRP bars is formulated based on beams reinforced with Glass FRP (GFRP) bars with no correction factor to account for CFRP bars. Although no data on CFRP bars was included in the calibration of Eqn. (2.7), ACI Committee 440 mentioned that "it is anticipated that the much larger stiffness of the CFRP bars will likely decrease the required development length." But ACI committee 440 recommended a material modification factor of 1.0 when CFRP bars are used.

In both the Canadian Highway Bridge Design Code (CAN/CSA-S6-06 2006) and Canadian Building Code CAN/CSA-S806-12, the development length varies linearly with the cross-sectional area and tensile strength of the FRP bar, and inversely with the square root of concrete compressive strength and cover thickness. The basic assumption in these two equations is the average bond stress is independent of the embedment length length. In other words, these two equations consider that the average bond stress for given concrete properties is independent of the embedment length. ACI 440.1R-06's equation, however, involved the embedment length-to-bar-diameter ratio. The available literature shows that the average bond stress decreases as the embedded length increases. The bond stress equation provided by the ACI 440.1R-06 report has captured this effect. ACI 440.1R-06 recommends this equation between (15 and 100) of embedment lengths to bar diameter ratio. However, most of the test beam results involved in this formulation had embedded length to bar diameter ratio less than $30d_b$ (Wambeke and Shield 2006). A few specimens that failed by splitting had an embedded length to bar diameter ratio between 30 and 95. No specimens with an embedded-length-to-bar diameter greater than 30 failed in a pullout mode of failure used in this database Wambeke and Shield (2006). More importantly, this equation is based on results from NVC specimens, with the majority of these beams reinforced with GFRP bars.

Recent studies have found that the bond strength of CFRP bars embedded in concrete is greater than that of GFRP bars in similar concrete due to the higher modulus of elasticity of the CFRP bars (Okelo and Yuan 2005, Newman, Ayoub, and Belarbi 2010). Furthermore, the development length for the CFRP bars based on ACI 440.1R-06 Eqn (2.8) gives values above $100d_b$, which is beyond the database range used to calibrate this equation. ACI committee 440 stated that using equation (2.7) to estimate

the FRP bar stress for embedment lengths greater than $100d_b$ is questionable due to limitations in the database (Wambeke and Shield 2006).

Therefore, the bond stresses of CFRP bars with a long embedment length in NVC need to be studied to address the existing gap in the current ACI development length prediction. Regarding the use of SCC, as discussed above, no guidelines are available for predicting the bond stress and development length of FRP bars embedded in SCC.

2.2.2.2 Bond behaviour of prestressing FRP tendons in concrete

In the late 1990s, several studies investigated the transfer and development lengths of CFRP tendons in normal vibrated concrete (NVC). Recently, the subject has captured the interest of many researchers, and the use of CFRP in prestressed applications has increased. In the following, a review of the published work on the subject is presented.

Abdelrahman and Rizkalla (1995) tested concrete T-beams pre-stressed with 8mm diameter CFRP bars. The concrete compressive strength was between 37.0 to 50.0 MPa, and the level of initial pre-stress ranged from 50% to 70%. The measured transfer lengths were 360mm and 500mm, for 50 and 70% prestress, respectively.

Taerwe and Pallemans (1995) reported the effect of concrete cover and concrete compressive strength, tendon diameter and initial pre-stress level on the transfer length. The parameters included were tendon diameters (5.3 and 7.5mm) and concrete compressive strength (42 and 65 MPa). The CFRP tendons were stressed to an initial pre-stress of 55% of the ultimate strength of the tendon. It was proposed that the transfer length for sand coated CFRP bars be $16d_b$, and the critical concrete cover be $2.6d_b$. The authors found that the concrete compressive strength has an insignificant effect on the transfer length.

Zaki et al. (1999) conducted research on the transfer and development length of CFRP pre-stressing strands in NVC. Concrete prism specimens were used to measure the transfer length. The main parameters were the concrete compressive strength, pre-stress level, shear reinforcement, time effect, and bar diameter and type (Leadline, CFCC, and steel strands). After the transfer length was measured, the prisms were subjected to pullout tests. Fifty-two beams were fabricated and tested for flexure to estimate their flexural bond length and flexural behaviour. The results of this work showed that the transfer length was increased by 10 and 17 percent when the shear reinforcement was omitted for Leadline and CFCC bars, respectively. The flexure bond length was not affected by the shear reinforcement for Leadline bars, and the CFCC prestressed beams exhibited an increase of 25 percent. After one year, the transfer length of Leadline bars was increased by 22 percent. This was not the case

for CFCC and steel strands, where no significant long-term changes were observed. Additionally, parameters such as bar diameter, and concrete compressive strength at release were found to be crucial factors that affect the transfer length. Based on their results, the authors suggested the following equations, which were later adopted by ISIS Canada and ACI 440.4R-04.

$$l_t = \frac{f_{pi}\, d_b}{\propto_t \; f_{ci}^{0.67}} \qquad (2.9)$$

$$l_{fb} = \frac{(f_{pu} - f_{pe})}{\propto_f \; f_{ci}^{0.67}} \qquad (2.10)$$

Where

l_t is the transfer length, mm;

f_{pi} is the initial prestress level, MPa;

d_b is the tendon diameter, mm;

α_t is a coefficient that depends on surface condition: 1.9 for leadline bars and 4.8 for CFCC strand;

f'_{ci} is the concrete compressive strength at transfer MPa;

l_{fb} is the flexural bond length, mm;

f_{pu} is the ultimate rupture strength of the tendon, MPa;

f_{pe} is the effective tendon prestress, MPa;

α_f is a coefficient that depends on surface condition: 1.0 for leadline bars and 2.8 for CFCC strand; and

f'_c is concrete compressive strength, MPa.

Zou (2003) evaluated the time-dependent effect on the transfer length of FRP bars. The main variables were the bars' size, configuration and surface condition, and the concrete compressive strength. Both CFRP and AFRP bars were used. The transfer length of CFRP Leadline 8 mm diameter bars with an indented surface was measured and found to be in the range of 300 to 800mm for 26 MPa and 63 MPa concrete specimens. In the case of high-strength concrete (63 MPa), CFRP and steel strands were found to have similar transfer lengths. In the case of sand-coated AFRP, the measured transfer length was found to be in the range of 170 – 270 mm. These results were very close to those of steel strands. In addition, the concrete compressive strength was found to have insignificant effect on the transfer length, and the time factor had no effect on the transfer length of AFRP specimens.

Xue et al. (2008) compared the bond behaviour of CFRP bars to that of steel strands. Pullout tests were carried out on CFRP bars embedded in cube specimens made from different materials: normal

concrete, high performance concrete, epoxy resin, and grout. The diameters of the CFRP bar were 12.5 and 15.2mm. Control specimens were made using steel strands with similar diameters. The ultimate tensile strength of the CFRP bars were 2400 MPa and 2330 MPa for 12.5mm 15.2 diameter, respectively. The embedded length used was 5 times the bar diameter. The findings of this work indicated that the ultimate bond strength of steel strands in concrete was 30 to 50% higher than that of CFRP in concrete; however, the allowable bond strength (stress at 1.0mm slip) of CFRP bars was about 1.3 to 1.4 times that of steel strands. The bar diameter had a moderate influence on the allowable bond strength. Based on this work, a development length equation was developed as follows:

$$l_{bf} = 0.083 \frac{f_{fu}\, d_b^{1.52}}{\sqrt{f_c'}} \qquad (2.11)$$

Where:

l_{bf} is the basic development length, mm;

f_{fu} is the ultimate rupture strength of the strand, MPa;

d_b is the strand diameter, mm; and

f_c' is the concrete compressive strength.

2.3 Summary and Discussion

2.3.1 Bond behaviour of reinforcement in SCC

It is clear that SCC, with its excellent fresh and hardened properties, has a great potential in structural applications. A general trend in the published literature indicated that the bond behaviour of steel reinforcement in SCC is similar or better to that in NVC. For non-prestressed concrete, most of the available literature indicates that the bond strength of steel reinforcement in SCC is similar to or greater than that in NVC. However, many of these research works used pullout specimens or short embedment length steel bars, which may not accurately represent the bond behaviour of flexural members. In the case of "top bar effect," and when slag cement is used, the bond strength in SCC could be reduced in comparison to NVC's. The researchers generally agree that the top bar effect is less in SCC, especially at low to moderate concrete compressive strength. At high compressive strength, both SCC and NVC behave similarly. Regarding the failure modes, steel bars in SCC tend to fail by slip rather than the typical splitting observed in NVC. This phenomenon may be attributable to the higher fines and lower coarse aggregate size than those of NVC. This type of failure is more ductile than a splitting failure mode.

In prestressed concrete, the research results indicate that both transfer and development lengths of steel strands in SCC meet the ACI specifications for NVC (Burgueno and Haq 2007). The recommended cover and clear spacing of the steel reinforcement to prevent splitting in SCC are similar to those required in NVC (Josef 2005). Previous research has shown that in the case of steel strands, the bond strength of SCC is about the same or better than that of NVC. These positive effects may become more evident as the fines content increases (Burgueno and Haq 2007). It is also found that fly ash powder could reduce the early compressive strength and decrease the bond strength, consequently increasing the transfer length. This factor could explain some of the results of fly ash specimens obtained by Burgueno and Haq (2007). Therefore, in general, SCC exhibits good bond properties in comparison to NVC. However, Burgueno and Haq (2007) indicated that the margin of safety is reduced when ACI 318 code equations are used to predict the bond and transfer length for SCC.

Based on the literature review, the study of the flexural behaviour of SCC members and validation of the current design guidelines is becoming increasingly important. To date, there are no design guidelines available by which design engineers can determine the development length of reinforcing bars embedded in SCC. The lack of such provisions has limited the use of SCC in construction

2.3.2 Bond behaviour of FRP bars in concrete

The bond strength of GFRP reinforcing bars in NVC has been extensively investigated; however, only a limited number of studies are available on the bond behaviour of CFRP bars in NVC. No research is available the literature on the bond behaviour of FRP bars in SCC.

Two types of factors affect the bond strength of FRP bars in concrete: FRP-material-related factors and concrete-material-related factors. The main FRP-material-related factors are FRP's stiffness, cross-sectional shape and surface conditions, type and volume of fibre and matrix, and the Hoyer effect (ACI 440.4R-04). The concrete-related factors are compressive strength, embedded length, cover thickness and confinement. In fact, the bond stresses are not uniform along the embedded length. The bond strength of FRP bars with a short embedded length is greater than those measured in long embedded lengths; however, the bond capacity, obviously, increases as the embedded length increases up to the full development length. Many researchers have reported that the bond strength increases as the concrete compressive strength increases. The bond strength is most likely to increase linearly with the square root of the concrete compressive strength.

The development length equation of the ACI 440.1R-06 design guideline is based mainly on GFRP bars embedded in NVC. The guide indicates that higher bond strength is expected for CFRP bars in

concrete than for GFRP bars due to their increased stiffness. However, ACI committee 440 does not provide a material correction factor for CFRP bars and instead recommends a value of 1.0. This knowledge gap needs to be appropriately addressed. The bond and flexural behaviour of SCC beams reinforced or prestressed with FRP bars needs to be addressed.

Chapter 3 – Experimental Program

3.1 Introduction

The experimental program was developed to investigate the bond and flexure behaviour of self-consolidating concrete (SCC) beams reinforced and prestressed with fibre reinforced polymer (FRP) bars. The study included non-prestressed and prestressed beams. The non-prestressed beams were used to examine the bond profile at various embedment lengths and determine the development length of different GFRP and CFRP bar diameters. For the prestressed beams, the study focused on determining both the transfer and development lengths of the CFRP bars at various prestressing levels. The study also included testing specimens made from normal vibrated concrete (NVC) to provide benchmark comparisons.

3.2 Test Program

Fifty six beam specimens were fabricated and tested. Forty specimens were non prestessed beams and sixteen specimens were prestressed beams. For the non-prestressed beams, sixteen specimens were made from SCC and reinforced with CFRP bars, and nine specimens were made from SCC and reinforced with GFRP bars. Fifteen specimens were made from NVC: twelve beams were reinforced with CFRP bars and three beams were reinforced with GFRP bars. The prestressed beams consisted of 12 specimens made from SCC and four specimens made from NVC. Both sets were prestressed with CFRP bars.

The bond stress of FRP bars were assessed based on tensile stresses in the FRP bars due to flexural loading. For each group of beams, flexural tests were carried at various shear spans to assess the effect of embedment length on bond stresses. The tensile stresses in the FRP bars were calculated based on the measured longitudinal strain by strain gauges mounted on the FRP bar. Two terms for bond stresses were evaluated: local bond stresses and average bond stresses. The local bond stress is the bond stress between two intermediate sections along the shear span and the average bond stress is the overall average bond stress along the shear span. A general overview of the experimental program is shown in Figure 3.1.

The main variable in the prestressed beams is the prestressing level. Three levels of prestressing were used: 30%, 45% and 60% of the guaranteed tensile strength of the FRP bar. Beams prestressed to 30% and 45% were considered as partially prestressed beams, flexural cracks are expected under service

load conditions while beams prestressed to 60% aimed to investigate the behaviour of fully prestressed beams: with no flexural cracks under service load conditions. The program was carried out in three main phases:

a) Exploratory phase: the main aim of this phase was to investigate the beam design and test setup. Only four non-prestressed beams and four prestressed beams were fabricated and tested.
b) Detailed phase: this phase contains the main experimental core of this study, with 36 SCC beams fabricated and tested
c) Comparison phase: in this stage, 12 specimens made from normal vibrated concrete (NVC) were fabricated and tested.

3.3 Test Parameters

The following test parameters were implemented in the experimental program.

a) Non-prestressed beams
   - Type of concrete: SCC and NVC
   - Type of FRP bar: CFRP and GFRP bars
   - FRP bar diameter: for the CFRP bars, bar diameters of 6.3, 9.5 and 12.7mm were used. For the GFRP bars, bar diameters of 9.5, 12.7 and 15.9mm were considered.
   - Concrete cover thickness: the main study was carried out on beams with a concrete cover thickness of $3d_b$. To study the effect of cover thickness, additional specimens were fabricated with cover thicknesses of 2.0db, $1.5d_b$ and $1.0d_b$.
   - Embedment lengths: three values of embedment length were selected in each group.
b) Prestressed beams
   - Type of concrete: SCC and NVC
   - Type of FRP bar: CFRP bar
   - Bar diameter: 12.7mm diameter was used
   - Prestressing level: 30%, 45%, and 60% of the guaranteed tensile strength of the CFRP prestressing bar.

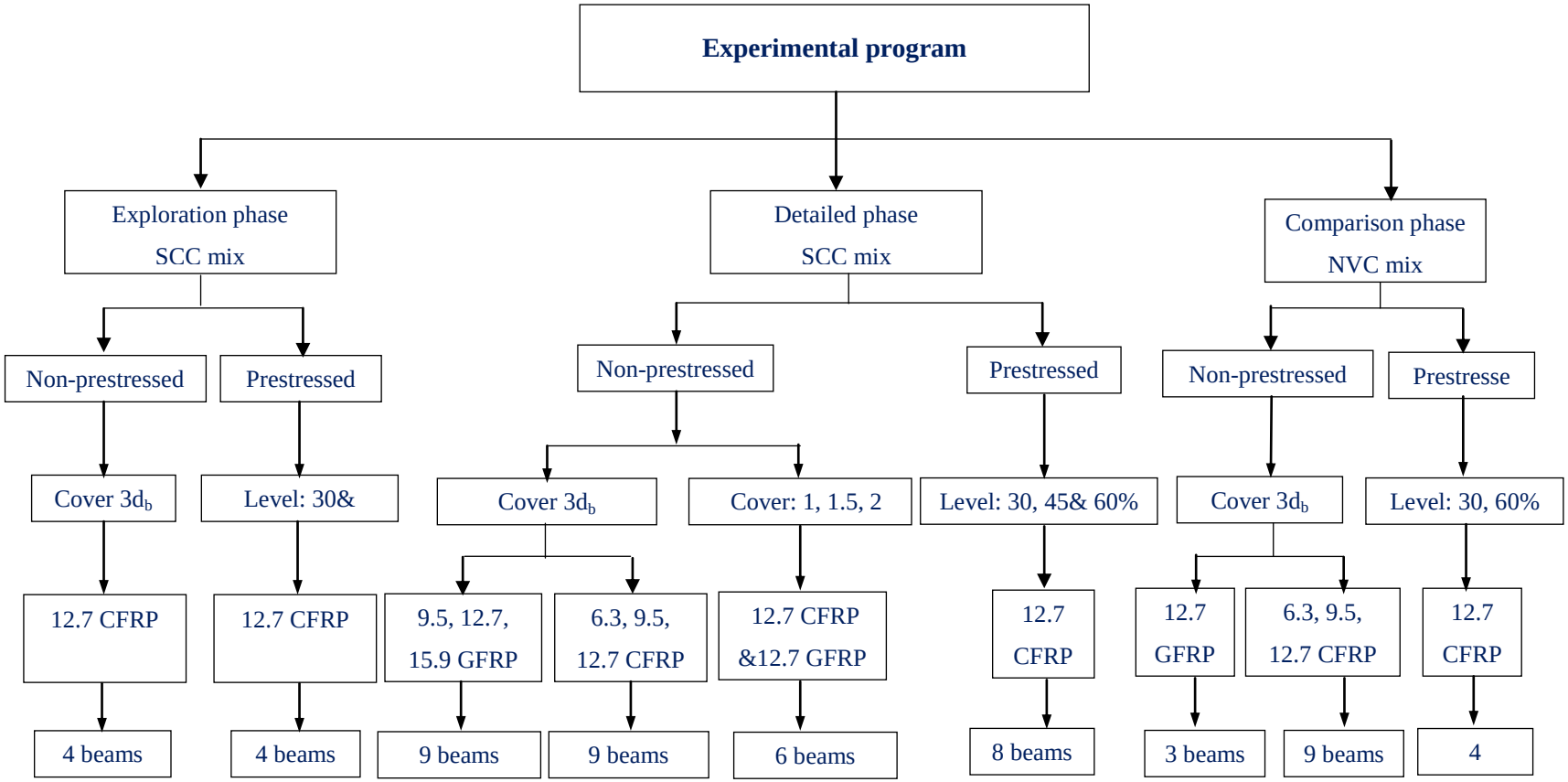

Figure 3.1 General overview of the experimental program

3.4 Specimen Selection and Test Matrix

Full-scale non-prestressed and prestressed beam specimens were constructed and tested. Beam specimens were selected because beam flexural testing provides the actual bond behaviour of flexural members. Figure 3.1 shows the typical beam geometry, reinforcement details and loading configuration. The length of the beams in each group was chosen to provide the required embedded length for testing and a constant moment region. The beam width was maintained constant at 150mm for all beams, while the beam depth was varied to maintain the reinforcement ratio at less than the balanced ratio and, at the same time, to provide a shear span to a depth ratio of above 3.0 to ensure slender beam behaviour with no deep beam effects. The beam configuration and section reinforcement design were selected to maintain a tension mode of failure in all beam specimens. The tension mode of failure provides the opportunity to explore the bond behaviour under a wide range of tensile stresses in the tension reinforcement. The detailed test matrices for the non-prestressed beams and prestressed beams are given in Tables 3.1 and 3.2, respectively. The beam nomenclature is shown in Figure 3.2.

All prestressed and non-prestressed beams were reinforced with a single CFRP bar in the tension zone. The concrete cover to the FRP bar was maintained constant to $3d_b$ except for specimens that were made to investigate the cover thickness effect. To avoid shear failure, all beams were reinforced with stirrups equally spaced throughout the beam length. The use of uniform shear reinforcement provides a constant confinement and simplifies the bond-strength analysis and evaluation. Various bar diameters were used in this study. For the prestressed beams, a single 12.7mm diameter CFRP bar was used as the prestressing reinforcement. In the non-prestressed beams: 6.3, 9.5 and 12.7mm diameter CFRP bars and 9.5, 12.7 and 19.5mm diameter GFRP bars were used as the main reinforcement. All beams were subjected to a four-point bending test. The embedment length of the FRP reinforcement in each beam was varied by increasing the shear span during testing. The shear span was varied within the same group to explore the transition of failure mode from a bond failure to bar rupture failure and hence to determine the bond stress profile for the minimum embedment length at onset of bar rupture.

Table 3.1 Detailed test matrix for non-prestressed beam specimens

Concrete type (f_c')	Group number	Beam label[(1)]	Beam size, $b \times h \times l$ mm	Bottom reinforcement					Shear reinforcement Size-spacing
				type	d, mm	Cover, mm	ρ	ρ_b	
Exploration Phase – SCC									
SCC-mix1 (66.6MPa)	ESC12.7	SC12.7-3.0-550	150×250×2200	CFRP	12.7	38.1	0.0041	0.0048	10M-100
		SC12.7-3.0-750							
		SC12.7-3.0-950							
		SC12.7-3.0-550							
Detailed Phase – SCC									
SCC-mix2 (49.6MPa)	SC6.3	SC6.3-3.0-350	150×150×1700	CFRP	6.3	18.9	0.0016	0.0059	8M-75
		SC6.3-3.0-450							
		SC6.3-3.0-600							
	SC9.5	SC9.5-3.0-550	150×200×2400		9.5	28.5	0.0028	0.0052	8M-75
		SC9.5-3.0-600							
		SC9.5-3.0-950							
	SC12.7	SC12.7-3.0-850	150×300×3000		12.7	38.1	0.0033	0.0041	8M-100
		SC12.7-3.0-1250							
		SC12.7-3.0-1400							
	SC12.7C	SC12.7-2.0-850	150×300×3000		12.7	25.4	0.0032	0.0041	8M-100
		SC12.7-1.5-850				19.1	0.0031		
		SC12.7-1.0-850				12.7	0.0030		
SCC-mix3 (70.9MPa)	SG9.5	SG9.5-3.0-300	150×200×2200	GFRP	9.5	28.5	0.0028	0.0094	8M-75
		SG9.5-3.0-450							
		SG9.5-3.0-600							
	SG12.7	SG12.7-3.0-350	150×200×2200		12.7	38.1	0.0054	0.0110	8M-75
		SG12.7-3.0-450							
		SG12.7-3.0-600							
	SG12.7 C	SG12.7-2.0-450	150×200×2200		12.7	25.4	0.0050	0.0110	8M-75
		SG12.7-1.5-450				19.1	0.0048		
		SG12.7-1.0-450				12.7	0.0047		
	SG15.9	SG15.9-3.0-450	150×300×2200		15.9	47.7	0.0054	0.0121	8M-100
		SG15.9-3.0-600							
		SG15.9-3.0-750							
Comparison Phase – NVC									
NVC-mix (64.5MPa)	NC6.3	NC6.3-3.0-350	150×150×1700	CFRP	6.3	18.9	0.0016	0.0072	8M-75
		NC6.3-3.0-450							
		NC6.3-3.0-600							
	NC9.5	NC9.5-3.0-550	150×200×2200		9.5	28.5	0.0041	0.0062	8M-75
		NC9.5-3.0-750							
		NC9.5-3.0-950							
	NC12.7	NC12.7-3.0-850	150×300×3000		12.7	38.1	0.0033	0.0049	8M-100
		NC12.7-3.0-1250							
		NC12.7-3.0-1400							
	NG12.7	NG12.7-3.0-350	150×200×2200	GFRP	12.7	38.1	0.0054	0.0100	8M-75
		NG12.7-3.0-550							
		NG12.7-3.0-550-2							

Table 3.2 Detailed test matrix for prestressed beam specimens

Concrete type (f_c')	Group label	Beam label[(1)]	Beam size, $b \times h \times l$ mm	Bottom reinforcement			Shear reinforcement Size-spacing
				Prestressing level, %	ρ	ρ_b	
Exploration Phase -SCC							
SCC-mix1 66.6MPa	S1-30	SC-30-1100	150×250×3600	30	0.00399	0.00641	10M-100
		SC-30-1250					
	S1-60	SC-60-1100		60	0.00399	0.00885	
		SC-60-1350					
Detailed Phase - SCC							
SCC-mix2 49.6MPa	S2-30	SC-30-1350	150×250×3600	30	0.00399	0.00519	10M-100
		SC-30-1500					
	S2-60	SC-60-1500		60	0.00399	0.00714	
		SC-60-1700					
SCC-mix 3	S3-45	SC-45-1100	150×250×3600	45	0.00399	0.00922	10M-100
		SC-45-1250					
		SC-45-1350					
		SC-45-1500					
Comparison Phase – NVC							
NVC mix	N-30	N30-1	150×250×3600	30	0.00399	0.00627	10M-100
	N-60	N60-2		60	0.00399	0.00866	
		N60-3					
		N60-4					

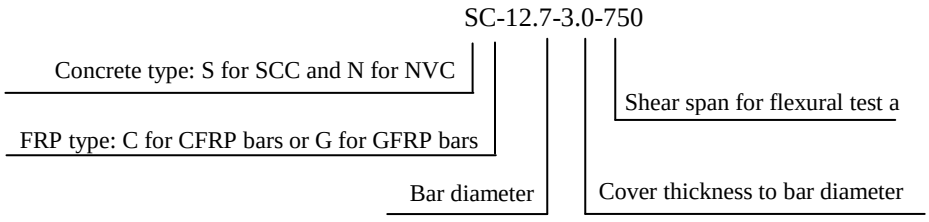

(a) Label definition of non-prestressed beams

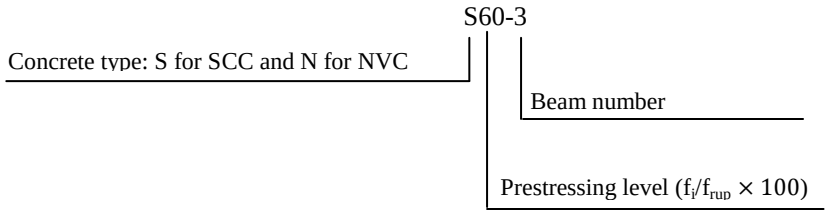

(b) Label definition of prestressed beams

Figure 3.2 Beam nomenclature

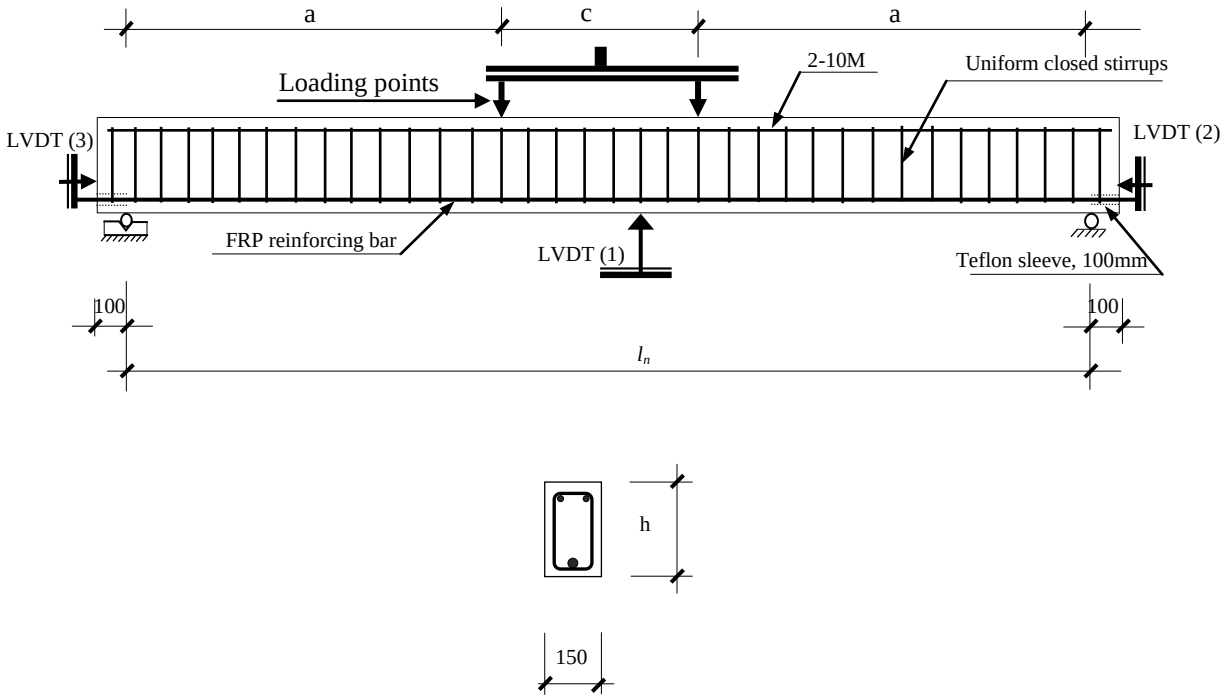

Where;

a is the shear span as defined in Tables 3.1 and 3.2

l_n is the clear beam testing span which is equal to the beam length minus 200mm

c is the length of the constant moment region which is equal to l_n minus twice the shear span

h is the overall cross section height as shown on Tables 3.1 and 3.2

Figure 3.3 Typical beam geometry and instrumentation arrangements

3.5 Material Properties

3.5.1 FRP Bars

Two types of FRP bars were used as main tensile reinforcement for the beam specimens: carbon fibre reinforced polymer (CFRP) bars, and glass fibre reinforced polymer (GFRP) bars. The FRP bars were manufactured by Pultrall Inc., Quebec, Canada. The FRP bars were made of continuous longitudinal fibres impregnated in a thermosetting vinyl ester resin, with a typical fibre content of 73% by weight for CFRP bars and 77.8% for GFRP bars. Both type of bars had their surfaces sand-coated to improve their bond ability with the surrounded concrete. The mechanical properties of the CFRP and GFRP bars are given in Table 3.3 (Pultrall Inc. 2007).

Table 3.3 Geometric and Mechanical properties of CFRP and GFRP bars (Pultrall Inc. 2007)

Bar type	Diameter, mm	Cross sectional area, mm^2	Guaranteed tensile strength, MPa	Tensile modulus, GPa	Tensile strain, %	Poisson's ratio
CFRP	6.3	31.67	1355.5	127.0	1.22	0.28
	9.5	71.26	1431.0	120.0	1.33	0.30
	12.7	126.70	1765.0	144.0	1.32	0.30
GFRP	9.5	71.30	765.0	45.4	1.89	0.21
	12.7	126.7	708.0	46.3	1.70	0.26
	15.9	197.9	683.0	48.2	1.56	0.25

3.5.2 Steel Bars

Deformed steel bars, No. 10M (d_b = 11.3 mm), were used as the top reinforcement for all beams and as shear reinforcement for most beams. The nominal yield stress of the deformed steel bars was 400 MPa. Smooth 8 mm diameter steel bars were used as shear reinforcement for the small cross-section beams. The nominal yield stress of the smooth bars was 340MPa.

3.5.3 Concrete

Four concrete batches were used to fabricate all the specimens of this study. All the four mixes were supplied by industrial concrete plant. SCC mix-1, SCC mix-3 and NVC mix were from the same supplier and SCC-2 was from another supplier. Both suppliers use a combination approach to obtain SCC mixes: increased fines and the use of viscosity modifying admixture VMA. Also, high range water reducing admixture HRWRA was used by both suppliers for the SCC mixtures. The maximum aggregate size for the SCC was 14mm and for the NVC was 25mm. The slump flow, J-ring and visual

segregation index for SCC mixes and slump measurements for the NVC mix were measured on the fresh concrete. Twenty-one concrete cylinders of 100mm diameter and 200mm height were cast from each batch. Three cylinders were tested at each of the following times: at transfer (3-5) days, 7 days, 14 days, 28 days and at flexural testing. Three cylinders were tested for modulus of elasticity at flexural testing, and three cylinders were tested for tensile strength (splitting test). Figures 3.4 to 3.7 show the fresh concrete tests during casting.

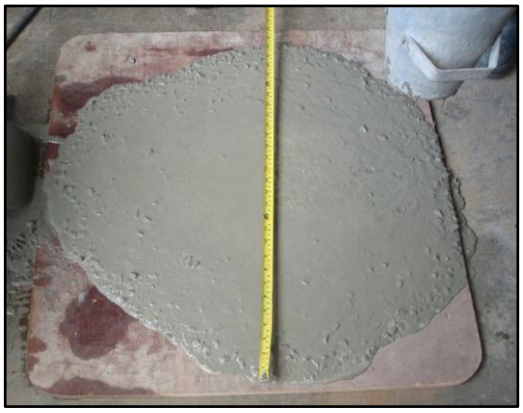

Figure 3.4 Slump flow measurement on SCC-mix1, VSI = 1.5

Figure 3.5 Slump flow measurement on SCC-mix2, VSI =1

Figure 3.6 Slump flow measurement on SCC-mix3, VSI =0

Figure 3.7 J-ring flow measurements on SCC-mix 3

Test results for fresh concrete properties of each concrete batch are given in Table 3.4. The slump flow and confined flow for the SCC mixes were between 650mm and 720mm. The confined flow J-ring test results for the SCC mix were between 625mm and 690mm. Visual stability index (VSI) for the SCC mixes were evaluated. The VSI is an indication of SCC mix static stability: ability of the mix to maintain homogenous distribution of its various constituents. ACI 237 (2007) classifies VSI results as: 0 = highly stable, 1.0 = stable, 2 = unstable and 3 = highly unstable. Results indicated that both SCC mix-1 and SCC mix-2 had VSI. of 1.5 and 1.0. SCC mix-1 had VSI of 0. These results are within the definition of the SCC fresh properties as prescribed by ACI 237 (2007). However, SCC mix-1 and SCC mix-2 were susceptible to segregation risk since they were on the border limit of passing ability requirement. SCC mix-3 showed the best fresh properties among the three mixes. It is important to note that both SCC mix-1 and SCC mix-3 were delivered from the same source and had exactly the

same mix proportion while SCC mix-2 were delivered from another source. All of the three SCC mixes used high range water reducer admixture and a combination of increased fines and VMA admixture to achieve the mix stability and segregation resistance.

Table 3.4 Summary of concrete fresh properties of all mixes

Test	Mix			
	SCC mix1	SCC mix2	SCC mix3	NVC mix
Slump flow, mm	720	680	650	150
Confined flow J-ring, mm	690	625	640	-
Segregation VI	1.5	1.0	0.0	-

Table 3.5 summarizes the compressive strength results. All mixes showed similar rates of strength development. The concrete compressive strengths at three days (prestess force release) of SCC mix-1, mix-2, and mix-3 were 30.4MPa, 26.1MPa and 40.1MPa, respectively. The concrete compressive strength at release of the NVC mix was 37.0MPa. The concrete compressive strength at flexural tests of SCC mix-1, mix-2, and mix-3 were 62.1MPa, 49.6MPa and 70.9MPa, respectively and for the NVC mix was 64.5MPa.

Table 3.5 Concrete compressive strength results

Test		Mix			
		SCC mix1	SCC mix2	SCC mix3	NVC mix
Average Compressive Strength, MPa	3 days (at release)	30.4	26.1	40.1	37.0
	7 days	35.1	35.2	46.0	42.1
	14	48.2	41.0	57.0	53.4
	21	57.5	44.0	62.0	59.5
	28 days	62.1	48.4	64.0	61.8
	at flexural testing(1)	62.1	49.6	70.9	64.5

(1) Specimens made from SCC mix-1 were tested approximately 28 day to 35 days from casting. Specimens made from SCC mix-2 were tested approximately 210 days from casting. Specimens made from SCC mix-3 were tested approximately 180 day from casting. Specimens made from NVC mix were tested approximately 45 days from casting.

Table 3.6 gives the splitting tensile strength results. Tensile test results showed that SCC had lower tensile stress than NVC. The ratio of tensile stress to square root of the concrete compressive strength of SCC mixes ranged from 0.70 to 0.85 with an average of 0.79 while for NVC, it ranged from 0.86 to

0.90 with an average of 0.88. Therefore, SCC mixes had about 12% less tensile strength relative to $\sqrt{f_c'}$than NVC. The possible explanation of this finding could be related to the larger maximum aggregate size in NVC mix as compared to the SCC mixes. Also, the coarse aggregate content in NVC mix was greater than those of SCC mixes. Although the concrete compressive strength in SCC mixes was typically higher than that of NVC mix due to the inherently low w/c ratio, its tensile strength was not improved..The opposite was observed with further reduction in the tensile strength to square roof of concrete compressive strength for SCC mixes as compared to the NVC mix.

Table 3.6 Concrete splitting tensile strength test results

Mix label	No.	Splitting tensile strength [1]		
		Experimental, MPa (1)	Average Experimental, (STDEV) MPa	(1)/$\sqrt{f_c'}$
SCC mix-1	SCC-1-1	6.72	6.31 (0.60)	0.85
	SCC-1-2	5.62		0.71
	SCC-1-3	6.59		0.83
SCC mix-2	SCC-2-02	4.94	5.63 (0.37)	0.70
	SCC-2-05	5.75		0.81
	SCC-2-06	5.22		0.74
	SCC-2-09	5.63		0.80
	SCC-2-11	-		-
SCC mix-3	SCC-3-01	7.14	6.94 (0.22)	0.85
	SCC-3-07	6.71		0.79
	SCC-3-08	6.97		0.83
NVC mix	NVC-15	7.11	7.07 (0.16)	0.89
	NVC-16	7.21		0.90
	NVC-17	6.89		0.86

[1] Tensile strength test is done on concrete cylinders (indirect tensile strength test).

ACI 318M–2008 provides two equations to predict the modulus of elasticity of normal-density concrete. These equations are permitted for use with SCC by ACI 237–07. However, ACI 237-07 expects that the modulus of elasticity of SCC will be 10 to 15% lower than that of NVC of similar compressive strength. ACI 237-07 suggests to experimentally determining the modulus of elasticity if the modulus of elasticity is critical. The two ACI 318M- 2008 equations are given in Eqns. (3.1) and (3.2).

$$E_c = 4700\sqrt{f_c'} \qquad (3.1)$$

$$E_c = W_c^{1.5}\left(0.043\sqrt{f_c'}\right) \qquad (3.2)$$

Where

E_c is the modulus of elasticity of concrete, MPa;

f_c' is compressive strength of concrete, MPa; and

W_c is density (unit weight) of concrete, Kg/m^3.

Testing for the modulus of elasticity was carried out according to ASTM C 469-02 "Standard Test Method for Static Modulus of Elasticity and Poisson's Ratio of Concrete in Compression." Table 3.7 gives the test results of the modulus of elasticity for all mixes. The average measured modulus of elasticity of SCC mix-1 was 27.8GPa, SCC mix-2 was 22.7GPA, and SCC mix-3 was 30.6GPa. The modulus of elasticity of the NVC mix was 37.5GPa. The experimental values of the modulus of elasticity of SCC ranged from 0.67 to 0.82 of that predicted by ACI 318 design code- Eqn. (3.1) - and from 0.65 to 0.80 based on Eqn. (3.2). The modulus of elasticity of SCC mix-1, which had a similar concrete compressive strength to the NVC mix, was about 75% of that of the NVC. The measured modulus of elasticity of the NVC mix met the ACI prediction with an average ratio of 0.99. A graphical comparison between the modulus of elasticity of SCC and NVC is shown in Figure 3.8. This result agrees with those in the literature. The possible explanation of this trend in the modulus of elasticity of the SCC mixes is related to less coarse aggregate content and smaller maximum aggregate size than that typically used in NVC mixes. The decreased coarse aggregate content in SCC versus NVC increases the mortar volume fraction in SCC which influences the modulus of elasticity.

Table 3.7 Modulus of elasticity test results of all concrete mixes

Mix label	No.	Unit wt. Kg/m^3	Modulus of Elasticity, MPa				(1)/(2)	(1)/(3)
			Experimental (1)	Average Experimental	ACI prediction (2)	ACI prediction (3)		
SCC mix-1	SCC-1-1	2483.4	28284	27820	37037	41937	0.76	0.67
	SCC-1-2	2492.2	27324			42158	0.74	0.65
	SCC-1-3	2379.0	27852			39320	0.75	0.71
SCC mix-2	SCC-2-02	2129.4	23737	22714	33101	29757	0.72	0.80
	SCC-2-05	2127.9	22657			29726	0.68	0.76
	SCC-2-06	2122.1	22145			29605	0.67	0.75
	SCC-2-09	2117.1	22754			29499	0.69	0.77
	SCC-2-11	2138.9	22278			29957	0.67	0.74
SCC mix-3	SCC-3-01	2380.5	32438	30617	39575	42053	0.82	0.77
	SCC-3-07	2244.7	29847			38507	0.75	0.78
	SCC-3-08	2301.0	29568			39963	0.75	0.74
NVC mix	NVC-15	2388.2	37482	37392	37746	40300	0.99	0.93
	NVC-16	2358.1	36582			39542	0.97	0.93
	NVC-17	2295.6	38112			37968	1.01	1.00

Where: (1) is experimental measurement; (2) ACI 318M-2008 prediction Eqn. (3.1) and (3) ACI 318M-2008 prediction Eqn. (3.2).

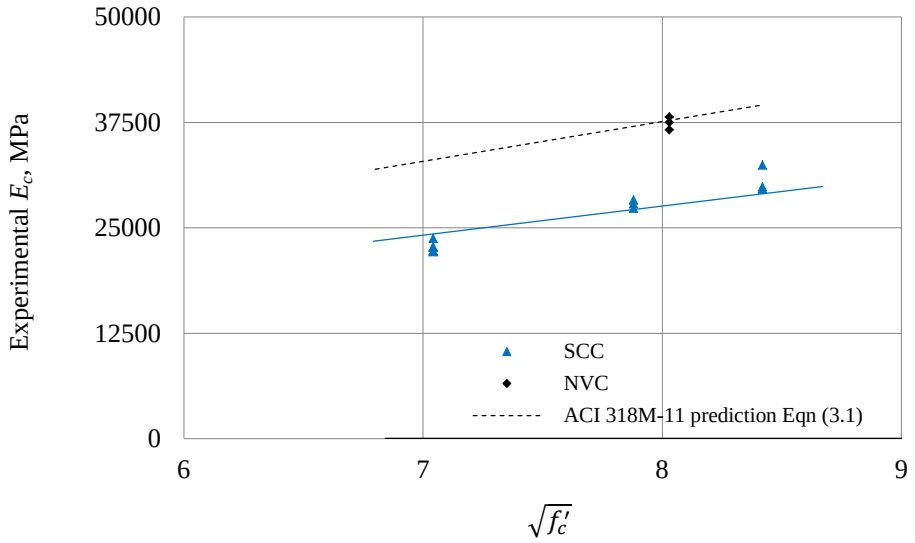

Figure 3.8 Experimental modulus of elasticity versus concrete compressive strength

3.6 Specimen fabrication

3.6.1 Installation of strain gauges

Several electrical resistance strain gauges (5mm in length) were mounted on the FRP bars. The purpose of these gauges was to provide the actual strains in the reinforcing FRP bar at the locations of interest. Knowing the strain, the tensile stress in the FRP bar can be calculated, and then the bond transfer between the reinforcing bar and the concrete can be determined and the bond profile can be established. The strain gauge installation procedure involved sanding the gauge location, and smoothing and cleaning the surface of the bar. The strain gauges were attached using special glue, and they were coated for protection from moisture.

3.6.1.1 Non-prestressed beams

Each beam was instrumented with several strain gauges mounted on the FRP bars within the shear span. The number of strain gauges used in each beam varied accordingly. One strain gauge (60mm in length) was placed on the concrete compression face at the extreme fibre at the midspan. Typical strain gauge layout is shown in Figure 3.9. Details of the strain gauge locations for all non-prestressed beams are given by Table 3.8.

3.6.1.2 Prestressed beams

Each prestressed CFRP bar was instrumented with six strain gauges (5 mm in length) mounted at 150, 350, 600, 950, 1250, and 1700 mm from one end of the beam. Several beams had fewer strain gauges. In each group, two beams had the strain gauges located at the live end and two beams had gauges located at the dead end. Live end is the beam end side where the prestressing load is being applied to the prestressing bar and released to the concrete beam and the dead end is the beam end where the anchorage set before the prestressing load application. The strain gauges were distributed along the length of the CFRP bar to capture the strains in the prestressed bars during the prestress operation and to determine the strain profile after prestessing force release. The strain gauges were also used to capture the strain in the CFRP bar during subsequent flexural tests. Typical strain gauge layout on prestressed CFRP bars is shown in Figure 3.10. Table 3.9 gives the location of strain gauges for all prestressed beams.

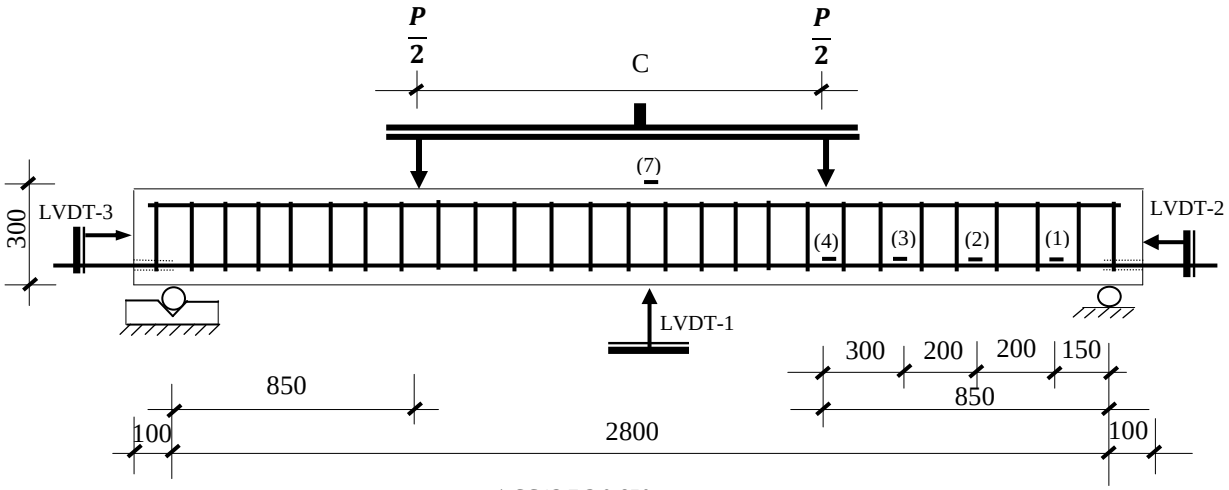

a) SC12.7-3.0-850

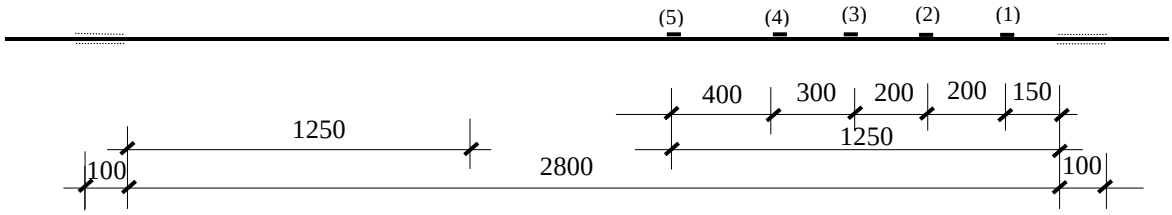

b) SC12.7-3.0-1250

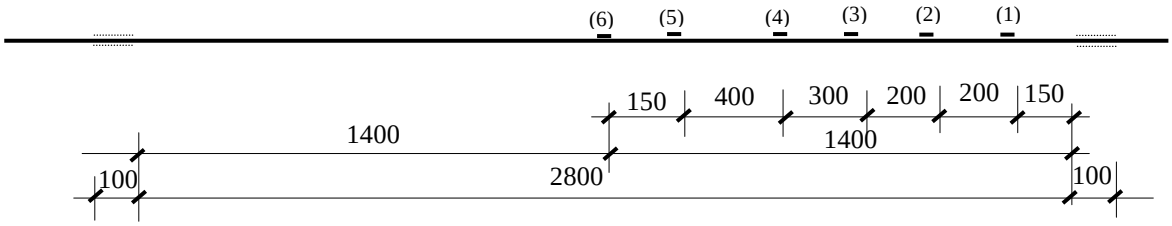

c) SC12.7-3.0-1400

Figure 3.9 Strain gauge locations and testing scheme of Group SC12.7

Table 3.8 Strain gauge locations on the FRP bars of non-prestressed beams

Type of FRP bar	Beam label	*ln* mm	a mm	c mm	Strain gauge locations FRP bar
GFRP reinforced beams	SG9.5-3.0-300	2000	300	1400	150, 300
	SG9.5-3.0-450		450	1100	150,350, 450
	SG9.5-3.0-600		600	800	150,350, 450, 600
	SG12.7-3.0-350	2000	350	1300	150, 350
	SG12.7-3.0-450		450	1100	150, 350, 450
	SG12.7-3.0-600		600	800	150, 350, 450, 600
	SG12.7-2.0-450	2000	450	1100	150, 350, 450
	SG12.7-1.5-450		450	1100	150, 350, 450
	SG12.7-1.0-450		450	1100	150, 350, 450
	SG15.9-3.0-450	2000	450	1100	150, 350, 450
	SG15.9-3.0-600		600	800	150, 350, 450, 600
	SG15.9-3.0-750		750	500	150, 350, 450, 600, 750
	NG12.7-3.0-350	2000	350	1300	200, 350
	NG12.7-3.0-550		550	900	200, 350, 550
	NG12.7-3.0-550-2		550	900	200, 350, 550, 750
CFRP reinforced beams	SC6.3-3.0-350	1500	350	800	150, 350
	SC6.3-3.0-450		450	600	150, 350, 450
	SC6.3-3.0-600		600	300	150, 350, 450, 600
	SC9.5-3.0-550	2000	550	900	200, 550
	SC9.5-3.0-750		750	500	200, 550, 750
	SC9.5-3.0-950		950	100	200, 550, 750, 950
	SC12.7-3.0-850	2800	850	1100	200, 550, 850
	SC12.7-3.0-1250		1250	300	200, 550, 850, 1250
	SC12.7-3.0-1400		1400	0	200, 550, 850, 1250, 1400
	SC12.7-2.0-850	2800	850	1100	200, 350, 550, 850
	SC12.7-1.5-850		850	1100	200, 350, 550, 850
	SC12.7-1.0-850		850	1100	200, 350, 550, 850
	NC6.3-3.0-350	1500	350	800	150, 350
	NC6.3-3.0-450		450	600	150, 350, 450
	NC6.3-3.0-600		600	300	150, 350, 450, 600
	NC9.5-3.0-550	2000	550	900	200, 550
	NC9.5-3.0-750		750	500	200, 550, 750
	NC9.5-3.0-950		950	100	200, 550, 750, 950
	NC12.7-3.0-850	2800	850	1100	200, 550, 850
	NC12.7-3.0-1250		1250	300	200, 550, 850, 1250
	NC12.7-3.0-1400		1400	0	200, 550, 850, 1250, 1400

Where: l_n is clear span (distance between supports); *a* is the shear span (distance from support to the point load) and c is the constant moment region length (distance between the two point loads).

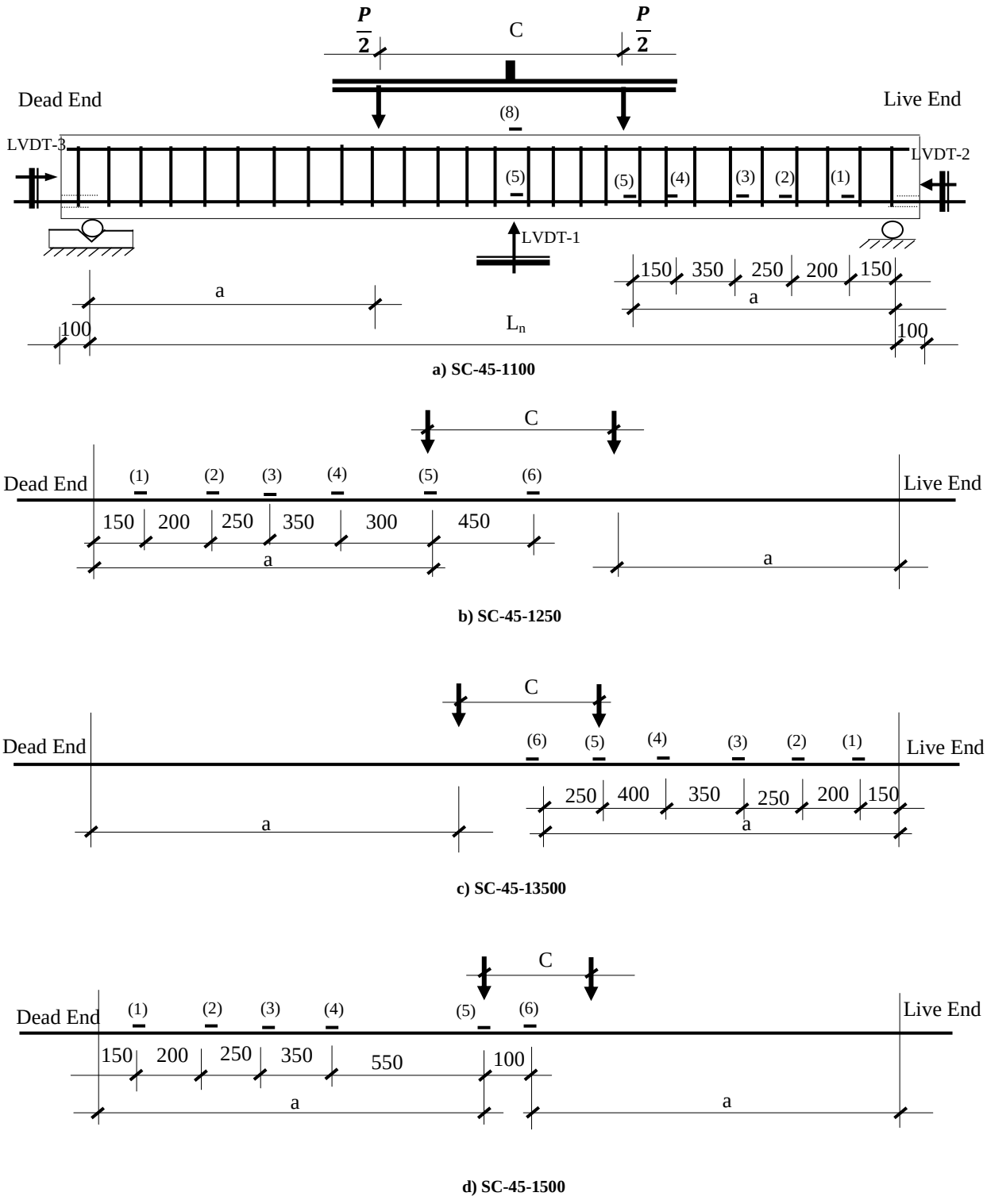

Figure 3.10 Strain gauges locations and testing layout of Group S45

Table 3.9 Strain gauge locations on the prestressing CFRP bars

Group	Beam label	*ln* mm	a mm	c mm	Strain gauge locations
					FRP bar
S30	SC-30-1100	3400	1100	1200	150, 350, 1700
	SC-30-1250	3400	1250	900	150, 350, 600, 1700
	SC-30-1350	3400	1350	700	150, 350, 600, 950, 1250, 1700
	SC-30-1500	3400	1500	400	150, 350, 600, 950, 1700
S45	SC-45-1100	3400	1100	1200	150, 350, 600, 950, 1100, 1700
	SC-45-1250	3400	1250	900	150, 350, 600, 950, 1250, 1700
	SC-45-1350	3400	1350	700	150, 350, 600, 950, 1350, 1700
	SC-45-1500	3400	1500	400	150, 350, 600, 950, 1500, 1700
S60	SC-60-1100	3400	1100	1200	150, 350, 600, 900, 1700
	SC-60-1350	3400	1350	700	150, 350, 1700
	SC-60-1500	3400	1500	400	150, 350, 600, 950, 1250, 1700
	SC-60-1700	3400	1700	0	150, 350, 600, 950, 1250, 1700
N30	NC-30-1350	3400	1350	700	1700
N60	NC-60-1250	3400	1250	900	1700
	NC-60-1350	3400	1350	700	200, 400, 600, 950, 1250, 1700
	NC-60-1500	3400	1500	400	200, 400, 600, 1700

Where: l_n is clear span (distance between supports); a is shear span (distance from support to the point load) and c is the constant moment region length (distance between the two point loads).

3.6.2 Caging and formwork

Reinforcement cage fabrication and formwork assembly were very similar for both types of specimens, prestressed and non-prestressed beams. During beam fabrication, steel stirrups, top steel rebars and the bottom FRP bar were assembled. Wire ties were used only on steel to steel (stirrups and top steel bar) connections and to fix the end sleeves (covering the FRP bar at the beam ends) to the stirrups. In addition, one plastic tie attached the CFRP bar to the stirrup at mid span. The formwork used to fabricate the beams was designed with a combination of plywood and structural steel sections. The sides were fair finish plywood, 18mm thick, and the bottom was a steel channel, 150mm width. This design allows for the sides to be removed easily for transfer length measurements without moving the beam from the casting bed. The forms were oiled, and then the cages were placed in the forms.

3.6.3 Prestressing operation

A special self-reacting steel frame was designed and fabricated to be used as a prestressing bed for prestressing operations. Figure 3.11 shows the schematic layout of this frame, and Figure 3.12 shows a cross section of the frame with the beams in position for casting. The serviceability requirement (small deformations under axial prestressed force) was the main factor that governed the design of this frame. The frame consisted of two side beams of W10×39 and double channels (2C12×20.7) at both ends. The two channels were centered at mid-height of the frame and had a gap of 37.5mm to allow for free passage of the prestressed FRP bars. All connections were similar and made using 8 bolts of one inch diameter, so the frame could be easily assembled and disassembled for storage. The frame provided a clear working space of 1360mm wide and 4500mm long. It has adjustable leveling bolts to allow for precise controls of the concrete cover thickness of the prestressing bar. The system has the ability to mechanically lock the prestressing force, adjust the tendon prestress level and gradually release the load. These advantages make this frame appropriate for a wide range of prestressing applications.

Wedge type anchors were used to grip the prestressing CFRP bars (Figure 3.13 a). These anchor system was developed at University of Waterloo,. The sand coating on the CFRP bars along the location of the anchorage system was removed to allow for uniform grip (Figure 3.13 b). At the live end, each anchorage barrel was fastened to a steel coupler which has an extended threaded steel rod passing through the steel frame and a 30T single-acting-hydraulic jack (Figure 3.14 a). A load cell of 240 kN was installed at the dead end of each beam. The load from the anchorage barrel at the dead-end was transferred to the steel frame. Then the anchorage system at the dead end was seated and placed against the load cell with a spacer plate in between the load cell and the anchorage barrel (Figure 3.14 b). The prestressing force was applied gradually using an electrical hydraulic pump. When the target load was achieved, a locking nut on the steel rod was fastened to the steel frame to maintain the load mechanically.

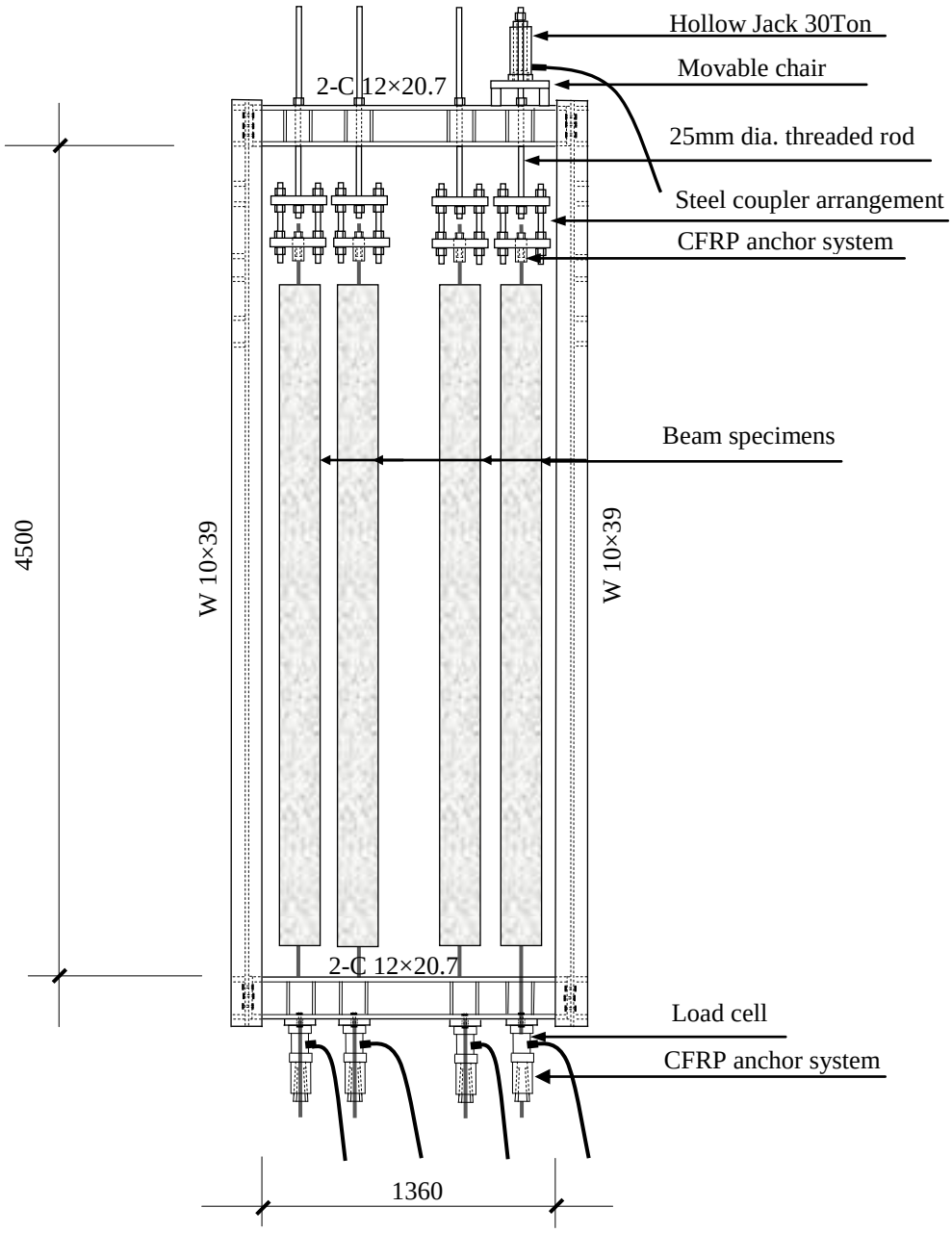

Figure 3.11 Prestressing steel frame plan

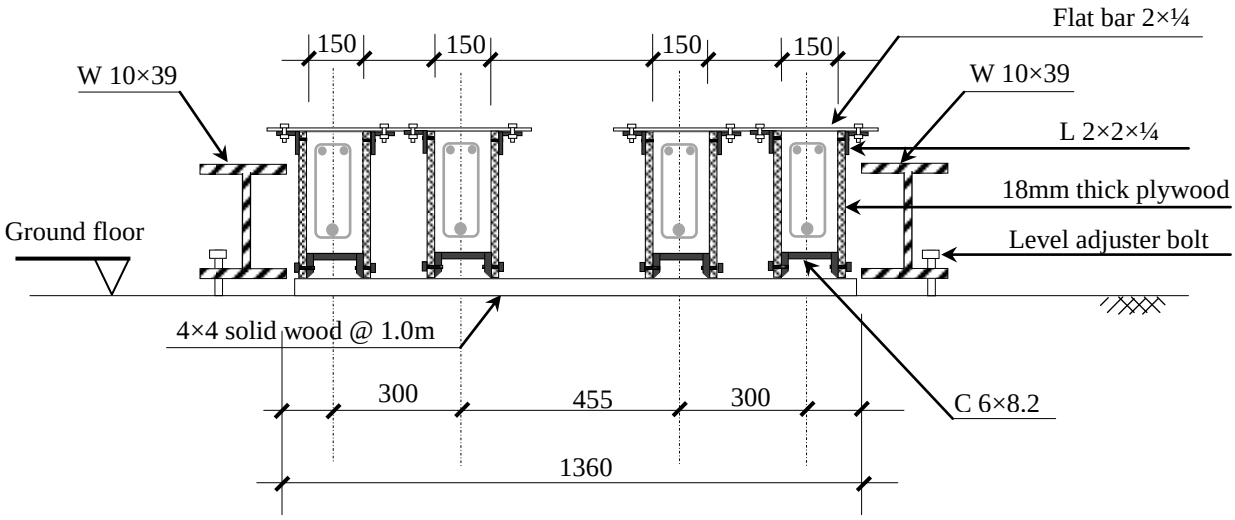

Figure 3.12 Beam formwork cross sectional details

3.6.4 Casting and curing

Ready-mix concrete was delivered to the casting bed by a truck. No vibration was used in the casting process of the SCC specimens, while an internal vibrator was used to compact the NVC specimens. Typically for SCC, the truck chute was placed at the mid-length of each beam, SCC was able to flow for 1.8m without use of vibration, and was able to completely encapsulate the caging and fill all the formwork. The beam surfaces were finished by trowel. After the concrete was set, all beams were covered with wet burlap and plastic sheets. The specimens and cylinders were kept under continuous moist curing for three days at normal room temperature; then the specimens were left to dry in air. At approximately two weeks from casting, the beams were stacked in the structural laboratory until 28 days before flexural testing.

Four prestressed beams and fifteen cylinders were cast from each batch. The beams and the cylinder specimens were subjected to wet curing for three days, as described above. On day four, the prestressing force was released gradually, and transfer length measurements were carried out. Load cells and strain gauge readings were continuously monitored and recorded during prestressing and up to when the release process was complete, using a National Instruments data acquisition system.

(a) Before seating

(b) Seated anchorage

Figure 3.13 Prestressed CFRP bar anchorage device

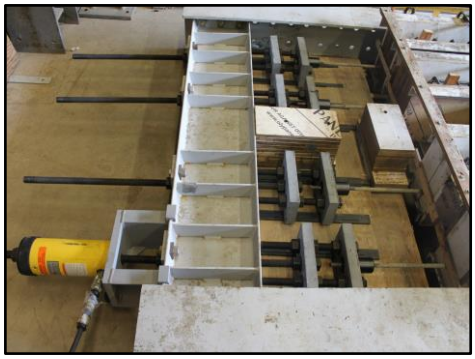

(a) Live end

(b) Dead End

Figure 3.14 Prestressing setup

3.7 Testing Procedure

3.7.1 Transfer length measurements in the prestressed beams

The transfer length of the CFRP bar in the prestressed beams was estimated by two methods: end-slip measurement and Demec point measurement. The end-slip measurements were recorded at both ends for all pretressed beams, while Demec point measurements were taken for only the two inner beams. The space available for the two other beams was not sufficient to place the Demec gauge and take an accurate reading. However, using this testing arrangement, for each cast, twelve independent transfer length measurements were provided. The two methods are described in detail below.

3.7.1.1 Concrete strain profile

Concrete strain profiles are widely used to estimate transfer length (Russell and Burns 1996, Andrew et al. 2011). The method is also known as the "95% Average Maximum Strain Method." In this method, reference (Demec) points are glued to the concrete surface on the beam side at the level of the prestressing bar before load release. The initial readings between Demec points are recorded. After release of the prestressing force, another set of readings between Demec points are recorded. The concrete strains are calculated by measuring the change in the Demec gauge readings relative to the initial readings. In this study, Demec points were placed at 50 mm (2 in) spacing (Figure 3.15 a). A gauge device of 200 mm gauge length and 0.001mm resolution was used to measure the distances between the Demec points (Figure 3.15 b). The calculated strain values were smoothed to remove local noise in the measurements, using Eqn. (3.3).

$$\varepsilon_i = \frac{\varepsilon_{i-1} + \varepsilon_i + \varepsilon_{i+1}}{3} \qquad (3.3)$$

Where

ε is measured strain in the concrete beam at the level of the prestressing bar, and (*i-1, i, i+1*) represents Demec points along the beam side surface.

The procedure to determine the transfer length based on longitudinal concrete strain profile can be summarized as follows:

(a) Plot the "smoothed" strain values along the beam's longitudinal axis (strain profile),

(b) Determine the "Average Maximum Strain (AMS)" by computing the numerical average of all the strains within the strain plateau of the effective prestress force,

(c) Take 95% of the "AMS" and draw a horizontal line corresponding to this value on the strain profile, and

(d) The transfer length is determined as the intersection of the 95% AMS line with the smoothened strain profile.

(a) General view of Demec points

(b) Measuring distance between two Demec points

Figure 3.15 Demec strain gauge measurements

3.7.1.2 Draw-in Measurements

Draw-in method is based on measuring the deformation of the prestressed strands due to prestressing stress (Logan 1997, Marti-Vargas et al. 2007). In this study, the deformation of the CFRP prestressing bars due to release of the prestressing force was measured at both ends using linear variable differential transducers (LVDTs) of ±12.5 mm range and 0.001mm resolution (Figure 3.16).

By measuring the slip (deformation) of the prestressing strand relative to the beam end due to release prestressing force, the length of the prestressing strand contributing to this deformation can be estimated based on mechanics of the materials. The deformation of a prestressing strand due to an applied prestress force is determined using Eqn. (3.4).

$$\Delta = \frac{P\,L}{A\,E} = \frac{1}{E}\int_{x_1}^{x_2} f(x)\,d_x \qquad (3.4)$$

Where

Δ represents the deformation of the bar;

P is the applied load;

L is the length of the stressed bar;

A is the cross section area of the bar;

E is the modulus of elasticity of the prestressing tendon; and

f (x) is the stress function over a specific length from x_1 to x_2.

Figure 3.16 End slip measurement during prestress load release

Assuming that the stress in the prestressing bar varies linearly from zero at the beam end to where the stress becomes uniform over a distance of the transfer length then the integration in Eqn. (3.4) can be done as follows:

$$\int_{x_1}^{x_2} f\ (x) d_x = \frac{f_{pi}}{2}\ l_t \qquad (3.5)$$

Where:

f_{pi} is the initial prestressing stress in the prestressed bar.

Combining Eqns. (3.4) and (3.5) gives Eqn. (3.6), which can be re-written in terms of transfer length in Eqn. (3.7):

$$\Delta = \left(\frac{1}{2}\ f_{pi}\right)\frac{l_t}{E_{frp}} \qquad (3.6)$$

$$l_t = \frac{2(\Delta\ E_{frp})}{f_{pi}} \qquad (3.7)$$

It important to note that only the net deformation of the bonded prestressing bar portion should be considered in determined transfer length based on Eqn. (3.7). The shortening of the prestressed bar from the LVDT clamp point to where the bar extends from the concrete should be subtracted from the LVDT measurement with the arrangement shown in the Figure 3.16.

3.7.2 Flexural testing

Flexural tests were carried to determine the maximum possible bond stress for each type of FRP reinforcing bar in this study and to establish the bond stress profile. All prestressed and non-prestressed beams were tested under a four-point static bending regime using a universal testing frame of 330kN capacity. The flexural tests were completed under displacement control at a rate of 1.0mm/minute. The shear span in the beam tests varied as given in Tables 3.1 and 3.2. The distances between the point loads were varied from beam to beam to vary the shear span. The beam was leveled in the loading frame and centered over the support centerlines. Measurements of load, midspan deflection (LVDT 1), bar slip at beam ends (LVDT 2 and LVDT 3), strain in CFRP bar, and strain in the concrete at the end of the shear span were collected using a National Instrumentation Data Acquisition System connected to a lab computer. Measurements were recorded at a 0.5 second time increment. Figure 3.17 shows the test arrangement.

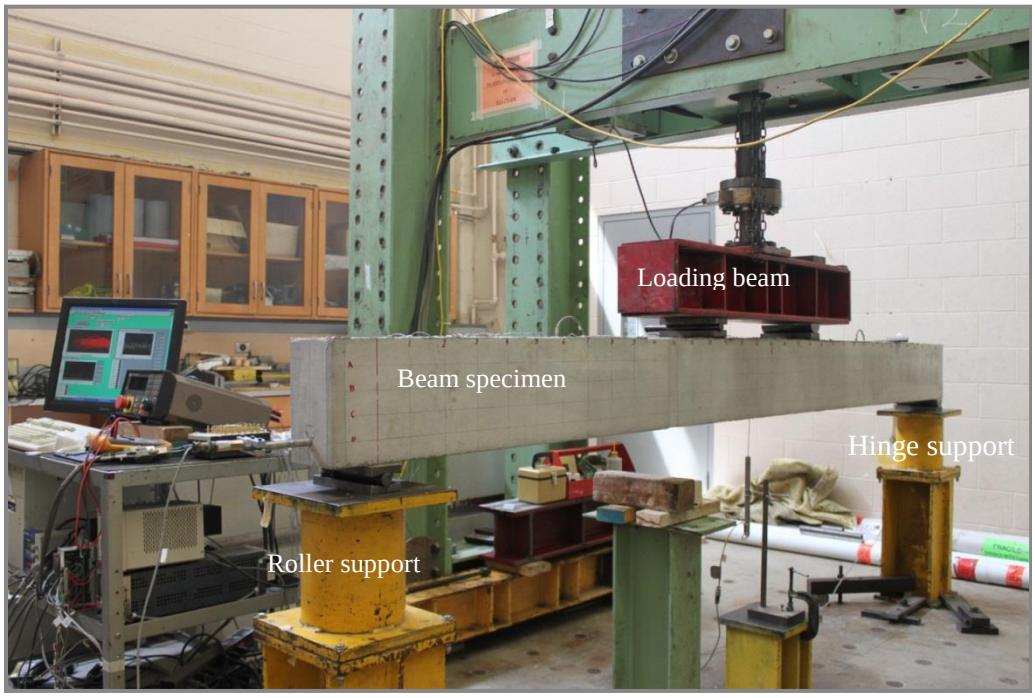

Beam specimen in the testing frame

LVDT - 2

LVDT - 1

LVDT - 3

Figure 3.17 Typical flexural test arrangement

Chapter 4 - Test Results and Discussion of non-prestressed FRP Reinforced Concrete Beams

4.1 Introduction

This chapter presents the results and discussion of the non-prestressed FRP reinforced concrete beams testing. As described in Chapter 3, reinforced concrete beams with both carbon and glass FRP bars were fabricated. Forty non-prestressed beam specimens were fabricated and tested. Twenty-five beams were reinforced with CFRP bars and fifteen beams were reinforced with GFRP bars. All beams were designed to have flexural tension failure. Parameters included in this study were the concrete type and compressive strength, type of FRP bar, bar diameter, cover thickness and embedment length. The test matrix was divided into groups of three beams, each based on the bar size and concrete type. Beams in the same group were reinforced with the same bar type and diameter and had similar dimensions, except for two groups used to study the effect of cover thickness on bond stress. The only variable between beams of the same group was the length of the shear span during the flexural testing. The shear span length was varied to explore the bond behaviour at various embedment lengths, and to experimentally obtain the minimum development length of each FRP bar used in this program. The shear span lengths implemented in this test program were very close to the expected development length, for which the bond profile will be similar to those used in the actual reinforced concrete structure.

All beams were tested under monotonic loading with deflection control of 1.0mm/minute. During the tests, load, midspan deflection, tensile strains in the FRP bars, and compression strains in the concrete top compression fibre were recorded using a data acquisition system at increments of 0.5 second. Analysis of failure modes and measured test results was done. Then the bond stress profiles of the FRP bars along the embedment length were calculated at various stages of loadings. A relationship between the average bond stress and concrete compression strength, embedment length, bar diameter and concrete cover thickness for both types of the FRP bars was formulated.

The presentation of results is divided into three main sections. Section 4.2 describes the modes of failure of the test specimens. Test results of the beams reinforced with GFRP bars are presented in section 4.3, while results of beams reinforced with CFRP bars are presented in section 4.4.

4.2 Modes of failure

Two failure modes were observed: bond failure and rupture of the tension FRP reinforcing bar. Bar rupture was a clear mode of failure where the tension reinforcing FRP bar suddenly ruptured and the load dropped to zero instantly. Bond failure, however, was relatively gradual. Two types of bond failures were observed: bond pullout failure and bond splitting failure.

The bond failure occurred when the available embedment length was not sufficient to sustain the longitudinal tensile stresses in the reinforcing bar. The first mode of bond failure, bond pullout failure, occurred when the bond stresses between the reinforcing bar and concrete reached the ultimate bond strength. Typical bond pullout failure was associated with excessive widening of the flexural crack close to the end of the shear span. Excessive rigid body motion around the failure crack was observed and combined with a slippage of the FRP reinforcing bar. In other words, the curvature continuity at the failure crack was lost due to excessive bar slippage. Beams that failed by bond pullout showed a gradual load degradation while the slippage continued to occur. The failure criteria used to define the bond pullout failure was when the bar recorded a slippage of 0.25mm at either beam end under testing. The bond pullout failure typically occurred at the end of the shear span. The bond failure occurred at the interface between the sand coating and the fibers of the reinforcing bar, Figure 4.1 (d). Figure 4.1 shows a typical beam that failed by bond pullout. The second mode of bond failure, bond splitting failure, occurred when the available concrete cover was not able to sustain the tensile stresses. Beams that failed in this manner showed a longitudinal crack parallel to the reinforcing bar (Figure 4.2).

Bar rupture occurred when the longitudinal tensile stresses reached the ultimate tensile strength of the bar. Most of the bars ruptured at tensile stresses greater than the guaranteed tensile strength reported by the manufacturer. Typical bar-rupture failures occurred in the midspan region where the applied moment was the highest along the beam length. Figure 4.3 shows a typical beam that failed by bar rupture. In this mode of failure, the experimental bond stresses were less than those reached in similar beams that failed by bond pullout. Therefore, beams that failed by bond pullout were more beneficial, in terms of defining the upper limits of bond stress, than beams that failed by bar rupture. On the other hand, if the embedment length was too short, the bond stresses could be significantly higher than those associated with cases when the embedment length was equal to the development length. This finding was mainly due to the fact that the bond stresses could be affected by embedment length or the embedment length-to-bar-diameter ratio and that the bond stresses resulting from a short embedment length might give unconservative values as compared to the bond stresses at an embedment length equal to the development length.

(a) Beam SC12.7-3.0-850 before flexural

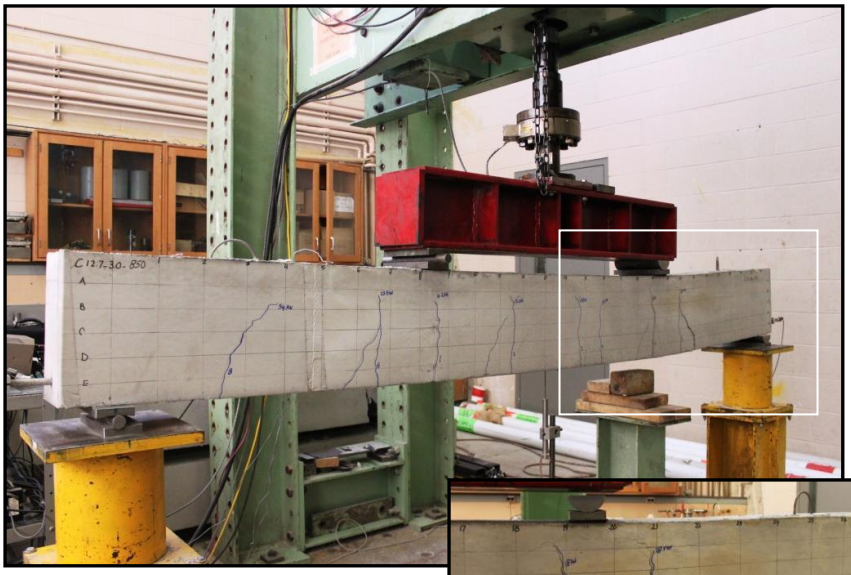

(b) Beam SC12.7-3.0-850 after failure

c) Failure crack at the end of the shear span

(e) Close up view of failure crack

d) Bond failure interface

Figure 4.1 Pullout bond failure: Beam SC12.7-3.0-850

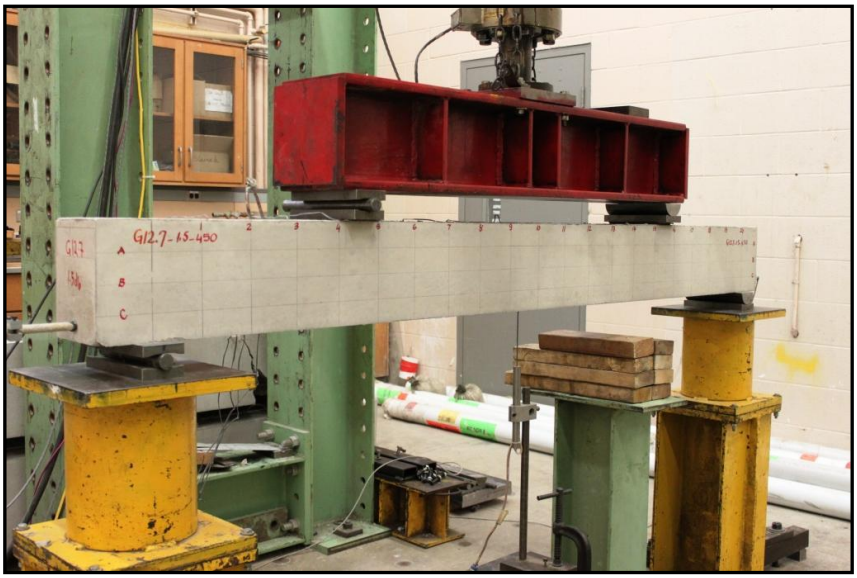

(a) Before the test

b) After failure

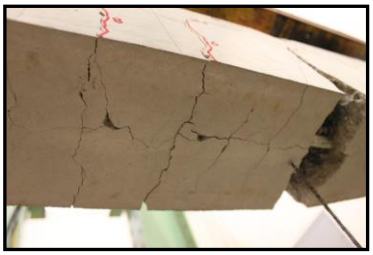

c) Splitting crack on left side

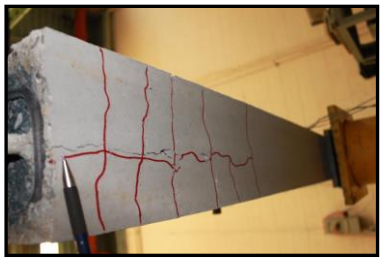

d) Splitting crack on the right side

Figure 4.2 Splitting bond failure: Beam SG12.7-1.5-450

(a) Beam before the test

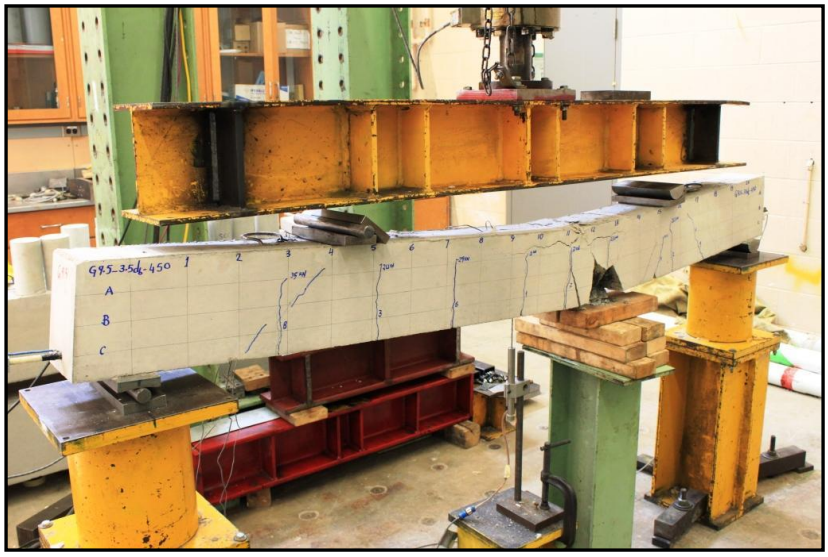

b) Beam after failure

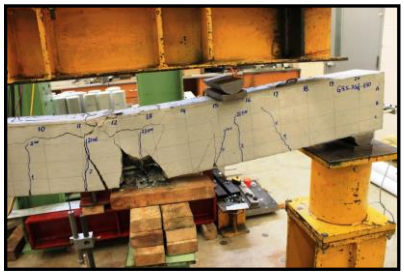

c) View of ruptured GFRP bar

(d) Close up view of failure side

Figure 4.3 Bar rupture failure mode: Beam SG12.7-3.0-450

4.3 Beams reinforced with GFRP bars

Fifteen beams were reinforced with GFRP bars: twelve beams were made from self consolidating concrete (SCC) and three beams were made from normal vibrated concrete (NVC). The SCC specimens were cast from two batches and the NVC specimens from one batch. As described in Chapter 3, the beam specimens were divided into four groups (SG9.5, SG12.7, SG15.9, and SG12.7C) made from SCC and one group (NG12.7) made from NVC. Each group had three beams. The cover thicknesses were maintained constant for all beams at $3d_b$, except beams of Group SG12.7-C, in which each beam had a different cover thickness: $2.0d_b$, $1.5d_b$ and $1.0d_b$. The applied moment versus midspan deflection and applied moment versus end slip results for beams reinforced with GFRP bars are presented in Section 4.3.1. The longitudinal tensile stress in the reinforcing GFRP bars and bond stresses are presented in section 4.3.2. The complete test results (moment versus deflection, crack mapping, strains in the GFRP bars and in the concrete and bond stress profile) for all beams reinforced with GFRP bars are presented in Appendix A.

4.3.1 Flexural test responses of beam reinforced with GFRP bars

All beams were tested statically under four-point bending. During the test, the applied load, midspan deflection and end slip, if any, were collected using a National Instrumentation Data Acquisition System connected to a computer. The applied moments were calculated based on the load and the actual shear span for each beam. The results of the applied moment versus midspan deflection of the beams made from SCC and from NVC are discussed separately in the following sections.

4.3.1.1 Flexural responses of beams made from SCC and reinforced with GFRP bars

Figures 4.4 to 4.8 show the moment versus deflection response for all groups. All beams showed a bilinear moment-deflection behaviour. The initial linear segment of the curve had a very steep slope, which corresponds to the uncracked stiffness. At the end of the first segment, flexural cracks started to form in the beam. Typically, the first crack occurred in the constant moment region. After the first crack, the beam's stiffness was significantly reduced, and flexural cracks continued to form. The slope of the second segment was less than the slope of the first part. The deflection rate was higher after the beam cracked, which is an indication of the stiffness reduction. As the load increased, more cracks formed, but the load deflection behaviour remained linear up to failure. Some of these beam showed jumps in the moment deflection responses possibly due to flexural crack formations and the local slip in the bar close to failure. The general trend of the beams within each group was for the midspan deflection to decrease for a given applied moment as the shear span increased. Figure 4.4 (a) shows that the midspan deflection for Group SG9.5 beams with shear spans of 300, 450 and 600mm were

43mm, 35mm, and 27mm, respectively. A similar trend was recorded for beams in Groups SG12.7 and SG15.9. This reduction in deflection can be attributed to the fact that as the shear span increased, the length of the constant moment region decreased, leading to less deflection at a given applied moment.

In Group SG9.5, Beam SG9.5-3.0-300 failed due to bond pullout failure and the other two beams failed due to bar rupture. The pullout of the GFRP bar of Beam SG9.5-3.0-300 was recorded by the LVDT at the beam end (Figure 4.4 b). There was no slip recorded up to the peak moment of 6.8kN.m. Then a slip of 0.10 mm was recorded by one LVDT and slowly increased to 0.21mm at a moment of 6.7kN.m. Then the load suddenly dropped to zero, and the end slip increased to 4.0mm. During this process, a loud noise was heard when complete bond pullout failure occurred. The maximum longitudinal strain and stress in the GFRP bar were 1.66% and 680.0MPa, respectively. The strain in the concrete top fibre at midspan was 1594με.

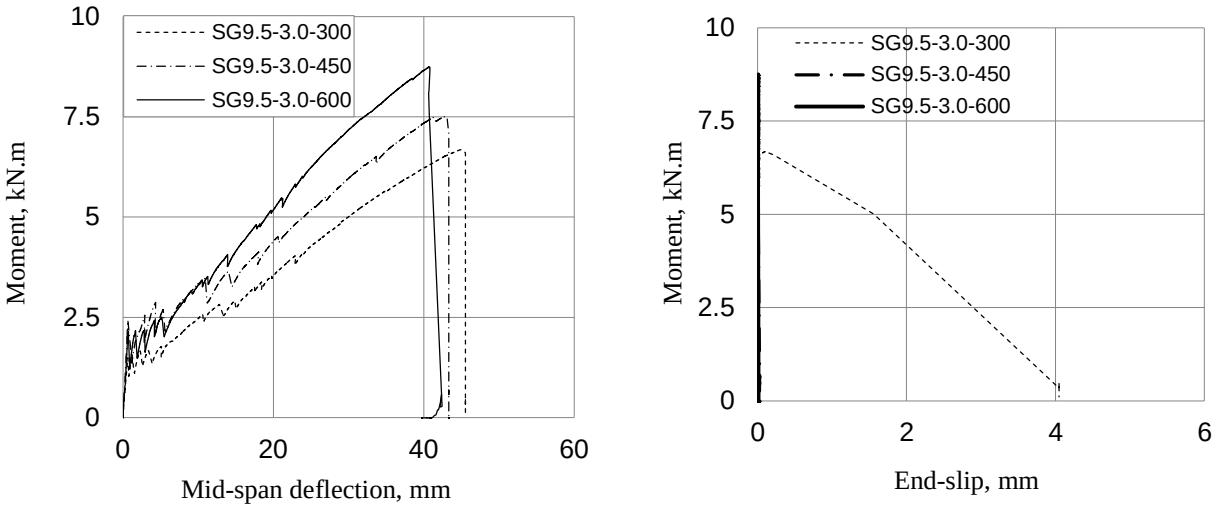

(a) Moment versus midspan deflection

b) Moment versus -end slip

Figure 4.4 Flexural test responses of SCC beams - Group SG9.5

The two other beams from Group SG9.5-3.0 failed by bar rupture. The GFRP bar strains at failure were 1.75% and 1.74%, with the tensile stresses of 750.0MPa, and 765.6MPa for Beams SG9.5-3.0-450 and SG9.5-3.0-600, respectively. The guaranteed tensile strength and rupture strain of the 9.5mm GFRP bars were reported by manufacturer as 765MPa and 1.89%, respectively. The achieved results of two beams were very close to the reported guaranteed tensile strength and slightly less than rupture strain. The concrete strains at the top compression fibre at failure were 1823με and 1663με for Beams SG9.5-3.0-450, and SG9.5-3.0-600, respectively. The concrete did not crush at failure for these beams.

Beams in Group SG12.7 were tested at shear spans of 350, 450 and 600mms. A bond pullout failure was recorded for the shortest shear span of 350mm while the other two beams failed due to bar rupture. Beam SG12.7-3.0-350 showed less deflection than these other two beams. However, the differences were small and could be attributed to the concrete mechanical properties or dimensions of the beam cross section. The longitudinal strains in the GFRP bars of Beams SG12.7-3.0-350, SG12.7-3.0-450, and SG12.7-3.0-600 were 1.1%, 1.29% and 1.37%, with tensile stress of 518, 570, and 614MPa, respectively. The guaranteed tensile stress of the 12.7 GFRP bar was reported as 708MPa.

For Beam SG12.7-3.0-350, which failed by bond pullout, the initiation of end slip was recorded at a moment of 14.94kN.m, with an end slip of 0.1mm. Then both the end slip and moment slightly increased. The end slip reached 0.15mm at a moment of 15.9kN.m. At a moment of 16.1kN.m, the end slip was 0.21mm. Then the end slip increased dramatically, with sudden drop in load. Beam SG12.7-3.0-450, which failed by bar rupture, showed a tendency of bond pullout failure, indicated by initiation of bar slip at peak load; however, the bar ruptured before excessive end slip. This result indicated that the development length of this bar embedded in this type of concrete will be very close to 450mm. However, it is important to note that the tensile stress of the GFRP bars varied, and the most important thing is to establish a development length relationship which is in a function of the tensile stress rather than assigning a fixed value to each bar diameter.

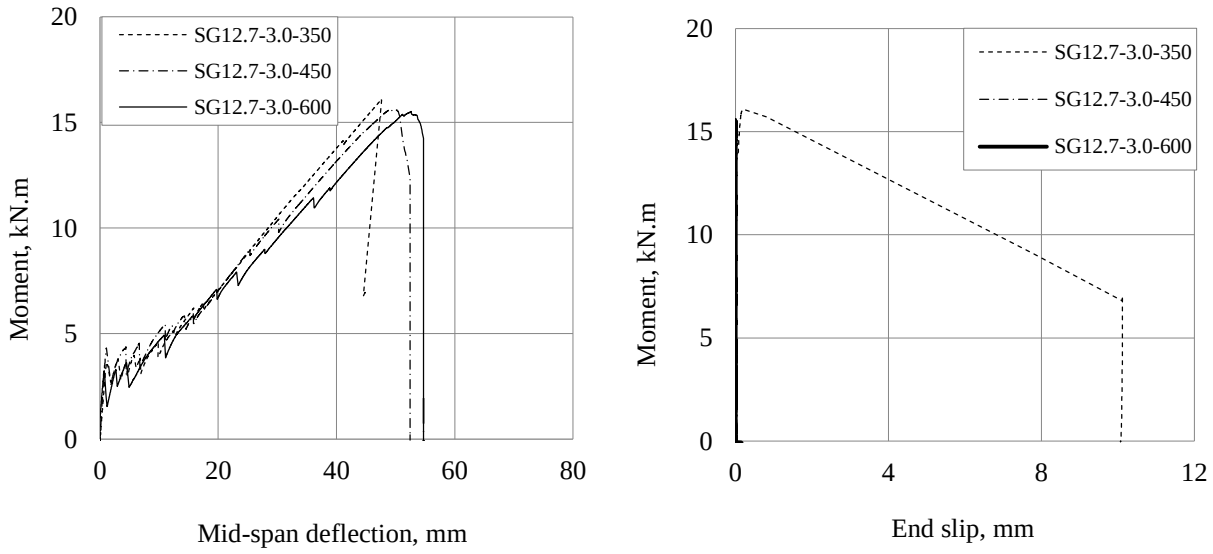

(a) Moment versus midspan deflection

(b) Moment versus end slip

Figure 4.5 Flexural test responses of SCC beams - Group SG12.7

The beams of Group SG15.9 were tested at shear spans of 450, 600 and 750mm. Figure 4.6 (a) shows the moment versus midspan deflection, and Figure 4.6 (b) shows the moment versus end slip for the three beams. Again, the beam with the shortest shear span failed due to bond pullout at a moment of 33.2kN.m. The other two beams, SG15.9-3.0-600 and SG15.9-3.0-750 failed by bar rupture at a moment of 45.5 and 37.7kN.m, respectively. No concrete crushing was observed in any of the three beams.

The maximum longitudinal strains and tensile stresses in the GFRP bars of the beams in this group were 1.17% and 514.8MPa for Beam SG15.9-3.0-450; 1.42%, 627.8MPa for Beam SG15.9-3.0-600; and 1.49% and 655.0MPa for Beam SG15.9-3.0-750. The guaranteed rupture strain and tensile stress of the 15.9mm GFRP bar were 1.56% and 683.0MPa, respectively. The concrete strains at the top compression fibre at the midspan were 1248με, 2327με, and 2060με for Beams SG15.9-3.0-450, SG15.9-3.0-600, and SG15.9-3.0-750, respectively. Beam SG15.9-3.0-450, which failed by bond pullout, the GFRP bar did not reach its ultimate tensile strength due to insufficient bond available to sustain large tensile stress. In other words, the GFRP bar had an insufficient embedment length in this beam. The other two beams failed by bar rupture when the GFRP bars reached their ultimate tensile strength. In these beams, the GFRP bar ruptured below the guaranteed tensile strength by 8.1% and 4.1% for beams SG15.9-3.0-600 and SG15.9-3.0-750, respectively.

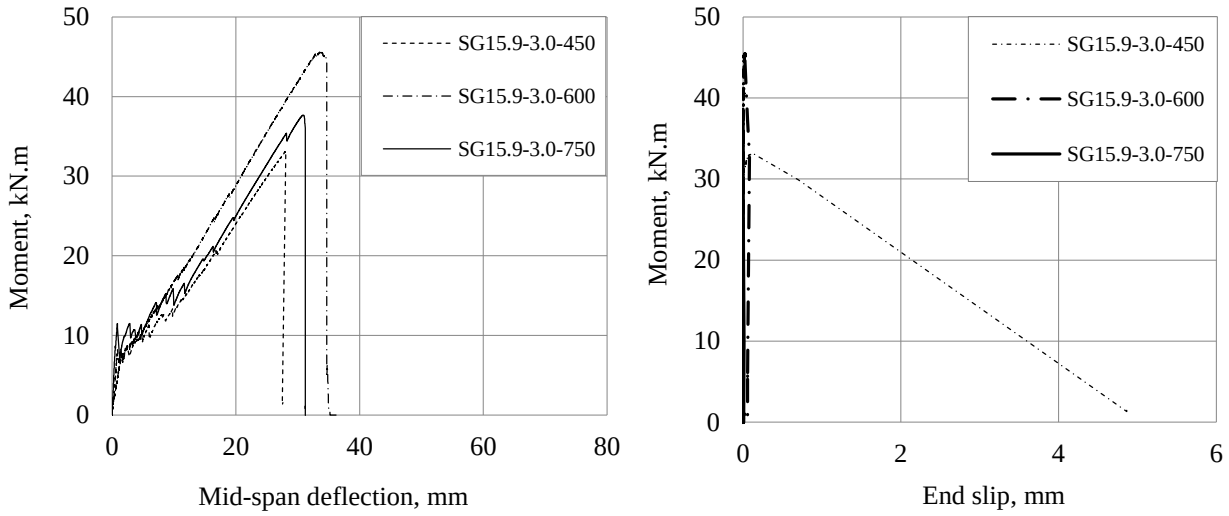

(a) Moment versus midspan deflection

(b) Moment versus end slip

Figure 4.6 Flexural test responses of SCC beams - Group SG15.9

The effect of concrete cover thickness on the flexural behaviour was examined by comparing results from three beams in Group SG12.7-C and one beam from Group SG12.7. Figure 4.7 (a) and Figure 4.7 (b) show the moment versus midspan deflection and moment versus end slip for these beams. These beams had cover thicknesses of $3.0d_b$, $2.0d_b$, $1.5d_b$ and $1.0d_b$. All beams in this comparison were tested at the same shear span of 450mm. However, the variation in the concrete compressive strength and in the effective depth among these four beams should be taken in consideration when comparing their peak moment and tensile stresses in the GFRP bars. The concrete compressive strength of the beams in Group SG12.7-C was 70.9MPa, while the concrete compressive strength of beam SG12.7-3.0-450 was 49.8MPa. The effective depth in Beams SG12.7-3.0-450, SG12.7-2.0-450, SG12.7-1.5-450 and SG12.7-1.0-450 were 155.55, 168.25, 174.6, 180.95mms, respectively.

The two beams that had cover thicknesses of $3.0d_b$ and $2.0d_b$ failed by bar rupture with splitting cracks. The beams with cover thicknesses of $1.5d_b$ and $1.0d_b$ failed due to bond splitting failure. The failure moments of these four beams (SG12.7-3.0-450, SG12.7-2.0-450, SG12.7-1.5-450 and SG15.9-1.0-450) were 15.6kN.m, 22.1kN.m, 21.1kN.m and 22.9kN.m, respectively. The tensile stresses in the GFRP bars of these four beams (SG12.7-3.0-450, SG12.7-2.0-450, SG12.7-1.5-450 and SG15.9-1.0-450) were 570MPa, 637MPa, 556MPa and 553MPa, respectively. The beam with a cover thickness of $3.0d_b$ (Beam SG12.7-3.0-450) had a lower stiffness, probably due to the smaller effective depth and lower concrete strength than the other three beams in this group. This beam failed at a moment of 15.6kN.m by bond pullout combined with bar rupture. The beam with a cover thickness of $2.0d_b$ failed due to bar rupture with no end slip. The beam with a cover thickness of $1.5d_b$ had an end slip of 0.13mm at a peak moment with splitting cracks. The beam with a cover thickness of $1.0d_b$ failed due to bond splitting with an end slip of 5.4mm. The initiation of end slip for this beam occurred at a moment of 22.6kN.m, with a value of 0.1mm, and the end slip at of 22.8kN.m was 0.25mm. The end slip at the peak moment value of 22.9kN.m was 2.1mm. As shown in Figure 4.7 (a) and (b), this beam showed a step-like behaviour at the tip of the moment-deflection curve. All of these beams had similar shear reinforcement, i. e. similar confinement by shear reinforcement.

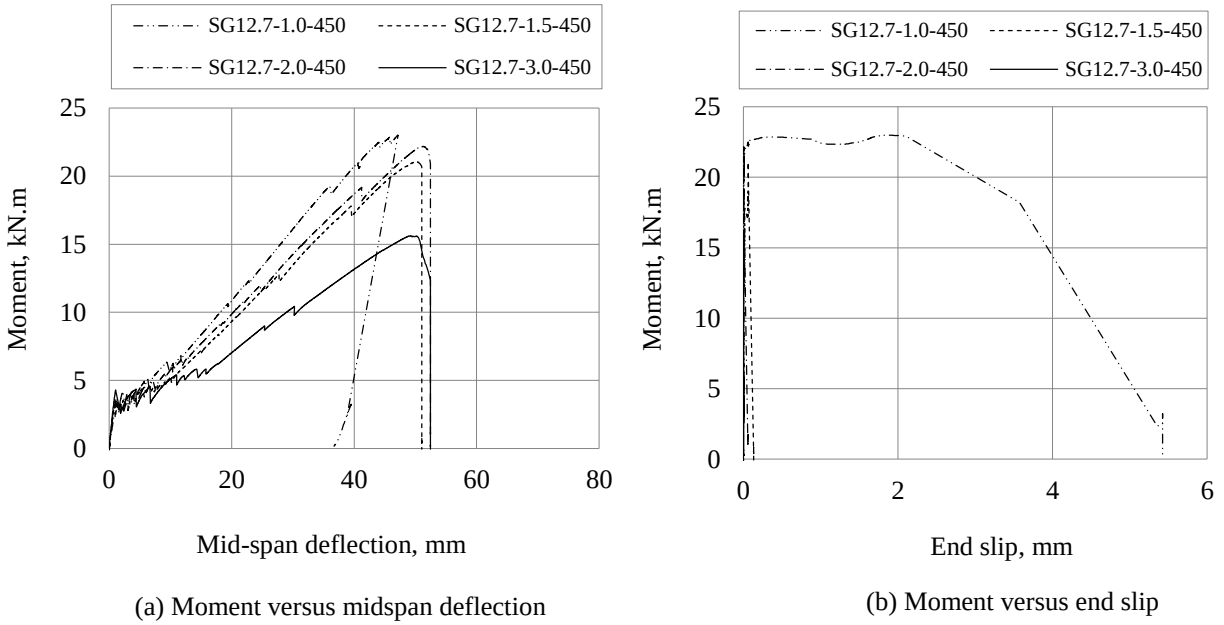

(a) Moment versus midspan deflection

(b) Moment versus end slip

Figure 4.7 Flexural test responses of SCC beams - Group SG12.7C

4.3.1.2 Flexural responses of beams made from NVC and reinforced with GFRP bars

The moment versus midspan deflection of beams in Group NG12.7, which were made from NVC, is shown in Figure 4.8 (a) and their moment versus end slip in Figure 4.8 (b). As the shear span increased, the midspan deflection was decreased for a given moment. Beam NG12.7-3.0-350 failed by bond pullout failure. An end slip of 3.0mm was recorded for this beam. The peak moment of this beam was 14.4kN.m, which was slightly greater than that of a similar beam made from SCC, SG12.7-3.0-450, that had a peak moment of 12.9kN.m. This result indicates that the reinforcing GFRP bar in the NVC beam achieved a higher tensile stress than that in the SCC beam. Beam NG12.7-3.0-550 failed due to bar rupture; however, an end slip of 0.05mm was recorded. For this reason, the third beam was tested with the same shear span of 550mm to confirm this result. No end slip was recorded during testing of the third beam. The peak moments of these two beams NG12.7-3.0-550 and NG12.7-3.0-550-2 were 15.3kN.m and 15.9kN.m, respectively. The companion beams made from SCC, SG12.7-3.0-450 and SG12.7-3.0-600 failed by bar rupture at applied moments of 14.4kN.m and 16.9kN.m, respectively.

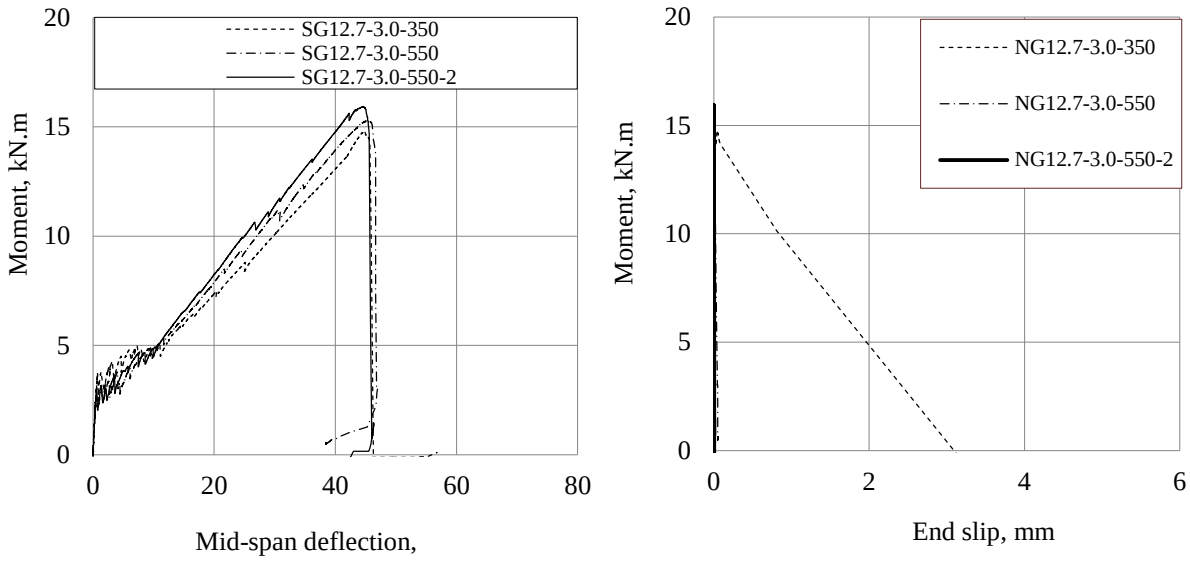

(a) Moment versus midspan deflection

(b) Moment versus end slip

Figure 4.8 Flexural test responses of NVC beams - Group NG12.7

4.3.1.3 Summary of flexural test results of all beams reinforced with GFRP bars

A summary of the flexural test results is shown in Table 4.1. In spite of the higher compressive strength of SCC mix-3, the average cracking moment of beams made from SCC-mix3, Group SG12.7, and beams made from NVC, Group NG12.7, was similar. This is attributed to similar tensile strength of the two mixes. However, the average midspan deflection of beams made of SCC was about 1.5 times the midspan deflection of beams made from NVC. The increased midspan deflection of the SCC beams can be attributed to the lower modulus of elasticity of SCC than NVC. Crack mapping indicated that at similar applied moments, the crack spacing was slightly less in SCC specimens as compared to NVC specimens. The average crack spacing within the constant moment region for beams that failed by bar rupture in Group SG12.7 was 140mm versus 180mm for beams in Group NG12.7. No crack width measurements were taken; however, visual inspection indicated that SCC beams had more flexural cracks with lesser crack widths. This result implies that SCC had better local bond performance than NVC; however, when flexural cracks occurred the local bond stress was negatively affected and as a result the average bond stress of SCC specimens were decreased.

As discussed above, Beam SG15.9-3.0-600 failed by bar rupture at a moment of 45.5kN.m, which is greater than that for Beam SG15.9-3.0-750. The reason can attributed to the variation in tensile stress of the GFRP bar at rupture. The GFRP bar of Beam SG15.9-3.0-600 reached a value of 627.8MPa as compared to the GFRP bar of Beam SG15.9-3.0-750, which ruptured at a tensile stress of 655.0MPa.

Table 4.1 Summary of the flexural test results of beams reinforced with GFRP bars

Group	Beam label*	Cracking		Ultimate		Mode of failure
		Moment kN.m	Deflection mm	Moment kN.m	Deflection mm	
SG9.5	SG9.5-3.0-300	2.9	0.91	6.7	45.5	pullout
	SG9.5-3.0-450	2.7	0.85	7.5	43.0	rupture
	SG9.5-3.0-600	3.1	0.94	8.7	40.8	rupture
SG12.7	SG12.7-3.0-350	3.5	1.06	14.1	41.1	pullout
	SG12.7-3.0-450	4.3	1.07	15.6	49.2	pullout/rupture
	SG12.7-3.0-600	3.2	0.91	15.5	52.6	rupture
SG15.9	SG15.9-3.0-450	8.2	0.85	33.2	27.7	pullout
	SG15.9-3.0-600	7.9	1.60	45.5	33.5	rupture
	SG15.9-3.0-750	8.6	0.75	37.7	30.9	rupture
SG12.7C	SG12.7-2.0-450	3.4	0.83	22.1	51.0	rupture
	SG12.7-1.5-450	3.2	0.89	21.1	49.9	pullout/splitting
	SG12.7-1.0-450	3.6	1.10	22.9	47.1	splitting
NG12.7	NG12.7-3.0-350	3.7	0.73	14.4	43.9	pullout
	NG12.7-3.0-550	2.9	0.59	15.3	44.7	pullout/rupture
	NG12.7-3.0-550-2	3.1	0.62	15.9	44.1	rupture

4.3.2 Bond stress analysis of GFRP bars

The equilibrium of forces between any two arbitrary sections or two strain gauge locations is shown schematically in Figure 4.9. The average bond stress within these sections is determined as described below.

The equilibrium of the horizontal forces acting on element ΔL can be written as in Eqn 4.1.

$$T_i = \mu \pi d_b \Delta L + T_{i-1} \qquad (4.1)$$

Where

T_i and T_{i-1} are the tensile forces in the reinforcing FRP bar at Section (*i*) and Section (*i-1*), respectively;

μ is the average local bond stress between Section (*i*) and Section (*i-1*);

d_b is the FRP bar diameter; and

ΔL is the distance between Section (*i*) and Section (*i-1*).

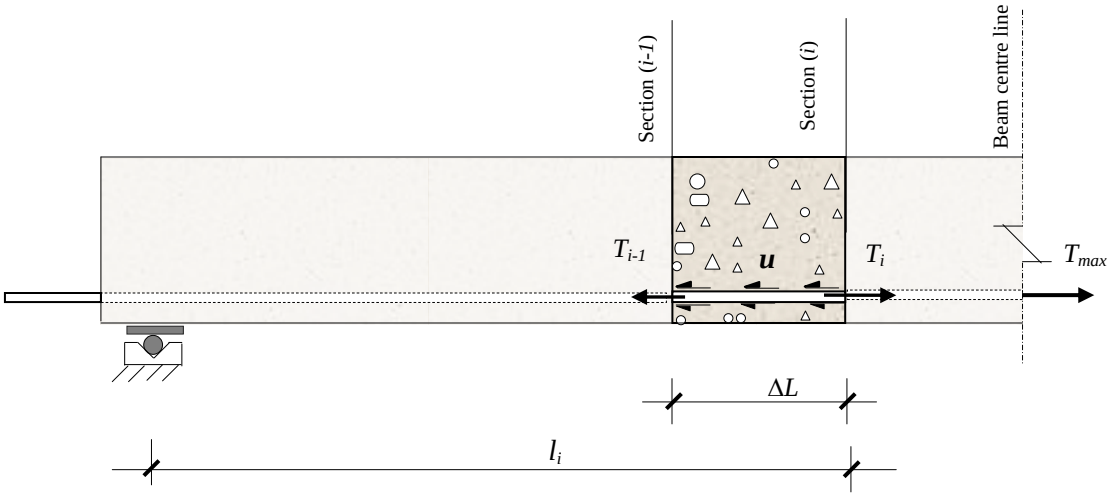

Figure 4.9 Tensile forces equilibrium in the tensile GFRP reinforcing bar

The tensile force "*T*" can be calculated based on the strain reading at that point and the bar properties, Eqn. (4.2).

$$T_i = \varepsilon_{(frp)_i} E_{(frp)_i} A_{(frp)_i} \quad (4.2)$$

Where

ε_{frp} is the longitudinal strain in the FRP bar;

E_{frp} is the modulus of elasticity of the GFRP bar; and

A_{frp} is the cross sectional area of the GFRP bar.

Therefore, the average local bond stress between Sections (*i*) and (*i+1*) can be calculated as in Eqn (4.3).

$$\mu = \frac{T_i - T_{i-1}}{\pi\, d_b\, \Delta L} \quad (4.3)$$

Therefore, the bond stress profile of the GFRP bar can be determined by calculating bond stress within various sections along the length of the GFRP bar using the strain gauge data.

Another term was used for bond analysis: the average bond stress. The average bond stress of the GFRP bars for a given embedment l_e was calculated as the tensile force in the GFRP bar at that section divided by the circumference area of the FRP bar from that section to the support as shown in Eqn. (4.4).

$$\mu_{average} = \frac{T_i}{\pi\, d_b\, l_i} \quad (4.4)$$

4.3.2.1 Tensile and bond stresses of GFRP bars in SCC beams

Ideally, the tensile stress in a reinforcing bar along a beam subjected to flexural loading should follow the bending moment diagram if there is perfect bond between the bar and concrete and the concrete is in the elastic range. Typical moment versus longitudinal strain responses of a typical SCC beam that failed due bond pullout and an SCC beam that failed due to bar rupture are shown in Figure 4.10 (a) and Figure 4.11 (a), respectively. Based on the strain responses the tensile and bond stress profiles along the length of the GFRP bar at several load levels were calculated for all beams. Figure 4.10 (b) and (c) show the tensile and bond stress profiles of Beams SG12.7-3.0-350, which had bond pullout failure. Figures 4.11 (a) and (b) show the tensile and bond stress of the GFRP bar at several load levels of Beam SG12.7-3.0-600, which had bar rupture failure. Before concrete cracking, the strain in the GFRP bar and concrete at the level of the bar were similar, and there was a minimal bond stress transfer. However, when the concrete in the tension face cracked, all the tensile force was carried by the tensile reinforcement, and bond stress transfer between the two materials occurred. When the first crack occurred at the end of the shear span, the strain gauge located at this location recorded a jump in strain reading due to the transfer of tensile forces from the concrete to the reinforcing GFRP bar. This jump in strain of both Beams SG12.7-3.0-350 and SG12.7-3.0-600 (Figures 4.10 and 4.11) resulted in a jump in tensile forces within the embedment length associated with a jump in bond stress at a moment of 5.0kN.m. At this stage, the bond stresses at the end of the shear span was 2.6MPa and 3.9MPa for Beams SG12.7-3.0-350 and SG12.7-3.0-600, respectively. The bond stress profile vanished quickly towards the support where the concrete was not cracked. As the loading increased, the concrete cracking front moved towards the supports and more jumps were recorded by other strain gauges located closer to the supports (Figure 4.10 a) and (Figure 4.11 a). Also, as the loading increased, the bond stress wave moved towards the support where the concrete was still uncracked and was able to sustain larger bond stresses (Figure 4.10 c) and (Figure 4.11 c). At the same time, there was a drop in the peak bond stress that was reached earlier at the first cracking. This trend can be seen more clearly in Beam SG12.7-3.0-600, which had multiple strain gauges attached to its reinforcing GFRP bar.

At a peak load level of 14.1kN.m for Beam SG12.7-3.0-350, which failed by bond pullout, the peak bond stress of 7.9MPa was located close to the support, and the minimum bond stress at the end of the shear span was 1.8MPa. On the other hand, Beam S12.7-3.0-600, which failed due bar rupture at a peak moment of 15.5kN.m, had a peak bond stress of 5.9MPa, and the bond stress at the end of the shear span was about 2.0MPa.

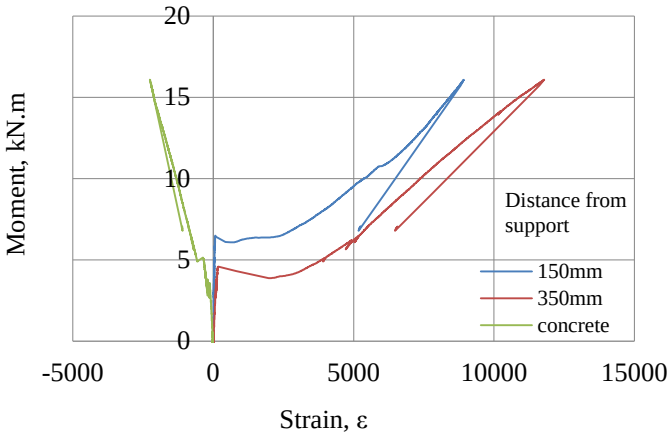

(a) Strain behaviour

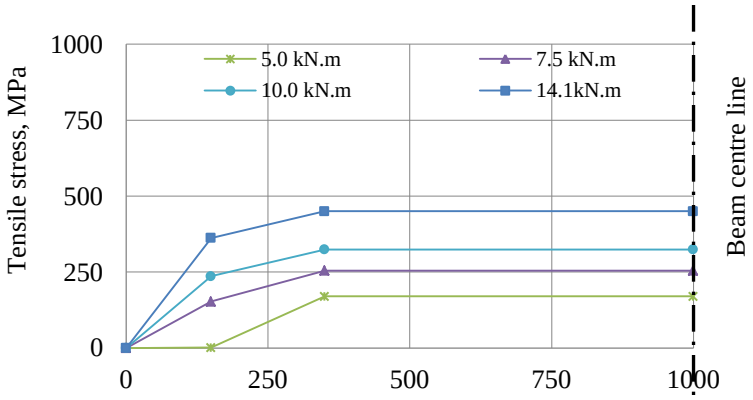

(b) Tensile stress profile

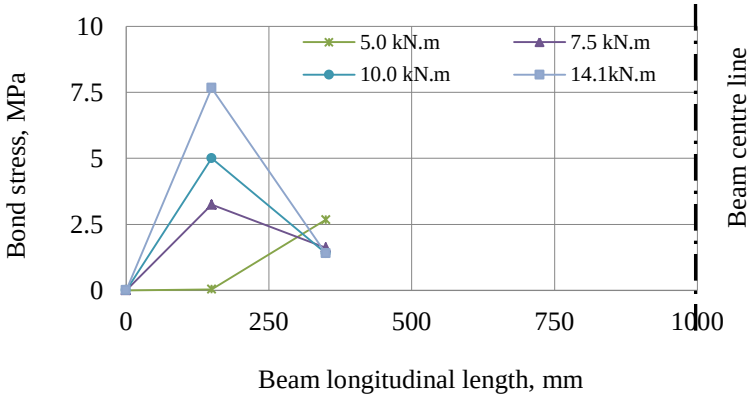

(c) Average local stress profile

Figure 4.10 Strain behaviour, tensile and bond stress profiles of Beam SG12.7-3.0-350 (failed by bond pullout)

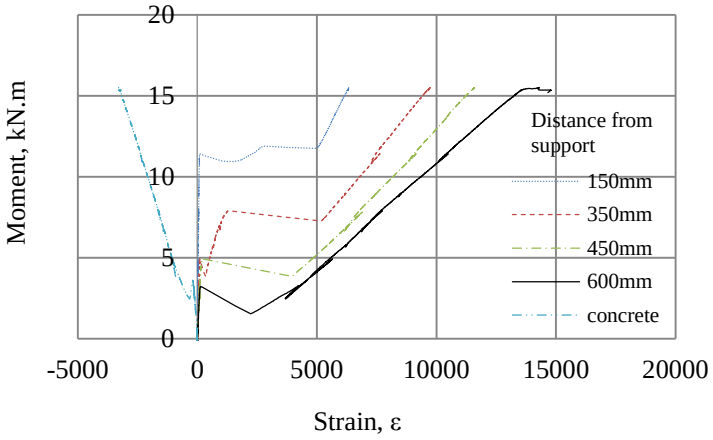

(a) Strain behaviour

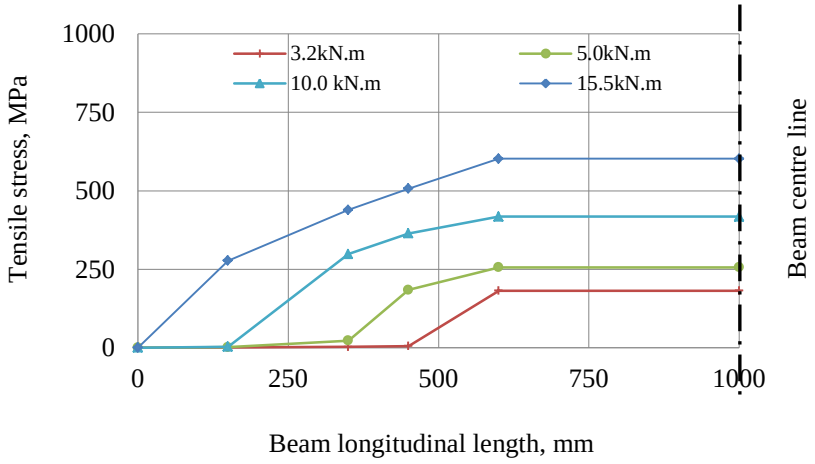

(b) Tensile stress profile

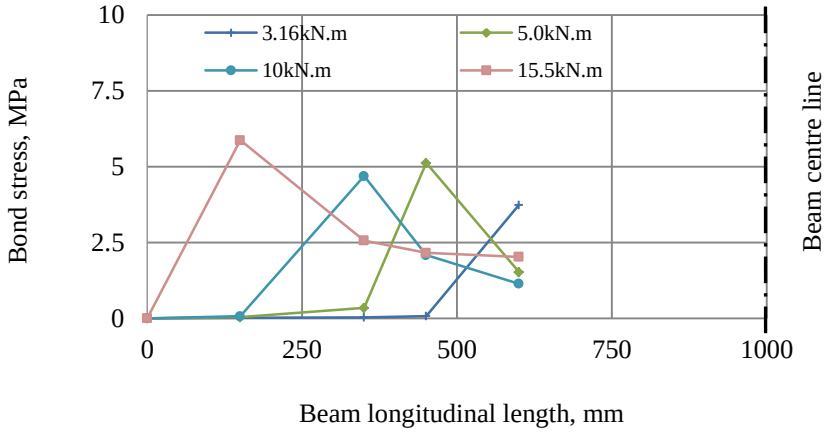

(c) Average local bond stress

Figure 4.11 Strain behaviour, tensile and bond stress profiles for Beam SG12.7-3.0-600 (failed by bar rupture)

The general shape of the tensile stress profile in the GFRP bars and the peak bond stress values were affected by their mode of failure. Beam SG12.7-3.0-350, which failed by bond pullout had a nonlinear tensile stress profile along the embedment length. Also, the bond stresses in the uncracked region, close to the support, had larger values than Beam SG12.7-3.0-600, which failed by bar rupture. At the same time, the bond stress at the end of the shear span, cracked region, in Beam SG12.7-3.0-350 (pullout bond failure) was less than that in the beam that failed by bar rupture. The possible explanation of this finding is that, in the case of bond pullout failure, the bond stresses in the uncracked region of the beam were at the ultimate bond strength, while in the case of bar rupture, the tensile strength of the GFRP bar was reached before the ultimate bond strength was reached.

The results of the tensile stress and bond stresses calculated for all beams made from SCC are presented in Tables 4.2. The table gives the values of experimental tensile stress, local bond stress, average bond stress, and normalized average bond stress. As described in Section 4.3.2, the local bond stress represents the average local bond between the strain gauges mounted on the GFRP bars, and the average bond stress at a given strain gauge location represents the overall average bond stress from that point to the beam support. For example, the average bond stress of Beam SG12.7-3.0 450 at 350mm is the tensile stress in the GFRP bar at this section divided by the circumference area of the bar from this section to the end of the bonded bar length which, in this case, is 350mm.

The general trend of the bond stress profiles was similar in all beams. At failure, the bond stress was not uniform. The peak bond stress occurred close to the support, while the bond stress at the end of the shear span, cracked region, had a lower bond stress. It was found that, as the embedment length increased, the average bond stress decreased. For example, the average bond stress of Beam SG9.5-3.0-300 was 5.38MPa, the average bond stress for Beam SG9.5-3.0-450 was 3.96MPa, and that of Beam SG9.5-3.0-600 was 3.03MPa, possibly because the cracked region had a greater influence on average bond stress in long embedment lengths versus short embedment lengths. In fact, the cracked region to uncracked region of beams with long embedment lengths is larger than in beams with a short embedment length. Long cracked regions with low bond stress values reduced the overall average bond stress.

The effect of changing cover thickness showed that there was a drop in the average bond stress when the cover thickness was reduced. The peak bond stresses for Beams SG12.7-2.0-450, SG12.7-1.5-450 and SG12.7-1.0-450 were 8.03, 7.39, and 6.62 MPa, respectively; and the average bond stresses of these beams were 4.49, 3.92 and 3.90MPa, respectively. Further discussion on the effect of cover thickness on tensile and bond stresses of the GFRP bars is provided in Section 4.3.2.5.

Table 4.2 Experimental results of tensile and bond stress of GFRP bars in SCC beams

Beam	l_e, mm (1)	l_e/d_b	f_{frp}, MPa (2)	Local bond stress, MPa (3)	Average, μ MPa (4)	$\frac{\mu}{\sqrt{f'_c}}$ (MPa)$^{1/2}$
SG9.5-3.0-300	150	15.8	512.4	8.11	8.11	0.96
	300	31.6	680.0	2.65	5.38	0.64
SG9.5-3.0-450	150	15.8	358.2	5.67	5.67	0.67
	350	31.6	559.5	3.19	4.43	0.53
	450	47.4	750.0	3.02	3.96	0.47
SG9.5-3.0-600	150	15.8	254.4	4.03	4.03	0.48
	350	31.6	412.2	2.50	3.26	0.39
	450	47.4	698.4	4.53	3.69	0.44
	600	63.2	765.6	1.06	3.03	0.36
SG12.7-3.0-350	150	11.8	372.6	7.89	7.89	1.12
	350	27.6	518.2	2.31	4.70	0.67
SG12.7-3.0-450	150	11.8	320.2	6.78	6.78	0.96
	350	27.6	504.0	2.92	4.57	0.65
	450	35.4	569.8	2.09	4.02	0.57
SG12.7-3.0-600	150	11.8	277.4	5.87	5.87	0.83
	350	27.6	425.7	2.35	3.86	0.55
	450	35.4	550.7	3.97	3.89	0.55
	600	47.2	614.2	1.34	3.25	0.46
SG15.9-3.0-450	150	9.4	313.7	8.31	8.31	0.99
	350	22.0	470.9	3.12	5.35	0.64
	450	28.3	514.8	1.75	4.55	0.54
SG15.9-3.0-600	150	9.4	301.2	7.98	7.98	0.95
	350	22.0	521.5	4.38	5.92	0.70
	450	28.3	577.9	2.24	5.10	0.61
	600	37.7	627.8	1.32	4.16	0.49
SG15.9-3.0-750	150	9.4	216.5	5.74	5.74	0.68
	350	22.0	362.0	2.89	4.11	0.49
	450	28.3	465.4	4.11	4.11	0.49
	600	37.7	576.5	2.94	3.82	0.45
	750	47.2	655.0	2.08	3.47	0.41
SG12.7-2.0-450	150	11.8	379.2	8.03	8.03	0.95
	350	27.6	583.4	3.24	5.29	0.63
	450	35.4	636.7	1.69	4.49	0.53
SG12.7-1.5-450	150	11.8	349.3	7.39	7.39	0.88
	350	27.6	523.6	2.77	4.75	0.56
	450	35.4	556.2	1.04	3.92	0.47
SG12.7-1.0-450	150	11.8	312.6	6.62	6.62	0.79
	350	27.6	463.5	2.40	4.20	0.50
	450	35.4	552.6	2.83	3.90	0.46

Where: (1) L_e is the embedment length from the support to the strain gauge location; (2) f_{frp} is the experimental tensile stress in the GFRP bar at the same location; (3) local bond stress is the average bond stress between the two gauges locations; (4) μ is the average bond stress within the embedment length.

4.3.2.2 Tensile and bond stress of GFRP bars in NVC beams

The results of the strain behaviour, tensile stress profile, and bond stress profile of the GFRP bars of Beams NG12.7-3.0-350 and NG12.7-3.0-550 are shown in Figures 4.12 and 4.13, respectively. Beam NG12.7-3.0-350 failed by bond pullout, and Beam NG12.7-3.0-550 failed by bar rupture. The tensile stress in the GFRP bar at failure was 601.2MPa. This value is greater than that for the companion beam made from SCC, SG12.7-3.0-350, which had a tensile stress in the GFRP bar of 518.2MPa. This trend was consistent with the NVC beam having a higher failure moment. However, the tensile stress profile in the GFRP bars within the embedment length of these two beams was different: nonlinear for the SCC beam and linear for the NVC beam.

The GFRP bar in the SCC had higher bond stresses within the uncracked region than those in NVC beams. The peak bond stress in the uncracked region of the NVC beam was 6.26MPa, as compared to 7.89MPa of a similar beam made from SCC (Figure 4.10 (c) and Figure 4.12 (c)). On the other hand, the local bond stress within the cracked region (350mm from the support) was 4.37 for the NVC beam and 2.31MPa for the SCC beam. The average bond stresses over the embedment length for the NVC and SCC beams were 5.45MPa and 4.7MPa, respectively. Therefore, SCC beams had higher bond stresses than NVC beams within uncracked regions, and vice versa in the cracked region. The average bond stress in NVC was about 15% higher than that in SCC beams in this group. This phenomena supports the earlier discussion that SCC mixes had better bond stress performance; however, closer flexural crack spacing negatively affected the average bond stress within the cracked region.

Table 4.3 Experimental results of tensile and bond stress of GFRP bars in NVC beams

Beam	l_e, mm (1)	l_e/d_b	f_{frp}, MPa (2)	Local bond stress, MPa (3)	Average, μ MPa (4)	$\frac{\mu}{\sqrt{f_c'}}$ $(MPa)^{1/2}$
SG12.7-3.0-350	200	15.8	394.6	6.26	6.26	0.80
	350	27.6	601.2	4.37	5.45	0.69
SG12.7-3.0-550	200	15.8	326.4	5.18	5.18	0.66
	350	27.6	503.5	4.57	4.57	0.58
	550	43.3	651.6	3.76	3.76	0.48
SG12.7-3.0-550-2	200	15.8	214.2	3.40	3.40	0.43
	350	27.6	484.1	5.71	4.49	0.56
	550	43.3	603.5	1.90	3.38	0.44

Where: (1) L_e is the embedment length from the support to the strain gauge location; (2) f_{frp} is the experimental tensile stress in the GFRP bar at the same location; (3) local bond stress is the average bond stress between the two gauges locations; (4) μ is the average bond stress within the embedment length.

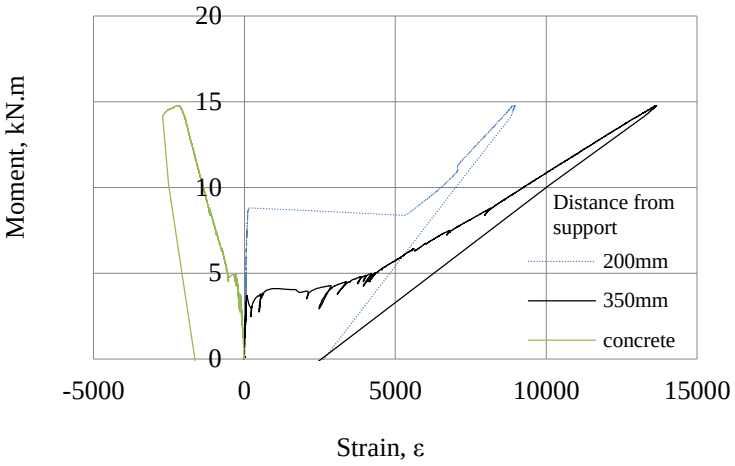

(a) Strain behaviour

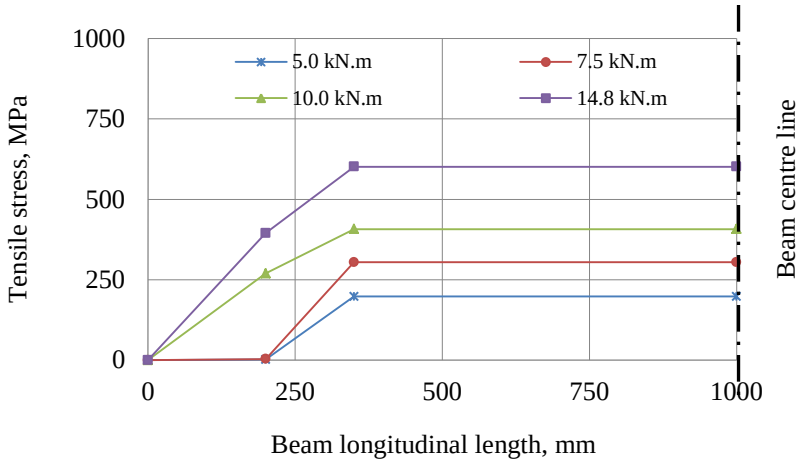

(b) Tensile stress profile

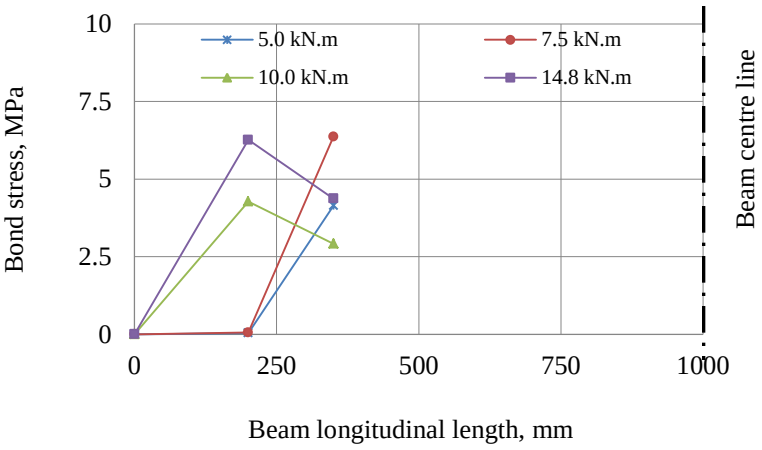

(c) Average local bond stress profile

Figure 4.12 Strain behaviour, tensile stress, and bond stress profiles of Beam NG12.7-3.0-350 (failed by bond pullout)

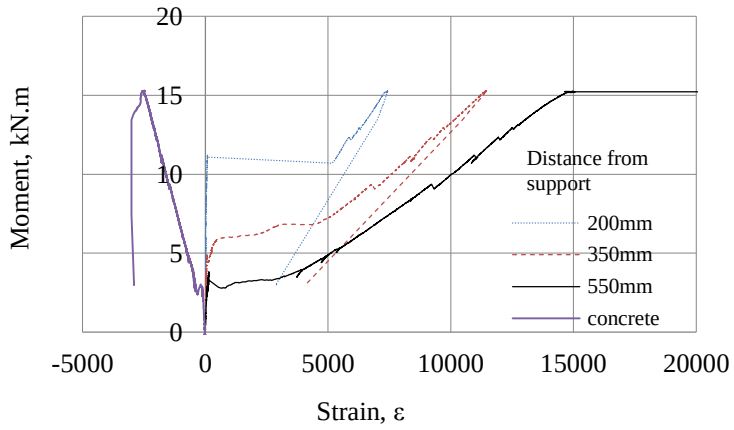

(a) Strain behaviour

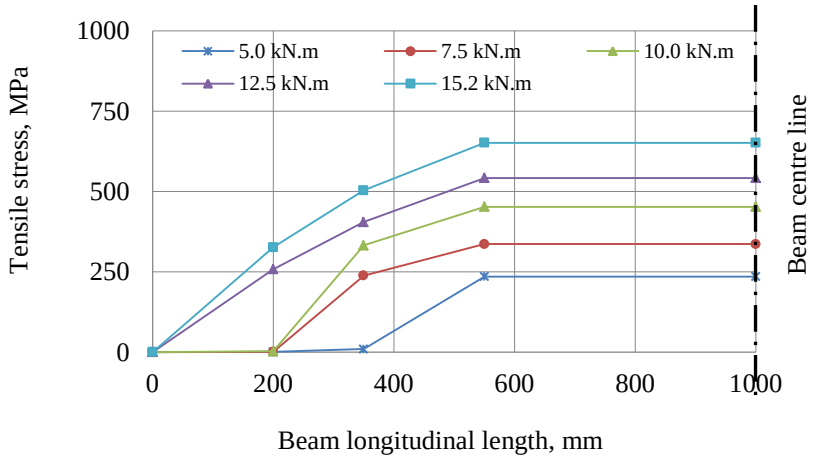

(b) Tensile stress profile

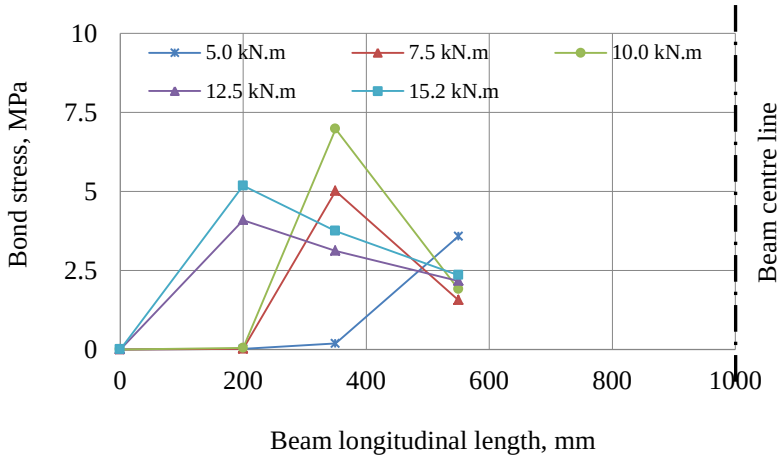

(c) Average local bond stress profile

Figure 4.13 Strain behaviour, tensile stress, and bond stress profiles for Beam NG12.7-3.0-550 (failed by bar rupture)

This result explains why SCC had a higher bond stress than NVC based on pullout specimens as reported in literature. The possible explanation of SCC having higher bond stresses within the uncracked region is because the concrete around the bar is more homogeneous in SCC and able to perfectly encapsulate the FRP reinforcing bar. Studying the bond and interfacial properties of steel reinforcement, Zhu et al. (2004) found that SCC provides 10 – 40% higher bond strength than NVC.

4.3.2.3 Effect of concrete type on normalized average bond stress of GFRP bars

The normalized bond stress versus normalized embedment length for beams that failed by bond pullout are presented graphically in Figure 4.14. Beams that failed by bar rupture were not included in this analysis because the GFRP bars in these beams reached the rupture tensile stress before the bond strength was reached. Figure 4.14 shows that for both types of concrete, the normalized bond stress and normalized embedment length have a nonlinear relationship. The normalized bond stress of the GFRP bars in SCC beams was about 20% larger than that in NVC beams at an embedment length to bar diameter ratio of 10. The difference in normalized bond stress between the SCC and NVC decreased as the normalized embedment length increased, and vanished at an embedment length to bar diameter ratio of about 37.5. No data from this work was available with an embedment length to bar diameter ratio above 45. The reason for this omission is that all GFRP bars implemented in this study ruptured at embedment length to bar diameter ratios greater than 45.

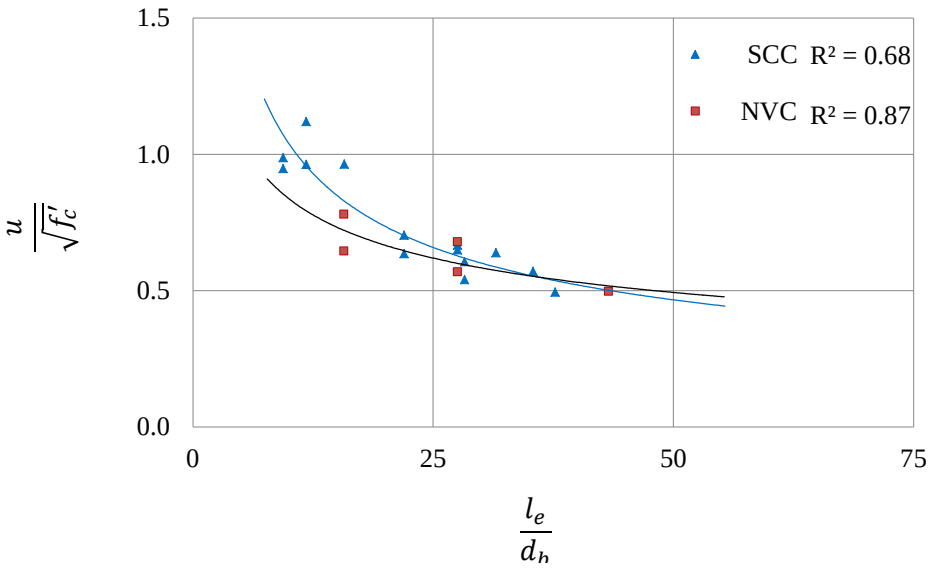

Figure 4.14 Normalized average bond stress versus normalized embedment length of SCC and NVC beams reinforced with GFRP bars

4.3.2.4 Effect of bar diameter on the normalized average bond stress of GFRP bars in SCC

The normalized average bond stress of beams that failed by bond pullout versus the embedment length to bar diameter ratio is presented in Figure 4.15. Based on the results obtained, the effect of the bar diameter on normalized average bond stresses is not clear if the data is plotted against the embedment length. A clear trend of the effect of bar diameter was evident when the normalized bond stress was plotted against the normalized embedment length. This trend could possibly be due to differences in beam stiffness because the beam sizes were not similar. In other words, at the same distance from the support and the same moment, a stiffer beam might not crack and the average bond stress could be less. The figure shows that when the bar diameter was increased from 9.5mm to 12.7mm, the decrease in the normalized bond stress was insignificant, and there was a slight decrease in normalized average bond stress when the bar diameter was increased from 12.7mm to 15.9mm. Although only two points are available for a bar diameter 9.5mm, the nonlinear relationship plotted was similar to that for the other two bar diameters.

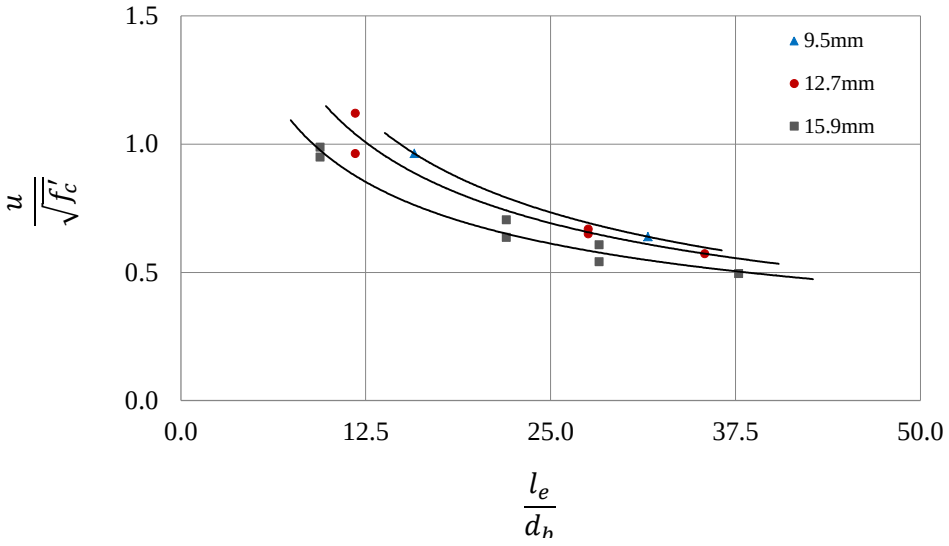

Figure 4.15 Effect of bar diameter on normalized average bond stress of SCC beams reinforced with GFRP bars

4.3.2.5 Effect of concrete cover thickness on the normalized average bond stress of GFRP bars in SCC

The results for beams in Group SG12.7C from Table 4.2 are presented graphically in Figures 4.16 and 4.17. Figure 4.16 shows the normalized average bond stress profiles for beams with a cover thickness range of $3.0d_b$, $2.0d_b$, $1.5d_b$ and $1.0d_b$. All beams in this comparison had a similar cross section, were reinforced with the same bar diameter, and were tested at a similar shear span. The data plotted on Figure 4.16 shows almost parallel curves of normalized average bond stress versus normalized embedment length. The results indicate that the normalized average bond stress decreases as the cover thickness decreases. A significant drop in bond stress was recorded when the cover thickness dropped below $2.0d_b$. This result was consistent with the observed mode of failure, which changed from bond pullout failure to bond splitting failure when the cover thickness dropped from $2.0d_b$ to $1.5d_b$. Both beams with cover thicknesses of $1.5d_b$ and $1.0d_b$ had bond splitting failure. Thus, due to insufficient confinement, the bond stress of these beams did not reach a bond stress similar to that of beams with a larger cover thickness.

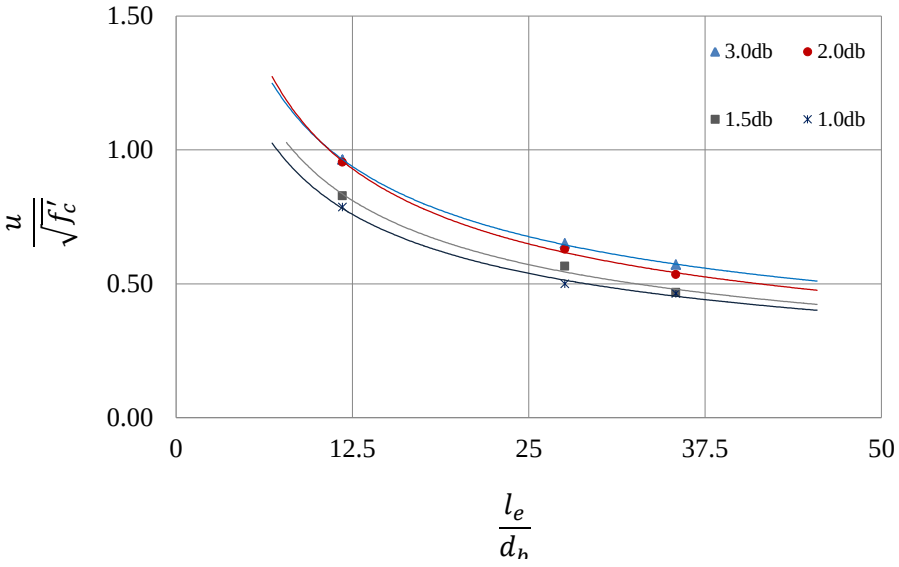

Figure 4.16 Normalized bond stress profile of SCC beams reinforced with GFRP bars at various cover thicknesses, Group SG12.7C

Figure 4.17 shows the effect of cover thickness on the normalized average bond stress at embedment lengths of 150mm, 350mm and 450mm. Linear relationship were used to represent the effect of cover thickness. The linear relationship had an acceptable fit and provided a simple relationship that can be

used to formalize a bond equation. Obviously, the line representing the normalized bond stress at an embedment of 150mm had larger values than the other two lines. At an embedment length of 450mm, the data indicated that the normalized bond stresses dropped from 0.571 when the cover thickness was $3.0d_b$ to 0.534 when the cover thickness decreased to $2.0d_b$ (a 6.5% drop in normalized bond stress). The most significant drop was recorded when the cover thickness dropped from $2.0d_b$ to $1.5d_b$, and a negligible drop was recorded when the cover thickness dropped from $1.5d_b$ to $1.0d_b$. A similar relationship was found at embedment lengths of 150mm and 350mm. It is important to note that all of these beams were reinforced with shear reinforcement that was sufficient to prevent shear cracks and that was equal to the maximum spacing allowed by CSA A23.3 Standard.

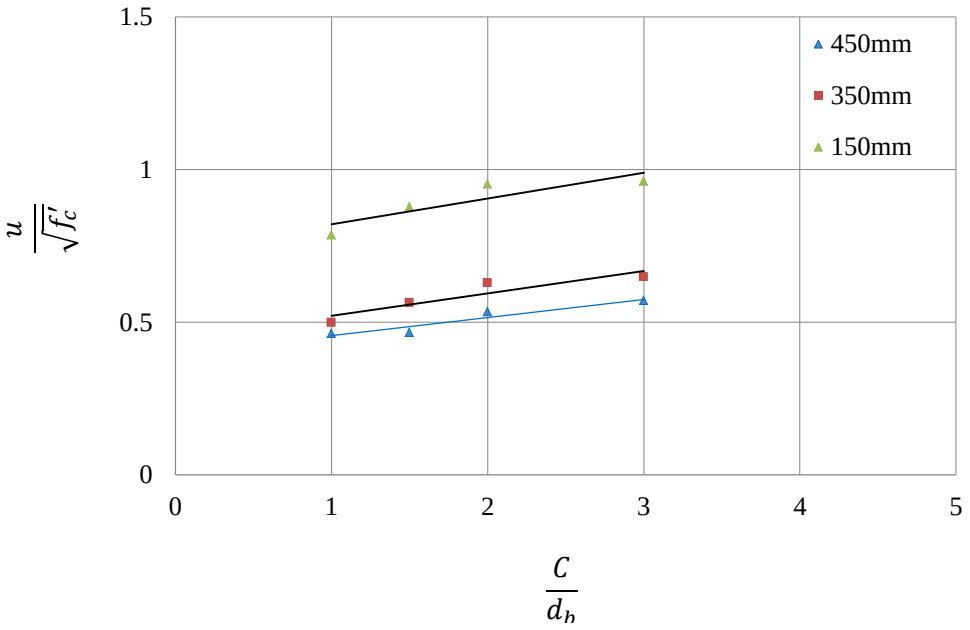

Figure 4.17 Average normalized bond stress versus normalized cover thickness of beams reinforced with GFRP bars

Relationships between the normalized bond stress and cover thickness were formulated from the data in Figure 4.17 at embedment lengths of 150mm, 350mm and 450mm, as given in Eqns. (4.6), (4.7) and (4.8).

At 150mm

$$\frac{\mu}{\sqrt{f_c'}} = 0.084\left(\frac{C}{d_b}\right) + 0.737 \qquad R^2 = 0.78 \qquad (4.6)$$

At 350mm

$$\frac{\mu}{\sqrt{f_c'}} = 0.073\left(\frac{C}{d_b}\right) + 0.448 \qquad R^2 = 0.85 \qquad (4.7)$$

At 450mm

$$\frac{\mu}{\sqrt{f_c'}} = 0.059\left(\frac{C}{d_b}\right) + 0.398 \qquad R^2 = 0.91 \qquad (4.8)$$

For

$$1.0 \leq \left(\frac{C}{d_b}\right) \leq 3.0$$

Where

μ is the average bond stress, MPa;

f_c' is the concrete compressive strength, MPa;

C is the cover thickness, mm; and

d_b is the bar diameter, mm.

The average slope from the three relationships is shown in Eqn (4.9).

$$\frac{\mu}{\sqrt{f_c'}} \propto 0.072\left(\frac{C}{d_b}\right) \qquad (4.9)$$

4.3.2.6 Formulation of bond stress equation for GFRP bars in SCC

Following the same approach used by Orangun et al. (1974) and Wambeke and Shield (2006), a relationship between the normalized average bond stress of GFRP bars embedded in SCC and the bar diameter to embedment length ratio of all beams that failed due to bond pullout can be formulated from the data plotted in Figure 4.18 as shown in Eqn 4.10.

$$\frac{\mu}{\sqrt{f_c'}} = 6.479\left(\frac{d_b}{l_e}\right) + 0.379 \qquad (4.10)$$

Where:

μ is average bond stress, MPa;

f_c' is concrete compressive strength, MPa;

l_e is the embedment length, mm; and

d_b is the bar diameter, mm.

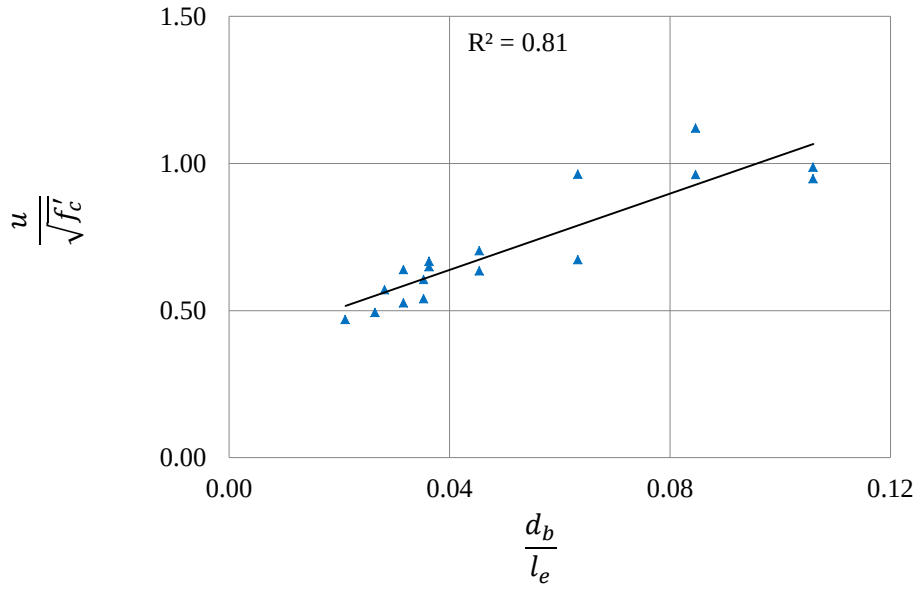

Figure 4.18 Normalized average bond stress versus inverted normalized embedment length of SCC beams reinforced with GFRP bars

Equation (4.10) involved data with embedment length to bar diameter ratios between 9.5 and 50. This data range covered bond stress results to the point where the rupture of the GFRP bars occurred. Three bar diameters, 9.5mm, 12.7mm, and 15.9mm were used in formulating this equation. However, Eqn (4.10) was derived based on the data of beams with a cover thickness of $3d_b$. To account for the effect of cover thickness, an additional term $\left(0.072\ \frac{C}{d_b} - 0.216\right)$ is added to the normalized bond stress Eqn. (4.10). This term is determined using Eqn. (4.9). At a C/db = 3, this term drops to zero.

$$\frac{\mu}{\sqrt{f_c'}} = \left[6.479\left(\frac{d_b}{l_b}\right) + 0.379\right] + \left[0.072\left(\frac{C}{d_b}\right) - 0.216\right]$$

Or,

$$\frac{\mu}{\sqrt{f_c'}} = 6.479\left(\frac{d_b}{l_e}\right) + 0.072\left(\frac{C}{d_b}\right) + 0.163 \qquad (4.11)$$

with

$$1.0 \leq \left(\frac{C}{d_b}\right) \leq 3.0$$

$$10.0 \leq \left(\frac{l_e}{d_b}\right) \leq 50$$

Where

μ is average bond stress, MPa;
$f_c^{'}$ is concrete compressive strength, MPa;
l_e is the embedment length, mm;
C is cover thickness, mm; and
d_b is the bar diameter, mm.

A comparison of the predicted normalized average bond stress values based on the proposed equation (Eqn. 4.11) and the experimental normalized average bond stress values is given in Table 4.4. The results show a good agreement between the experimental and the predicted values. The experimental to predicted ratio ranged from 0.89 to 1.22, with a mean value of 1.04 and a standard deviation of 0.093. A ratio of less than (1.0) means that the prediction was unconservative with respect to the measured experimental results. This was the case for five readings from Group SG15.9, possibly because the normalized bond stress was decreased slightly as the bar diameter increased (Figure 4.15). The bar diameter effect was indirectly incorporated in Eqn. (4.11). However, adding another term to account for bar diameter is possible, but the formulated equation was kept similar to the existing equation for the GFRP bars in NVC..

Table 4.4 Comparison between the experimental and predicted normalized average bond of GFRP bars in SCC

Beam	l_e, mm	$\frac{d_b}{l_e}$	$\frac{C}{d_b}$	Experimental $\frac{\mu}{\sqrt{f'_c}}$ (MPa)$^{1/2}$	Predicted $\frac{\mu}{\sqrt{f'_c}}$ (MPa)$^{1/2}$	$\frac{\text{Experimental}}{\text{Predicted}}$
SG9.5-3.0-300	150	15.8	3.0	0.964	0.789	1.22
	300	31.6	3.0	0.639	0.584	1.09
SG12.7-3.0-350	150	11.8	3.0	1.120	0.928	1.21
	350	27.6	3.0	0.667	0.614	1.09
SG12.7-3.0-450	150	11.8	3.0	0.962	0.928	1.04
	350	27.6	3.0	0.649	0.614	1.06
	450	35.4	3.0	0.571	0.562	1.02
SG15.9-3.0-450	150	9.4	3.0	0.987	1.066	0.93
	350	22.0	3.0	0.635	0.673	0.94
	450	28.3	3.0	0.540	0.608	0.89
SG15.9-3.0-600	150	9.4	3.0	0.948	1.066	0.89
	350	22.0	3.0	0.703	0.673	1.04
	450	28.3	3.0	0.606	0.608	1.00
	600	37.7	3.0	0.494	0.551	0.90
SG12.7-2.0-450	150	11.8	2.0	0.953	0.856	1.11
	350	27.6	2.0	0.629	0.542	1.16
	450	35.4	2.0	0.534	0.490	1.09
SG12.7-1.5-450	150	11.8	1.5	0.828	0.820	1.01
	350	27.6	1.5	0.564	0.506	1.11
	450	35.4	1.5	0.466	0.454	1.03
SG12.7-1.0-450	150	11.8	1.0	0.786	0.784	1.00
	350	27.6	1.0	0.499	0.470	1.06
	450	35.4	1.0	0.463	0.418	1.11

4.4 Beams reinforced with CFRP bars

Twenty-five beams were reinforced with CFRP bars: sixteen beams were made from self consolidating concrete (SCC) and nine beams from normal vibrated concrete (NVC). The beam specimens were divided into eight groups, including the exploratory Group SC12.7-E. This exploratory group was used to refine the test specimen configurations of the main experimental program. The groups consisted of a set of three beams, except for the exploratory group, which had four beams. The concrete cover thickness was constant for all beams at $3d_b$, except for the beams of Group SC12.7-C, which had various cover thicknesses- $2.0d_b$, $1.5d_b$, and $1.0d_b$. Results from the flexural tests are presented and discussed below. Detailed results of each beam (including crack pattern, moment versus deflection, moment versus end slip, strain gauge readings and tensile and bond stress profiles of the CFRP reinforcing bars) are provided in Appendix B.

4.4.1 Moment deflection responses of beams reinforced with CFRP bars

Results for beams made from SCC and NVC are presented separately in Sections 4.4.1.1 and 4.4.1.2, respectively. The results from each group are compared in terms of the moment versus midspan deflection and the moment versus end slip. Section 4.4.1.3 gives a summary of flexural test results.

4.4.1.1 Flexural responses of beams made from SCC and reinforced with CFRP bars

Figures 4.19 - 4.21 show the moment versus deflection response and moment versus end slip for all beams made from SCC. Each figure shows the results of one group. Generally, all beams showed a bilinear moment-deflection behaviour. The initial linear segment of the response had a very steep slope, which corresponded to the uncracked beam stiffness. This segment was ended when the first crack initiated. The second segment had a reduced slope (stiffness) with a higher rate of deflection versus moment. Within each group, the behaviour of all beams was similar before cracking. Typically, the first crack occurred within the constant moment region. As the applied load increased, more cracks formed, and the crack front moved toward the sides of the constant moment region. Beams that failed by bond pullout had a lower ultimate moment than those that failed by flexure (bar rupture). Pullout failure started with widening of the crack closest to the end of the shear span and initiation of bar slippage at one side. A “tic-tac” sound was heard at the initiation of the bond failure. The beams exhibited a rigid body motion around the slippage point during the failure stage. At failure, a loud noisy “ping/pop” sound was heard and the bar slip suddenly increased. Typically, slip was recorded on one side of the two shear spans. On the other hand, beams that failed by bar rupture had a similar loud “ping/pop” noise when the bar ruptured and the load dropped to zero. The failure happened suddenly,

and there was no indication of a plastic joint. Beams with both failure modes showed similar curvature response and flexural cracks.

Examining the effect of varying the length of the shear span on the moment-deflection responses, it is evident that as the shear span increased, the midspan deflection decreased at the same moment value. This decrease is attributed to the decrease in the constant moment region length, which had a larger influence on midspan deflection than region close to supports. Yet, the midspan deflection at failure was larger because the beam with a larger shear span reached a higher failure moment than beams that failed by bond failure at lower loads.

All beams in Group I experienced bond pullout failure (Figure 4.19). Beam SC6.3-3.0-350 showed load oscillation during testing. Examination of the test data reveals that there was a hydraulic system disturbance during the test because of another fatigue test running at the same time. Results from this beam were not including in any further discussion. Beams: SC6.3-3.0-450, SC6.3-3.0-600 showed similar slippage characteristics (Figure 4.19 (b)). The moment-deflection response of Beam SC6.3-3.0-450 showed a slight degradation of stiffness at a moment of 5.1kN, but the initiation of the end slip was recorded at a moment of 5.9kN.m (Figure 4.19 (a)). The strain gauge attached to the CFRP bar at 450mm from the support showed an overflow in readings at a moment of (5.1kN.m), which may indicate that local slippage occurred. Beam SC6.3-3.0-600 showed a slight stiffness improvement, and it failed at a moment of 6.5kN.m due to bond pullout mode of failure.

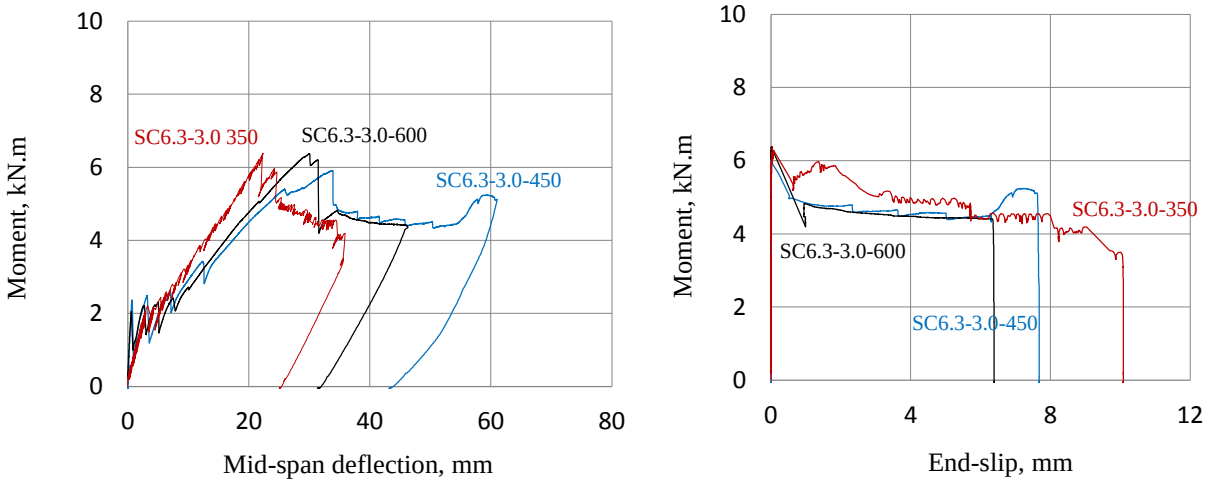

a) Moment-deflection responses b) Moment-end slip

Figure 4.19 Flexural test of SCC beams reinforced with 6.3mm CFRP bars, Group SC6.3

Beams of Group II had the typical trend of the effect of embedment length on moment deflection behaviour (Figure 4.20). The midspan deflection decreased as the shear span increased at a similar moment. The peak moment for Beam SC9.5-3.0-550, tested at a shear span of 550mm, was 12.7kN.m, and that for Beam SC9.5-3.0-750, tested at a shear span of 750mm, was 16.2kN.m, and that for Beam SC9.5-3.0-950, tested at a shear span of 950mm, was 16.0kN.m. The first two beams failed by bond pullout and the third failed due to bar rupture. As shown in Figure 4.20, the first two beams exhibited a post-failure response with a lower load as bar slippage increased. The tests of these two beams were terminated manually after significant slippage was recorded: 6.5mm and 4.5mm for Beam SC9.5-3.0-550 and SC9.5-3.0-750, respectively. Beam SG9.5-3.0-950 showed small jump-like-steps in load close to failure. This behaviour was possibly due to fiber rupture of the CFRP bar. When there were insufficient fibers to take up the load, the remaining fibers of the CFRP bar ruptured at once and the load dropped to zero instantly. Examining the strain gauge results (Appendix B) reveals that the tensile stress of the CFRP bar in Beam SG9.5-3.0-950 ruptured at 1435MPa, while the maximum tensile stress of the CFRP bar in Beam SC9.5-3.0-750 was 1375MPa and in Beam SC9.5-3.0-550 was1063MPa.

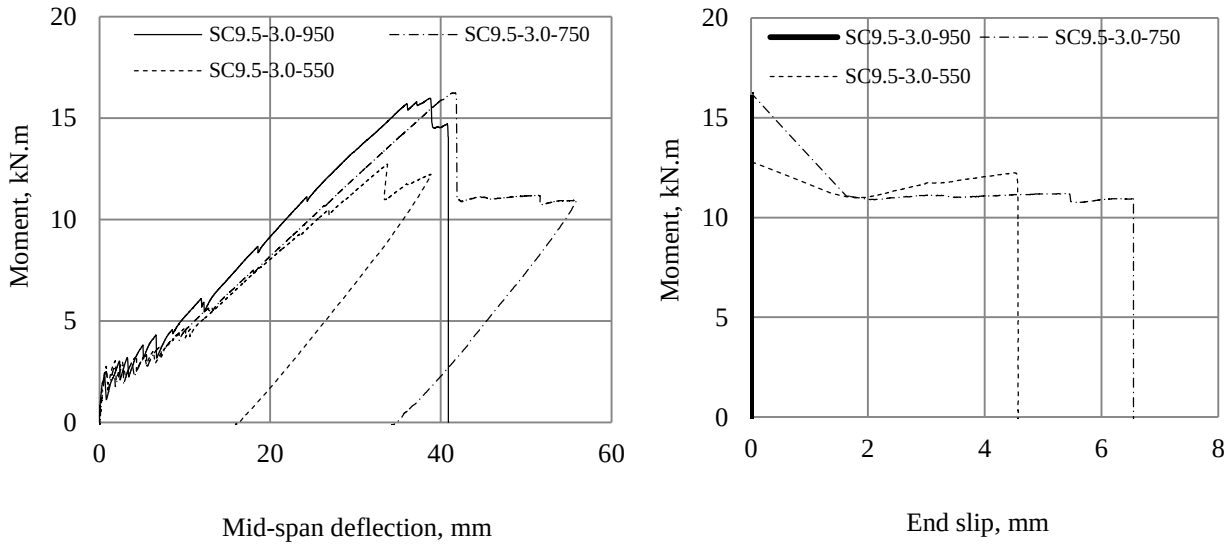

(a) Moment-deflection responses (b) Moment-end slip

Figure 4.20 Flexural test results of SCC beams reinforced with 9.5mm CFRP bar, Group SC9.5

Beams in Group III also showed the effect of the embedment length with respect to moment-deflection responses, Figure 4.21. Three beams were tested at embedment lengths of 850, 1250, and 1400mm.

The failure moments of these beams were 32.4kN.m (l_e = 850mm), 38.5kN.m (l_e = 1250mm), and 43.6kN.m (l_e = 1400mm). The first two beams failed by bond pullout, and the third beam showed a combined mode of failure with bar rupture at the onset of slip initiation.

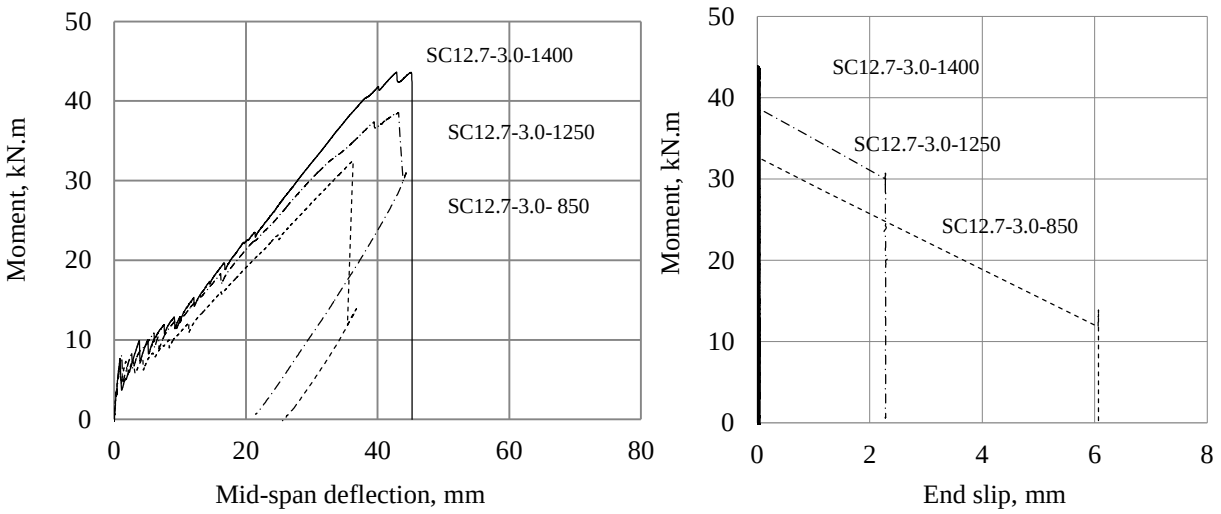

(b) Moment-deflection (b) Moment-end slip

Figure 4.21 Flexural test results of SCC beams reinforced with 12.7mm CFRP bars, Group SC12.7

To assess the effect of concrete cover thickness on the flexural behviour of SCC beams, different cover thicknesses of $3.0d_b$, $2.0d_b$, $1.5d_b$ and $1.0\ d_b$ were compared. It is important to note that the concrete compressive strength of the beam that had a cover thickness of $3.0d_b$ was 49.8MPa, and that for the other three beams was 70.8MPa. The peak moment of the beam with a cover of $3.0d_b$ was 32.4kN.m, the beam with a cover of $2.0d_b$ was 38.4kN.m, the beam with a cover of $1.5d_b$ was 34.7kN.m, and the beam with a cover of $1.0d_b$ was 32.4kN.m. There are two competing parameters in these four beams: effective depth and cover thickness. As the cover thickness reduced, the effective depth increased. The increase in the effective depth increases the beam stiffness and the resistance moment as compared with beams with a smaller effective depth, but the increased effective depth, in this group of beams, was associated with a decrease in the cover thickness, which might have reduced the bond strength and ultimately the moment capacity. The beams with cover thicknesses of $1.5d_b$ and $1.0d_b$ had a lower peak moment than the beam with cover thickness of $2.0d_b$, due to bond splitting failure. On the other hand, the deflection at midspan decreased as the effective depth increased, due to increased stiffness of the beam. This trend in results appeared after cracking when the effective depth had a significant contribution on the beam stiffness.

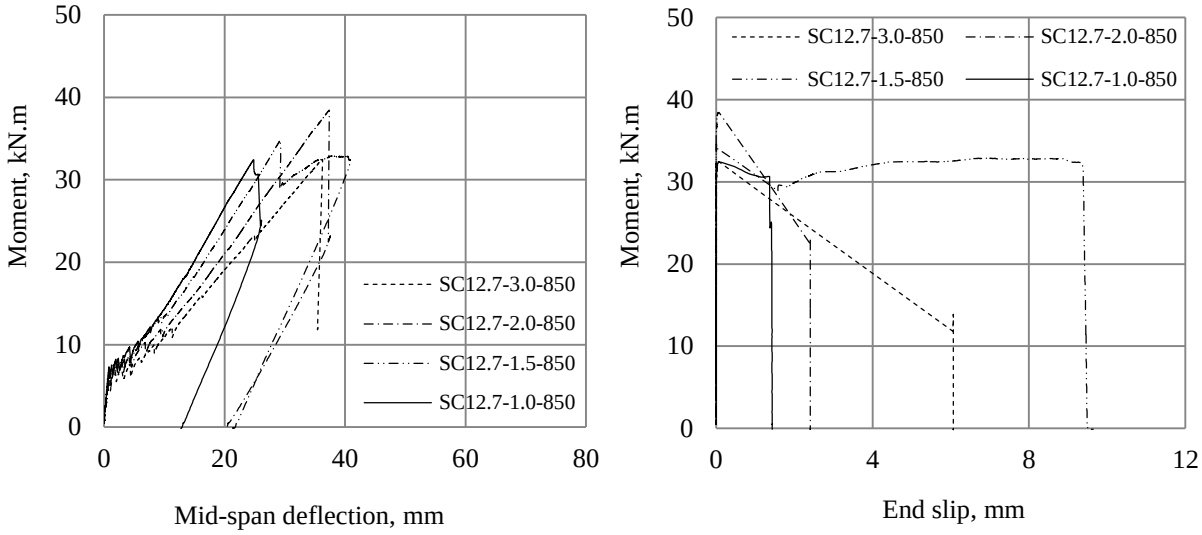

(c) Moment-deflection (b) Moment-end slip

Figure 4.22 Flexural test results of SCC beams reinforced with 12.7mm CFRP bars and various cover thicknesses, Group SC12.7C

4.4.1.2 Flexural responses of beams made from NVC and reinforced with CFRP bars

Beams made from NVC had a similar trend of flexural response to that of beams made from SCC (Figures 4.23 – 4.25). All beams showed bilinear moment-deflection responses. Figure 4.23 shows the results for Group NC6.3. The two beams tested at a shear span of 350mm and 450mm failed by bond pullout at a moment of 5.9kN.m and 8.0kNm, respectively. These beams had higher failure loads than those achieved by similar beams made from SCC. Beam NC6.3-600 failed by bar rupture at a moment of 8.6kN.m. The concrete compressive strength of the NVC was 64.4MPa and that for the SCC mix was 49.8MPa.

Figure 4.24 shows the moment versus midspan deflection of beams reinforced with a 9.5mm diameter CFRP bar (Group NC9.5). All beams in this group failed by bond pullout failure. However, the failure moments of NVC beams were higher than those for similar beams made from SCC, Group SC9.5. The peak moments were 15.4kN.m, 18.4kN.m and 19.9kN.m for Beams NC9.5-3.0-550, NC9.5-3.0-750 and NC9.5-3.0-950, respectively. The end slip ranged from 1.9mm to 4.8mm. The CFRP reinforcing bar in Beam NC9.5-3.0-950 reached higher tensile stress than that of the bar in similar beam made from SCC.

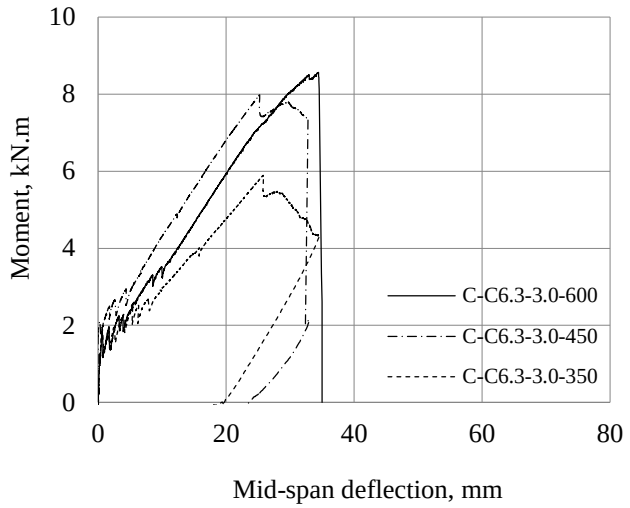

Moment-midspan deflection responses

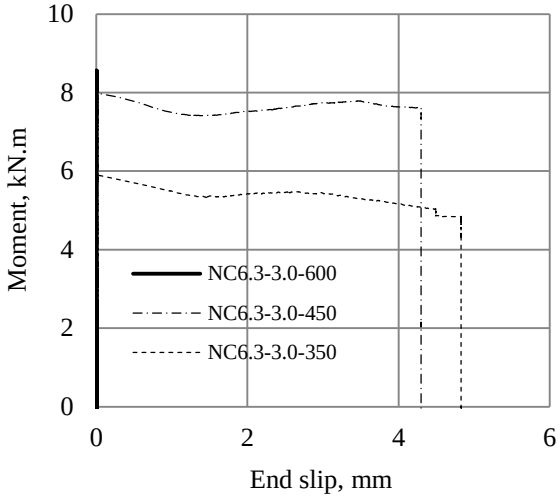

Moment end slip responses

Figure 4.23 Flexural test results of NVC beams reinforced with 6.3mm CFRP bars, Group NC6.3

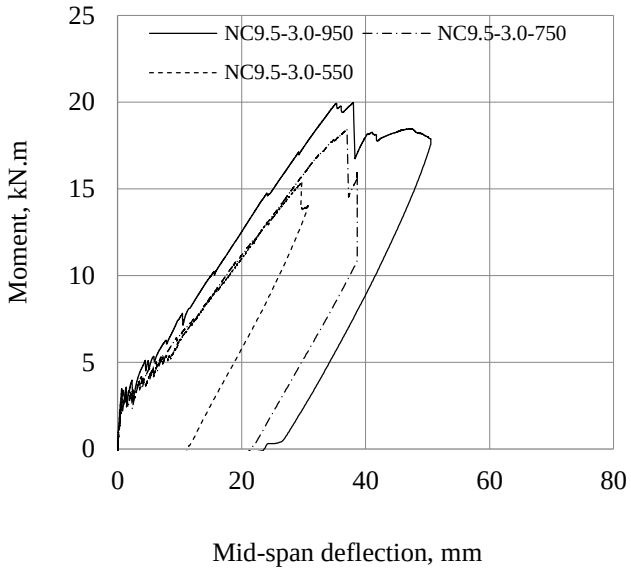

Moment-midspan deflection responses

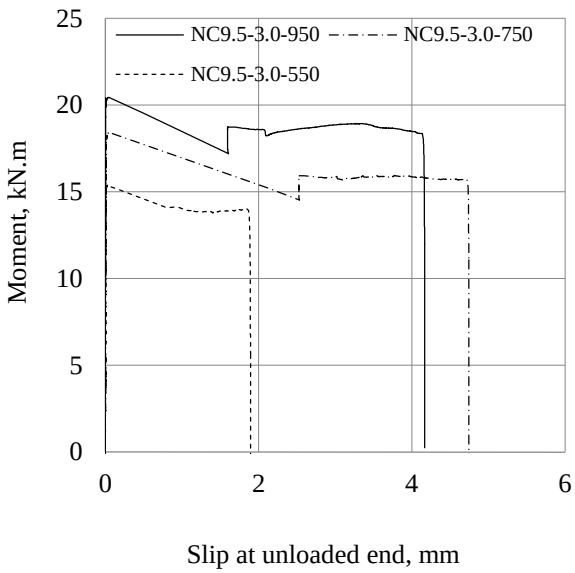

Moment slip at unloaded end responses

Figure 4.24 Flexural test results of NVC beams reinforced with 9.5mm CFRP bars, Group NC9.5

Figure 4.25 shows the moment deflection responses of beams reinforced with a 12.7mm diameter CFRP bar, Group NC12.7. The three beams in this group were tested at shear spans of 850mm, 1250mm and 1400mm. Beam NC12.7-850 and Beam NC12.7-1250 experienced bond pullout failure and Beam NC12.7-1400 failed by bar rupture. All beams in this group followed the typical response after cracking: as the shear span increased, the midspan deflection decreased at a similar applied moment. Beams made from NVC had higher peak moment values than beams made from SCC for a similar shear span. The highest peak moment was 49.8kN.m for Beam NV12.7-3.0-1400. The other two Beams, NC12.7-3.0-850 and NC12.7-3.0-1250, had peak moments of 39.3kN.m and 45.2kN.m, respectively. The end slip at failures was 4.5mm and 3.8mm for Beams NC12.7-3.0-850 and NC12.7-3.0-1250, respectively.

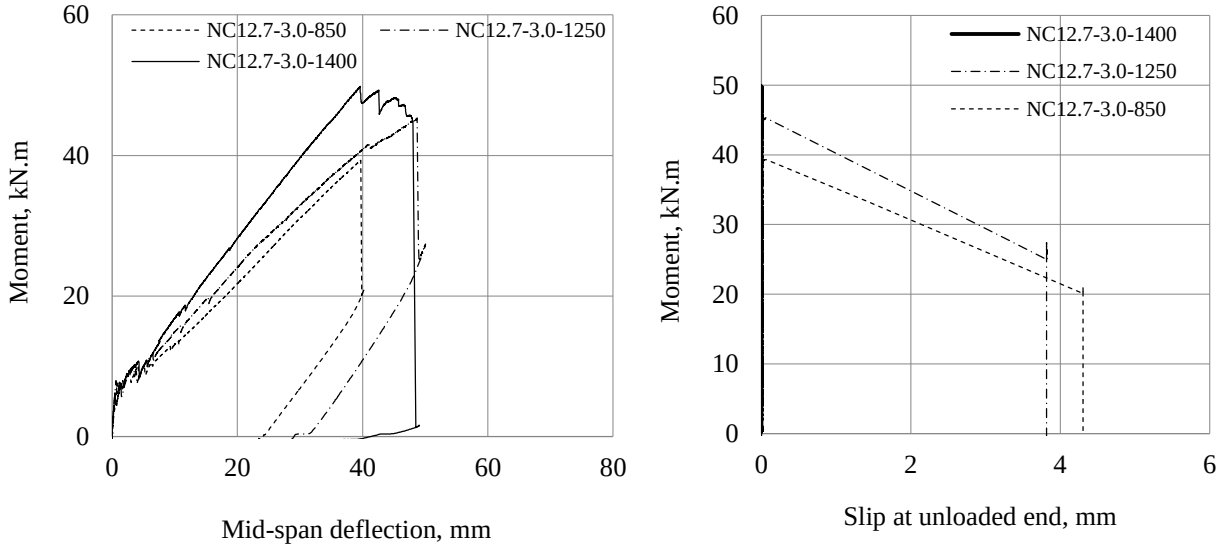

Moment-midspan deflection responses

Moment end slip responses

Figure 4.25 Flexural test results of NVC beams reinforced with 12.7mm CFRP bars, Group NC12.7

4.4.1.3 Summary of flexural test results of beams reinforced with CFRP bars

Table 4.5 summarizes the flexural test results of all beams reinforced with CFRP bars. All beams made from NVC except beams reinforced with 6.3mm diameter CFRP bars, had a slightly higher cracking moment than those beams made from SCC. There was no clear trend of the cracking moment for those found in GFRP beams.

Beam specimens made from NVC achieved higher moment resistance than those made from SCC and tested at similar shear spans. One of the reasons for this similarity was that the concrete compressive strength of the NVC mix was higher than that of SCC mix-2 (64.5MPa versus 49.8MPa). NVC beams with sufficient embedment length failed by rupture of the CFRP bar. The achievable tensile stresses in the CFRP bars should be investigated for both cases to evaluate whether there was a bond deficiency in the SCC specimens as compared to the NVC specimens. This analysis is presented in the next section.

Table 4.5 Flexural test results of beams reinforced with CFRP bars

Group	Beam designation	Beam size (b×h×L), mm	f'_c, MPa	Cracking		Ultimate		Mode of failure
				Δ_{cr} mm	M_{cr} kN.m	Δ_{max} mm	M_{max} kN.m	
SC6.3	SC6.3-3.0-350	150×150×1700	49.6	3.26	2.20	21.4	6.3	B
	SC6.3-3.0-450			0.61	2.05	29.8	6.3	B
	SC6.3-3.0-600			0.69	2.37	31.2	6.5	B
SC9.5	SC9.5-3.0-550	150×200×2200	49.6	0.75	2.75	33.7	12.7	B
	SC9.5-3.0-750			0.80	2.50	41.6	16.2	B
	SC9.5-3.0-950			0.61	2.44	38.8	16.0	R
SC12.7	SC12.7-3.0-850	150×300×3000	49.6	0.85	6.90	36.3	32.4	B
	SC12.7-3.0-1250			1.04	7.80	43.2	38.5	B
	SC12.7-3.0-1400			0.86	7.64	42.6	43.6	B/R
SC12.7-E	SC12.7-3.0-550	150×250×2200	62.1	-	-	22.0	23.0	B
	SC12.7-3.0-650			0.49	4.20	24.5	26.7	B
	SC12.7-3.0-750			0.58	4.30	28.1	31.0	B
	SC12.7-3.0-950			2.84*	7.60*	31.5	35.0	B
SC12.7C’	SC12.7-2.0-850	150×300×3000	70.9	1.01	6.80	37.4	38.4	B/S
	SC12.7-1.5-850			0.79	6.30	29.3	34.7	S
	SC12.7-1.0-850			0.77	6.90	24.8	32.4	S
NC6.3	NC6.3-3.0-350	150×150×1700	64.5	0.63	1.95	25.8	5.9	B
	NC6.3-3.0-450			*	1.91	25.2	8.0	B
	NC6.3-3.0-600			0.66	1.90	34.4	8.6	R
NC9.5	NC9.5-3.0-550	150×200×2200	64.5	0.88	3.40	29.7	15.4	B
	NC9.5-3.0-750			1.29	3.23	37.0	18.4	B
	NC9.5-3.0-950			0.67	3.48	35.3	19.9	B
NC12.7	NC12.7-3.0-850	150×300×3000	64.5	0.94	7.66	39.4	39.3	B
	NC12.7-3.0-1250			0.64	7.93	48.5	45.2	B
	NC12.7-3.0-1400			1.06	7.50	39.5	49.8	R

Where: S refers to self consolidating concrete; N refers to normal consolidating concrete, C refers to CFRP bars; E refers to the explanatory group; C’ refers to the group of beams that had varied cover thickness; M_{cr} is the experimental cracking moment; Δ_{cr} is the deflection at onset of first crack; M_{max} is the peak moment achieved before failure; Δ_{max} is the deflection associated with M_{max}; B refers to bond pullout failure; R refers to bar rupture failure; and S refers to bond splitting failure.

4.4.2 Tensile and bond stresses development in CFRP Bars

The typical strain response, tensile stress profile, and bond stress profile of selected CFRP reinforced concrete beams are discussed in this section. The tensile and bond stress results of all beams reinforced with CFRP bars are given in Appendix B. A procedure similar to that used for beams reinforced with GFRP bars was utilized in this section. The tensile stress in the CFRP bar was calculated based on the strain readings using Eqn. (4.2). The average bond stress profiles along the embedment length were determined using the difference in tensile stress between the strain gauge locations, Eqn. (4.4). The bond stress profile gives information on the initiation of the local bond slip if any. The effect of embedment length, cover thickness, bar diameter and concrete type on the tensile and bond stress profiles of the CFRP bars are discussed.

4.4.2.1 Tensile and bond stress of the CFRP bars in SCC Beams

Figures 4.26 and 4.27 show the strain response, tensile stress and bond stress profiles of the CFRP reinforcing bar of Beams SC12.7-3.0-850 and SC12.7-3.0-1400, respectively. Beam SC12.7-3.0-850 failed due the bond pullout while Beam SC12.7-3.0-1400 failed due to bar rupture. Figure 4.26 (a) shows the strain response at 200, 550 and 850mm from the support of Beam SC12.7-3.0-850. The CFRP strain results showed that when concrete in the tension face cracked, the strain gauge reading at the end of the shear span, 850mm from the support, suddenly increased in tensile strain in the CFRP bar when the tensile force transferred from the concrete to the CFRP bar. As the applied moment increased, similar jumps along the bar length in the tensile strain of the CFRP bar were recorded by strain gauges at other locations.

The tensile stress profile of the CFRP bar of Beam SC12.7-3.0-850 (Figure 4.26 (b)) showed that the sudden jumps in tensile stress coincided with cracking propagation from the midspan toward the support. As the applied moment approached the peak moment, the tensile stress profile within the shear span became nonlinear. The bond stress profile at this stage showed that the bond stress at the cracked region decreased as the moment increased, which was an indication of bond degradation at this region. The possible reason is that each crack reset the bond stress to zero at the crack location. Therefore, the local bond stress within the cracked region remained low. A large portion of the tensile stress was transferred to the concrete in the uncracked beam region (the region close to the support where the actual moment is less than the cracking moment).

Figure 4.26 (c) shows the bond stress profile of the CFRP bar in Beam SC12.7-3.0-850. When the first crack occurred, at an applied moment of 6.90kN.m, the bond stress at 850mm increased suddenly to

2.1MPa and then further increased to 3.9MPa after cracking. There was a minimal bond stress transfer in the region where the applied moment was less than the cracking moment, from the support to 550mm away from the support. When a second crack appeared (in the vicinity of 550mm from the support) at a moment of 10.0kN.m, the bond stress went from 0.0 to 1.9MPa. The jump in bond stress at 550mm was associated with a drop in bond stress at 850mm from 3.9MPa to 2.6MPa. As the applied moment increased, a similar pattern was recorded. Before bond slip occurred, a maximum bond stress of 8.26MPa was recorded close to the support region while the bond stress in the cracked region ranged between 1.6 to 2.0MPa. This pattern indicated that the bond stress in the cracked region had deteriorated due to flexural cracks and the peak bond stress shift towards the support or uncracked section. The results show that the beam failed by bond pullout at a tensile stress of 1119.6MPa in the CFRP bar. The bond failure occurred between the sand coating and the fibres of the CFRP bar.

Beam SC12.7-3.0-1400, which failed due to bar rupture, showed different tensile and bond stress profiles in the CFRP bar. Figure 4.27 shows the strain response, stress and bond stress profile at various load levels. Similar to the beam that failed by bond pullout, jumps in the longitudinal strain of the CFRP due to concrete cracking occurred, Figure 4.27 (a). The sudden increases in the longitudinal strains were associated with the initiation of bond stress at that location (Figure 4.27 (b)). However, the main difference from the previous beam was that the tensile stress profile in the CFRP tended to be linear after crack stabilization (Figure 4.27 (b)). As the load increased, the bond stress waves propagated towards the uncracked region in a manner similar of Beam SC12.7-3.0-850 (Figure 4.27 (c)). The bond stresses within the cracked region at the peak moment ranged between 1.90 and 4.72MPa, with an average bond stress within the cracked region of 3.40MPa. This value was slightly larger than that of Beam SC12.7-3.0-850, possibly because the moment gradient of Beam SC12.7-3.0-1400 was steeper than that of Beam SC12.7-3.0-850. The peak bond stress in the uncracked region (close to the support) of Beam SC12.7-3.0-1400 was 5.5MPa which was lower than that of the Beam SC12.7-3.0-850, which failed in bond pullout. Beam SC12.7-3.0-1400 showed no significant end slip, and failed due to bar rupture at a tensile stress of 1617.2MPa. Therefore, the ultimate bond strength of the CFRP bar was not reached.

These two examples of failure modes showed that if the embedment length of the CFRP bar is insufficient, the bond stress before pullout occurs will utilize the full bond strength to resist the slip. In the first case, the bond stress in the uncracked region reached an ultimate bond stress of 8.26MPa, while in the second case, the CFRP bar ruptured at a maximum bond stress of 5.5MPa in the uncracked region. The average bond stress in the beam that failed by bond pullout was 4.19MPa and in the beam that failed by bar rupture was 3.67MPa. When sufficient embedment length was available, the bond

stress was distributed over a larger length, and the tensile strength of the CFRP bar was reached. However, in the case of bond pullout failure when the embedment length was less than the required development length of the CFRP bar to reach its tensile strength, the bond stress waves propagated to the support, where the section was uncracked, due to a possible local bond slip at the end of the shear span. The results showed a flattening in the tensile stress profile within the cracked region which is an indication of bond stress deteroration at the end of the shear span..

Table 4.6 gives the bond stress results of all beams made from SCC with a cover thickness of $3d_b$. The data presented includes the local bond stress, average bond stress and normalized average bond stress at failure at several locations for each beam. The table also shows that the average bond stress decreases as the embedment length to bar diameter ratio increases. Also, for the same diameter bars, the average bond stress decreases as the embedment length to bar diameter ratio increases.

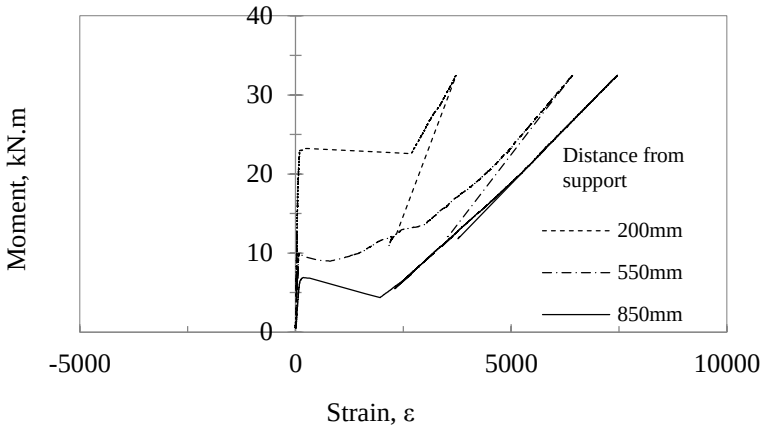

(a) Strain profile response

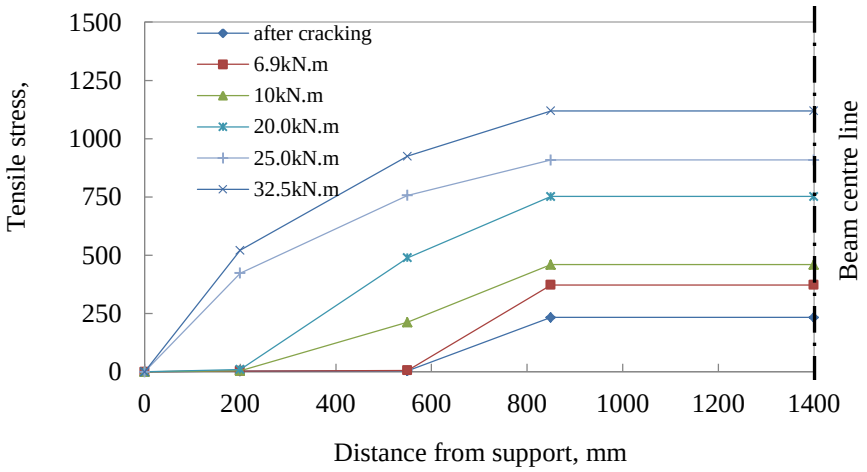

(b) Tensile stresses profile at various load levels

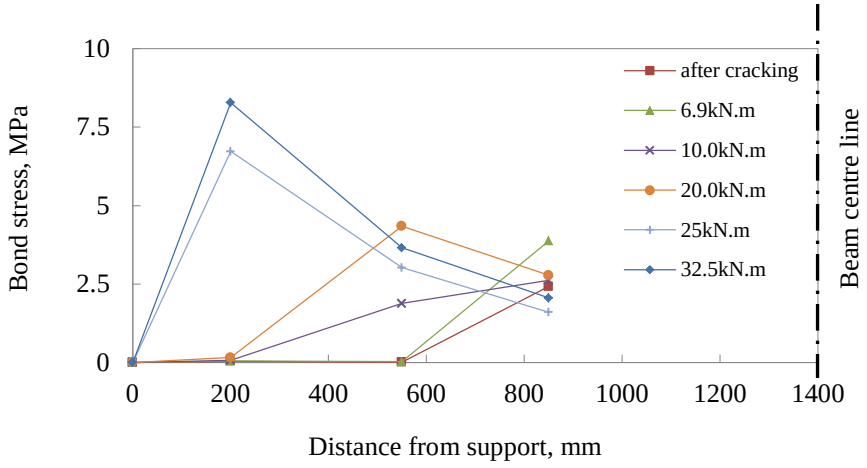

(c) Average local bond stress profile

Figure 4.26 Strain response, (b) tensile stress profile and (c) bond stress profile in CFRP bar of Beam SC12.7-3.0-850

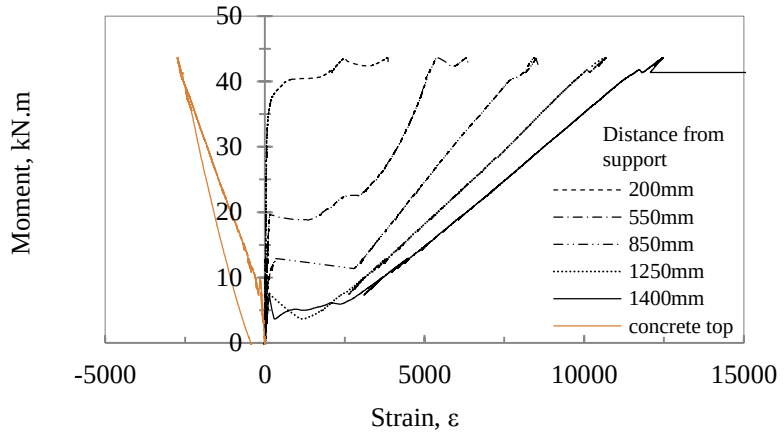

(a) Strain response in the CFRP bar and concrete

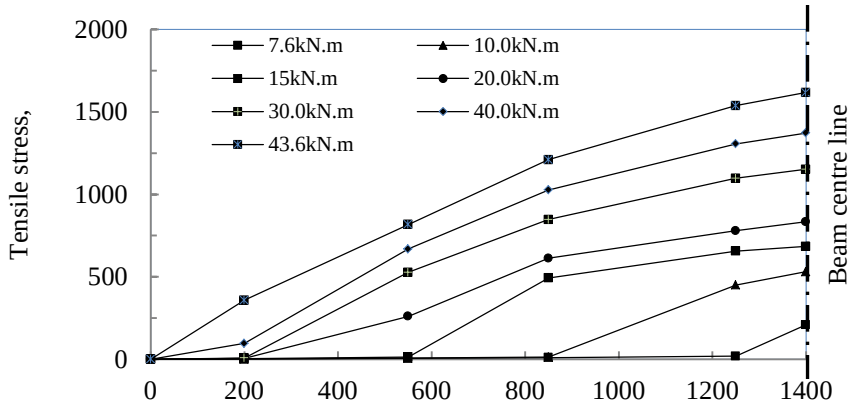

(b) Tensile stresses profile at various load levels

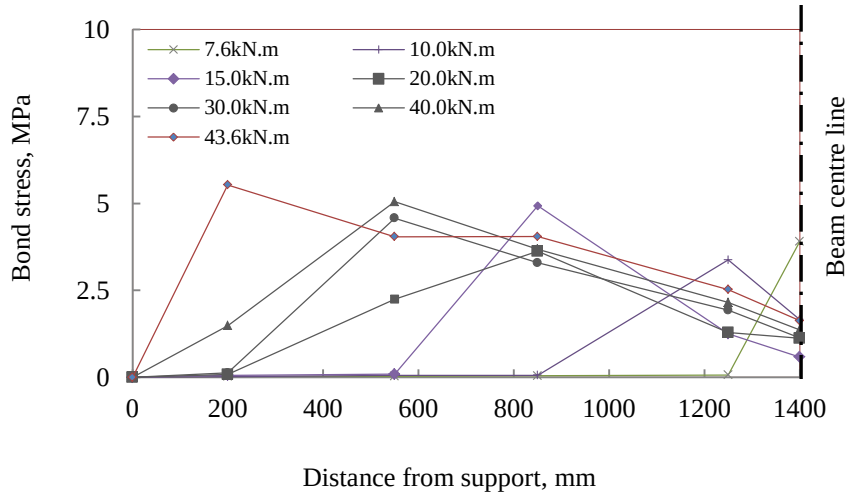

(c) Average local bond stress profile

Figure 4.27 (a) Strain response, (b) tensile stress profile and (c) bond stress profile in CFRP bar of Beam SC12.7-3.0-1400

Table 4.6 Bond stresses of SCC beams reinforced with CFRP with cover thickness of $3d_b$

Group	Beam	l_e, mm (1)	l_e/d_b	f_{frp}, MPa (2)	Local bond stress MPa (3)	Average bond stress μ MPa (4)	$\frac{\mu}{\sqrt{f_c'}}$ $(MPa)^{1/2}$
SC6.3	SC6.3-3.0-350	150	23.8	715.5	7.51	7.51	1.067
		350	55.5	971.3	2.01	4.37	0.621
	SC6.3-3.0-450	150	23.8	832.2	8.74	8.74	1.241
		350	55.5	1120.7	2.27	5.04	0.716
		450	71.4	1205.9	1.34	4.22	0.599
	SC6.3-3.0-600	150	23.8	822.1	8.63	8.63	1.226
		350	55.5	1206.5	3.03	5.43	0.771
		450	71.4	1557.5	5.53	5.45	0.774
		600	95.2	1660.7	1.08	4.36	0.619
SC9.5	SC9.5-3.0-550	200	21.1	663.1	7.88	7.88	1.119
		550	57.9	1063.1	2.71	4.59	0.652
	SC9.5-3.0-750	200	21.1	656.2	7.80	7.80	1.108
		550	57.9	1061.8	2.75	4.59	0.651
		750	78.9	1375.2	3.72	4.35	0.618
	SC9.5-3.0-950	200	21.1	499.9	5.94	5.94	0.843
		550	57.9	875.1	2.55	3.78	0.537
		750	78.9	1183.7	3.66	3.75	0.532
		950	100.0	1435.1	2.99	3.59	0.509
SC12.7	SC12.7-3.0-850	200	15.75	551.6	8.76	8.76	1.244
		550	43.3	925.3	3.39	5.34	0.758
		850	66.9	1119.6	2.06	4.18	0.594
	SC12.7-3.0-1250	200	15.7	574.3	9.12	9.12	1.295
		550	43.3	894.6	2.91	5.16	0.733
		850	66.9	1159.2	2.80	4.33	0.615
		1250	98.4	1424.1	2.10	3.62	0.514
	SC12.7-3.0-1400	200	15.7	358.5	5.69	5.69	0.809
		550	43.3	878.5	4.72	5.07	0.720
		850	66.9	1210.5	3.51	4.52	0.642
		1250	98.4	1537.9	2.60	3.91	0.555
		1400	110.2	1617.1	1.68	3.67	0.521

Where: (1) L_e is the embedment length from the support to the strain gauge location; (2) f_{frp} is the experimental tensile stress in the CFRP bar at the same location; (3) local bond stress is the average bond stress between the two gauges' locations; (4) μ is the average bond stress within the embedment length.

4.4.2.2 Tensile and bond stress of the CFRP bars in NVC Beams

Typical strain responses, tensile stress profiles and bond stress profiles of selected CFRP reinforced beams are presented and discussed in this section. The strain response, tensile stress profile and bond stress profile of all beams reinforced with CFRP bars are given in Appendix B. Figures 4.28 and 4.29 show the strain response, tensile stress profile and bond stress profile of Beam NC12.7-3.0-850 and Beam NC12.7-3.0-1400, respectively. Beam NC12.7-3.0-850 failed by bond pullout failure and Beam NV12.7-3.0-1400 failed by bar rupture. Similar recorded patterns are used to compare the NVC beams with corresponding beam made from SCC. However, the achieved tensile and bond stresses in the CFRP bar were not similar.

In Beam NC12.7-3.0-850, which failed by bond pullout, the maximum tensile stress in the CFRP bar at failure was 1332.3MPa. This stress was higher than the stress recorded in Beam SC12.7-3.0-850. The bond stress at the end of the shear span, in the cracked region, was between 2.1 and 3.5MPa. The peak bond stress at 200mm from the support, in the uncracked region, was 8.24MPa. Since the concrete compressive strength of the SCC and NVC are not the same, a normalized bond stress was calculated. Table 4.6 gives the results for beams made from SCC, and Table 4.7 gives the results of beams made from NVC. The normalized bond stress in the SCC beams was higher in the uncracked region than that in the NVC beams, but the opposite was found within the cracked region. Generally, the beams made from SCC showed higher normalized bond stress in the uncracked region and the opposite in the cracked region. The average normalized bond stresses at an embedment length of 850mm were very similar for both Beams SC12.7-3.0-850, NC12.7-3.0-850, with values of 0.59 and 0.62, respectively.

The maximum tensile stress in the CFRP bar of Beam NC12.7-3.0-1400, which failed by bar rupture, was 1688.4MPa. Because both beams NC12.7-3.0-1400 and SC12.7-3.0-1400 failed due to bar rupture, comparison of the bond stresses of these two beams at failure might not be valid. For this reason, the bond stresses were compared at a tensile stress of 1617.2MPa in the CFRP bar. This tensile stress is the maximum tensile stress of the CFRP in the SCC beam. The applied moments at this tensile stress in the two beams were very similar: 41.2kN.m in the NVC and 43.4kN.m for the SCC. The tensile stress and bond stress profiles of the CFRP bar in the NVC beam were calculated from strain data and plotted in Figure 4.30 in comparison with the failure tensile and bond stress profiles of the CFRP bar in the SCC beam. The tensile stress in the CFRP bar of the SCC beam at 200mm from the support was larger than that in the NVC beam. The bond stress did not initiate at the 200mm from the support in the NVC beam, while the bond stress in the SCC beam reached its peak value. The NVC beam showed a larger bond stress in the cracked region and this beam was able to sustain the required bond stress to achieve a high tensile stress. The SCC beam had a lower bond stress in the cracked

region for the same tensile stress level at the end of the shear span; thus, bond stress was initiated in regions close to the support to supplement the deficiency in bond in the cracked region and sustain the required tensile stress in the CFRP bar.

Table 4.7 gives the tensile stress, local bond stress, average bond stress and normalized average bond stress results of all beams that made from NVC. The data shown in this table are the peak values before failure. Similar trends to the SCC beams were recorded in the NVC beams; however, the values were different. Generally the tensile stresses in the CFRP bars in the NVC beams were slightly higher than those recorded in the SCC beams. The local bond stresses in the uncracked region were less in the NVC than in the SCC beams. The results indicate that the average normalized bond stresses decreased as the bar diameter increased. Moreover, the same bar diameter, the normalized average bond stress decreased as the embedment length increased.

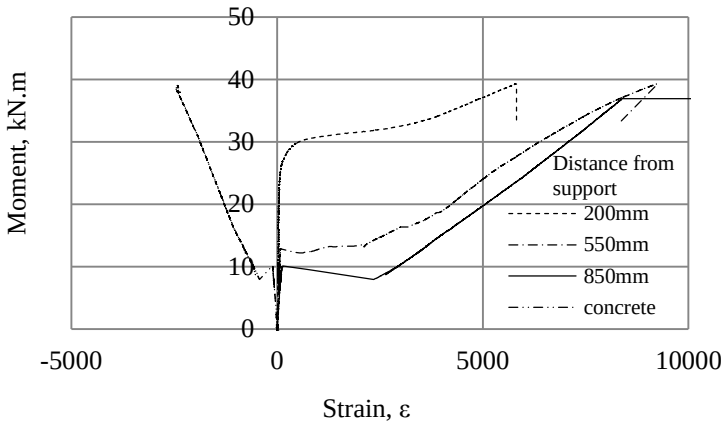

(a) Strain response in CFRP bar and in top compression fiber of concrete at the midspan

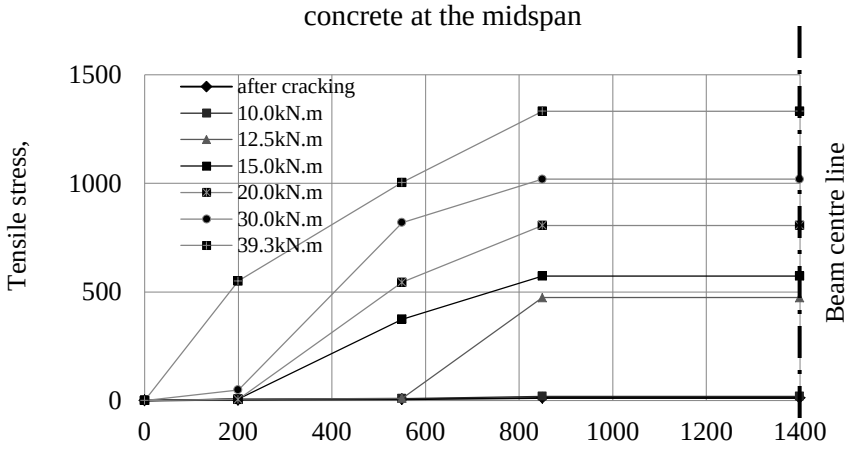

(b) Tensile stresses profile at various load levels

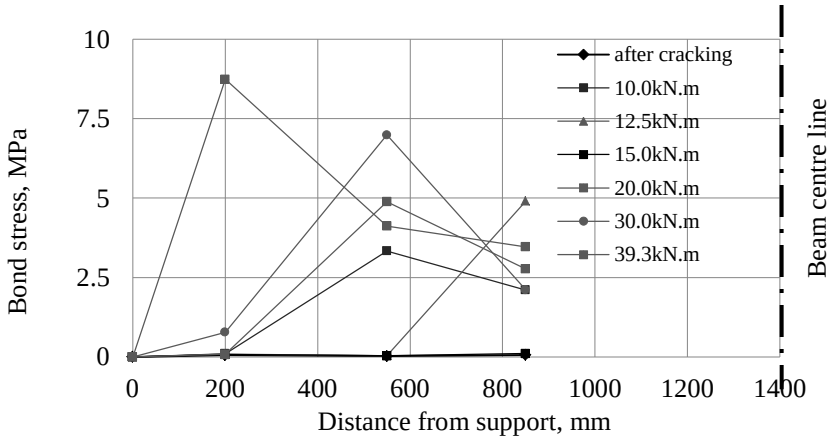

(c) Average local bond stress profile

Figure 4.28 Strain response (a), tensile stress profile (b) and local bond stress profiles (c) in the CFRP bar of Beam NC12.7-3.0-850

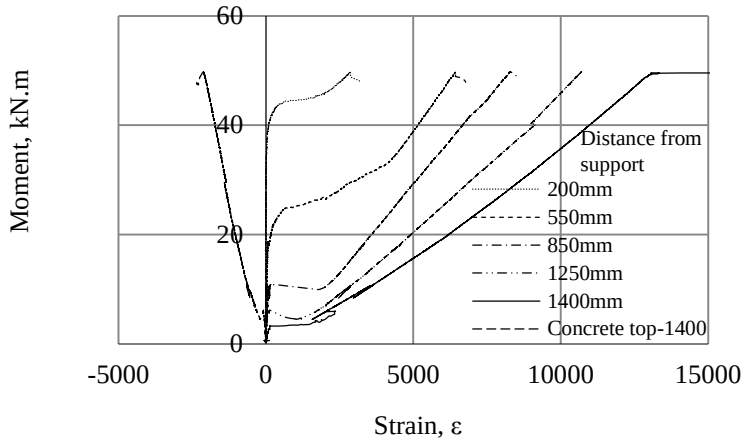

(a) Strain response in CFRP bar and in top fiber of concrete at midspan

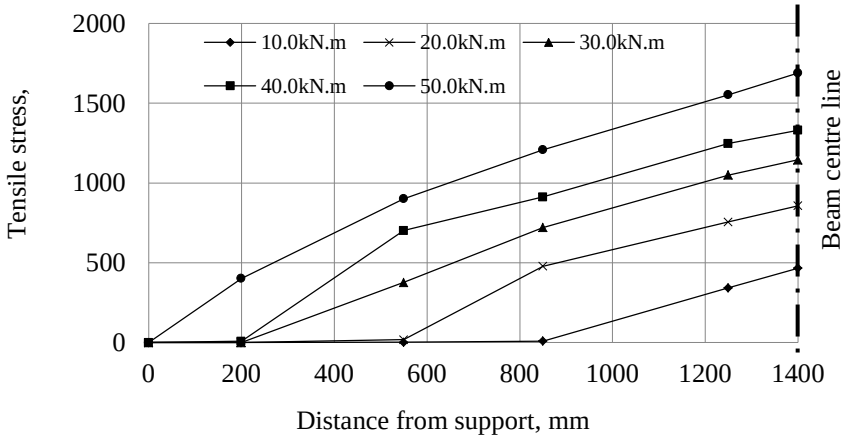

(b) Tensile stresses profile in the CFRP bar at various load

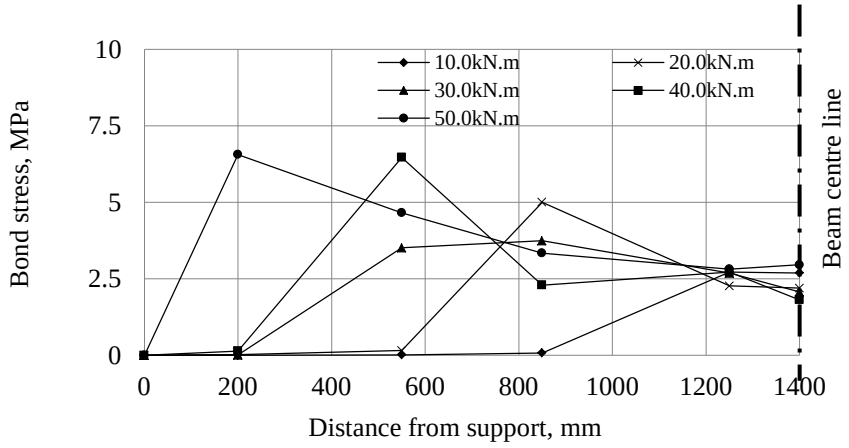

(c) Average local bond stress profile

Figure 4.29 Strain response (a), tensile stress profile (b), and local bond stress profile (c) in the CFRP bar of Beam NC12.7-3.0-1400

Table 4.7 Bond stresses of NVC beams reinforced with CFRP bars

Group	Beam	l_e, mm (1)	l_e/d_b	f_{frp}, MPa (2)	Local bond stress MPa (3)	Average bond stress μ MPa (4)	$u/\sqrt{f'_c}$, $(MPa)^{1/2}$
NC6.3	NC6.3-3.0-350	150	23.8	808.3	8.49	8.49	1.057
		350	55.5	1207.5	3.14	5.43	0.677
	NC6.3-3.0-450	150	23.8	821.5	8.63	8.63	1.074
		350	55.5	1412.3	4.65	6.36	0.791
		450	71.4	1556.8	2.28	5.45	0.678
	NC6.3-3.0-600	150	23.8	823.5	8.65	8.65	1.077
		350	55.5	1355.0	4.19	6.10	0.759
		450	71.4	1599.4	3.84	5.60	0.697
		600	95.2	1822.0	2.34	4.78	0.596
NC9.5	NC9.5-3.0-550	200	21.1	623.6	7.41	7.41	0.922
		550	57.9	1112.1	3.31	4.80	0.598
	NC9.5-3.0-750	200	21.1	617.9	7.34	7.34	0.914
		550	57.9	1295.0	4.59	5.59	0.696
		750	78.9	1593.6	3.55	5.05	0.628
	NC9.5-3.0-950	200	21.1	595.8	7.07	7.07	0.881
		550	57.9	1122.0	3.57	4.85	0.603
		750	78.9	1714.1	7.03	5.43	0.676
		950	100.0	1900.8	2.22	4.75	0.592
NC12.7	NC12.7-3.0-850	200	15.75	519.2	8.24	8.24	1.026
		550	43.3	1132.6	5.56	6.54	0.814
		850	66.9	1332.3	2.11	4.98	0.620
	NC12.7-3.0-1250	200	15.7	543.3	8.62	8.62	1.074
		550	43.3	958.9	3.77	5.54	0.689
		850	66.9	1271.1	3.30	4.75	0.591
		1250	98.4	1723.9	3.59	4.38	0.545
	NC12.7-3.0-1400	200	15.7	413.8	6.57	6.57	0.818
		550	43.3	926.6	4.65	5.35	0.666
		850	66.9	1195.3	2.84	4.46	0.556
		1250	98.4	1577.1	3.03	4.01	0.499
		1400	110.2	1688.4	2.36	3.83	0.477

Where: (1) L_e is the embedment length from the support to the strain gauge location; (2) f_{frp} is the experimental tensile stress in the CFRP bar at the same location; (3) local bond stress is the average bond stress between the two gauges' locations; (4) μ is the average bond stress within the embedment length

4.4.2.3 Effect of concrete type on tensile and bond stress in the CFRP bars

A comparison between results of the tensile and bond stress in the 12.7mm CFRP bar of Beams SC12.7-3.0-1400 and NC12.7-3.0-1400 is shown graphically in Figure 4.30. The profile of the CFRP bar in SCC represents the tensile and bond stress profile at failure; however, the profiles of the CFRP bar in NVC were calculated from the data when the tensile stress of the CFRP bar was equal to 1617.1MPa (failure stress in SCC beams) at the end of the shear span. The comparison shows that the NVC beam had higher bond stress profile from about 450mm from the support to the end of the shear span. The bond stress of the CFRP bar in SCC was pushed back to the support. This result was consistent with the local bond stresses, which showed that the SCC beams had lower bond stress in the cracked region.

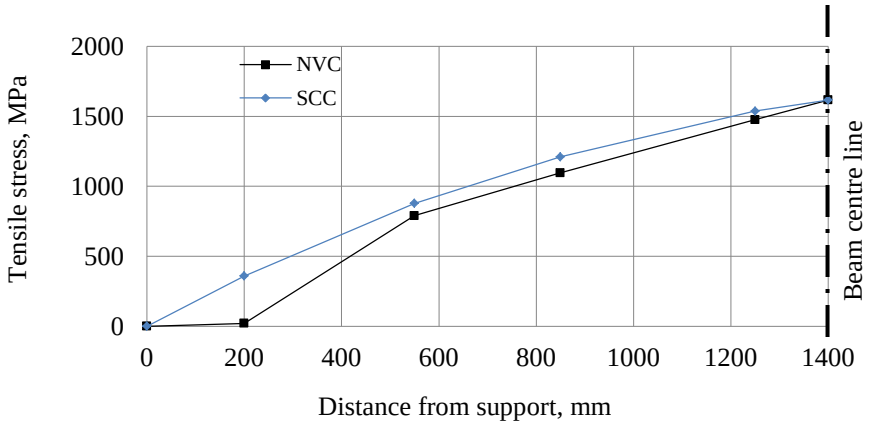

(b) Tensile stresses profiles

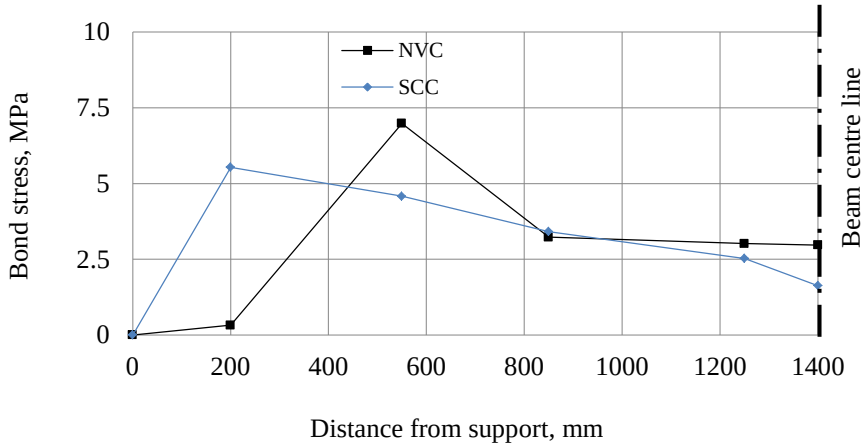

(b) Bond stress profiles

Figure 4.30 Comparison between Beam NC12.7-3.0-1400 and Beam SC12.7-3.0-1440 at same tensile stress of 1617MPa

Normalized average bond stresses from Tables 4.6 and 4.7 are graphically presented in Figure 4.31. Only the beams that failed by bond pullout failure are included in this figure. Beams that failed by bar rupture do not give the ultimate bond strength; however, those beams provide information on the development length of the CFRP bars. The figure shows that the bond stress of CFRP bars in SCC is slightly less than those of NVC at a similar embedment length to bar diameter ratio.

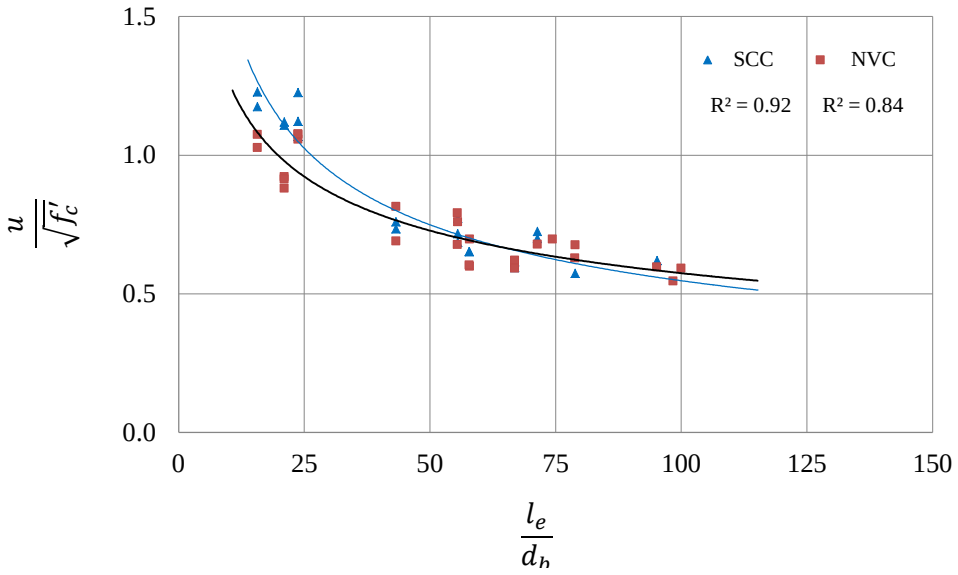

Figure 4.31 Normalized bond stress profile vs. normalized embedment length of all beams reinforced with CFRP bars

4.4.2.4 Effect of bar diameter on the normalized average bond stress of CFRP bars in SCC

The normalized average bond stress of beams that failed by bond pullout failure versus the embedment length to bar diameter ratio is presented in Figure 4.32. The general shape of the relationship between the normalized average bond stress and the embedment length is nonlinear. The figure shows that as the normalized embedment length increased, the normalized average bond stress decreased. Also, the data on the figure shows that the normalized average bond stresses of the bar diameters, 6.3mm, 9.5mm and 12.7mm, had parallel curves. The 6.3mm CFRP bar had the largest normalized bond stress of these CFRP bars. There was a slight decrease in normalized bond stress between the 9.5mm CFRP bar and the 12.7mm CFRP bar.

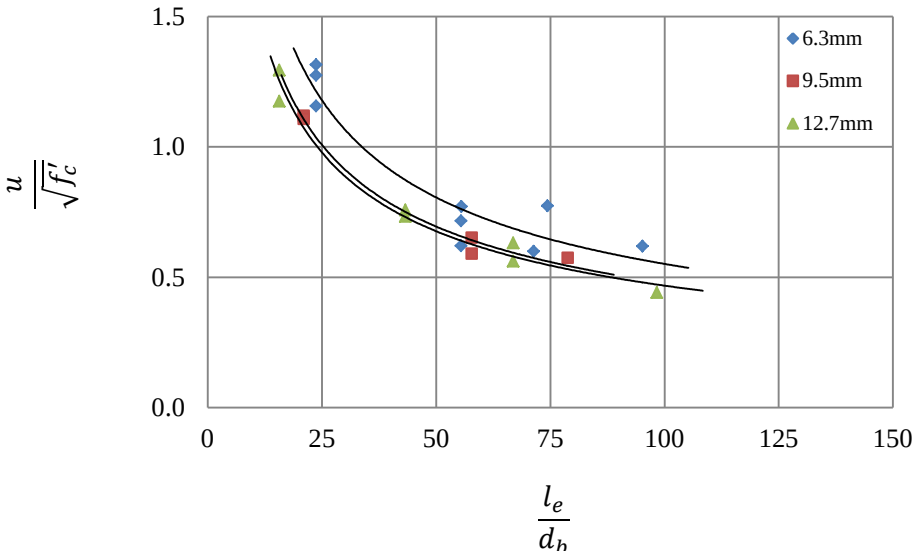

Figure 4.32 Effect of bar diameter on normalized average bond stress of SCC beams reinforced with CFRP bars

4.4.2.5 Effect of cover thickness on the tensile and bond stresses of the CFRP bars in SCC beams

Four cover thicknesses were used in this program: $3.0d_b$, $2.0d_b$, $1.5d_b$ and $1.0\ d_b$. This set of beams consisted of beams from Group SC12.7C and Beam SC12.7-3.0-850 from Group SC12.7. All beams in this comparison had a similar cross section, were reinforced with the same bar diameter, and were tested at the same shear span. Beams with cover thicknesses of $3.0d_b$ and $2.0d_b$ failed by bond pullout, although the beam with a cover thickness of $2.0d_b$ showed only minor visible splitting crack. Beams with cover thicknesses of $1.5d_b$ and $1.0d_b$ failed by bond splitting and had clearly visible longitudinal cracks of the soffit parallel to the reinforcing bar.

Figure 4.33 shows the strain response, tensile stress profile, and bond stress profile of Beam SC12.7-1.0-850. Comparing the results for this beam to those of a companion beam with cover thickness of $3.0d_b$ –Beam SC12.7-3.0-850, Figure 4.27– the achieved tensile stress in the CFRP bar decreased when the cover thickness decreased. Data for all beams from Group SC12.7C is given in Table 4.8.

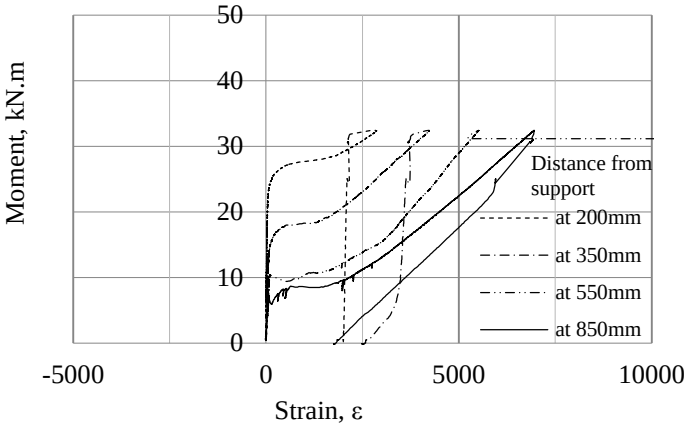

(a) Strain response

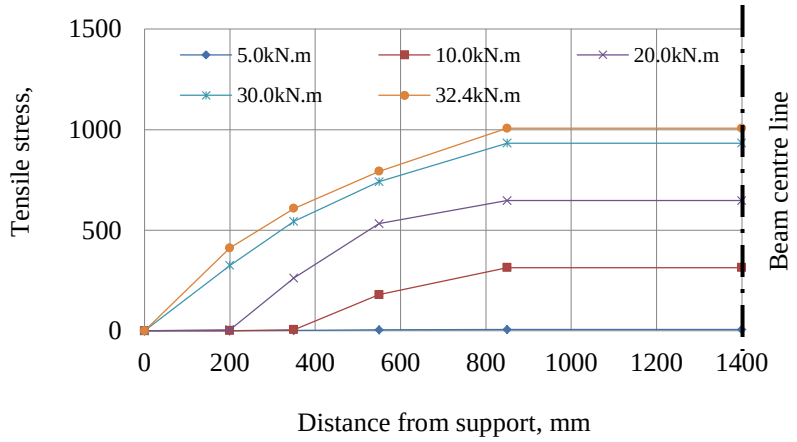

(b) Tensile stresses profile

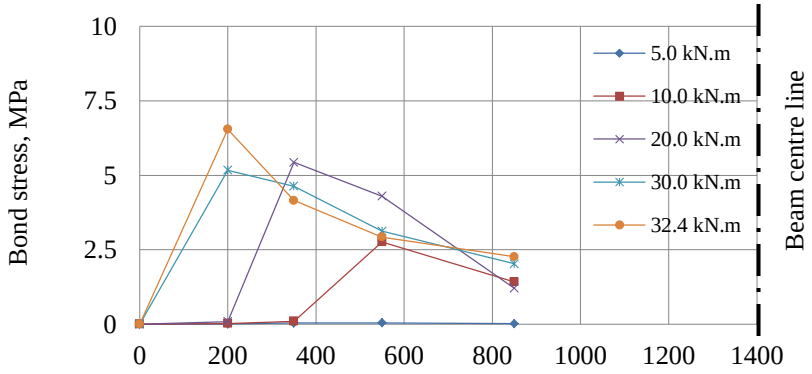

(c) Average local bond stress profile

Figure 4.33 Strain response (a), tensile stress profile (b) and bond stress profile in the CFRP bar of Beam SC12.7-1.0-850

Table 4.8 Summary of tensile and bond stresses in the CFRP bars of SCC beams of Group SC12.7C

Group	Beam	l_e, mm (1)	l_e/d_b	f_{frp}, MPa (2)	Local bond stress MPa (3)	Average bond stress μ MPa (4)	$\frac{\mu}{\sqrt{f'_c}}$ $(MPa)^{1/2}$
-	SC12.7-3.0-850	200	15.75	551.6	8.76	8.76	1.244
		550	43.3	925.3	3.39	5.34	0.758
		850	66.9	1119.6	2.06	4.18	0.594
SC12.7C	SC12.7-2.0-850	200	15.75	521.8	8.28	8.28	0.984
		350	27.56	748.9	4.81	6.79	0.807
		550	43.3	960.0	3.35	5.54	0.658
		850	66.9	1142.8	1.93	4.27	0.507
	SC12.7-1.5-850	200	15.75	420.1	6.67	6.67	0.792
		350	27.56	669.0	5.27	6.07	0.721
		550	43.3	867.9	3.16	5.01	0.595
		850	66.9	1064.6	2.08	3.98	0.472
	SC12.7-1.0-850	200	15.75	412.2	6.54	6.54	0.777
		350	27.56	608.5	4.16	5.52	0.656
		550	43.3	792.7	2.92	4.58	0.543
		850	66.9	1006.6	2.26	3.76	0.447

Where: (1) L_e is the embedment length from the support to the strain gauge location; (2) f_{frp} is the experimental tensile stress in the CFRP bar at the same location; (3) local bond stress is the average bond stress between the two gauges locations; (4) μ is the average bond stress within the embedment length

Figure 4.34 graphically represents the data from Table 4.8 and the results of Beam SC12.7-3.0-850. As discussed above, the normalized average bond stress significantly decreased when the mode of failure changed from bond pullout to bond splitting. The results indicate that the normalized average bond stress decreased as the cover thickness decreased A significant drop in bond stress was recorded when the cover thickness dropped from $3.0d_b$ to $2.0d_b$. Then the average bond stresses were slightly decreased as the concrete cover thickened from $2.0d_b$ to $1.0d_b$. A cover thickness of $3.0d_b$ was considered to be the critical cover thickness to avoid bond splitting mode failure of CFRP bars in SCC. This value was higher than that obtained for the GFRP bars. The possible explanation of this trend is that the CFRP bars had larger tensile stresses and needed greater confinement than did the GFRP bars.

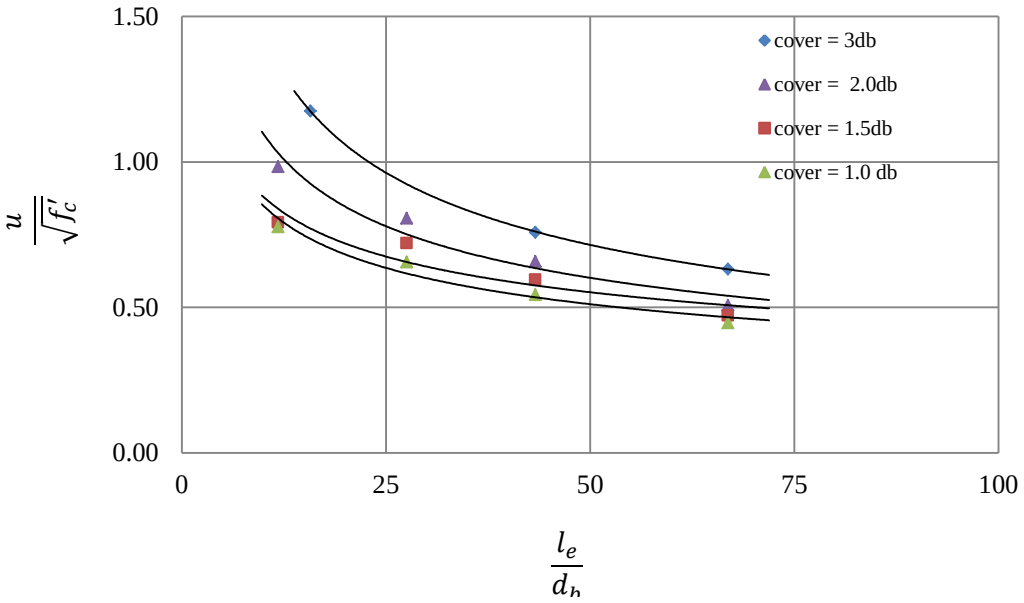

Figure 4.34 Normalized bond stress profile of SCC beams reinforced with CFRP bars at various cover thicknesses

To quantify the effect of cover thickness on the normalized average bond stress, the normalized bond stress at embedment lengths of 200mm, 550mm and 850mm of the CFRP bar in beams of Group SC12.7C and Beam SC12.7-3.0-850 are plotted in Figure 4.35. Linear relationships are used to represent the effect of cover thickness. The linear relationship has an acceptable fit and provides simple formulation of a bond equation. The relationships between the normalized bond stress and cover thickness were formulated from the data in Figure 4.35 at embedment lengths of 200mm, 550mm and 850mm as shown in Eqns. (4.12), (4.13) and (4.14)

l_e = 200mm

$$\frac{\mu}{\sqrt{f_c'}} = 0.177\left(\frac{C}{d_b}\right) + 0.641 \qquad R^2 = 0.99 \qquad (4.12)$$

l_e = 550mm

$$\frac{\mu}{\sqrt{f_c'}} = 0.108\left(\frac{C}{d_b}\right) + 0.436 \qquad R^2 = 1.00 \qquad (4.13)$$

l_e = 850mm

$$\frac{\mu}{\sqrt{f_c'}} = 0.075\left(\frac{C}{d_b}\right) + 0.365 \qquad R^2 = 0.99 \qquad (4.14)$$

For

$$1.0 \leq \left(\frac{C}{d_b}\right) \leq 3.0$$

Where

μ is average bond stress, MPa;

f_c' is the concrete compressive strength, MPa;

C is cover thickness, mm; and

d_b is the bar diameter, mm.

The average slope of the three relationships between the normalized average bond stress and cover to bar diameter ration from Eqn (4.12), (4.13) and (4.14) was calculated and shown in the relationship in (4.15)

$$\frac{\mu}{\sqrt{f_c'}} \propto 0.120\left(\frac{C}{d_b}\right) \qquad (5.15)$$

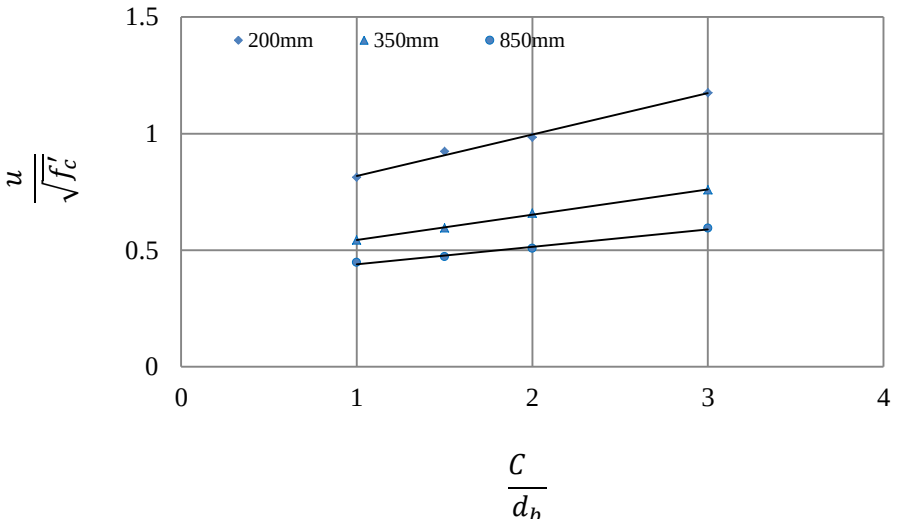

Figure 4.35 Normalized average bond stress versus normalized cover thickness of CFRP bars in SCC beams

4.4.3 Formulation of bond stress equation for CFRP bars in SCC

Following the same approach used by Orangun et al. (1974) and Wambeke B. and Shield C. (2006), a relationship between the normalized average bond stress of CFRP bars embedded in SCC and the bar diameter to embedment length ratio of all beams that failed due to bond pullout can be formulated from the data plotted in Figure 4.36, as shown in Eqn. (4.16).

$$\frac{\mu}{\sqrt{f_c'}} = 13.76\left(\frac{d_b}{l_e}\right) + 0.45 \qquad (4.16)$$

Where

μ is average bond stress, MPa;

f_c' is concrete compressive strength, MPa;

l_e is the embedment length, mm; and

d_b is the bar diameter, mm.

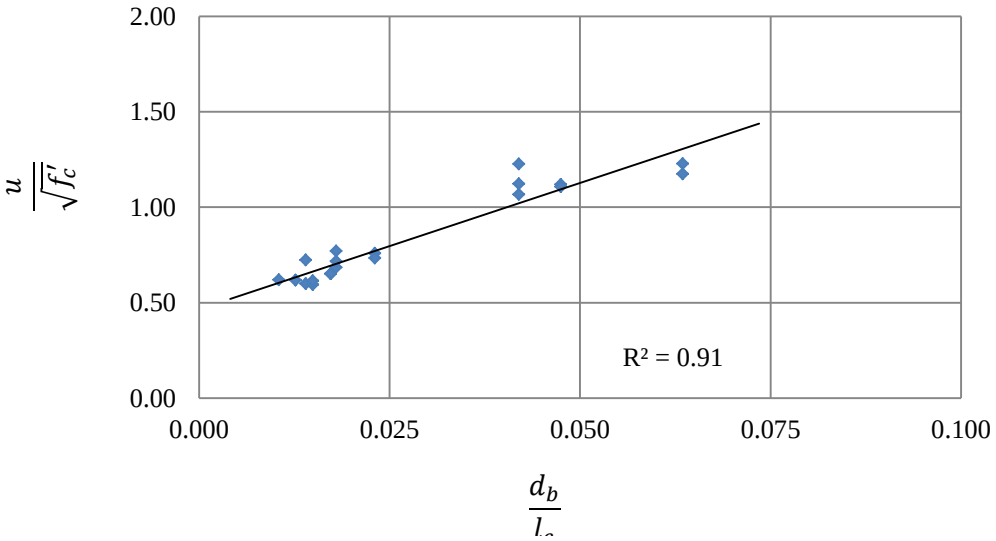

Figure 4.36 Normalized average bond stress versus the bar diameter to embedment length ratio of CFRP bars in SCC beams

Eqn. (4.16) involved data with an embedment length to bar diameter ratio from 15.0 to 100.0. This data range covered bond stress results to approximately the point when rupture of the CFRP bar occurred. Three bar diameters - 6.3mm, 9.5mm and 12.7mm - were used in formulating this equation.

Eqn. (4.16) was derived based on data of beams with a cover thickness of $3d_b$. To account for the effect of the cover thickness (C/d_b ratio), an additional term of $\left[0.12\left(\frac{C}{d_b}\right) - 0.36\right]$ is added to the normalized bond stress in Eqn. (4.16). This term is determined using the relationship (4.15); this term drops to zero at a cover thickness of $3.0d_b$.

$$\frac{\mu}{\sqrt{f_c'}} = \left[13.76\left(\frac{d_b}{l_e}\right) + 0.45\right] + \left[0.12\left(\frac{C}{d_b}\right) - 0.36\right]$$

Therefore,

$$\frac{\mu}{\sqrt{f_c'}} = 13.76\left(\frac{d_b}{l_e}\right) + 0.12\left(\frac{C}{d_b}\right) + 0.09 \qquad (4.17)$$

and

$$1.0 \leq \left(\frac{C}{d_b}\right) \leq 3.0$$

$$15 \leq \left(\frac{l_e}{d_b}\right) \leq 100$$

Where

μ is the average bond stress, MPa;
f_c' is the concrete compressive strength, MPa;
l_e is the embedment length, mm;
C is cover thickness, mm; and
d_b is the bar diameter, mm.

4.4.4 Validation of the proposed model

The predicted normalized average bond stress values based on the proposed equation (4.17) and the experimental normalized average bond stress values are compared in Table 4.9. The results show a good agreement between the experimental and the predicted values. The experimental/predicted ratio ranged from 0.76 to 1.20. The mean value of the ratios is 1.004 and the standard deviation is 0.089. A

ratio of less than (1.0) means that the predicted value is less than the experimental values. The cases with the experimental/predicted ratio less than 1.0 are at an embedment length of 200mm in beams from Group SC12.7-C. The data of the experimental normalized average bond stress from Table 4.9 is presented graphically in Figure 4.37. The proposed relationship correlated well with the experimental results.

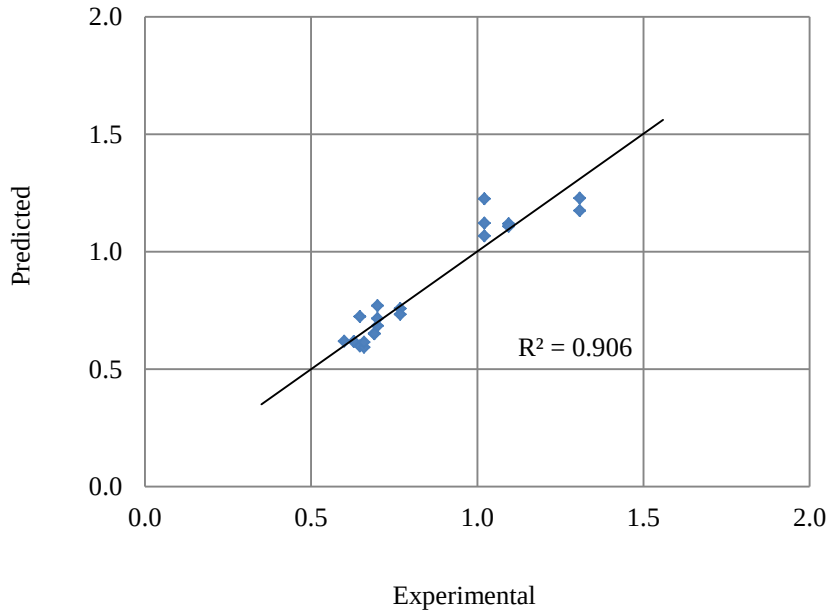

Figure 4.37 Comparison between the predicted and the experimental normalized average bond stress of all SCC beams reinforced with CFRP bars and failed by bond pullout

Table 4.9 Comparison between the experimental and proposed equation for the normalized average bond of CFRP bars in SCC

Group	Beam	l_e, mm	$\frac{l_e}{d_b}$	$\frac{C}{d_b}$	Experimental $\frac{\mu}{\sqrt{f'_c}}$ (MPa)$^{1/2}$	Proposed $\frac{\mu}{\sqrt{f'_c}}$ (MPa)$^{1/2}$	$\frac{\text{Experimental}}{\text{Proposed}}$
SC6.3	SC6.3-3.0-350	150	23.8	3.0	1.067	1.049	1.04
		350	55.5	3.0	0.621	0.700	0.98
	SC6.3-3.0-450	150	23.8	3.0	1.241	1.022	1.10
		350	55.5	3.0	0.716	0.701	1.02
		450	71.4	3.0	0.599	0.647	0.93
	SC6.3-3.0-600	150	23.8	3.0	1.226	1.022	1.20
		350	55.5	3.0	0.771	0.701	1.10
		450	71.43	3.0	0.774	0.647	1.12
		600	95.2	3.0	0.619	0.600	1.03
SC9.5	SC9.5-3.0-550	200	21.1	3.0	1.119	1.095	1.02
		550	57.9	3.0	0.652	0.691	0.94
	SC9.5-3.0-750	200	21.1	3.0	1.108	1.095	1.01
		550	57.9	3.0	0.651	0.691	0.94
		750	78.9	3.0	0.618	0.629	0.98
SC12.7	SC12.7-3.0-850	200	15.75	3.0	1.244	1.309	0.90
		550	43.3	3.0	0.758	0.769	0.99
		850	66.9	3.0	0.594	0.660	0.90
	SC12.7-3.0-1250	200	15.7	3.0	1.295	1.309	0.94
		550	43.3	3.0	0.733	0.769	0.95
		850	66.9	3.0	0.615	0.660	0.93
		1250	98.4	3.0	0.514	0.596	0.92
SC12.7C	SC12.7-2.0-850	200	15.75	2.0	0.984	1.189	0.83
		350	27.6	2.0	0.807	0.825	0.98
		550	43.3	2.0	0.658	0.649	1.01
		850	66.9	2.0	0.507	0.540	0.94
	SC12.7-1.5-850	200	15.75	1.5	0.792	1.129	0.82
		350	27.6	1.5	0.721	0.765	0.94
		550	43.3	1.5	0.595	0.589	1.01
		850	66.9	1.5	0.472	0.480	0.98
	SC12.7-1.0-850	200	15.75	1.0	0.777	1.069	0.76
		350	27.6	1.0	0.656	0.705	0.93
		550	43.3	1.0	0.543	0.529	1.06
		850	66.9	1.0	0.447	0.420	1.06

Results from the exploratory Group (SC12.7-E) were used as an independent data to validate the prediction of the normalized average bond stress by Eqn. (4.17). This comparison is given in Table 4.10. The overall results agreed with experimental data. However, there was an unconservative result in the case of B1. This comparison was limited by the number of beams. Further discussion and comparison with the available equations is provided in Chapter 6.

Table 4.10 Comparison between the experimental and proposed equation for the normalized average bond of CFRP bars in SCC

Group	Beam	d_b, mm	l_e, mm	$\frac{l_e}{d_b}$	$\frac{C}{d_b}$	Experimental $\frac{\mu}{\sqrt{f_c'}}$ (MPa)$^{1/2}$	Proposed $\frac{\mu}{\sqrt{f_c'}}$ (MPa)$^{1/2}$	$\frac{\text{Experimental}}{\text{Proposed}}$
SC12.7E	B1	12.7	550	43.3	3.0	0.562	0.769	0.73
	B2	12.7	650	51.2	3.0	0.689	0.721	0.96
	B3	12.7	200	15.75	3.0	1.098	1.309	0.84
		12.7	550	43.3	3.0	0.845	0.769	1.10
		12.7	750	59.1	3.0	0.694	0.686	1.01
	B4	12.7	200	15.75	3.0	1.229	1.309	0.94
		12.7	550	43.3	3.0	0.870	0.769	1.13
		12.7	750	59.1	3.0	0.751	0.686	1.09
		12.7	950	74.8	3.0	0.647	0.639	1.01

Chapter 5 – Test Results and Discussion of Beams Prestressed with CFRP Bars

5.1 Introduction

Sixteen prestressed beam specimens were fabricated and tested. All beams were prestressed with 12.7mm carbon fibre reinforced polymer (CFRP) bars. Full details of the fresh and hardened properties of the concrete and the CFRP bar properties were presented in Chapter 3. The beams were divided into four groups. Beams of Groups I, II and III were made from self consolidating concrete (SCC), and prestressed to 30%, 45%, and 60% of the guaranteed tensile strength of the CFRP bar, respectively. Beams of Group IV were made from normal vibrated concrete (NVC). One beam of Group IV was prestressed to 30%, and the other three beams were prestressed to 60% of the guaranteed tensile strength of the CFRP bars.

This chapter presents the experimental results, including analysis of the bond stress development of the prestressed CFRP bars in SCC and the flexural behaviour of CFRP prestressed concrete beams. Section 5.2 presents the prestressing data and the concrete compressive strength results. Bond stress due to prestress load release and transfer lengths of CFRP bars in SCC are given in section 5.3. A proposed equation to predict the transfer length is presented in this section. Section 5.4 presents the flexural test results and flexural bond stress analysis. A detailed examination of the mode of failure is done. Comparison of the experimental results with the predictions using design equations are presented and discussed in Sections 5.3 and 5.4.

5.2 Prestressing data

As described in Chapter 3, four prestressed beams were fabricated and cast from each concrete batch. The prestressing operation went smoothly, except for three cases were the CFRP bar did not reach the target prestressing level of 60%. Two of these cases occurred during the first prestressing operation during the casting of beams of Group III. Two out of four prestressed CFRP bars of this group, Beam S60-1 and Beam S60-2, were stressed to 60% of the guaranteed tensile strength. However, the other two bars did not attain the 60% level; a cracking noise was heard from the prestressed bars at a stress of about 726MPa. A possible shear crack of the resin matrix or fiber cracked occurred in these two bars. The prestressing level was then reduced to 30%, and these beams were regrouped as Group I and named Beam S30-1 and Beam S30-2. A complementary number of beams of these two groups, I and

III, were fabricated and cast during the next batch. The third case that failed to attain the 60% prestress level was a beam from Group IV. The original plan was to prestress all NVC beams to a 60% prestress level; however, one beam, Beam N30-1, was only prestressed to 30%. Useful results were obtained from this beam as it provided a comparison between SCC and NVC at a lower prestressing level.

Table 5.1 gives the prestressing data (force and stress) at jacking and release as well as the concrete compressive strength at release and 28 days. The table provides the initial jacking load and the load before release. The jacking load is the maximum load applied to the CFRP bars by the hydraulic pump during the prestressing operation. The load was mechanically locked to the prestressing steel frame, and the pump was moved to the next bar. During prestressing of the other bar, there was a slight loss in the prestressing force of the seated bars as a result of the elastic shortening of the prestressing steel frame. After completion of the prestressing operation on the four bars, the concrete casting was performed the next day. The load before release (F_i), or the initial prestressing stress (f_i), is the longitudinal force/stress in the CFRP bars just before release of the prestress force was begun. The loss in the prestressing stress between the jacking and the initial pretressing involves a loss due to the locking mechanism, seating of the anchor system, early relaxation in the CFRP bars, and elastic shortening in the prestressing steel fame. Shrinkage in concrete also will contribute to changing the initial prestressing force. Detailed discussion of these losses is beyond the scope of this work.

The prestressing load was measured and monitored by means of load cells, which were mounted at the ends of each prestressed bar. While the target prestressing stress for each group was the same, small variations in the prestressing force at jacking existed within each group. The reasons for this variation can be attributed to the fine control of the hydraulic electric pump system and the interaction between the prestressed bars during the prestressing operation. The test results were analyzed based on the actual prestressing load for each beam, which eliminated the effect of the variation in the target force.

Table 5.1 Prestressing data and average concrete compressive strength results

Group/ Beam labels		Nominal prestressing level	Jacking		Before release		Concrete compressive strength, MPa	
			Load F_j, kN	Stress f_j, MPa	Force, F_i kN	Stress, f_i MPa	At release	At 28 days
I	S30-1	30	77.6	612.5	72.0	568.3	30.4	62.1
	S30-2		76.1	600.6	70.0	552.5		
	S30-3		92.0	726.1	82.0	647.2	41.0	49.6
	S30-4		82.0	647.2	79.0	623.5		
II	S45-1	45	102.2	806.6	96.8	764.1	35.0	70.9
	S45-2		112.0	884.0	103.2	814.5		
	S45-3		106.6	841.3	100.9	796.4		
	S45-4		102.0	805.1	96.3	760.1		
III	S60-1	60	124.1	979.5	121.7	960.5	30.4	62.1
	S60-2		139.0	1097.1	130.0	1026.0		
	S60-3		127.7	1007.9	121.0	954.7	41.0	49.6
	S60-4		133.3	1052.1	127.1	1003.2		
IV	N30-1	30	80.4	634.6	73.7	582.0	37.0	64.5
	N60-2	60	148.0	1168.1	141.0	1112.9		
	N60-3		142.0	1120.8	134.3	1060.3		
	N60-4		146.1	1153.1	139.5	1101.3		

5.3 Transfer Length Results

Two methods were used to estimate the transfer length: concrete strain profile and draw-in methods. The transfer length results of all prestressed beams based on the two methods are presented and discussed below.

5.3.1 Concrete Strain Profile Method

Concrete longitudinal profile measurement was done on two beams from each cast. The process of measurement and calculation of the longitudinal strain were presented in detail in Chapter 3. The concrete strain profile was determined for a total of nine beams out of sixteen prestressed beams. Demec gauge measurements were taken at the casting location and prior to moving the beams, to avoid any disturbance or strain change due to the weight of the beams. The method involves calculation and plotting the longitudinal concrete strain profile. Then, the average maximum strain (AMS) was

calculated for each beam. The AMS is the average longitudinal concrete strain at the level of the prestressing bar with the plateau region of the beam. A line representing 95% of the AMS is drawn. The transfer length is estimated as the distance from the end of the beam to where the longitudinal concrete strain profile line crosses the 95% AMS line. The longitudinal strain profile and estimated transfer length are presented and discussed below.

Figures 5.1 and Figure 5.2 show the longitudinal strain profile due to the release of the prestressing force of one beam from each prestress level for both SCC and NVC, respectively. For both cases, as expected when the prestressing force decreased, the longitudinal strain values decreased; however, the rate of decrease was not linear for SCC specimens. The 95%AMS of beam S30-1 was 257 με, for Beam S45-2 was 276 με, and for Beam S60-1 was 374 με. All other beams made of SCC showed similar strain patterns. The results revealed that the concrete strains in SCC beams were higher than those in NVC beams at the same prestressing stress level. The 95% AMS of SCC beams prestressed to 60 % ranged between 360 to 390 με and for NVC beams prestressed to the same level were between 220 and 250 με. Similarly, at a 30% prestress level, the 95% AMS of SCC specimens were between 240 to 275 με and for NVC specimens ranged from 170 to 200 με. The ratio of the longitudinal strains of SCC beams to that of NVC beams prestressed to the same level ranged between 1.4 and 1.6. This finding is possibly due to SCC having a lower modulus of elasticity than the NVC. Even though the early modulus of elasticity of the concrete has not been tested, results of the modulus of elasticity of hardened concrete showed that the SCC had a modulus of elasticity of 27.8, 22.7 and 30.6GPa for SCC-mix1, SCC mix-2 and SCC mix-3, respectively. The modulus of elasticity of the NVC mix was found to be 37.4GPa. It is expected that similar difference between the modulus of elasticity of the SCC mixes and the NVC mix may still exit during the prestressing force release. Thus, SCC showed larger values of compression strain than the NVC specimens did.

Table 5.2 gives a summary of the transfer length results based on the longitudinal strain profile. For a prestress level of 60% the transfer length of CFRP bars in SCC ranged between 610 mm and 750 mm, while in NVC beams, it ranged between 550 mm and 620 mm. On average, the transfer length was 14% longer in SCC than in NVC. At a 30% prestress level, the transfer lengths of the CFRP bars in SCC ranged from 340 to 370mm, while in the NVC beams they were between 290 and 310mm. On average, the transfer length in SCC was about 15% longer than in NVC. It is evident that as the prestressing force was increased from 30% to 60%, the transfer lengths of the CFRP bars in SCC beams increased significantly. Results show that generally the transfer length at the live end was slightly larger than that at the dead end for the same beam. The increase in transfer length in live end could be a result of the dynamic impact of releasing the CFRP bar.

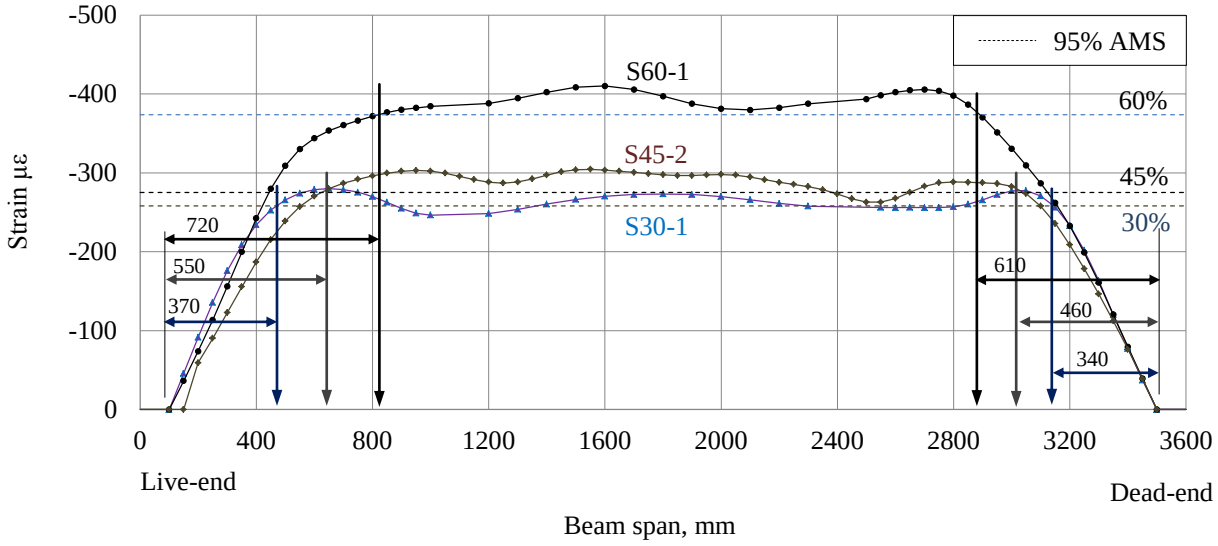

Figure 5.1 Longitudinal concrete strain profiles due to release of prestressing force in SCC Beams S30-1, S45-2, and S60-1

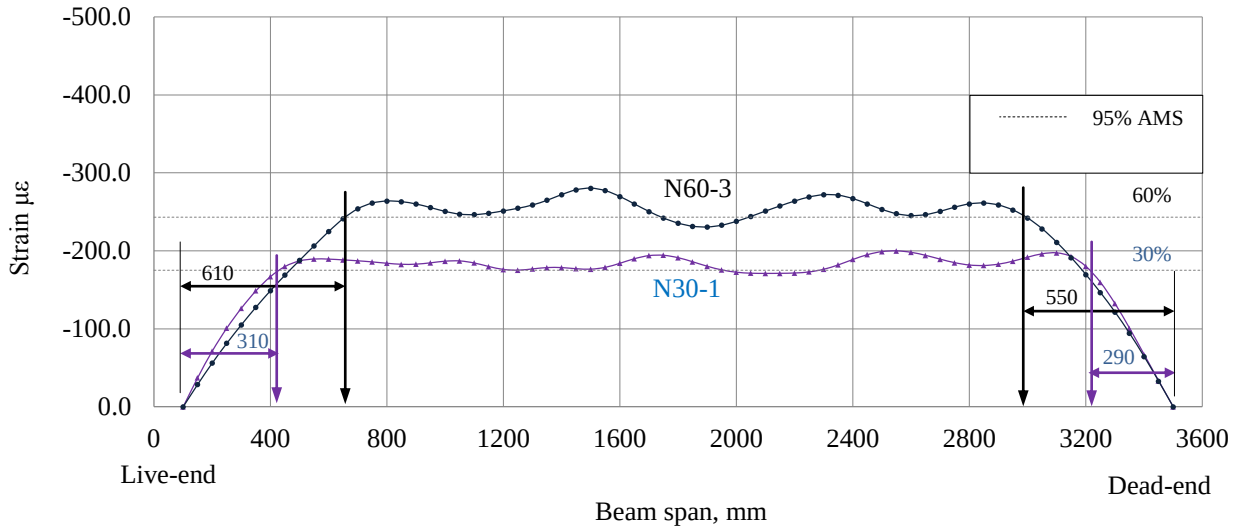

Figure 5.2 Concrete strain profiles due to release of prestressing force in NVC Beams N30-1 and N60-3

The average bond stresses within the transfer length were calculated based on the initial prestress levels and the experimentally measured transfer length for each side of the beam using Eqn (5.1) and presented in Table 5.2. The results show that average bond stresses in NVC beams were higher than the bond stresses in SCC beams at similar prestressing levels. More in-depth analysis of the bond stresses is provided in Sections 5.3.4 and 5.3.5.

$$u_t = \frac{f_i \ A_b}{\pi \ d_b \ l_t} \qquad (5.1)$$

Where

u_t is the average bond stress over the transmission zone due to prestress force release, MPa;

f_i is the initial prestressing, MPa;

A_b is the prestressing bar cross section area, mm^2; and

d_b is the prestressing bar diameter, mm; and

l_t is the experimentally measured transfer length, mm.

Table 5.2 Transfer length results – concrete strain profile method

Group/Beam label		Initial stress, f_i MPa	Live end		Dead End		Average transfer length, mm
			Transfer length, mm	Average bond stress, MPa	Transfer length, mm	Average bond stress, MPa	
I	S30-1	568.3	-	-	-	-	-
	S30-2	552.5	370	4.74	340	5.16	355
	S30-3	647.2	-	-	-	-	-
	S30-4	623.5	-	-	-	-	-
II	S45-1	764.1	-	-	-	-	-
	S45-2	814.5	550	4.70	460	5.62	505
	S45-3	796.4	520	4.86	540	4.68	530
	S45-4	760.1	-	-	-	-	-
III	S60-1	960.5	720	4.23	610	5.00	655
	S60-2	1026.0	-	-	-	-	-
	S60-3	954.7	750	4.04	640	4.74	695
	S60-4	1003.2	730	4.36	630	5.05	650
IV	N30-1	582.0	310	5.96	290	6.37	300
	N60-2	1112.9	-	-	-	-	-
	N60-3	1060.3	610	5.52	550	6.12	580
	N60-4	1101.3	620	5.64	560	6.20	590

- No measured data

5.3.2 Draw-in Method

When the prestressed CFRP bar was released, the prestressing force was transferred to the concrete by the bond between the CFRP prestressed bar and the concrete. The transfer length is the distance required to accommodate deformation equal to the measured slip in the CFRP bar relative to the concrete as a result of releasing the initial prestressing force. As described in Chapter 3, the CFRP bar had an unbonded length of 100mm at both ends of all beams. The LVDTs used to measure the draw-in displacement were fastened 70mm away from the beam end surface. The deformations of the prestressed CFRP bar due to prestress release in the short unbonded length were included in the LVDT reading. The shortening of the unbonded bar portion was subtracted from the total displacement measured by the LVDTs to obtain the net draw-in displacement. The shortening in length of the unbonded bar portion was calculated using the actual initial prestressing stress and the geometric and mechanical properties of the CFRP bar, using Equation 5.2. The net draw-in displacements are presented in Table 5.3. The calculated transfer lengths values are given in the same table. The modulus of the elasticity of the CFRP bars used in the calculations was 144GPa as reported by the manufacturer; test results by Soudki (2010) showed that the average measured modulus of elasticity of similar bars was 146.3GPa. Average bond stresses were calculated for the live end and dead independently using Eqn. (5.1) and the results are tabulated in the Table 5.3.

$$\Delta_{net} = \Delta_{LVDT} - \frac{f_i}{E_{cfrp}} l_{un} \qquad (5.2)$$

Where

Δ_{net} is the net draw-in displacement, mm;

Δ_{LVDT} is the total measured displacement by LVDT, mm;

f_i is the initial prestressing stress, MPa;

E_{cfrp} is the modulus of elasticity of the CFRP bar; and

l_{un} is the total unbonded length of the CFRP bar between the LVDT clamp point to where the CFRP bars is bonded.

Table 5.3 gives the net draw-in, transfer length and average bond stress of both live and dead ends of all beams. Similar to the concrete strain profile method, the transfer length results showed that SCC specimens experienced a longer transfer length than to the NVC specimens did at similar initial prestress levels. At a 60% prestress level, the average transfer length of CFRP bars in SCC ranged between 629 mm and 733 mm, while for NVC beams it ranged between 478 mm and 527 mm. At a 30% prestress level, only one NVC had draw-in method measurements. The results from these beams

showed that the average transfer length of the CFRP bars in SCC ranged between 259 mm and 337 mm, as compared to 250 mm in NVC beams. The result of the bond stresses calculation showed that the average bond stress of the CFRP bar in NVC was higher than that in the CFRP bar in SCC by about 24% and 40% at prestressing levels of 30% and 60%, respectively. Also, the results clearly confirm that the average bond stresses decreased as the initial prestress increased, for both types of concrete; however, the decrease was steeper in the SCC beams than in the NVC beams (Table 5.3). The average bond stress dropped by about 25% when the prestress level increased from 30% to 60% in SCC, as compared to about 9% in the case of the NVC beams. More discussion on the bond stress behaviour is presented in Section 5.3.4.

Table 5.3 Experimental transfer length results –draw-in method

Group/ Beam label		f_i, MPa	Net draw-in, mm		Live end		Dead end		Average transfer length, mm
			Live end	Dead end	l_t, mm	u_t, MPa	l_t, mm	u_t, MPa	
I	S30-1	568.3	1.478	0.604	749**	-	306	5.90	306
	S30-2	552.5	0.443	0.549	231	7.59	286	6.13	259
	S30-3	647.2	0.784	0.730	349	5.89	325	6.32	337
	S30-4	623.5	0.688	0.697	318	6.22	322	6.15	320
II	S45-1	764.1	1.393	1.438	525	4.62	542	4.48	534
	S45-2	814.5	1.406	1.374	497	5.20	486	5.32	492
	S45-3	796.4	1.432	1.327	518	4.88	480	5.27	499
	S45-4	760.1	1.320	1.251	500	4.83	474	5.09	487
III	S60-1	960.5	2.164	2.351	649	4.70	705	4.32	677
	S60-2	1026.0	2.572	2.647	722	4.51	743	4.38	733
	S60-3	954.7	2.105	2.062	635	4.77	622	4.87	629
	S60-4	1003.2	2.508	2.323	720	4.42	667	4.77	694
IV	C30-1	582.0	0.539	0.469	267	6.63	232	7.63	250
	C60-2	1112.9	2.075	1.994	537	6.58	516	6.85	527
	C60-3	1060.3	1.826	1.932	496	6.79	525	6.41	511
	C60-4	1101.3	1.908	1.747	499	7.01	457	7.65	478

** This value is not included in the average value calculation

5.3.3 Comparison of the results from concrete strain profile and draw-in measurement

Both concrete strain profile and draw-in methods showed similar trends of experimental to prediction ratio. However, the concrete strain profile method gave slightly higher transfer length values than the

draw-in method did possibly because the draw-in method assumes that the CFRP bar stress development varies linearly from zero at the beam end to the full effective prestressing stress at the end of the transfer length. On the other hand, the longitudinal concrete strain profile, which is based on Demec point measurements, showed that the stress profile trends to be nonlinear, with a reduced stress gain close to the end of the transfer length. Furthermore, concrete strain profile is based on experimental measurements while the draw-in method is based on experimental measured draw-in displacement and the mechanical properties of the prestressing CFRP bar.

5.3.4 Concrete type effect on the transfer length

The measured results from both methods are plotted versus the initial prestressing stress in Figure 5.3. It is evident that as the prestressing level increases, the transfer length of CFRP bars in SCC shows a slightly nonlinear trend with the prestress level. At a 30% prestress level, both types of concrete showed similar values of transfer length. As the prestressing level increased, the transfer length of the SCC beam increased in a non-linear fashion. The NVC specimens kept a linear relationship between the transfer length and the prestressing level. The transfer length at a 60% prestress level of the SCC specimens was about 1.25 that of the NVC specimens. A possible explanation of this trend is in the difference in the stress-strain behaviour of SCC versus NVC at early ages. SCC mixes had larger paste volume and increased admixture dosage as compared to NVC mix which results in a change in the microstructure of concrete matrix especially the interfacial zone between the prestressed CFRP bars and concrete. SCC exhibited higher compressive strain values than NVC did at similar prestressing force (see Figures 5.1 and 5.2). The low early modulus of elasticity of SCC could be an indication of a slow bond strength development in the SCC mixes. More research is needed to verify this hypothesis. NVC specimens showed a linear relationship between the transfer length and the prestressing level.

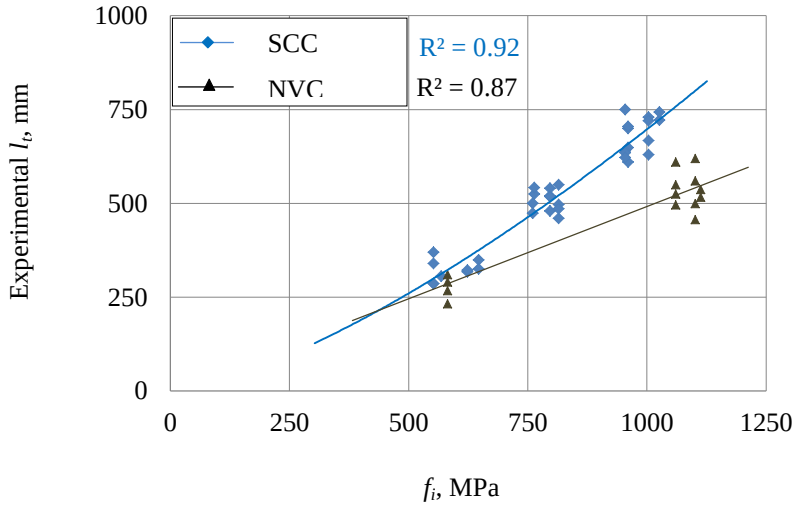

Figure 5.3 Transfer length results of SCC and NVC specimens

5.3.5 Immediate prestress loss and bond stress analysis along the transmission zone

The development of prestressing stress within the transmission zone is crucial for shear design and serviceability analysis of the prestressed flexural members. In this section, the stress development in the prestressed CFRP bars is presented and analyzed. The strain gauge data were used to determine the prestress loss, longitudinal prestressing stress profile before and after load release and the bond stress profile along half of the beam length.

5.3.5.1 Immediate prestress loss

The immediate loss in the initial prestressing stress due to load release was calculated based on the average drop in the three strain gauges located close to midspan of the beam. The strain gauges were located at 1050mm, 1350mm, and 1800mm from the beam end. The strain readings used to estimate the prestress loss were taken just before release, the initial prestressing force, and about two hours after the release process of the prestressing force. A summary of the prestress losses and the effective prestress for all the beams is presented in Table 5.4.

Table 5.4 Prestress data: initial prestress, immediate loss and the effective prestressing stress

Group/ Beam labels		Initial Prestress, f_{pi}, MPa		Average strain gauge readings, με		Immediate Prestress loss, %	Effective prestress f_{pe}, MPa
		nominal	Actual	Before release(1)	After release(1)		
I	S30-1	30	568.3	3864	3739	3.23	549.9
	S30-2		552.5	3763	3643	3.20	534.8
	S30-3		647.2	4733	4581	3.21	626.4
	S30-4		623.5	4239	4112	3.00	604.8
II	S45-1	45	764.1	5290	5194	1.80	750.3
	S45-2		814.5	5587	5448	2.48	794.3
	S45-3		796.4	5583	5444	2.49	776.6
	S45-4		760.1	5353	5224	2.41	741.8
III	S60-1	60	960.5	6742	6547	2.89	932.7
	S60-2		1026.0	7210	6994	2.99	995.3
	S60-3		954.7	6729	6486	3.60	920.3
	S60-4		1003.2	7122	6915	2.90	974.1
IV	N30-1	30	582.0	4159	4024	3.23	563.2
	N60-2	60	1112.9	8680	8391	3.32	1076.0
	N60-3		1060.3	8157	7895	3.20	1026.4
	N60-4		1101.3	8340	7973	4.39	1052.9

(1) Average of the three strain gauges at 1050, 1350 and 1800mm

5.3.5.2 Longitudinal stress and bond stress profile along the transfer zone

Typical longitudinal stress profiles before and after prestress force release and bond stress profiles from each group are shown in Figures 5.4 to 5.7. Stresses in the prestressed CFRP bar were calculated using measurements from the strain gauges mounted along the bar.

Figures 5.4 (a), 5.5 (a) and 5.6 (a) compare the effect of the prestressing level on the tensile stress profile of the CFRP bar in the SCC specimens. Before release, the prestress stress profile was almost constant along the beam length. The tensile profile exhibited nonlinear stress development along the transmission zone after release of the prestress force. The general shape of the tensile stress development of the CFRP bar in SCC is similar for all prestress levels, except that as the prestress level increased, the tensile stress development occurred over a longer length.

Figures 5.4 (b), 5.5 (b) and 5.6 (b) show the bond stress profile after release of a typical SCC beam prestressed to 30%, 45% and 60%, respectively. The bond stress was zero at the free end (100mm from the beam end) and increased sharply to its peak value very close to the beam ends. Then the bond stress gradually dropped to zero toward the midspan of the beam. The peak bond stress recorded for the 30% prestress level was 7.71MPa, and at 45% prestress, it was 6.46MPa, and at 60% prestress it was 6.30MPa. This finding indicates that the transfer length has a nonlinear relationship with the pretressing stress within the range of this study. The nonlinearity of the stress development supports the finding of the transfer length results.

Figure 5.7 shows the tensile stress and bond stress profiles for NVC specimen N60-4. The tensile stress profile was similar to that of SCC specimen but had a shorter transfer length. The peak bond stress recorded for Specimen N60-4 was 7.55MPa, which is 20% higher than that of a similar SCC specimen (S60-4).

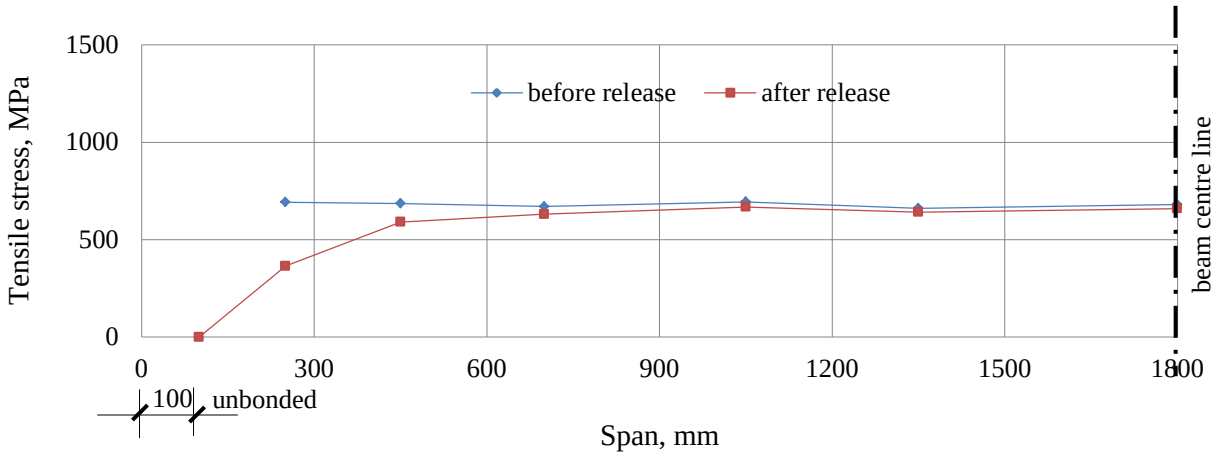

(a) Longitudinal tensile stresses profile in the CFRP bar

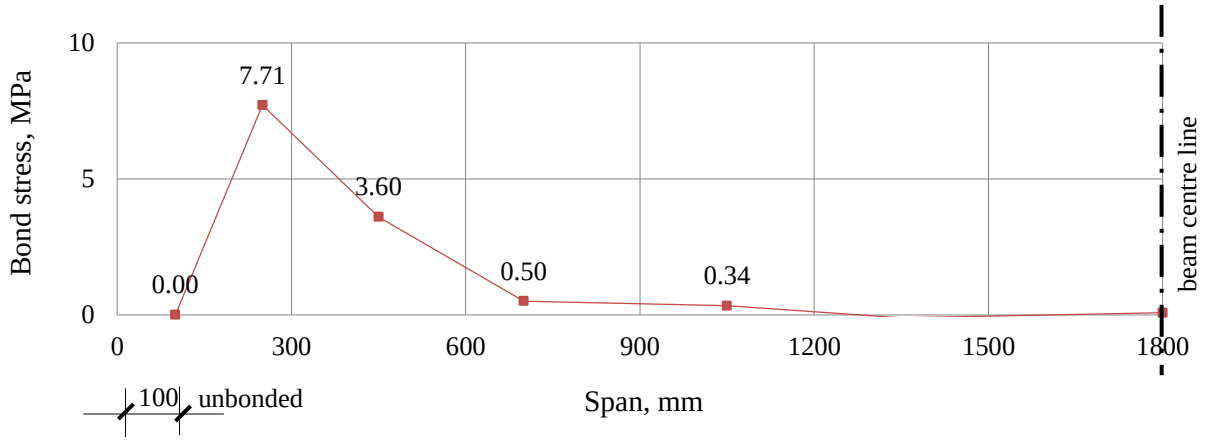

(b) Bond stress profile after release

Figure 5.4 Longitudinal tensile and bond stresses of Beam S30-3

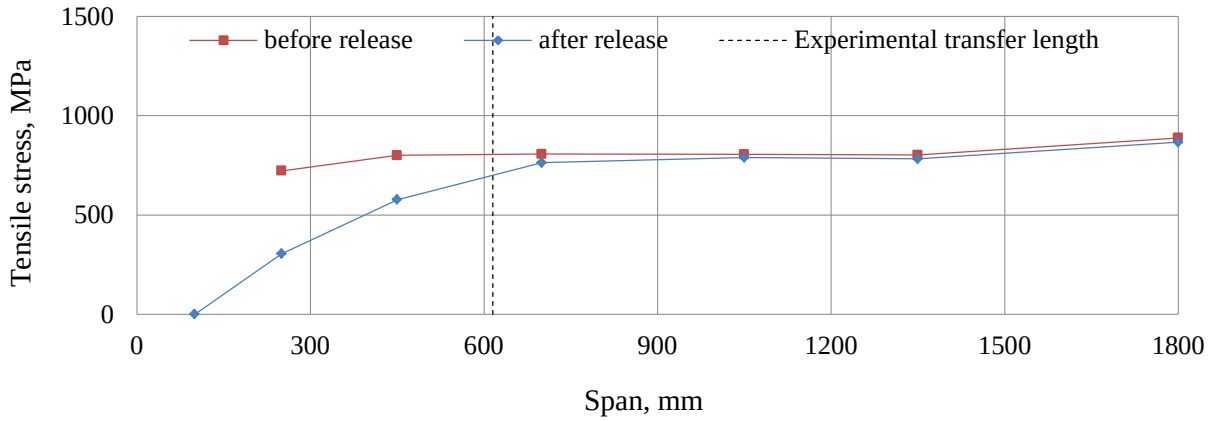

(a) Longitudinal tensile stress profile in the CFRP bar

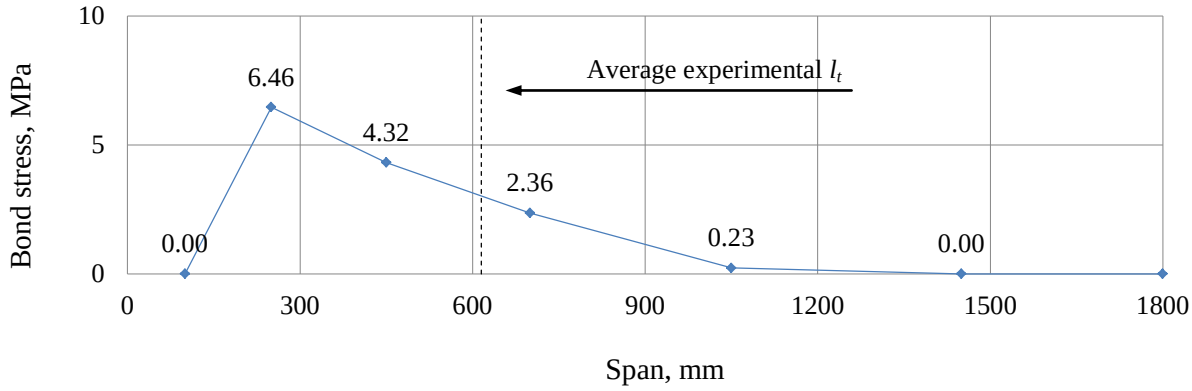

(b) Bond stress profile after release

Figure 5.5 Longitudinal tensile and bond stresses of Beam S45-3

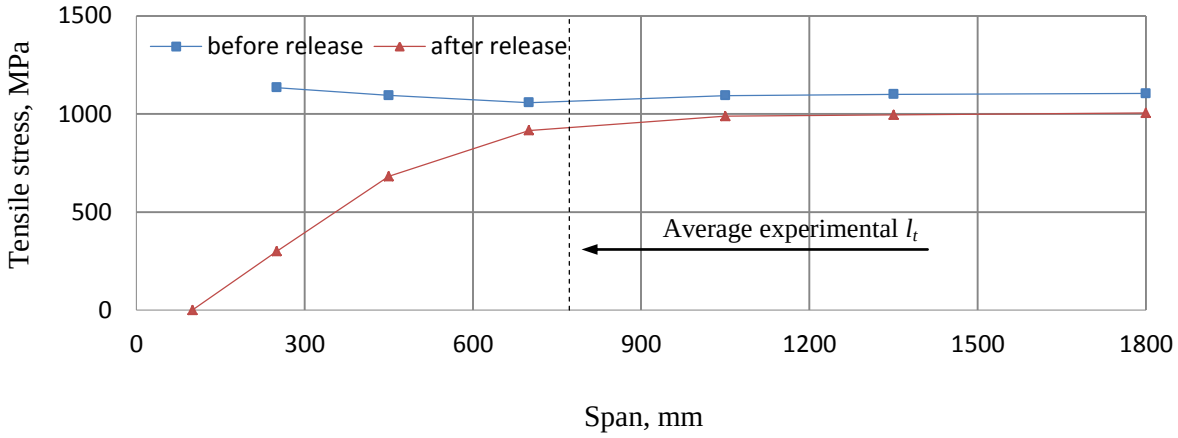

(a) Longitudinal tensile stress profile of the CFRP bar

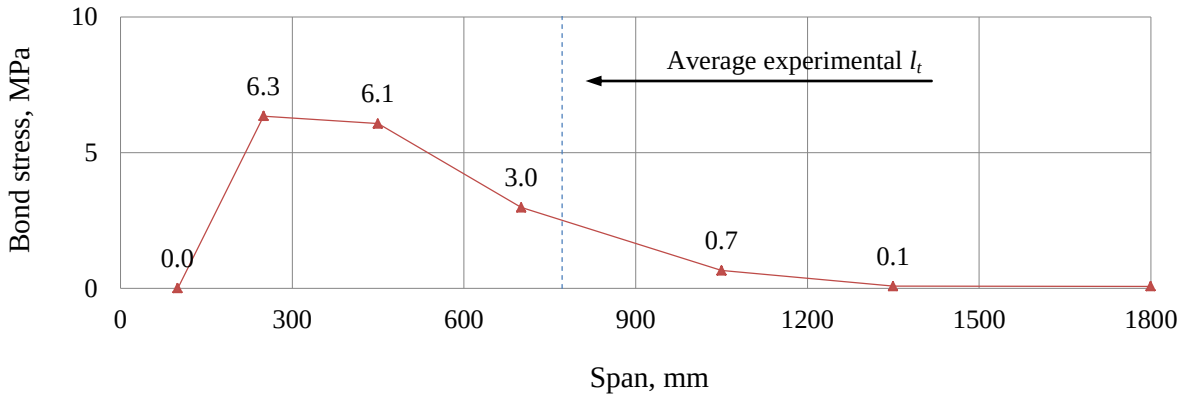

(b) Bond stress profile after release

Figure 5.6 Longitudinal tensile and bond stresses of Beam S60-4

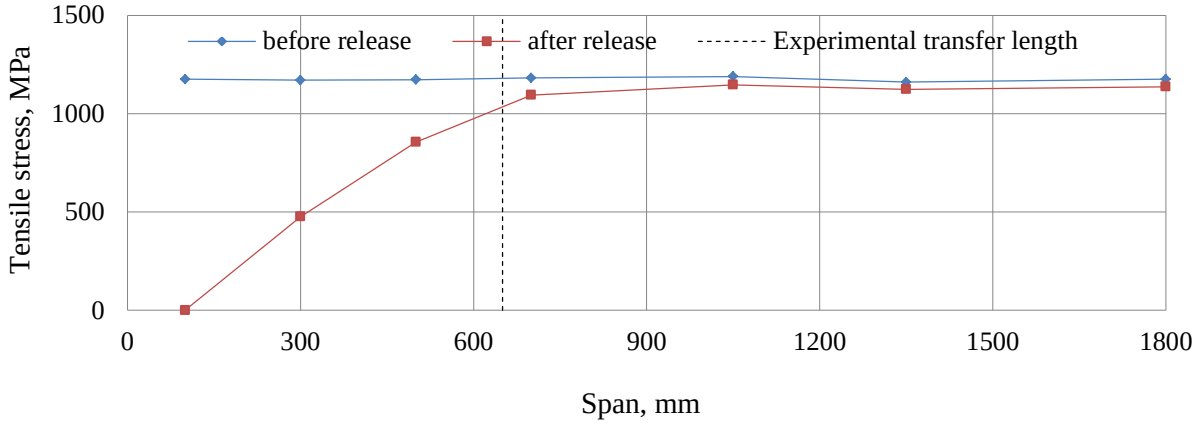

(a) Longitudinal tensile stress in the prestressed CFRP bar

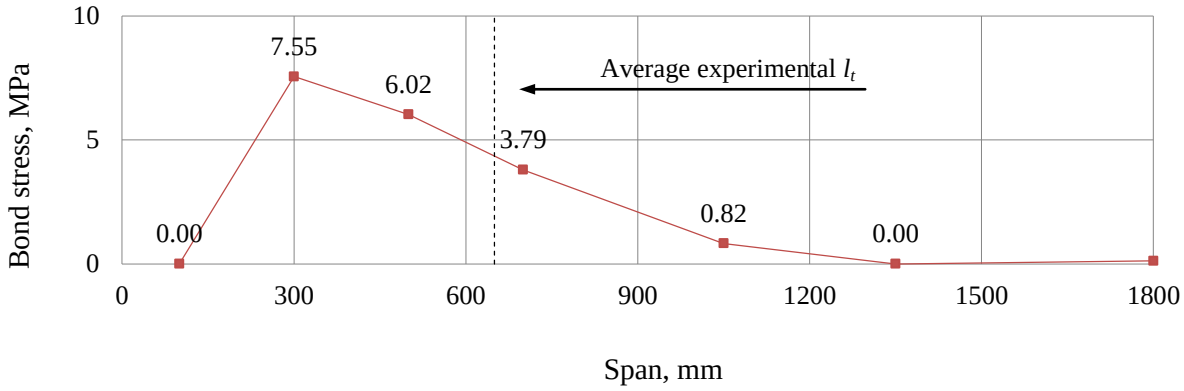

(b) Bond stress profile after release

Figure 5.7 Longitudinal tensile and bond stresses of Beam N60-4

5.3.6 Average bond stress along the transmission zone of SCC beams

Tables 5.2 and 5.3 give the average bond stress results based on the concrete strain profile and draw-in method, respectively. The average bond stresses of the CFRP bar in SCC were calculated using the actual initial prestressing stress and the average experimental transfer length for each beam. The results show that the average bond stress decreased as the prestressing level increased. The effect of the concrete compressive strength at release and the prestressing level are discussed in the following.

(a) Effect of Concrete Compressive Strength

Figure 5.8 is a plot of the bond stress data versus the concrete strength at transfer raised to the power of 0.67. The data plotted are for two prestress levels (30% and 60%) and two concrete compressive strengths (30.4MPa and 41.0 MPa). Because the results had only two groups of points of the concrete compressive strength, the relationship between the bond stress and f_{ci} cannot be, ideally, assessed; however, based on the data available, the bond stress to concrete compressive strength at transfer to the power of 0.67 is relatively constant. Therefore, the concrete compressive strength of this range had no significant effect on the bond stress of the CFRP bars in SCC. This finding differs from what reports in the literature that the bond stress of CFRP bars varies linearly with $f_{ci}^{0.67}$ in NVC.

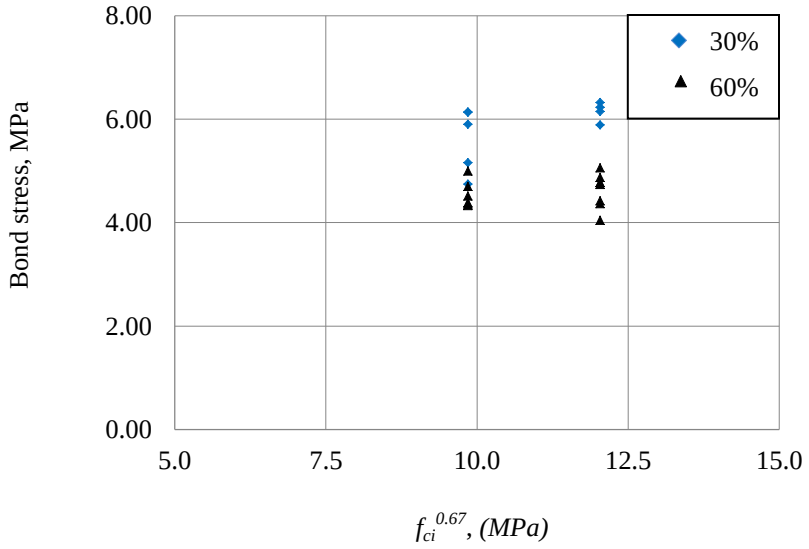

Figure 5.8 Bond stress of CFRP bar in SCC versus fci$^{0.67}$

(b) Effect of the Prestressing Level

Figure 5.9 shows the relationship between the normalized bond stress and initial prestressing stress. The normalized bond stress was taken as the average bond stress divided by $f_{ci}^{0.67}$ to account for

differences in the concrete compressive strength at transfer. The data shown in Figure 5.9 includes all transfer length results at the live end and dead end based on the two measurement methods. It is evident from Figure 5.9 that the average bond stress decreases as the prestressing level increases.

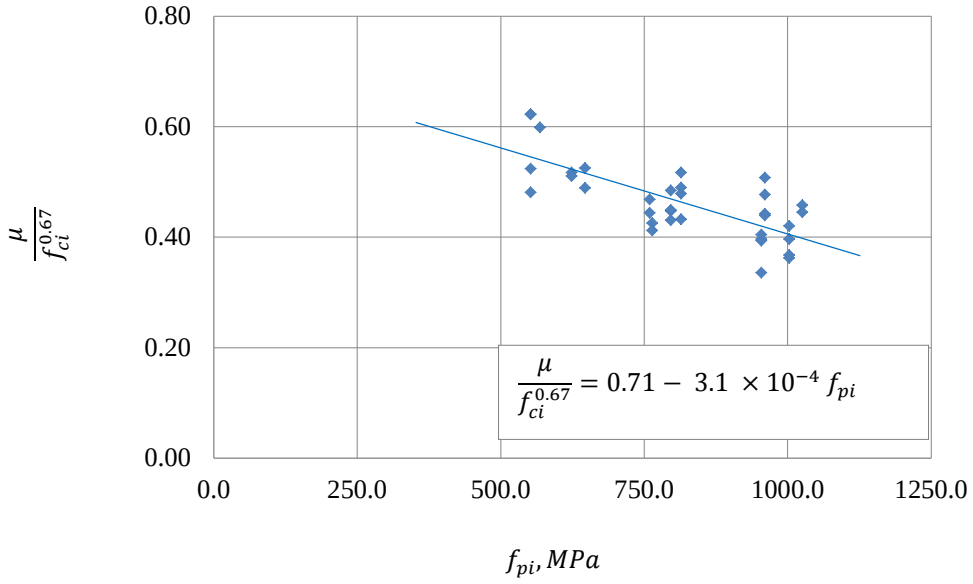

Figure 5.9 Normalized bond stress of CFRP bar in SCC versus initial prestressing stress

A linear relationship was used as the best fit curve for the normalized bond stress data versus the initial prestress in SCC as given in Eqn. (5.3). This approach is consistent with the bond equation used for NVC specimens. The linear relationship provided an acceptable fit with R^2 of 0.72. It should be noted that there was no improvement for the higher degree relationship between the normalized bond stress and the initial prestress of this data. Also, this relationship is valid within the prestressing limits in this study. While this range is the most widely used in construction, this relationship needs to be verified for other prestressing ranges.

$$\frac{\mu_t}{f_{ci}^{0.67}} = 0.71 - 3.1 \times 10^{-4} f_{pi} \qquad (5.3)$$

Where

f_{pi} is the initial prestressing stress, MPa;

μ_t is the average bond stress due to prestress load release, MPa; and

f_{ci} is the concrete compressive strength at release.

5.4 Flexural test results of the prestressed beams

All beams were subjected to four point static flexural testing. The load, midspan deflections, strain on the prestressed CFRP bar at various locations, strain of the concrete compression fiber at midspan, and end slip at both sides were recorded during the tests. Cracks were also monitored and marked. Test results and analysis of the obtained data are presented in the following sections.

5.4.1 Modes of failure

Two modes of failure were recorded: bond pullout failure and bar rupture failure. The bar rupture mode of failure can be simply defined and distinguished from other types of failure: the prestressed bar suddenly ruptures and the applied load drops to zero instantly. This failure was associated with a loud "ping" cracking sound. Figure 5.10 shows a typical bar rupture mode.

Bond pullout failure is defined when a slippage of 0.25mm was recorded at the unloaded end of the prestressed bar. This limit for pullout failure mode has been set by ASTM A882/A882M (1992) and used by other researchers (Zaki et al. 1996). When the bar pullout was initiated, a loud noise occurred, and the applied load dropped to a lower value (residual strength). The noise continued to occur while the beam continued to resist loading at a reduced stiffness. The beam was able to sustain and carry more loads at relatively reduced stiffness. The slippage appeared as a snap step-like-behaviour on the moment vs. deflection responses. These steps vary from one beam to the other. For small slippage, a second larger peak load value could be measured. However, in some cases, where a significant load drop occurred, the load was maintained at lower values before a complete failure occurred. In some cases, a slip value of above 5mm was recorded before complete failure occurred. Several prestressed CFRP bars were visually inspected after testing by cutting transverse concrete slices from the beam at selected locations. Then, a longitudinal cut was done to cut the CFRP bar in half. The results of this autopsy revealed two main findings. First, the bond failure occurred between the sand coating layer and the fibre interface of the CFRP bar. Second, the slippage was initiated within the transmission zone when the bond stress waves that result from loading approached the CFRP bar in the transmission zone. The bond failure between the sand coating and the fibers in the CFRP bar was common in the bond pullout failure cases. The beam continued to take load while the debonding of the CFRP bar propagated inwards to the constant moment region. Figure 5.11 shows a typical bond pullout failure mode. More analysis of the bond stress interaction due to prestress load release and flexural testing is presented and discussed in Section 5.4.4.

(a) Beam S45-4 before testing

(b) Just after failure

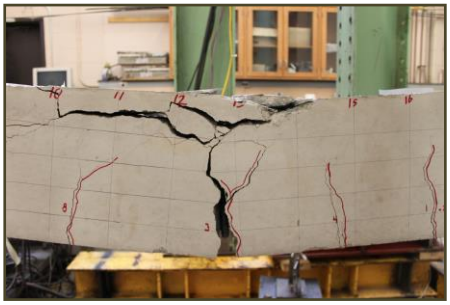

(c) Close view of the failure zone

(d) Concrete slice showed the CFRP bar still in complete contact with concrete

Figure 5.10 Typical bar rupture mode of failure, Beam S45-4

(a) Beam S60-2 before testing

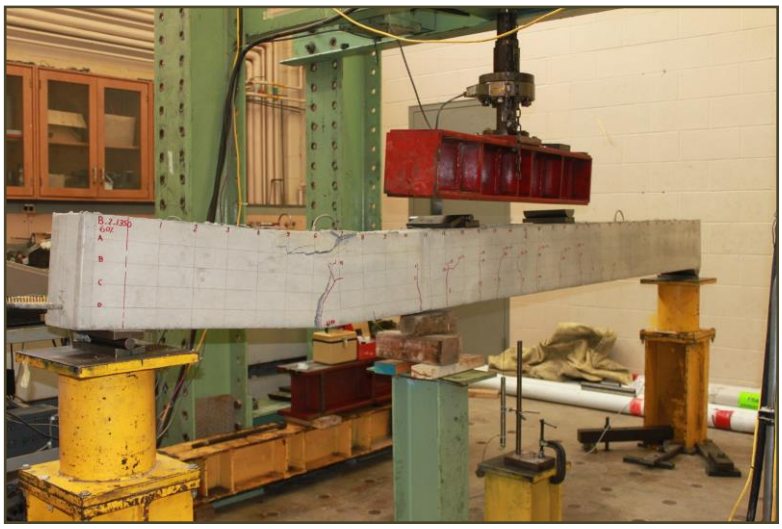

(b) Beam S60-2 after testing. Pullout bond failure occurred at the end of the transmission zone

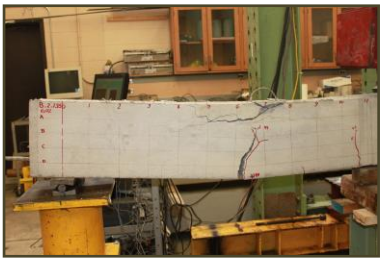

(c) Close view of the region of failure

(d) Cut off slices showing the bond failure

Figure 5.11 Bond pullout failure mode, Beam S60-2

The location of the failure crack for these two failure modes (bar rupture vs. bond failure) is clearly different. Typically, the bar rupture mode of failure occurred within the constant moment region or, less commonly, under one of the applied load points. In the case of bond failure, the flexural crack closest to the end of the transfer zone or between the ends of the transmission zone to the point of the applied load continued to widen significantly during the slippage of the CFRP bar from the concrete. The beams that failed by bond pullout showed a rigid body motion at the failure crack location (Figure 5.11 (b)).

A few beams exhibited combined modes of failure. The failure initiated as bond failure then the prestressed bar ruptured. No shear failure or concrete crushing was recorded as the main cause of failure.

5.4.2 Moment deflection responses

Table 5.5 gives a summary of the flexural test results. The moment and deflection values at initial cracking and at failure and the modes of failure are reported in this table. It should be noted that the deflection values do not include camber values. Also, the moment does not include moment due to the beam own weight. Two beams exhibited combined modes of failure, S30-2 and S60-4. In these beams, the failure started as pullout; however, during slippage, the beam was able to take additional load, and bar rupture occurred. Beam S30-4 had premature bar rupture mode of failure. The CFRP bar ruptured at low tensile stresses. This beam is one of the two beams that experienced bar cracking noises during the prestressing operation. The results of this beam are not discussed further in this chapter. The theoretical analysis showed that the ultimate moment capacity is 42.5kN.m. Experimental results showed that beams which failed by bar rupture slightly exceeded the theoretical moment capacity.

The average cracking moment was increased as the prestressing level increased, as expected. The average cracking moments of SCC beams prestressed to 30%, 45% and 60% were 11.5kN.m, 16.8kN.m and 18.4kN.m, respectively. The cracking moments of NVC beams prestressed to 30% and 60% were 10.5 and 18.7kN.m, respectively. The direct comparison might not be accurate due to the differences in concrete compressive strength and the slight differences in the effective prestressing force.

Table 5.5 Flexural test results

Group	Beam label	Shear span, mm	Cracking		Failure		Type of failure
			Moment, kN.m	Deflection, mm	moment, kN.m	Deflection, mm	
I	S30-1	1100	12.8	3.7	16.7	11.9	Pullout
	S30-2	1250	10.7	3.6	42.4	69.2	Rupture
	S30-3	1350	10.1	3.1	33.9	52.5	Pullout/Rupture
	S30-4	1500	12.5	3.6	17.8	25.4	Rupture*
II	S45-1	1100	17.1	4.7	34.0	35.9	Pullout
	S45-2	1250	16.8	4.6	36.8	35.7	Pullout
	S45-3	1350	14.6	3.4	36.9	31.5	Pullout
	S45-4	1500	18.7	3.7	43.5	40.6	Rupture
III	S60-1	1100	16.7	5.1	26.3	12.9	Pullout
	S60-2	1350	22.9	5.2	31.4	19.2	Pullout
	S60-3	1500	16.9	4.9	26.7	21.2	Pullout
	S60-4	1700	17.2	6.3	33.2	22.3	Pullout/rupture
IV	N30-1	1350	10.5	4.2	42.3	68.8	Rupture
	N60-2	1250	20.9	4.1	29.4	12.5	Pullout
	N60-3	1350	17.5	3.6	44.6	48.5	Rupture
	N60-4	1500	17.9	3.9	43.7	49.4	Rupture

* This beam failed by premature bar rupture failure. The flexural test results of this beam were excluded from any further discussion

The moment-deflection response of all beams showed a bilinear behaviour with a smooth transition between the two segments. Figures 5.12 to 5.15 show flexural test results of Groups I, II, III and IV, respectively. The initial linear part of the curve had a steep slope, which corresponds to the uncracked stiffness. In the second part, the beam stiffness decreased as a result of flexural cracking. As the loading increases, the flexural cracks propagate upward slowly due to the prestressing effect. The two types of failure modes, bar pullout, bar rupture, were recorded. No concrete crushing failure occurred; however, in some cases, the concrete crushed after excessive slippage and large deflections. Beams that failed by pullout bond failure showed a gradual degradation of the moment while the bar continued to slip.

Group I consists of four SCC beams with CFRP bars prestressed to 30% prestress level. Figure 5.12 shows the test results of Group I. Beam S30-1, which has a shear span of 1100mm, failed due to bond

at an applied moment of 16.7kN.m. When the shear span was increased to 1250mm, Beam S30-2 failed due to bar rupture at an applied moment of 33.9kN.m. This moment was less than predicted section capacity; yet the bar ruptured at a tensile stress less than guaranteed tensile strength. When the shear span was increased to 1350mm, the beam was able to attain section capacity; however, the bar slipped at a tensile stress very close to the guaranteed tensile strength. When the shear span was increased to 1500mm, the beam failed by premature bar rupture. Both Beams S30-2 and S30-4 experienced cracking sound during the pretressing operation. The results from Beam B30-04 were not included in the bond stress analysis and the development length equation formulation; but the results from Beam S30-2 were considered in the analysis. The results from Beam S30-2 fit the general trend of an increase in moment capacity with increase in the shear span. Test results of Group I suggest that the development length should be between 1350mm and less than 1500mm.

Group II are SCC beams prestressed to 45%. Group II results followed the expected trend: the moment capacity increased as the shear span was increased (Figure 5.13). The first three beams, S45-1, S45-2 and S45-3 failed due to bond pullout and the moment increased from 34.0kN.m to 39.0kN.m when the shear span was increased from 1100mm to 1350mm. Beam S45-4 with a shear span of 1500mm failed by bar rupture at an applied moment of 43.5kN.m. The test results of Group II suggest that the development length should be very close to 1500mm.

Group III are SCC beams prestressed to 60%. In Group III (Figure 5.14) Beams S60-1, S60-2 and S60-3 failed due to pullout bond failure while Beam S60-4 had combined bond/flexure mode of failure. The failure in this beam initiated due to bond pullout failure; however, shortly after slippage initiated, bar rupture occurred. Also, this beam had noticeable stiffness loss when the moment exceeded 38kN.m No end slip was recorded at this moment. The possible explanation of this response is that there was local slippage within the transmission zone. Therefore, the development length of this type of the CFRP bar prestressed to 60% falls above 1700mm.

Group IV are beams made from NVC with one beam (N30-1) prestressed to 30% and the three other beams prestressed to 60%. Test results of this group are shown in Figure 5.15. Beam N30-1 was tested at a shear span of 1350mm and failed due to bar rupture at an applied moment of 43.6kN.m. Beam N60-2 had a shear span of 1250mm and failed by bond pullout failure at an applied moment of 29.4kN.m. Beam N60-4 failed by bar rupture at an applied moment of 44.6kN.m. No improvement in failure moment was recorded when the shear span was increased to 1500mm. In fact, Beam S60-4 was tested before Beam S60-3. Otherwise, Beam S60-4 should be tested at a shear span less than 1350mm.

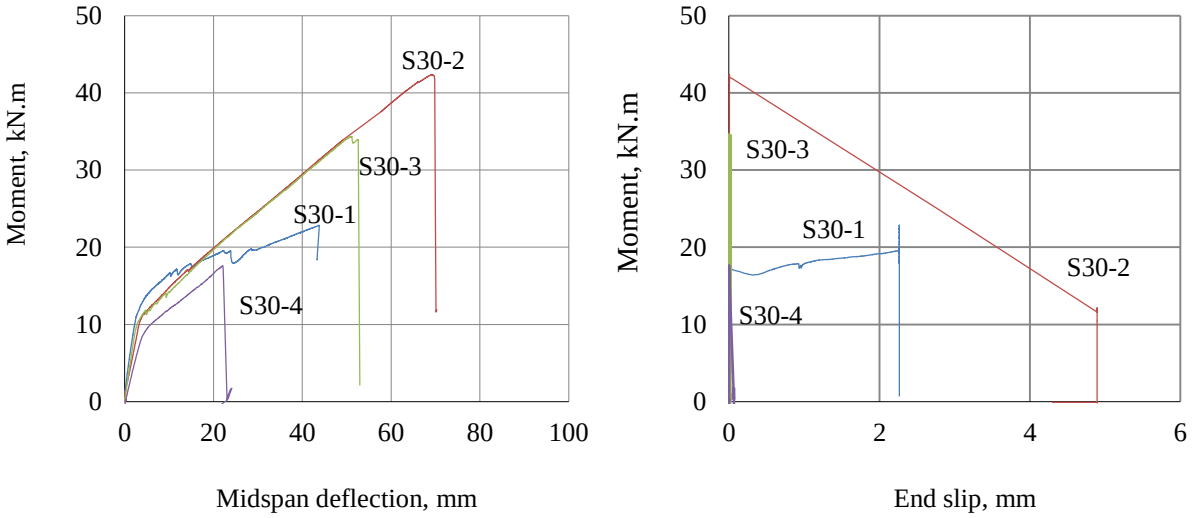

(a) (b)

Figure 5.12 Flexural test results of Group S30, (a) Moment–deflection responses, (b) Moment – end slip responses

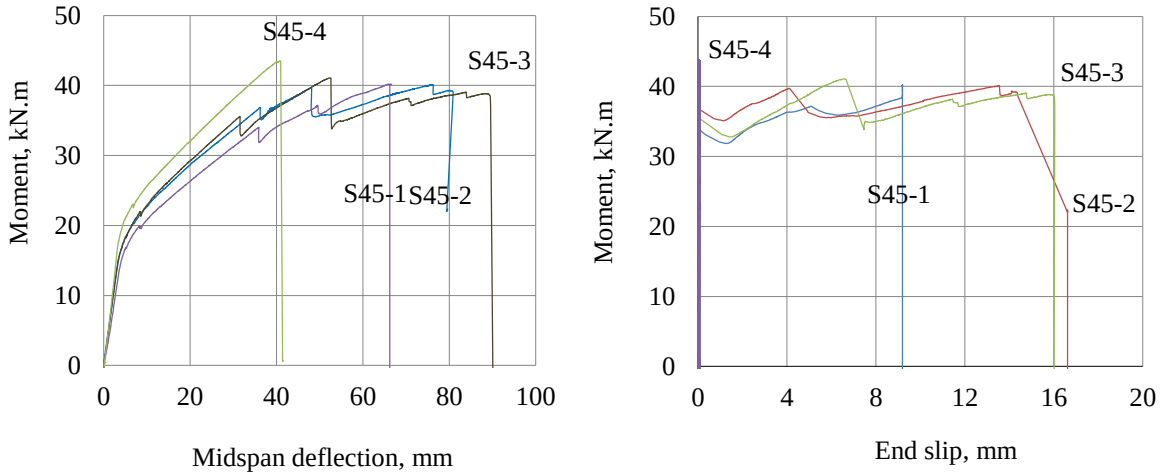

(a) (b)

Figure 5.13 Flexural test results of Group S45, (a) Moment–deflection responses, (b) Moment – end slip responses

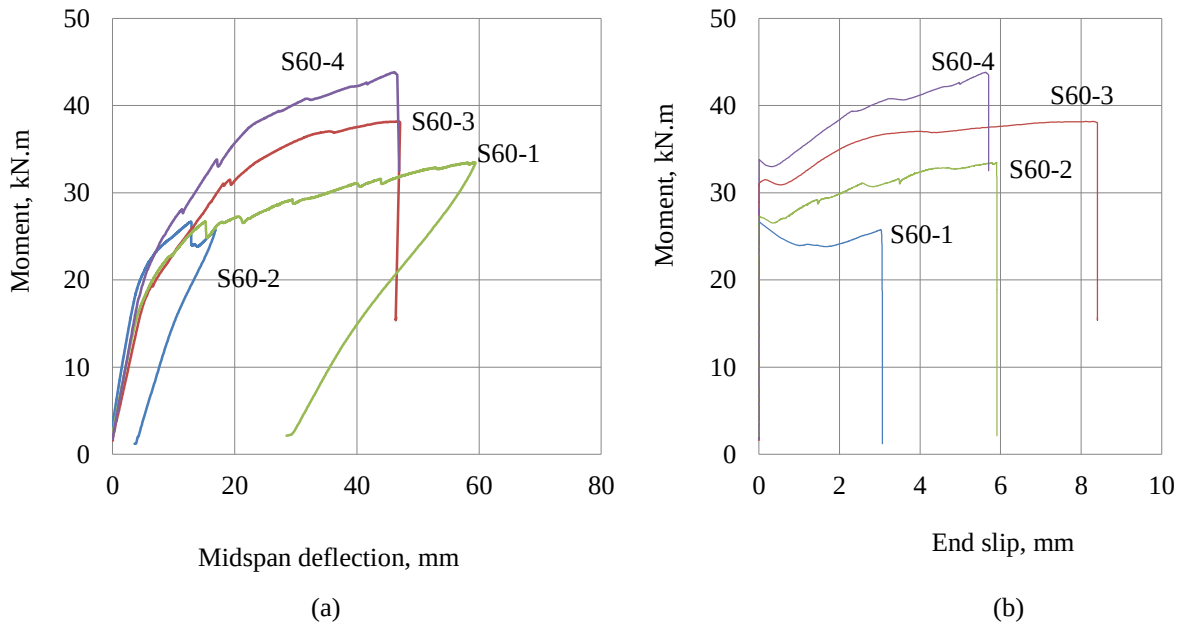

Figure 5.14 Flexural test results of Group S60, (a) Moment–deflection responses, (b) Moment – end slip responses

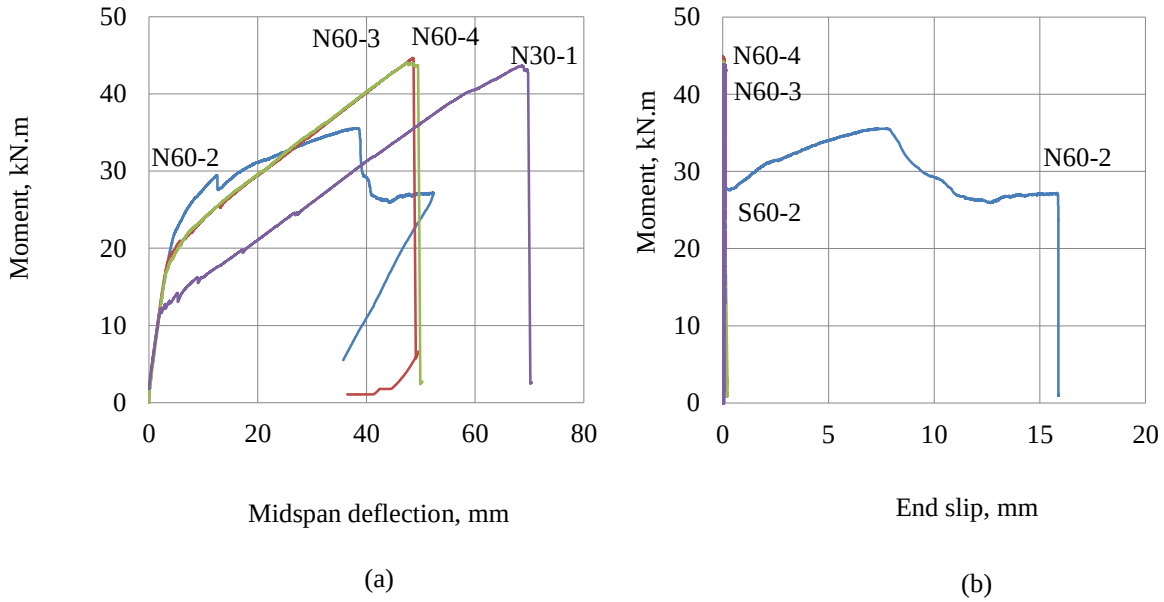

Figure 5.15 Flexural test results of Group N60, (a) Moment–deflection responses, (b) Moment – end slip responses

5.4.2.1 Effect of the prestressing level on the flexural behviour of SCC beams prestressed with CFRP bars

To assess the effect of the prestressing level, beams that failed due to bar rupture were compared. Figure 5.16 shows the flexural responses of Beams S30-3, S45-3 and S60-4. The deflection was normalized to the deflection of Beam S30-3, and the moment was normalized to failure moment of the same beam. The normalized deflection here is important to eliminate the effect of differences in the shear span on the deflections. The results showed that when the initial prestress increased from 30% to 45%, the deflection was decreased to 60% of the beam prestressed to 30%. Beam S60-4 had a bond pullout failure before bar rupture and this affected the deflection; however, based on the stiffness after cracking, the deflection was decreased to less than 50% when the prestress increased from 30% to 60%.

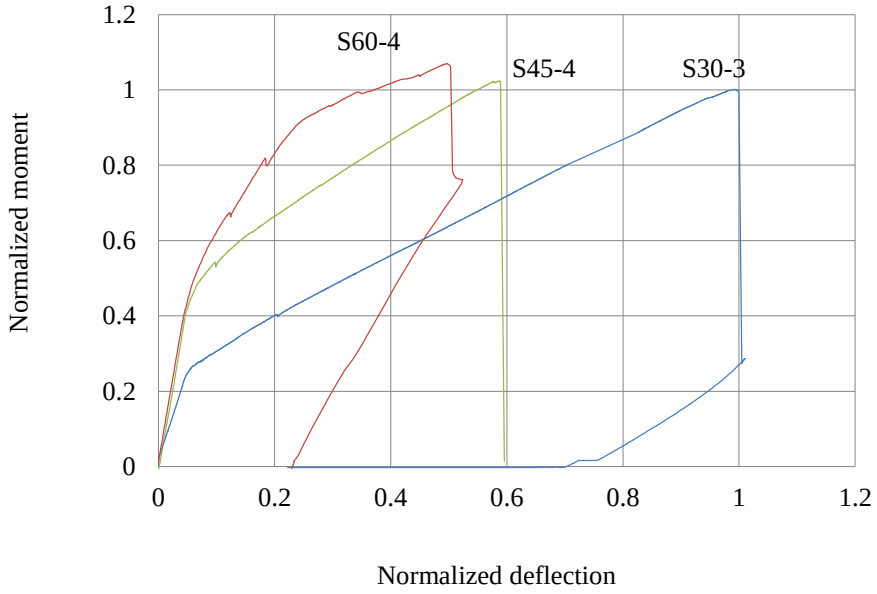

Figure 5.16 Effect of prestressing level on flexural responses of SCC specimens

5.4.2.2 Effect of the SSC on the flexural behviour of CFRP prestressed beams

To assess the effect of SCC on the flexural behaviour, SCC and NVC beams of same prestress level and tested at same shear span length were compared. Figure 5.17 (a) shows a comparison between Beams S30-3 and N30-1. Both of these two beams were prestressed to 30% and tested at a shear span of 1350mm. The flexural behaviour of these two beams was almost identical. There was no effect of

using SCC concrete on the flexural behviour. It is also important to mention here that the concrete compressive strength of Group I and Group IV were very similar: 62.1 MPa for the SCC specimens and 64.5MPa for the NVC specimens.

Figure 5.17 (b) compares of two beams prestressed to 60% and tested at a shear span length of 1350mm. Beam S60-3 was made from SCC and Beam N60-3 from NVC. The comparison here is limited due to the fact that Beam S60-3 failed before bar rupture due bond pullout failure. However, based on the segment of the curve before the slip failure occurred, the SCC specimen showed a slightly stiffer response after cracking. The reason could be related to the higher concrete compressive strength of 70.9MPa for the SCC compared to 64.5MPa for the NVC specimens. Therefore, SCC beams had a similar flexural response to the NVC specimens.

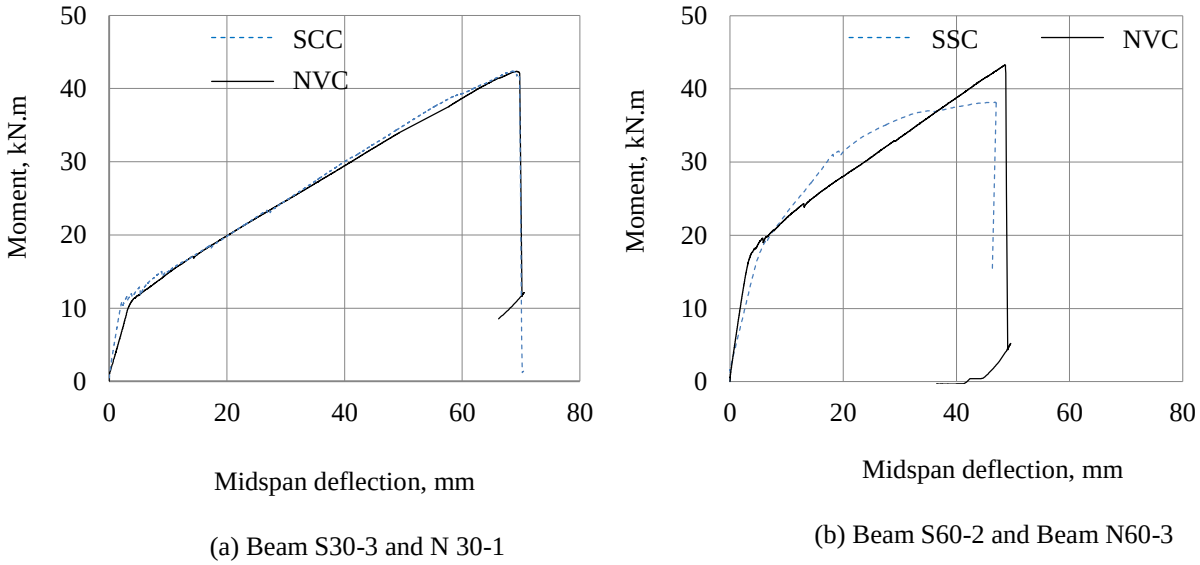

(a) Beam S30-3 and N 30-1

(b) Beam S60-2 and Beam N60-3

Figure 5.17 Flexural test responses comparison between SCC and NVC specimens

5.4.3 Longitudinal tensile stress development and bond stress profile

Stress development during the flexural test was monitored by means of strain gauges, which were distributed along the transfer length and flexural bond length. The tensile stress and bond stress development within the shear span was calculated based on the strain measurements. Figures 5.17 to 5.20 show the strain gauge locations, the tensile stress profile and bond stress profile at various applied moments for selected specimens.

Figure 5.18 shows the tensile stress and bond stress profiles of Beam S45-3 during the flexural test. The beam failed by bond pullout. The tensile stress in the prestressed CFRP bar decreased within the transfer length zone as the load was increased up to failure. When the slip initiated at an applied moment of 32.8kN.m, the tensile stress dropped to nil at the first strain gauge location (150mm from support) indicating that the bar debonded at that location. As the load increased, the reduction in the tensile stress in the bar progressed toward the midspan of the beam indicating further debonding of the bar with increased slip. The bond stress followed a similar pattern. There was no increase in bond stresses within transfer zone due to flexural loading. When the load reached the peak (35.5kN.m), the CFRP bar was not able to take any bond stresses within the transfer zone to resist the applied moment and the beam failed by bond pullout failure. Initially the bond stress peaked close to beam free end then dropped linearly towards midspan. As the load was increased and slip initiated, the peak bond stress moved inward with further debonding of CFRP bar with the transfer zone at onset of failure. This finding explains the observed failure cracks. All beams failed by bond pullout failure, the failure cracks were located very close to the end of the transfer zone.

Figure 5.19 shows the tensile stress and bond stress profiles for Beam S45-4 that failed by bar rupture. There was no increase in tensile or bond stress of the CFRP bar in the transfer zone due to flexural loading; however, the tensile stresses in the CFRP bar continued to increase within the flexural bond length. Due to the sufficient flexural length available in this beam, the bond stresses were able to provide the required anchorage for the prestressed CFRP bar and the beam failed due to bar rupture.

Figure 5.20 shows the tensile stress and bond stress profiles for Beam S60-4. Beam failure was initiated by bond pullout. Due to the flexural bond length available, the failure began with bond pullout but eventually the bar ruptured. The longitudinal tensile stress profile for the CFRP bar showed that there were losses in the tensile stresses as the slippage stated, but the flexural bond stresses were still effective and the beam was able to take load until the CFRP bar ruptured.

Beams made with NVC followed a similar pattern as SCC beams; however, the bond stress values were slightly larger and the rupture of the CFRP bars was reached at shorter embedment length. Figure 5.21 show the tensile stress and bond stress profiles of the CFRP bar for Beam N60-3. This beam was tested at a shear span of 1350mm and it failed by bar rupture. There was no increase in bond stress within the transfer length during the flexural loading.

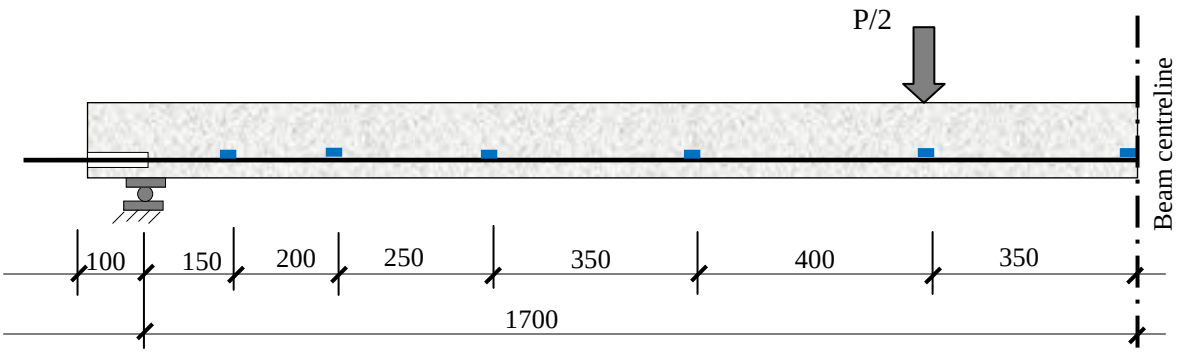

(a) Schematic shows the testing layout and the strain gauge locations

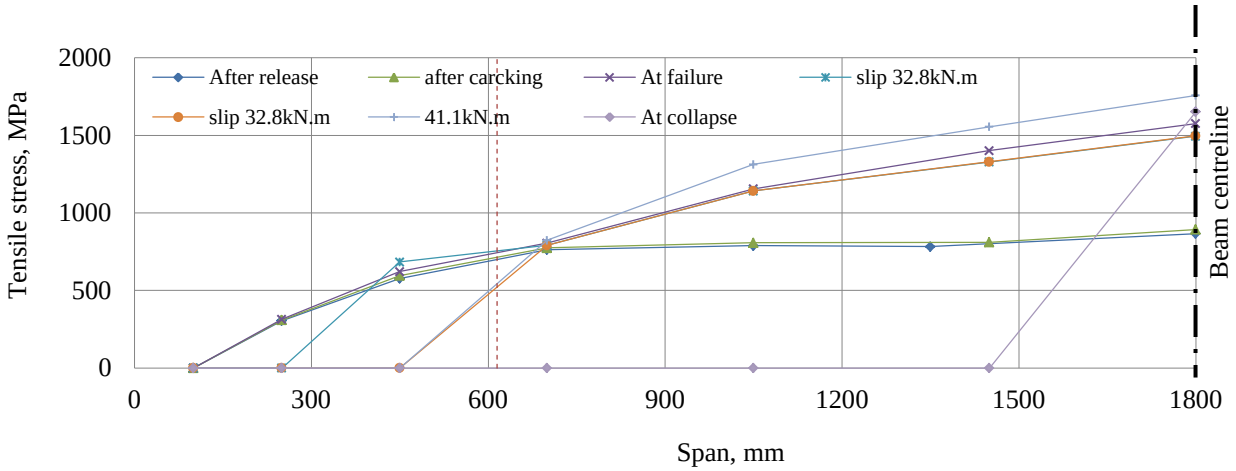

(b) Tensile stress in the prestressed CFRP bar

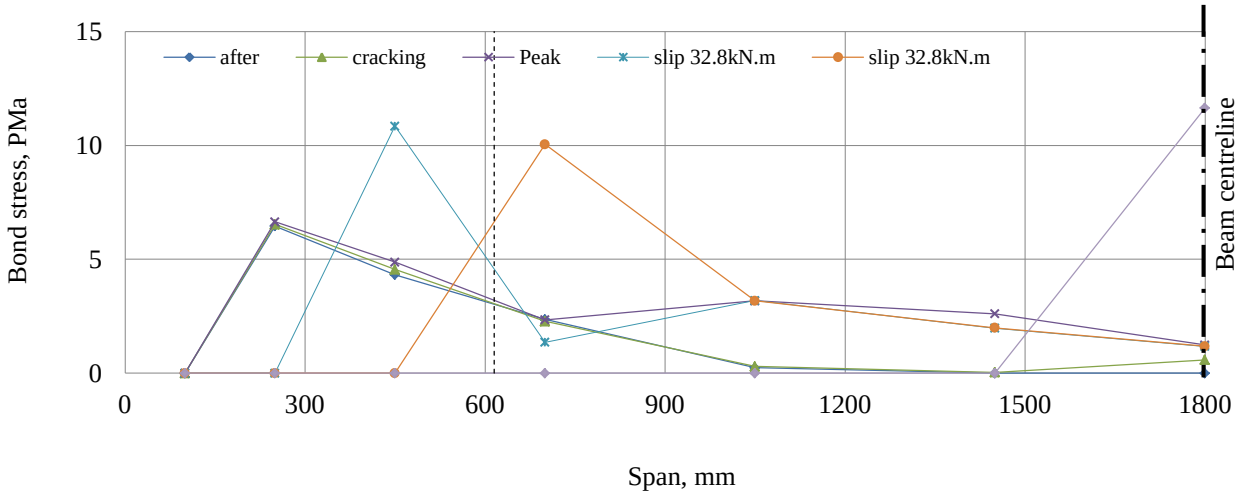

(c) Bond stress development due prestress release and flexural test

Figure 5.18 Tensile and bond stress development in the prestressed CFRP bars during the flexural test of Beam S45-3, shear span is 1350mm, and beam failed by pullout bond failure

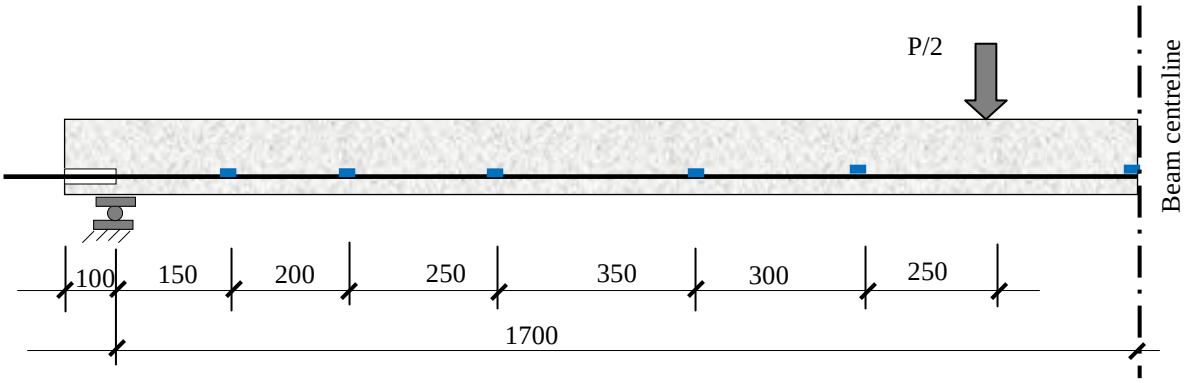

(a) Schematic shows the testing layout and the strain gauge locations

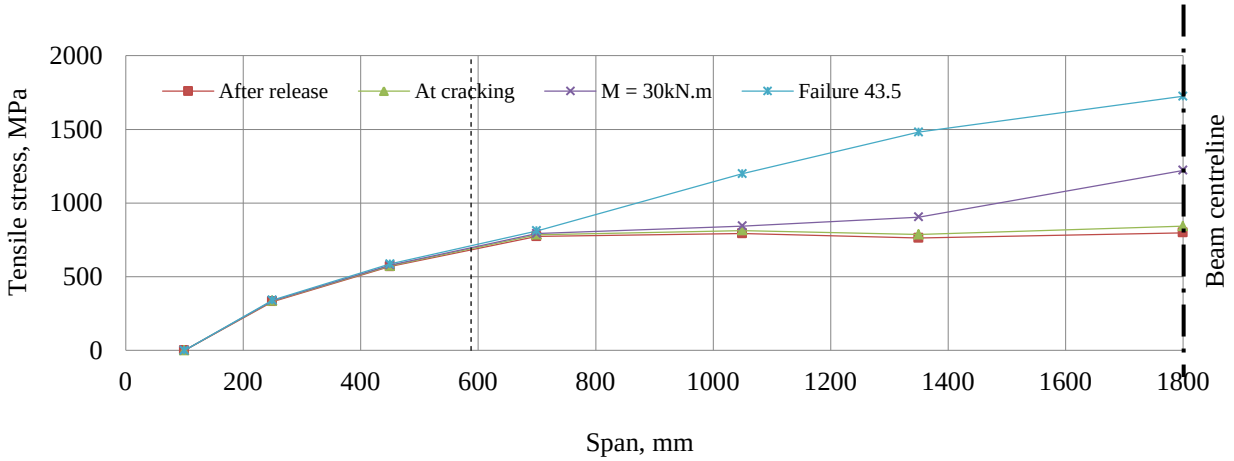

(b) Tensile stress in the prestressed CFRP bar

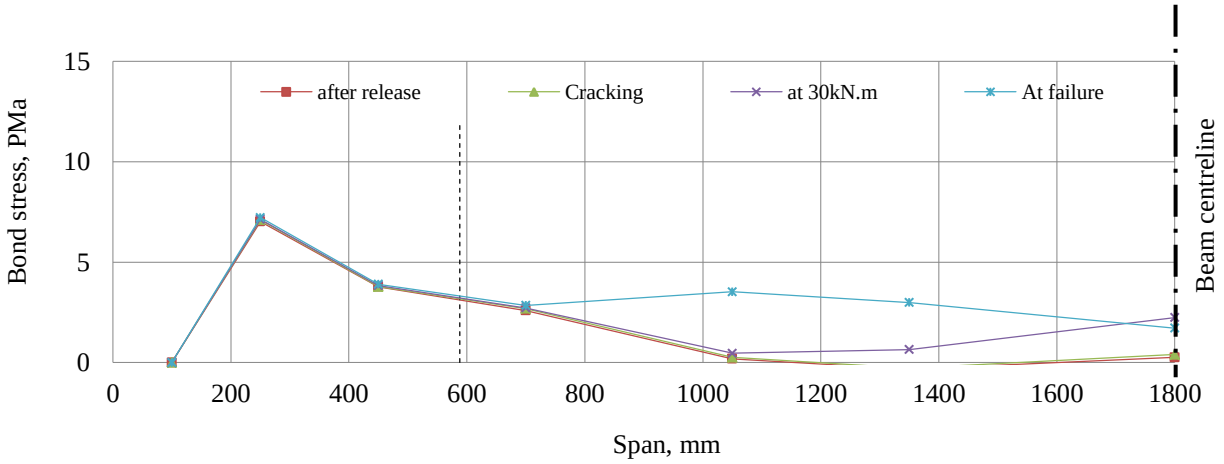

(c) Bond stress development due prestress release and flexural test

Figure 5.19 Tensile and bond stress development in the prestressed CFRP bars during the flexural test of Beam S45-4, shear span is 1500mm, and beam failed by pullout bond failure

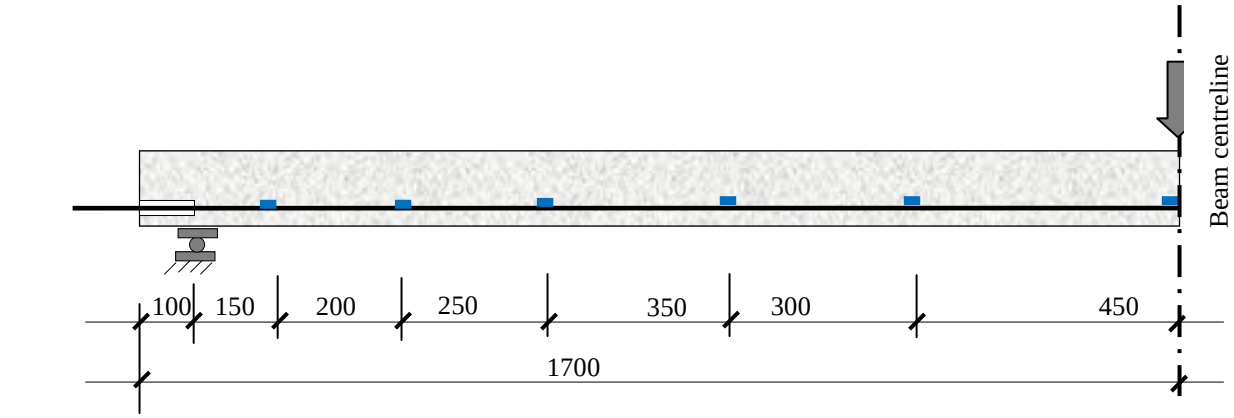

(a) Schematic shows the testing layout and the strain gauge locations

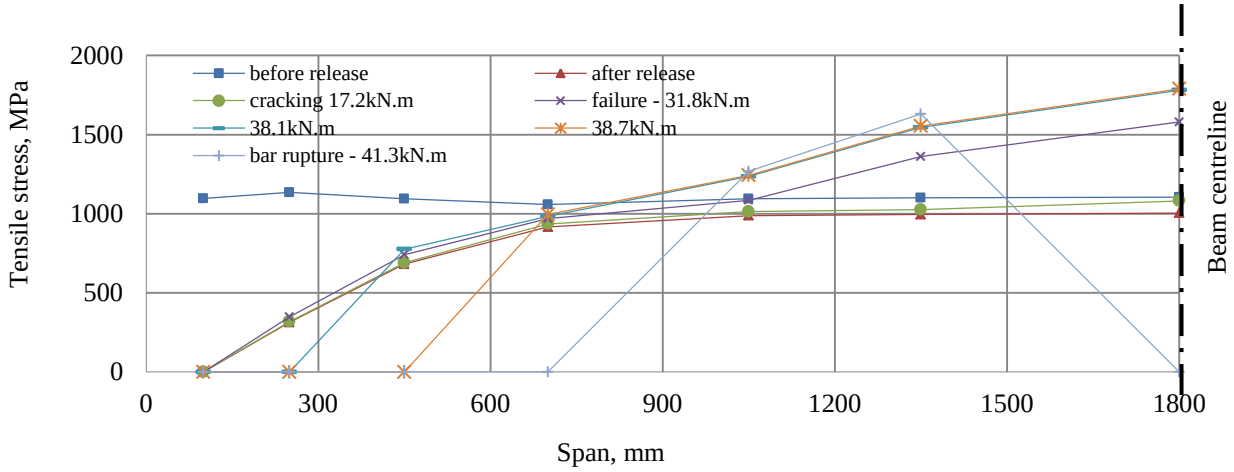

(b) Tensile stress in the prestressed CFRP bar

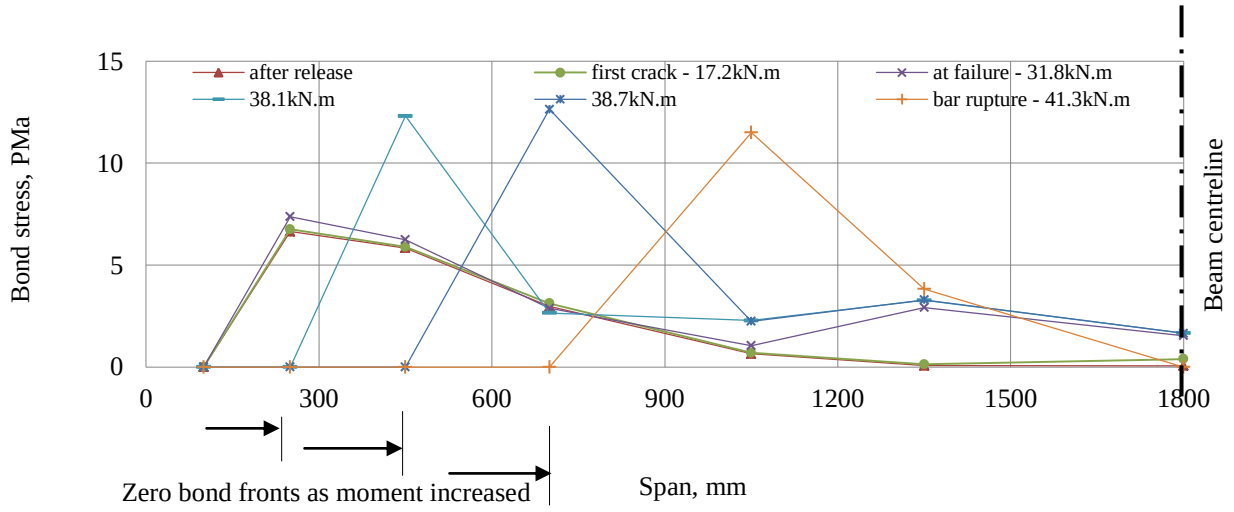

(c) Bond stress development due prestress release and flexural test

Figure 5.20 Tensile and bond stress development in the prestressed CFRP bars during the flexural test of Beam S60-4, shear span is 1700mm, and beam failed by pullout bond failure

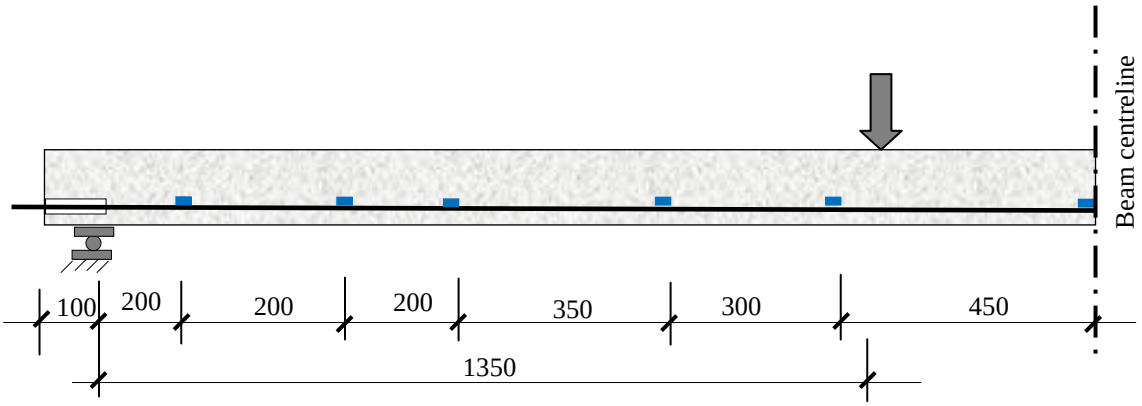

(b) Schematic shows the testing layout and the strain gauge locations

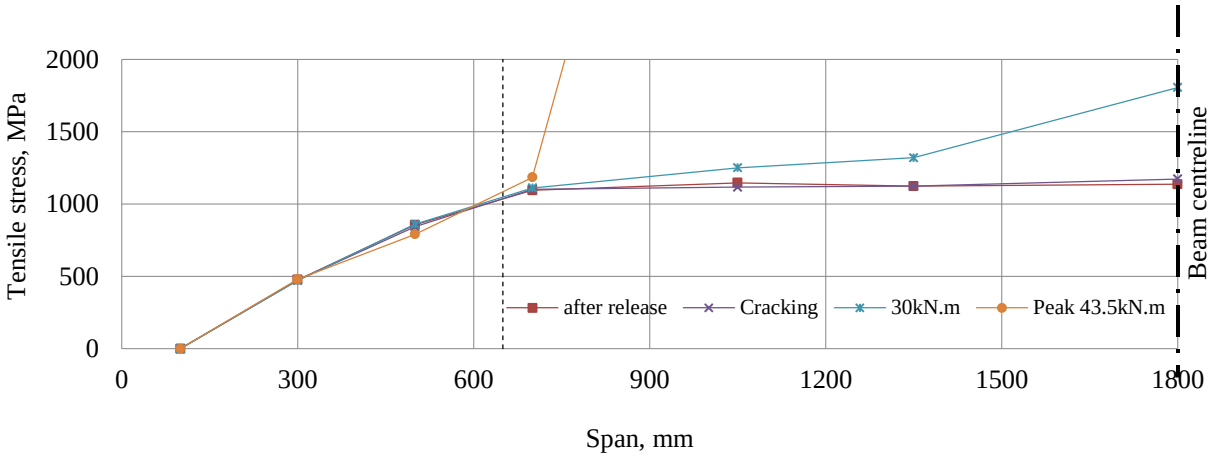

(b) Tensile stress in the prestressed CFRP bar

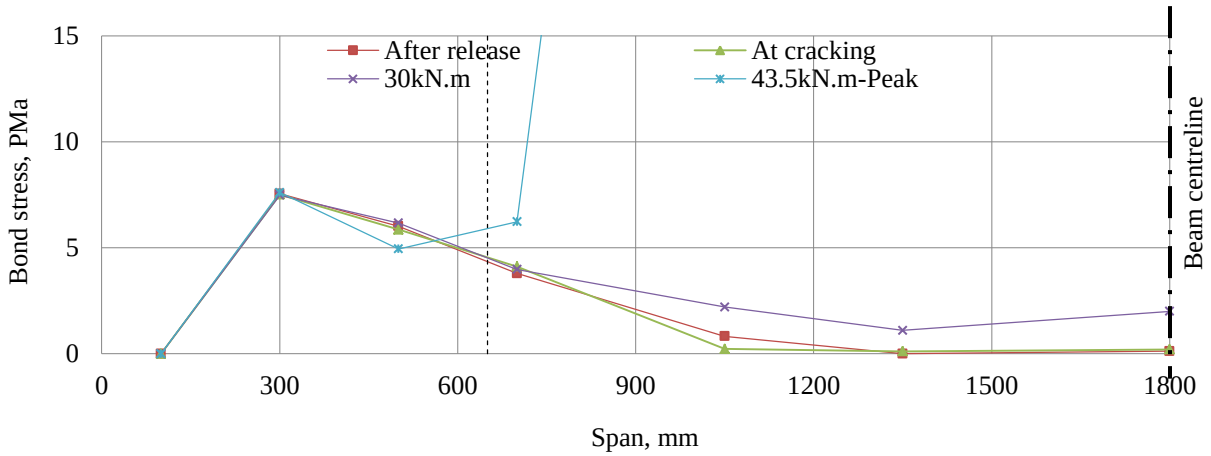

(c) Bond stress development due prestress release and flexural test

Figure 5.21 Tensile and bond stress development in the prestressed CFRP bars during the flexural test of Beam N60-3, shear span is 1350mm, beam failed by bar rupture

5.4.4 Average bond stress within the flexural bond length

The average bond stresses of the flexural bond region were calculated based on the measured increase in the tensile stresses in the CFRP bars during the flexural test. Table 5.6 gives the available flexural bond length, the increase in tensile stresses due to flexural load and the calculated average bond stresses. The results indicated that the flexural bond stresses were significantly less than the average bond stress developed within the transfer zone. The effect of the concrete compressive strength at release and the prestressing level are assessed below.

Table 5.6 Flexural test results

Group	Beam	f_e, MPa	l_{tr}, mm	Shear span, mm	Available l_f, mm	Increase in CFRP tensile stress, MPa	Average u_f, MPa	$\frac{u_f}{f_c'^{0.67}}$
I	S30-1	549.9	306.0	1100	794.0	810.5	3.2	0.19
	S30-2	534.8	301.8	1250	943.0	1357.5	4.5	0.27
	S30-3	626.4	337.0	1350	1013.0	1178.0	3.7	0.28
	S30-4	604.8	320.0	1500	1180	583.0	*	*
II	S45-1	750.3	533.5	1100	566.5	582.4	3.4	0.19
	S45-2	794.3	515.8	1250	751.8	714.7	2.9	0.17
	S45-3	776.6	514.5	1350	835.5	635.8	2.7	0.16
	S45-4	741.1	487.0	1500	1013.0	927.3	2.9	0.17
III	S60-1	932.7	668.5	1100	434.0	369.5	2.7	0.16
	S60-2	995.3	732.5	1350	617.5	478.6	2.5	0.15
	S60-3	920.3	661.8	1500	838.2	611.2	2.3	0.17
	S60-4	974.1	671.8	1700	1028.2	813.5	2.5	0.18
IV	C30-1	540.0	274.8	1350	1075.2	1291	3.8	0.23
	C60-2	1076.0	526.5	1250	723.5	540.0	2.4	0.15
	C60-3	1026.4	545.4	1350	804.6	791.0	3.1	0.19
	C60-4	1052.9	534.1	1500	965.9	806.2	2.6	0.16

* This beam failed by premature bar rupture. The flexural test results of this beam were excluded from the average bond stress analysis.

5.4.4.1 Effect of concrete compressive strength on the bond stress of SCC specimens

The effect of varying the concrete compressive strength on the bond strength of the CFRP bar in SCC is assessed based on beams that failed by pullout mode failure. Beams that failed by bar rupture did not reach the maximum bond stresses of those beams. Figure 5.22 shows a plot of the flexural bond stress,

u_f, versus concrete compressive strength on the day of testing raised a power of 0.67, $f_c^{'0.67}$. A linear relationship was used correlate the variation of bond stresses with concrete compressive strength. It is evident that the bond stresses increased linearly with the concrete compressive strength raised to the power of 0.67. Therefore, the flexural bond stress can be formulated linearly in terms of the concrete compressive strength raised to a power of 0.67, $f_c^{'0.67}$ as presented in the next section.

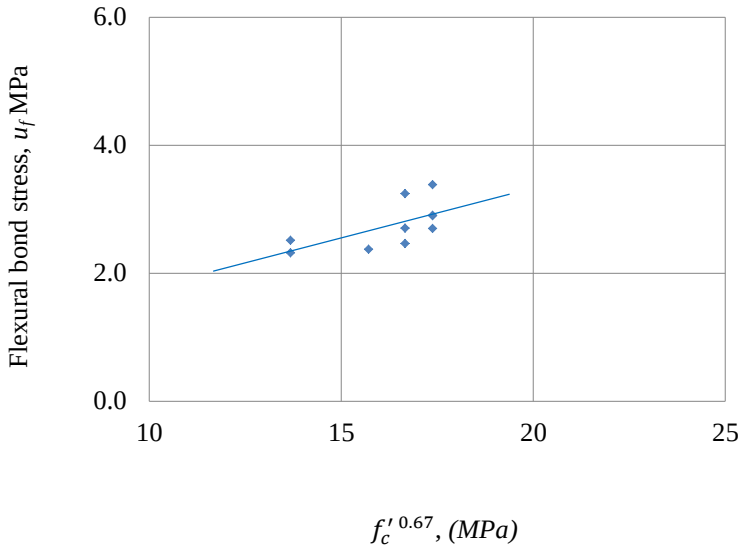

Figure 5.22 Flexural bond stress of prestressed CFRP bar in SCC versus $fci^{0.67}$

5.4.4.2 Effect of the prestressing level on the bond stress of SCC specimens

The increase in tensile stress in the prestressing CFRP bars due to load is defined as the flexural tensile stress. The data for normalized bond stress versus the flexural tensile stress of the CFRP bars is shown in Figure 5.23. Again here, only the beams that failed by bond pullout were used for the same reason discussed above. A linear relationship used to correlate the data. The relationship indicated that the normalized bond stress increases as the flexural tensile stress of the CFRP bar increases. SCC specimens showed similar normalized flexural bond stresses at a given flexural tensile stress as compared to NVC.

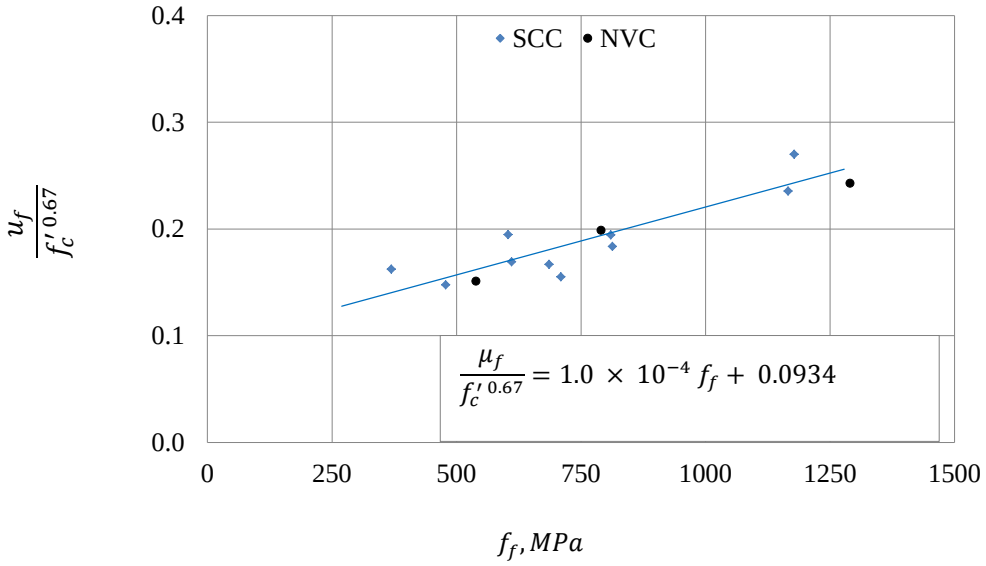

Figure 5.23 Normalized bond stress of CFRP bar in SCC versus flexural tensile stress

Based on the data shown in Figure 5.23, a relationship between the normalized flexural bond stress and flexural tensile stresses in a prestressed CFRP bar in SCC was formulated, Eqn 5.7. The equation is for bond pullout failure because sufficient concrete cover was available to prevent splitting bond failure.

$$\frac{u_f}{f_{ci}^{0.67}} = 1.0 \times 10^{-4} f_f + 0.0934 \qquad (5.7)$$

Where:

f_f is the flexural bond stress, MPa;

u_f is the flexural average bond stress, MPa; and

f'_c is the concrete compressive strength, MPa.

Chapter 6 – Analytical Modeling of non-Prestressed FRP Beams

6.1 Introduction

In this chapter an analytical model is proposed to calculate the flexural response of non-prestressed FRP beams. A complete moment-deflection response was analytically determined for selected beams that failed by bar rupture. The sectional analysis approach of the ISIS Canada design guideline (2007) was used to predict the moment capacity. This model was formulated for normal vibrated concrete (NVC) and validated in this thesis for use with self consolidating concrete (SCC). For each beam, the tensile stresses in the FRP bar and the strain in the top compression fibre of the concrete were calculated at a load level equal to the experimental failure moment. The predicted strains in the concrete compression fibre and the FRP bar were compared with the experimentally measured strains. The midspan deflection was calculated using two methods: a simplified approach based on the effective moment of inertia and a method based on elongation of the tensile reinforcement and curvature approach. Also presented in this chapter are models to predict the average bond stress between FRP bars and concrete. The experimental results and predictions using available design guidelines equations for the bond stresses and development length of FRP bars were compared. A correction factor for the ACI 440.1R-06 equation for the development length of FRP bars in NVC beams was proposed to account for CFRP bars. New equations for development length of CFRP and GFRP bars embedded in SCC beams were formulated.

6.2 Constitutive relationship for Concrete and FRP bars

Concrete was assumed to be in a linear elastic state before cracking. The concrete compressive strength, the modulus of rupture, and the modulus of elasticity for the concrete used in this analysis were obtained from material test results as tabulated in Table 6.1. The stress and strain relationship of concrete in compression incorporated in this analysis is represented according to a model proposed by Collins and Mitchell (1997).

$$f_c = f_c' \left[\frac{n \left({\varepsilon_t}/{\varepsilon_c'} \right)}{(n-1) + \left({\varepsilon_t}/{\varepsilon_c'} \right)^{nk}} \right] \qquad (6.1)$$

where

f_c the compressive stress in concrete at any corresponding strain ε_t

ε_t is the strain in the extreme concrete compression fibre

f_c' is the specified concrete compressive strength

ε_{cu} is the ultimate strain in concrete at failure taken as 0.0035;

n is curve-fitting factor equal to Ec/ (Ec=Ec')

E_c is the tangent stiffness when ε_t is zero,

E_c' is equal to f_c'/ε_{cu}; and

k is factor account to increase the post peak decay in stress.

Table 6.1 Concrete properties

Mix label	Modulus of Rupture, MPa	Modulus of Elasticity, GPa	Concrete Compressive Strength, MPa
SCC-Mix1	3.1	24.6	63.3
SCC-Mix2	3.4	22.8	48.9
SCC-Mix3	4.1	30.6	70.9
NVC	3.9	37.5	64.5

The relationship between the tensile stress and tensile strain of the FRP bars was assumed to be linear up to rupture (Eqn. 6.2). The modules of elasticity used in this analysis were as given in Table 3.4. These values were given by the manufacturer and confirmed through test carried Soudki and Martin (2010).

$$f_{frp} = \varepsilon_{frp} \; E_{frp} \qquad (6.2)$$

Where

f_{frp} is the tensile stresses in the FRP bar;

ε_{frp} is the longitudinal tensile strain in the FRP bar; and

E_{frp} is the modulus of elasticity of the FRP bar.

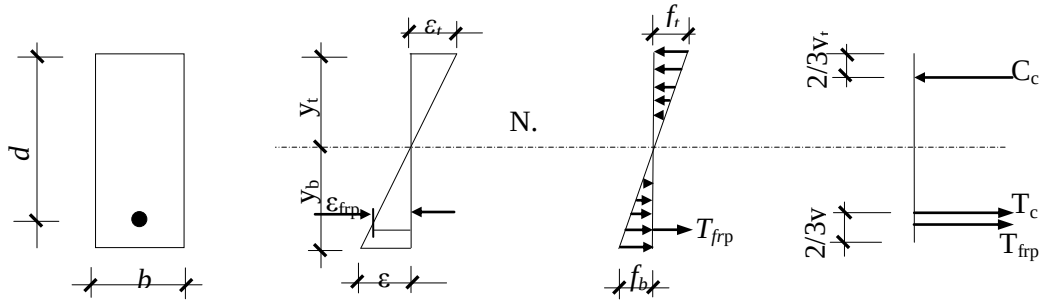

Cross | Strain compatibility | Stress distribution | Resultant forces

(a) Before concrete cracking

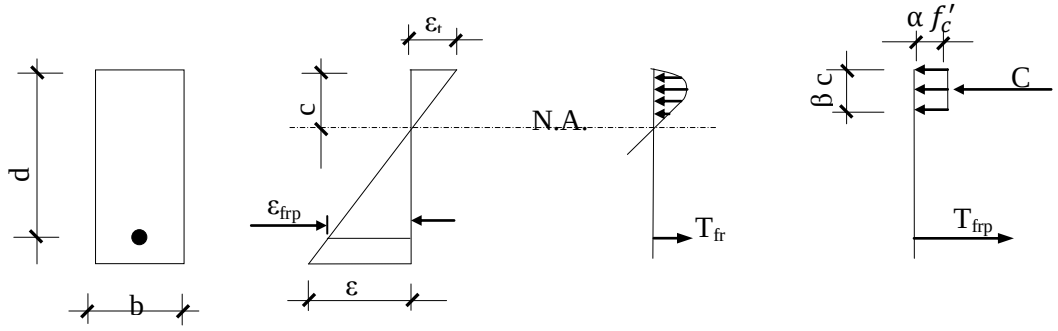

Cross Section | Strain compatibility | Actual stresses distribution | Idealized concrete stresses

(b) After concrete cracking

Figure 6.1 Section analysis model

6.3 Analytical model for flexural response

6.3.1 Model for moment resistance

The sectional analysis approach described in ISIS Canada design manual 3 (2008) was used to predict the moment resistance and the strains in the FRP bars and concrete. The model is based on forces equilibrium and strain compatibility approach. A schematic of the model is shown in Figure 6.1. A fully cracked section was assumed after the tensile stress at the extreme tension fiber of the concrete exceeded the modulus of rupture of the concrete (concrete tensile stresses and tension stiffening are neglected). The analysis is governed by the following equations.

The compression force in concrete is given by Eqn. (6.3):

$$C = \alpha \, \varphi_c \, f_c' \, \beta \, c \, b \qquad (6.3)$$

Where

C is the compressive force in the concrete in the compression region;

α is the stress factor to calculate the intensity of the average compressive stress in concrete over a depth of βc;

φ_c is the strength reduction factor for concrete taken to be 1.0 in this analysis;

f_c' is the concrete compressive strength at testing;

β is the factor for the depth of the equivalent compression stress block;

c is the depth of the neutral axis; and

b is the cross sectional depth.

Because all the beams were designed to fail due to rupture of the reinforcing FRP bar, the corresponding strain at the extreme compression fibre was less than the concrete crushing strain (ε_u). Thus the traditional rectangular stress block distribution cannot be used. The values of β and α used in this analysis account for the strain at the top compression fibre that is less than the ultimate strain of the concrete. The values of β and α used in this analysis were taken from ISIS Canada Design Manual 3. This manual provides the values of β and α at various strain levels and concrete compressive strengths.

The tensile force in the FRP bar is given by Eqn. (6.4):

$$T = A_{frp} \, \varphi_{frp} \, f_{frp} \qquad (6.4)$$

Where;

T is the tensile force in the FRP bar;

A_{frp} is the cross sectional area of the FRP bar;

φ_{frp} is the strength reduction factor for the FRP bars taken to be 1.0 in this analysis; and

f_{frp} is the tensile stresses in the FRP bar.

The strain compatibility over the cross-section depth is given in Eqn. (6.5).

$$\frac{c}{d} = \frac{\epsilon_t}{\varepsilon_t + \varepsilon_{frp}} \qquad (6.5)$$

Where

ε_t is the compressive strain at the extreme compression fibre of concrete;

d is the depth from the top compression fibre to the centroid of FRP bar.

Using equilibrium of the forces or C = T gives Eqn. (6.6):

$$\alpha\, \varphi_c\, f_c'\ \beta\, c\, b = A_{frp}\, \varphi_{frp}\, \varepsilon_{frp}\, E_{frp} \qquad (6.6)$$

Using an iterative procedure, a solution can be obtained for the two unknowns, c and ε_{frp}, in Eqn. (6.5). A spreadsheet was used to implement the iterative procedure of the model. Then the moment resistance can be calculated using Eqn. (6.7).

$$M_r = T\left(d - \frac{\beta\, c}{2}\right) \qquad (6.7)$$

6.3.2 Model for deflection

Two methods were used to calculate the midspan deflection in the FRP reinforced concrete beams: the first method is a simplified method based on the average effective moment of inertia along the beam span and the second method is based on curvature approach using the elongation in the FRP bar. The two methods are described below.

6.3.2.1 Simplified method for deflection

The midspan deflection is calculated based on the transformed moment of inertia before the concrete cracks. After cracking, the midspan deflection is calculated based on the effective moment of inertia of the beam's cross section. The effective moment of inertia is empirically derived for FRP-reinforced concrete flexural members (ISIS Canada 2007). The effective moment of inertia is based on the assumption of a uniform moment of inertia along the beam span.

$$I_e = \frac{I_t\, I_{cr}}{I_{cr} + \left(1.0 - 0.5\left(\frac{M_{cr}}{M_a}\right)^2\right)(I_t - I_{cr})} \quad (6.8)$$

$$I_{cr} = \frac{b\,(kd)^3}{3} + n_{frp}\, A_{frp}\,(d - kd)^2 \quad (6.9)$$

$$n_{frp} = \frac{E_{frp}}{E_c} \quad (6.10)$$

$$\rho = \frac{A_{frp}}{bd} \quad (6.11)$$

$$k = \sqrt{(\rho n_{frp})^2 + 2\,\rho n_{frp}} - \rho n_{frp} \quad (6.12)$$

Where;

I_e is the effective moment of inertia;

I_t is the moment of inertia of the uncracked transformed section;

I_{cr} is the moment of inertia of the cracked section;

M_{cr} is the cracked moment;

M_a is the applied moment;

n_{frp} is the modular ratio;

E_{frp} is the modulus of elasticity of the FRP bar;

E_c is the modulus of elasticity of concrete;

A_{frp} is the cross sectional area of the FRP bar;

d is the depth of the centre of the reinforcing FRP bar;

b is the width of the cross section;

k is a factor given by Eqn (6.11);

ρ is the reinforcement ratio, $\left(\rho = \frac{A_{frp}}{b\,d}\right)$.

The midspan deflections of a symmetrically simply supported beam under four point flexural loading (Figure 6.2) can be calculated based on the basic elastic beam analysis (Eqn. 6.13).

$$\Delta = \frac{P\,a}{24\,E_c\,I_e}\,(3\,l^2 - 4\,a^2) \quad (6.13)$$

Where

P is the applied load;

a is the shear span; and

l is the total beam span.

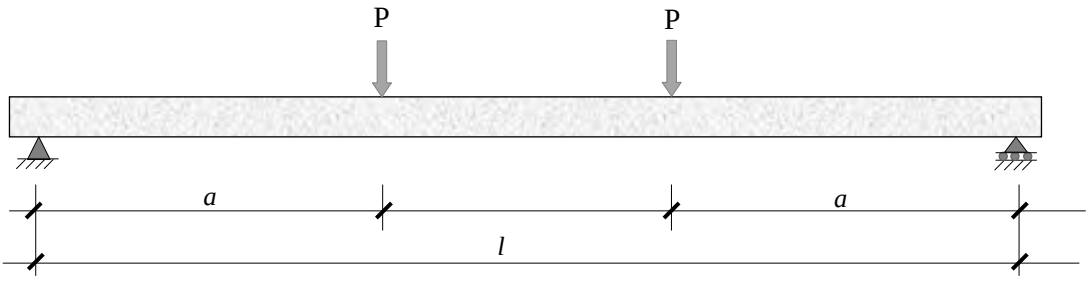

Figure 6.2 Four point flexural beam loading

6.3.2.2 Rigorous model for deflection calculation

6.3.2.2.1 Model concept and procedure

The midspan deflection is calculated by integrating the curvature along the beam length. The curvature is used to define the deformed shape of flexural members under flexural load. The curvature of a given beam element is defined as the rotation per unit length. For small deflections, the relative deflection of any two points along the beam length subjected to flexural loading can be written as in Eqn. 6.14 and shown schematically in Figure 6.3.

$$d\Delta = x\, d\theta \qquad (6.14)$$

Where

$d\Delta$ is the relative deflection

x is the distance from the support; and

$d\theta$ is the change in curvature.

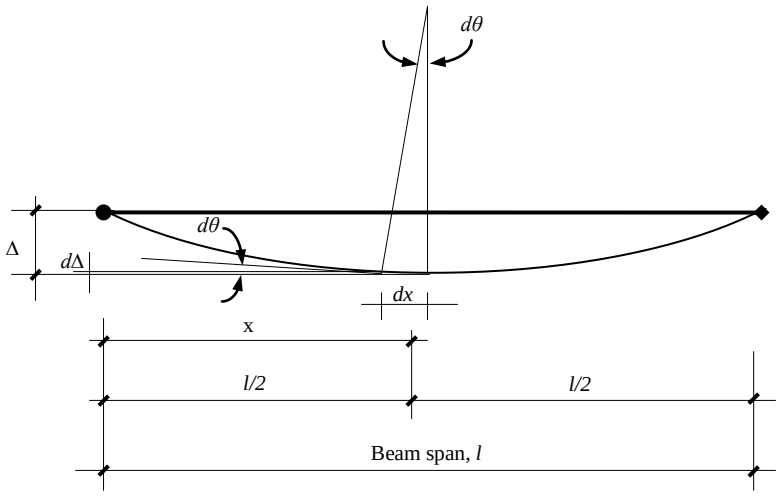

Figure 6.3 Beam curvature

El-Maaddawy (2004) proposed a new model to calculate the midspan deflection of a simply supported symmetrically loaded beam based on the elongation of the reinforcement and curvature approach. In this model, the beam is divided into a series of elements. The length of each member is equal to the predicted crack spacing. For each element, the applied external moment is assumed to be constant. The section analysis is performed at the middle of each element to determine the strain in the reinforcing bar and the neutral axis depth. Along the element length, the tensile forces in the reinforcement are transferred to the concrete by bond stresses, thus reducing the tensile forces in the reinforcing bar, resulting in less deflection. This bond is determined to be equal to the tension-stiffening effect.

The deflection is calculated from the elongation of the reinforcing bar within each element using Eqn. (6.15):

$$\Delta = \sum_{i=1}^{i=n} \frac{e_i}{d - c_i} x_i \qquad (6.15)$$

Where

n is the number of elements within half of the beam span;

e_i is the elongation in the reinforcing bar;

d is the depth from the extreme compression fibre of the concrete to the centroid of the reinforcing bar;

c_i is the neutral axis depth; and

x_i is the distance from the support to the centre of the element (i).

The elongation in the tensile reinforcement, e_i, is given by Eqn. (6.16):

$$e_i = \frac{s_m}{E_{frp}} \left(f_i - \frac{\mu \, s_m}{d_b} \right) \tag{6.16}$$

Where

s_m is the element length

f_i is the tensile stress in the reinforcing bar at the middle of the element (i)

μ is the bond stress within the element

d_b is the reinforcing bar diameter

E_{frp} is the Young's modulus of the reinforcing bar

The values of f_i and c_i for a given element at a given load level can be calculated from the section analysis described in Section 6.3.1.

6.3.2.2.2 Element length

The element length is taken to be equal to the crack spacing, s_m. The element length (crack spacing) used in this analysis is that proposed by El-Maaddawy (2004); however, because the type of tensile reinforcement used in this study is different (FRP versus steel rebar), this crack spacing might be different in beams reinforced with FRP bars. Increasing the element length might affect the calculation of the bond stress due to averaging the bond stress over a larger element length. The mean crack spacing is calculated using Eqn. (6.17).

$$s_m = 2 \left(C + \frac{s_b}{10} \right) + k_1 \, k_2 \, \frac{d_b}{p_{ef}} \tag{6.17}$$

$$p_{cf} = \frac{A_s}{A_{cef}} \tag{6.18}$$

$$k_1 = \begin{cases} 0.40 & \text{for deformed bars} \\ 0.80 & \text{for plain bars} \end{cases} \tag{6.19}$$

$$k_2 = 0.25 \, \frac{\varepsilon_1 + \varepsilon_2}{2 \, \varepsilon_1} \tag{6.20}$$

Where:

C is the clear concrete cover, mm;

s_b is the spacing between longitudinal reinforcing bars, mm;

d_b is the reinforcing bar diameter, mm;

A_s is the cross sectional area of the reinforcing bar, mm^2;

A_{cef} is the largest possible concrete area surrounding the reinforcing bar and has the same centroid as the reinforcing bar, mm^2;

k_1 is a coefficient that characterizes bond properties, taken as 0.8 in this study;

k_2 is a coefficient that accounts for the strain gradient within the effective embedment zone of the concrete;

ε_1 is the concrete strain at the bottom of the effective embedment zone; and

ε_2 is the concrete strain at the top of the effective embedment zone.

6.3.2.2.3 Bond stress

The bond stress between a reinforcing bar and concrete within the element length can be calculated using Eqn. (6.21), which is based on a bond-slip model specified by the CEB Model Code (1991).

$$\mu = \begin{cases} \dfrac{d_b}{2s_m}(f_{max} - n \quad f_r) & if\ \mu \leq \mu_{max} \\ \mu_{\max} & if\ s \leq s_1 \\ \mu_{max} - (\mu_{max} - \mu_{friction})\dfrac{(s - s_1)}{(s_2 - s_1)} & if\ s_1 < s \leq s_2 \\ \mu_{friction} & if\ s > s_2 \end{cases} \tag{6.21}$$

Where

μ is the average bond stress, MPa;

d_b is the reinforcing bar diameter, mm;

s_m is the crack spacing, mm;

f_{max} is the maximum tensile stress within the element, MPa;

$_n$ is the modular ratio of the reinforcing bar to the concrete;

f_r is the modulus of rupture of the concrete, MPa; and

s_1 and s_2 represent the bond stress slip model, mm.

This model represents the bond slip behaviour of a steel bar embedded in concrete. The model involves a linear reduction in the bond stress as the slip increases from s_1 to s_2. After s_2, the bond stress mainly depends on the friction stresses. The above model assumes that the full tensile force in the tensile bar is transferred to the concrete within the embedment length. This assumption does not represent the actual tensile forces of a given element from a beam subjected to flexural forces where only part of the tensile

force is transferred from the tensile bar to the concrete. Therefore, the equilibrium requirement might not be satisfied for a given element if "f_{max}" is used to calculate the bond stress.

Therefore, in the present study, the difference in tensile stresses between two adjacent elements is assumed to be carried by the concrete instead of "f_{max}." The bond stress model used for the deflection calculation is given in Eqn. (6.22).

$$\mu_i = \begin{cases} \frac{d_b}{2s_m}\left(\left(f_i - f_{i-1}\right) - n_{frp}\, f_r\right) & if\ \mu \le \mu_{max} \\ \mu_{\max} & if\ \mu \ge \mu_{max} \end{cases} \qquad (6.22)$$

Where

f_i and f_{i-1} are the tensile stresses in the tensile reinforcing bars in elements *(i)* and *(i-1)*, respectively;

n_{frp} is the modular ratio of the FRP bars;

f_r is the modulus of rupture of concrete; and

μ_{max} represents the maximum possible bond stress profile.

6.3.2.2.4 New proposed upper limits of local bond stress of FRP bars

El-Maadawy (2004) proposed a bond stress-slip model for steel reinforcing bars to estimate the maximum limiting bond stress. The model is described by CEB Model Code (1991). In this program, the local bond stress profile from the experimental results was used to describe the upper limit for the bond stress. The local bond stresses from the experimental results of beams that failed due bond pullout were plotted versus the ratio of the applied moment to cracking moment (M_a/M_{cr}) for each type of FRP bar and concrete. Beams that failed due to bar rupture were not included in this formulation as the local bond stress did not reach the bond strength of the FRP bars in these specimens.

Figures 6.4 (a), (b) and (c) show the maximum local bond stress profiles normalized to the square root of the concrete compressive strength versus the applied moment to cracking moment ratio of CFRP bars embedded in SCC beams, GFRP bars embedded in SCC beams, and CFRP bars embedded in NVC beams, respectively. No attempt was made to determine the maximum bond stress of the GFRP bars in NVC beams due to the limited number of specimens available under this category. Two constraints were implemented in each relationship: the lower limit of the applied moment-to-cracking moment ratio was taken as 1.0 and the upper limit of this ratio was taken as the maximum available from the experiment results. Generally, the normalized bond stress decreased as the applied moment to cracking moment ratio increased. There were no data for bond stress when the ratio of the applied moment to cracking moment was less than 1.0. Theoretically, the bond stress should be close to nil

when the section is not cracked ($M_a/M_{cr} < 1.0$) because the reinforcement and the concrete have similar strains at the level of the reinforcement. Furthermore, no bond stress data were available when the ratio of the applied moment-to-cracking moment was above than 6.0. However, the trend of bond stress versus (M_a/M_{cr}) ratio is expected to be flattened at similar levels beyond this limit of 6.0 until bond failure or bar rupture occur. The normalized local bond stress relationships were formulated mathematically using the data plotted in Figure 6.4. Eqns. (6.23), (6.24) and (6.25) give the proposed maximum limit of bond stress for the CFRP in SCC, GFRP in SCC, and CFRP in NVC, respectively.

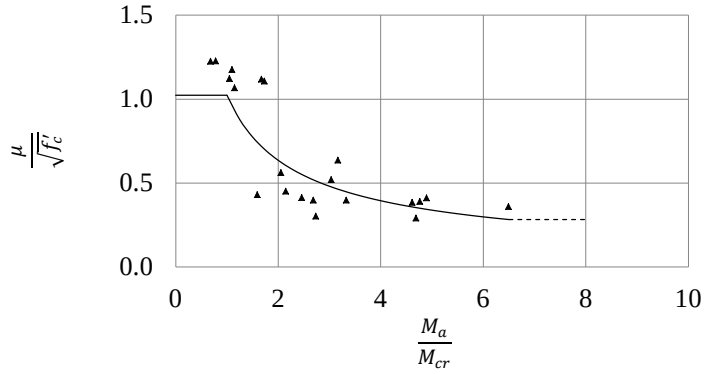

(a) CFRP bars in SCC

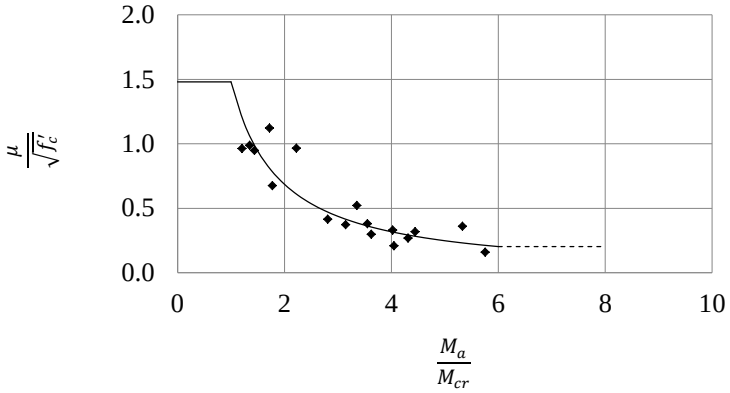

(b) GFRP bars in SCC

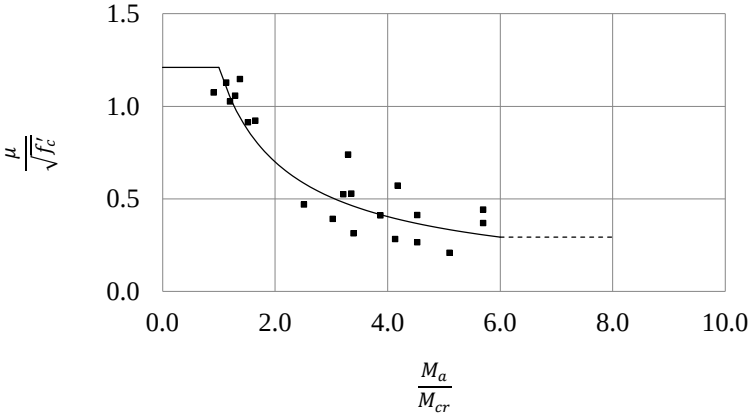

(c) CFRP bars in NVC

Figure 6.4 Maximum local bond stress profiles of CFRP and GFRP bars

a) CFRP bars embedded in SCC beams

$$\frac{u_{CFRP}}{\sqrt{f_c'}} \begin{cases} 1.02 & M_a \leq M_{cr} \\ 1.02\left(\frac{M_a}{M_{cr}}\right)^{-0.687} & M_{cr} < M_a \leq 6.0\,M_{cr} \\ 0.283 & M_a > 6.0\,M_{cr} \end{cases} \quad (6.23)$$

b) GFRP bars embedded in SCC beams

$$\frac{u_{GFRP}}{\sqrt{f_c'}} \begin{cases} 1.48 & M_a \leq M_{cr} \\ 1.48\left(\frac{M_a}{M_{cr}}\right)^{-1.11} & M_{cr} < M_a \leq 6.0\,M_{cr} \\ 0.203 & M_a > 6.0\,M_{cr} \end{cases} \quad (6.24)$$

c) CFRP bars embedded in NVC beams

$$\frac{u_{CFRP}}{\sqrt{f_c'}} \begin{cases} 1.21 & M_a \leq M_{cr} \\ 1.02\left(\frac{M_a}{M_{cr}}\right)^{-0.790} & M_{cr} < M_a \leq 6.0\,M_{cr} \\ 0.294 & M_a > 6.0\,M_{cr} \end{cases} \quad (6.25)$$

6.4 Analytical results

6.4.1 Beams reinforced with CFRP bars

Full flexural behaviour analysis was conducted on two beams: SC12.7-3.0-1400 and NC12.7-3.0-1400 using the approach described in Section 6.3. Table 6.2 gives the results of the sectional analysis for Beam SC12.7-3.0-1400. The table presents the strain in the concrete compression fibre, strain and tensile stress in the CFRP bar, moment resistance and curvature. The analysis was stopped when the tensile stress in the CFRP bar reached 1617MPa, which is equal to the measured rupture tensile stress of this beam.

Table 6.2 Sectional analysis results of Group SC12.7-3.0-1400

Condition of the section	$\varepsilon_t/\varepsilon_{cu}$	ε_t, ε	ε_{cfrp}, ε	f_{cfrp} MPa	M_r kN.m	Curvature, ($\times 10^6$)1/mm
	0.024	-82.3	53.3	7.7	3.88	0.51
Bottom concrete cracked	0.047	-164.6	106.5	15.3	7.75	1.09
	0.1	-350.1	1468.8	211.5	6.30	7.29
	0.15	-523.3	2152.8	310.0	9.21	10.72
	0.2	-700.0	2861.1	412.0	12.22	14.27
	0.25	-852.7	3513.9	506.0	15.00	15.00
	0.3	-1051.5	4256.9	613.0	18.15	21.27
	0.35	-1226.0	4951.4	713.0	21.10	24.75
	0.4	-1398.6	5645.8	813.0	24.05	28.23
	0.45	-1574.3	6340.3	913.0	27.00	31.72
	0.5	-1748.8	7034.7	1013.0	29.95	35.20
	0.55	-1924.3	7722.2	1112.0	32.87	38.66
	0.6	-2098.6	8409.7	1211.0	35.78	42.11
	0.65	-2274.3	9083.3	1308.0	38.63	45.51
	0.7	-2448.6	9756.9	1405.0	41.48	48.91
	0.75	-2624.4	10402.8	1498.0	44.19	52.20
	0.8	-2798.4	11048.6	1591.0	46.91	55.49
CFRP bar rupture	0.815	-2851.5	11229.2	1617.0	47.66	56.42

The analytical versus experimental results of the concrete and the CFRP strains at the midspan are presented graphically Figure 6.5. The predicted concrete strain matched the experimental data. However, the analytical CFRP strains were less than in the experimental results. After the concrete had cracked, both the analytical and the experimental strain curves followed a linear trend, confirming the expected linear behaviour of the SCC beams reinforced with FRP bars. The possible explanation of why the experimental strain in the CFRP bar was less than that in the analytical results is that of strain gauge was located close to a flexural crack. However, the results from other beams need to be reviewed and discussed to determine the overall trend for this comparison.

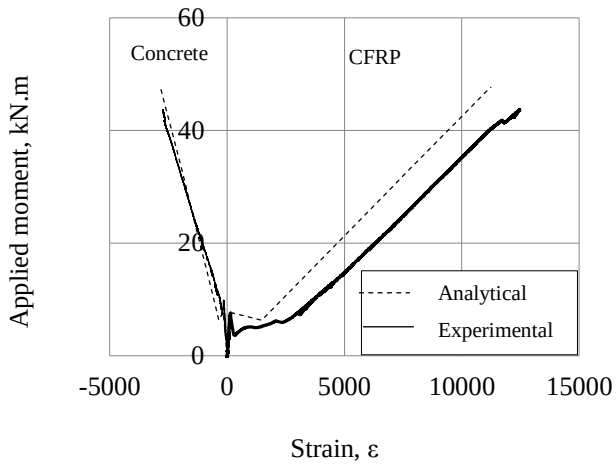

Figure 6.5 Comparison between the predicted and experimental strains in the concrete and CFRP bar at the midspan for Beam SC12.7-3.0-1400

The midspan deflection was calculated based on the simplified method and curvature approach. The tensile stress in the CFRP bars from the section analysis was used to calculate the midspan deflection. The tensile stress versus applied moment of this beam is shown on Figure 6.6. The relationship between the tensile stress in the CFRP bar of Beam SC12.7-3.0-1400 and the applied moment from Figure 6.6 is given by Eqn. (6.26).

$$f_{cfrp} = \begin{cases} \dfrac{M_a}{0.50} & 0.0 < M_a \leq M_{cr} \\ \dfrac{M_a - 0.210}{0.0285} & M_a > M_{cr} \end{cases} \qquad (6.26)$$

Where,

f_{cfrp} is the tensile stress in the CFRP bar, MPa

*M*a is applied moment, kN.mm; and

M_{cr} is cracking moment, kN.mm.

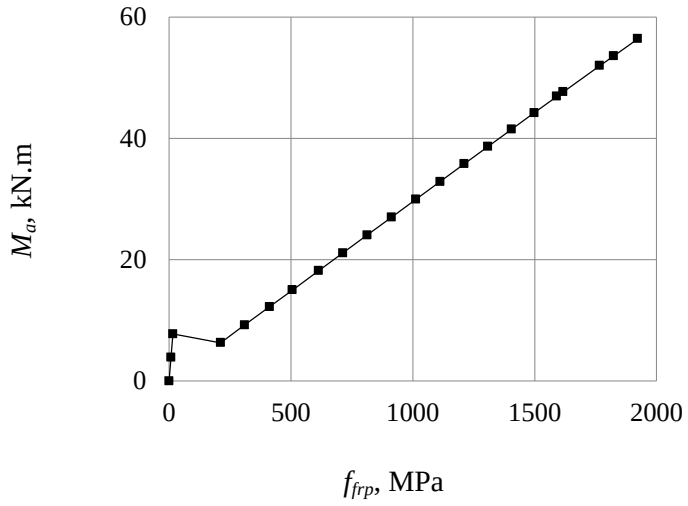

Figure 6.6 Model tensile stress of Beam SC12.7-3.0-1400

The comparison of the predicted versus measured moment versus midspan deflections results are shown in Figure 6.7. After the beam cracked, the analytical predictions gave deflection values less than those in the experimental results. Both the analytical and the experimental moment versus deflection curves were linear after cracking, as expected. However, the slopes of the analytical curves were steeper, which suggests that the actual beam stiffness is less than the analytical stiffness used for deflection calculation. When comparing the results at the experimental failure moment of 43.6kN.m, the experimental deflection was 42.6mm and the tensile stresses in the CFRP bar was 1617MPa. At the same applied moment, the analytical simplified results gave a midspan deflection of 32.4mm and a tensile stress in the CFRP bar of 1478MPa. On the other hand, analytical-rigorous results had excellent correlation with the experimental data, with a midspan deflection of 36.9mm. According to the guidelines, the simplified method should be used as a conservative method, but the results showed that it was unconservative. The possible explanation might be that the assumption of a uniform effective moment of inertia along the beam span might overestimate the actual stiffness of SCC beams reinforced with CFRP bars.

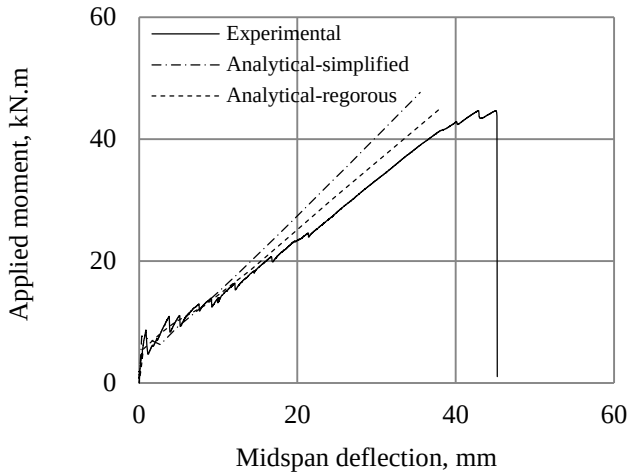

Figure 6.7 Moment versus midspan deflection for Beam SC12.7-3.0-1400: experimental versus predicted results

Table 6.3 compares the experimental data and predictions from the two analytical methods at various load levels. It is evident that between the service and ultimate load levels, the predicted midspan deflection by the simplified method was on average 79% of the experimental value, while based on the rigorous model it was about 88%.

Table 6.3 Comparison between the analytical and experimental methods of midspan deflections for Beam SC12.7-3.0-1400

Condition	Applied moment, kN.m	Midspan deflection, mm				
		Experimentally (1)	Simplified (2)	Rigorous (3)	(2)/(1)	(3)/(1)
Uncracked	3.87	0.39	0.18	0.38	0.46	0.97
	7.88	0.86	0.35	0.77	0.41	0.90
Cracked	9.32	4.73	4.87	4.23	1.03	0.89
	12.22	8.48	7.64	6.99	0.90	0.82
	18.14	15.27	12.63	13.75	0.83	0.90
	24.04	22.29	17.34	19.00	0.78	0.85
	29.95	27.77	21.94	24.29	0.79	0.87
	35.78	33.35	26.44	29.10	0.79	0.87
	41.44	39.71	30.81	34.86	0.78	0.88
	43.63	42.60	32.40	36.91	0.76	0.87

A similar flexural analysis was performed for Beam NC12.7-3.0-1400. The results of the sectional analysis are given in Table 6.4. A graphical comparison between the experimental and analytical concrete strains and CFRP strains is shown in Figure 6.8. The predicted results of both strains showed good agreement with the experimental data.

Table 6.4 Sectional analysis results of Group NC12.7-3.0-1400

Condition of the section	$\varepsilon_t/\varepsilon c_u$	ε_t, ε	ε_{cfrp}, ε	T_{cfrp} MPa	Mr, kN.m	Curvature, ($\times 10^6$)1/mm
	0.015	-52.6	36.3	5.23	4.47	0.34
Bottom concrete cracked	0.030	-105.2	72.7	10.46	8.94	0.70
	0.1	-350.8	1659.7	239.00	7.33	7.87
	0.15	-525.9	2458.3	354.00	10.84	11.68
	0.2	-695.4	3250.0	468.00	14.31	15.44
	0.25	-873.8	4034.7	581.00	17.75	17.75
	0.3	-1051.6	4833.3	696.00	21.24	23.03
	0.35	-1225.0	5618.1	809.00	24.68	26.78
	0.4	-1399.4	6388.9	920.00	28.06	30.48
	0.45	-1570.2	7215.3	1039.00	31.69	34.38
	0.5	-1746.6	7986.1	1150.00	35.06	38.09
	0.55	-1925.8	8763.9	1262.00	38.46	41.83
	0.6	-2098.5	9486.1	1366.00	41.62	45.33
	0.65	-2273.3	10291.7	1482.00	45.15	49.17
	0.7	-2449.4	11097.2	1598.00	48.68	53.01
CFRP bar rupture	0.725	-2545.0	11527.8	1660.00	50.56	55.07

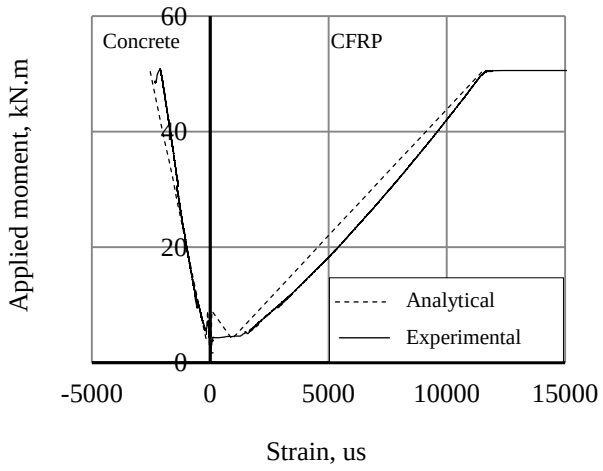

Figure 6.8 Comparison between the predicted and experimental strains in the concrete and the CFRP bar for Beam NC12.7-3.0-1400

The midspan deflection was calculated based on both simplified and rigorous models. The tensile stress in the CFRP bars used in the rigorous model was based on the sectional analysis. The tensile stress versus applied moment of this beam is shown in Figure 6.9. The relationship between the tensile stress in the CFRP bar and the applied moment from Figure 6.9 is given by Eqn. 6.27. The experimental moment versus midspan deflection results are compared with predicted results as shown in Figure 6.10 and given in Table 6.5. The predicted midspan deflection based on the simplified method had a slightly better correlation with experimental results versus the SCC specimen, but, the simplified method was still unconservative at higher applied moments. The rigorous model results had excellent agreement with the experimental results at all load levels.

$$f_{cfrp} = \begin{cases} \dfrac{M_a}{0.855} & 0.0 < M_a \leq M_{cr} \\ \dfrac{M_a - 0.142}{0.0303} & M_a > M_{cr} \end{cases} \qquad (6.27)$$

Where,

f_{cfrp} is the tensile stress in the CFRP bar, MPa

M_a is the applied moment, kN.mm; and

M_{cr} is the cracking moment, kN.mm.

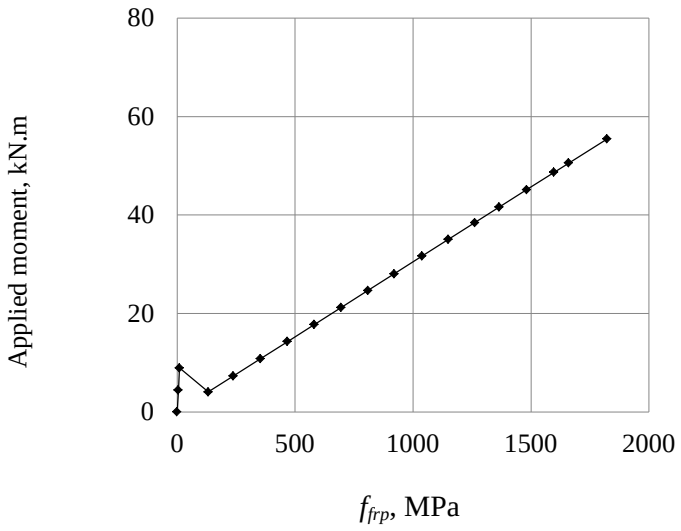

Figure 6.9 Model tensile stress of Beam NC12.7-3.0-1400

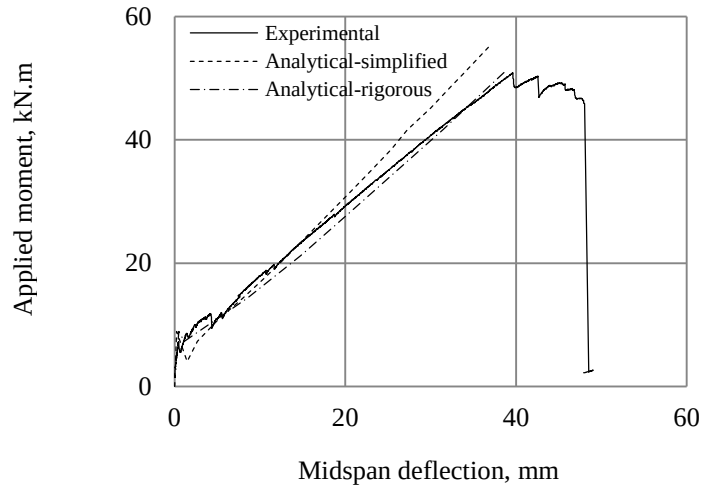

Figure 6.10 Moment versus midspan deflection for Beam NC12.7-3.0-1400: experimental versus prediction results

Table 6.5 Comparison between analytical and experimental midspan deflections for Beam NC12.7-3.0-1400

Condition	Applied moment, kN.m	Midspan deflection, mm,				
		Experimental (1)	Simplified model (2)	Rigorous Model (3)	(2)/(1)	(3)/(1)
Uncracked	4.47	0.21	0.12	0.24	0.57	1.14
	8.94	1.46	0.23	0.49	0.16	0.34
Cracked	7.33	1.62	2.67	1.12	1.65	0.69
	14.31	7.48	8.01	8.52	1.07	1.14
	21.24	14.14	13.24	14.80	0.94	1.05
	28.06	19.10	18.12	20.39	0.95	1.07
	35.06	25.07	23.02	26.12	0.92	1.04
	41.62	38.81	27.56	31.44	0.71	0.81
	48.68	37.49	32.42	36.88	0.86	0.98
	50.56	39.35	33.71	38.59	0.86	0.98

Results for the sectional analysis of all beams are given in Table 6.6. The general trend of the sectional analysis showed that the experimental values of the tensile stresses in the CFRP bars were larger than the analytical results at the same applied moment for beams made with a 6.3mm CFRP bar and were similar to the experimental results for beams reinforced with 9.5mm and 12.7mm CFRP bars. The analytical concrete strain results were within about ±10% of the measured values, with the exception of two Beams, NC9.5-3.0-550 and NC12.7-3.0-1400, which had analytical concrete strains about 20% higher than measured values. There was no clear trend for the tensile stress in the CFRP bars and strain in concrete between the SCC and the NVC specimens between the analytical and the experimental. For the NVC beams, results of the analytical analysis showed close prediction for the tensile stresses in the CFRP bars and midspan deflections. The only contradiction in this trend was in the beams reinforced with 6.3mm CFRP bars. Results of the tensile stresses of the CFRP bars in this group were significantly larger than the experimental values.

Table 6.6 Comparison between the experimental results and the analytical results for CFRP reinforced beams (SCC and NVC specimens)

	Beam	Moment, kN.m	Experimental		Analytical	
			Concrete strain, ε	f_{frp}, MPa	Concrete strain, ε	f_{frp}, MPa
SCC specimens	SC6.3-3.0-350	6.4	-1917	971.3	-2011	1606
	SC6.3-3.0-450	6.4	-1884	1205.9	-2011	1606
	SC6.3-3.0-600	6.5	-2183	1660.7	-2099	1707
	SC9.5-3.0-550	12.7	-	1063.1	-1950	1140
	SC9.5-3.0-750	16.2	-	1375.2	-2508	1450
	SC9.5-3.0-950	16.0	-	1435.1	-2475	1431
	SC12.7-3.0-850	32.4	-	1119.6	-1982	1069
	SC12.7-3.0-1250	38.5	-	1424.1	-2360	1267
	SC12.7-3.0-1400	43.6	-2450	1617.1	-2851.5	1428
NVCspecimens	NC6.3-3.0-350	5.9	-	1207.5	-1663	1497
	NC6.3-3.0-450	8.0	-2594	1556.8	-2305	2074
	NC6.3-3.0-600	8.6	-2817	1766.1	-2451	2218
	NC9.5-3.0-550	15.4	-1705	1112.1	-2099	1372
	NC9.5-3.0-750	18.4	-2544	1593.6	-2498	1640
	NC9.5-3.0-950	19.9	-2660	1900.8	-2712	1822
	NC12.7-3.0-850	39.3	-2424	1332.3	-2018	1320
	NC12.7-3.0-1250	45.2	-2185	1644.9	-2275	1482
	NC12.7-3.0-1400	49.8	-2117	1688.4	-2545	1660

- No data available

Results of midspan deflection of all beams based the two methods and the experimentally measured results are given in Table 6.7. Generally, the simplified method was unconservative in SCC beams rather than in NVC beams. The midspan deflection based on the analytical simplified method ranged from 76% to 90% of the experimental results for SCC beams, with the exception of Beam SC12.7-3.0-1250. The difference in midspan deflection was between 86% and 1.15% of the experimental values for the NVC beams, with the exception of Beams NC6.3-3.0-450 and NC12.7-3.0-1250. The midspan deflections based on the rigorous approach were in good agreement with the experimentally measured values for both SCC and NVC specimens. The ratio of the predicted midspan deflection based the rigorous method to experimental deflection ranged from 0.85 to 1.01 for the SCC beams and from 0.83 to 1.08 for the NVC beams. Beam NC6.3-3.0-450, which had the largest difference using both

methods, might have been subject to an error in the experimentally measured midspan deflection. The possible explanation of the results of the simplified method for the SCC beams might be related to the effective moment of inertia. The stiffness of the SCC beams after cracking could be less than predicted by Eqn. (6.10), which is used for the simplified method.

Table 6.7 Comparison between analytical and experimental midspan deflections for CFRP reinforced beams

	Beam	Moment, kN.m	Midspan deflection, mm				
			Experimental (1)	Simplified model (2)	Rigorous model (3)	(2)/(1)	(3)/(1)
SCC specimens	SC6.3-3.0-350	6.4	-	28.5	32.06	-	-
	SC6.3-3.0-450	6.4	29.8	26.7	29.71	0.90	1.00
	SC6.3-3.0-600	6.5	31.2	23.9	26.67	0.77	0.85
	SC9.5-3.0-550	12.7	33.7	29.6	34.03	0.88	1.01
	SC9.5-3.0-750	16.2	41.6	34.4	39.62	0.83	0.95
	SC9.5-3.0-950	16.0	38.8	29.4	33.94	0.76	0.87
	SC12.7-3.0-850	32.4	36.3	26.5	36.69	0.73	1.01
	SC12.7-3.0-1250	38.5	43.2	26.4	37.20	0.61	0.86
	SC12.7-3.0-1400	43.6	42.6	32.4	36.91	0.76	0.87
NVC specimens	NC6.3-3.0-350	5.9	25.8	24.1	27.92	0.93	1.08
	NC6.3-3.0-450	8.0	25.2	34.5	35.66	1.37	1.42
	NC6.3-3.0-600	8.6	34.4	32.9	34.37	0.96	1.00
	NC9.5-3.0-550	15.4	29.7	34.1	35.26	1.15	1.19
	NC9.5-3.0-750	18.4	37.0	37.2	38.70	1.01	1.05
	NC9.5-3.0-950	19.9	35.3	35.2	36.01	1.00	1.02
	NC12.7-3.0-850	39.3	39.4	34.7	40.98	0.88	1.04
	NC12.7-3.0-1250	45.2	48.5	33.0	40.12	0.68	0.83
	NC12.7-3.0-1400	49.8	39.4	33.71	38.59	0.86	0.98

- No data available

6.4.2 Flexural analysis results of beams reinforced with GFRP bars

Prediction of the flexural responses of two beams, each reinforced with a 12.7mm GFRP bar, was done. One beam was made from SCC (SC12.7-3.0-600), and the second beam was made from NVC (NG12.7-3.0-600). Both beams failed by bar rupture, and no concrete crushing was recorded. The sectional analysis was carried out at selected load levels. Table 6.8 gives the results of the sectional analysis of Beam SG12.7-3.0-600, and Figure 6.11 shows a graphical comparison between the analytical and experimental strains in the concrete and the GFRP bars for the same beam.

Table 6.8 Sectional analysis results of Group SG12.7-3.0-600

Condition of the section	$\varepsilon_t/\varepsilon_{cu}$	ε_t, ε	ε_{cfrp}, ε	f_{cfrp} MPa	Mr, kN.m	Curvature, ($\times 10^6$)1/mm
	0.025	-82.90	45.38	2.10	1.89	0.82
Bottom concrete cracked	0.05	-165.79	90.76	4.20	3.77	1.65
	0.1	-349.53	2105.83	97.50	1.84	15.79
	0.15	-526.61	3099.35	143.50	2.70	23.31
	0.2	-698.38	4103.67	190.00	3.57	30.87
	0.25	-876.23	5107.99	236.50	4.44	4.44
	0.3	-1050.88	6112.31	283.00	5.32	46.05
	0.35	-1223.76	7105.83	329.00	6.18	53.55
	0.4	-1398.90	8110.15	375.50	7.05	61.13
	0.45	-1574.56	9107.99	421.70	7.91	68.68
	0.5	-1749.85	10107.99	468.00	8.78	76.23
	0.55	-1924.08	11092.87	513.60	9.63	83.68
	0.6	-2098.79	12082.07	559.40	10.49	91.17
	0.65	-2274.81	13051.84	604.30	11.33	98.53
	0.7	-2449.47	14021.60	649.20	12.17	105.89
	0.75	-2624.69	14950.32	692.20	12.97	112.99
	0.8	-2801.60	15887.69	735.60	13.77	120.15
	0.85	-2974.40	16760.26	776.00	14.52	126.87
CFRP bar rupture	0.90	-3150.05	17645.79	817.00	15.27	133.69

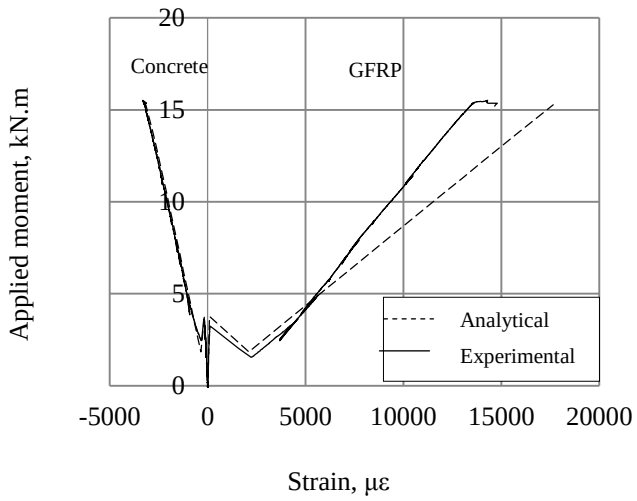

Figure 6.11 Comparison between the predicted and experimental strains in the concrete and the GFRP bar of Beam SG12.7-3.0-600

The results shown in Figure 6.10 indicate that the predicted concrete strains are in good agreement with the experimental strains. However, the predicted GFRP strains at midspan diverted from the experimental GFRP strains at a moment of 5.0kN.m. The experimental strains in the GFRP bar were less than the predicted strains after this moment. Comparing the reading of this strain gauge with those of other strain gauges that were attached on the GFRP bar of this beam (see Appendix B) suggests that the strain gauge was partially detached from the GFRP bar during the experimental measurement. The experimental strains of the GFRP bar did not maintain a linear relationship with applied moment as other strain gauges on the same bar did.

The midspan deflection was calculated based on the simplified and rigorous models. The tensile stress in the GFRP bars from the section analysis was used in the rigorous model. The tensile stress versus applied moment is shown on Figure 6.12 and given in Eqn. (6.28).

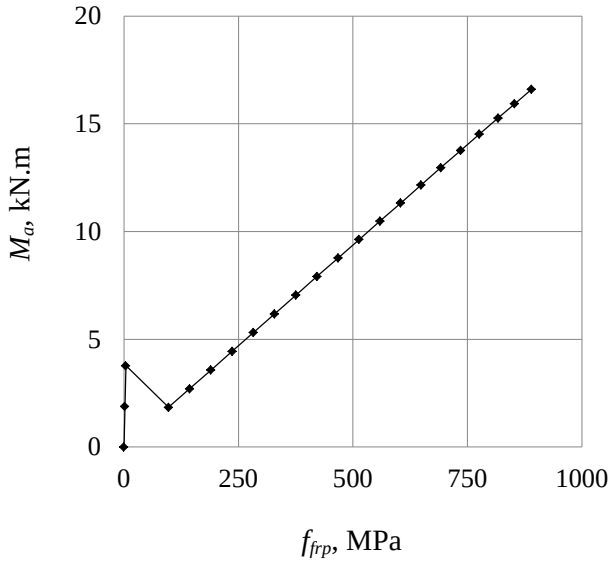

Figure 6.12 Tensile stress of the GFRP bar of Beam SG12.7-3.0-600

$$f_{cfrp} = \begin{cases} \dfrac{M_a}{0.90} & 0.0 < M_a \leq M_{cr} \\ \dfrac{M_a - 0.04}{0.019} & M_a > M_{cr} \end{cases} \qquad (6.28)$$

Where,

f_{cfrp} is the tensile stress in the GFRP bar, MPa

Ma is applied moment, kN.mm; and

M_{cr} is cracking moment, kN.mm

The results of moment versus midspan deflections based on the simplified method and rigorous model versus the experimental results are given in Table 6.9 and graphically compared in Figure 6.13. Generally, both methods gave close predictions as compared to the experimental results after cracking and poor correlation before cracking. The predicted deflection based on the simplified method was 10-12% greater than the experimental measurements. Specifically, the crack formations and load measurements were not stabilized during crack initiation and led to the errors. Predictions using the rigorous model were close to the experimental data, with a ratio of predicted to experimental results from 1.03 to 1.10. It is worth note that predictions of the deflection in GFRP reinforced beams were slightly higher than measured values which is possibly due to tension stiffening in the actual beam..

Table 6.9 Comparison between the methods of midspan deflection calculations of Beam SG12.7-3.0-600

Condition	Applied moment, kN.m	Midspan deflection, mm				
		Experimentally (1)	Simplified method (2)	Rigorous model (3)	(2)/(1)	(3)/(1)
Uncracked	1.89	0.46	0.18	0.35	0.39	0.76
	3.77	0.73	0.37	0.90	0.51	1.23
Cracked	1.84	1.77	3.65	2.99	2.06	1.69
	3.57	7.20	6.52	8.95	0.91	1.24
	5.32	14.10	15.36	15.50	1.10	1.10
	7.05	20.65	23.05	22.57	1.12	1.09
	8.78	27.21	30.27	29.45	1.11	1.08
	10.49	33.11	37.18	35.26	1.12	1.06
	12.17	40.03	43.82	41.09	1.09	1.03
	13.77	45.08	50.11	47.31	1.11	1.05
	15.27	50.75	55.95	52.78	1.10	1.04

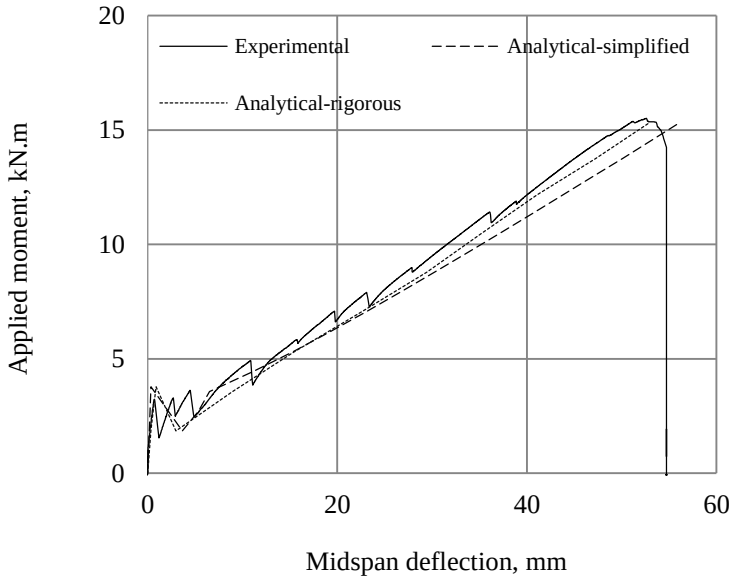

Figure 6.13 Moment versus midspan deflection for Beam SG12.7-3.0-600: predicted versus experimental results

Results for the sectional analysis of all beams are given in Table 6.10. The general trend of the analysis results showed that the experimental values of the tensile stresses in the GFRP bars were less than the predicted results at the same applied moment. The compression strains in the extreme compression fiber of the concrete were in good agreement with the experimental results at all load levels.

Table 6.10 Comparison between the experimental results and the analytical analysis beams reinforced with GFRP

Beam	Moment, kN.m	Experimental		Analytical	
		Concrete strain, ε	f_{frp}, MPa	Concrete strain, ε	f_{frp}, MPa
SG9.5-3.0-300	6.7	-1594	680.0	-1290	606
SG9.5-3.0-450	7.5	-1823	750.0	-1485	680
SG9.5-3.0-600	8.7	-1663	765.6	-1740	789
SG12.7-3.0-350	14.1	-2251	518.2	-2810	741
SG12.7-3.0-450	15.6	-2895	569.8	-3232	835
SG12.7-3.0-600	15.5	-3302	614.2	-3220	828
SG15.9-3.0-450	33.2	-1248	514.8	-2175	720
SG15.9-3.0-600	45.5	-2305	627.8	-3075	1009
SG15.9-3.0-750	37.7	-2061	655.0	-2448	802
NG12.7-3.0-350	14.4	-2241	601.2	-2610	770
NG12.7-3.0-550	15.3	-2609	651.6	-2705	820
NG12.7-3.0-550-2	15.9	-2948	603.5	-2870	850

Table 6.11 compares the measured versus predicted midspan deflections at the failure load for all beams. The comparison shows that deflection predictions using the simplified method were conservative by 10% to 20% on average of the experimental measurements. Predictions using rigorous model were less unconservative. The ratio of midspan deflection to prediction using the rigorous model ranged from 0.93 to 1.17, with the exception of two beams (SG9.5-3.0-600 and SG9.5-3.0-450). Those two beams had the slight unconservative predictions, which may be due to the error in experimental measurements.

Therefore, deflection predictions using the simplified method were highly unconservative for SCC beams reinforced with CFRP and less unconservative for NVC beams reinforced with CFRP bars. The simplified method was conservative for beam reinforced with GFRP bars (SCC beams and NVC beams). This is possibly due to using the effective moment of inertia. Beams reinforced with CFRP bars might have had stiffness less than that predicted by the simplified method. The difference was

higher when SCC was combined with CFRP bars. It is worth note here that SCC beams showed closer crack spacing than NVC beams, which may have an impact on the beam stiffness. Excellent predictions of midspan deflections were obtained using the rigorous model in all cases.

Table 6.11 Comparison of predicted versus measured midspan deflections for GFRP reinforced beams

Beam	Moment, kN.m	Midspan deflection, mm				
		Experimental (1)	Analytical (2)	Rigorous model (3)	(2)/(1)	(3)/(1)
SG9.5-3.0-300	6.7	45.5	36.9	41.3	0.86	0.91
SG9.5-3.0-450	7.5	43.0	40.3	43.9	0.93	1.02
SG9.5-3.0-600	8.7	40.8	45.9	47.9	1.13	1.17
SG12.7-3.0-350	14.1	47.5	56.2	53.05	1.18	1.12
SG12.7-3.0-450	15.6	49.2	61.5	57.66	1.25	1.17
SG12.7-3.0-600	15.5	52.6	55.95	52.78	1.06	1.00
SG15.9-3.0-450	33.2	27.7	31.4	25.64	1.13	0.93
SG15.9-3.0-600	45.5	33.5	41.1	40.73	1.23	1.22
SG15.9-3.0-750	37.7	30.9	33.6	30.62	1.09	0.99
NG12.7-3.0-350	14.4	43.9	55.2	-	1.26	-
NG12.7-3.0-550	15.3	44.7	54.5	-	1.22	-
NG12.7-3.0-550-2	15.9	44.1	58.2	-	1.32	-

6.5 Bond and development length analysis

The average normalized bond stresses of GFRP bars and CFRP bars embedded in concrete are calculated based available design guidelines and compared to the experimental values.

6.5.1 Bond and development of GFRP and CFRP bars in NVC beams

Figure 6.14 shows the normalized bond stresses versus normalized embedment length of both GFRP and CFRP bars embedded in NVC beams. Canadian guidelines (ISIS Canada M3 (2008) and CSA-S806-12) assume a constant normalized bond stress, which is independent of the embedment length. This assumption led to largely conservative results for short embedment lengths and unconservative results for long embedment lengths. In fact, this assumption does not capture the actual bond stress profiles of GFRP bars and CFRP bars embedded in NVC beams. On the other hand, the ACI440.1R-06 equation captured the trend of the normalized bond stresses of GFRP bars in NVC beams. The predicted values of the normalized bond stress based on the ACI equation for the GFRP bars in NVC beams agree well with the experimental results. The predicted results of the development length of the CFRP bars based on the ACI440.1R-06 equation were largely conservative, because ACI440.1R-06 does not consider the enhancement in normalized bond stresses of the CFRP bars as compared to GFRP bars. As presented in Chapter 2, ACI 440.1R-06 states that "No data exists in the database for CFRP bars; it is anticipated that the much larger stiffness of the CFRP bars will likely decrease the required development lengths and, correspondingly, its material modification factor. At this time, a material factor equal to 1.0 is recommended for CFRP bars."

A material modification factor can be estimated as the ratio of the measured/predicted ratio of the normalized bond stress of the CFRP bars at a similar normalized embedment length. Table 6.12 gives the results of experimental and predicted normalized bond stresses as well as a material modification factor for CFRP reinforced concrete beams in this study. Also, the table shows the data and predictions for the GFRP reinforced concrete beams to illustrate how well ACI equation predictions compare with measured bond stresses. The result for the CFRP reinforced concrete beams showed that this ratio ranges from 1.10 to 1.79, with a mean value of 1.44 and standard deviation of 0.05. The data used in this comparison had a cover-to-bar-diameter ratio of 3.0. Within probability of 95%, the modification factor for the CFRP bars in NVC was found to be 1.35.

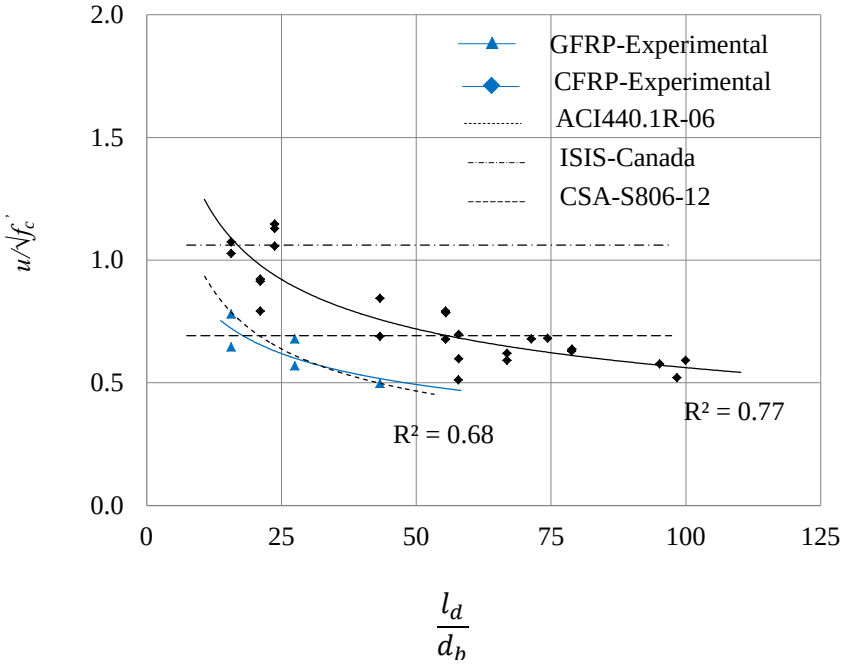

Figure 6.14 Experimental bond stresses of GFRP and CFRP bars in NVC as compared to predictions using available guidelines

Table 6.12 Comparison between the normalized average bond stresses of the CFRP and GFRP bars in NVC beams

Group	Beam	l_e, mm	l_e/d_b	$u/\sqrt{f'_c}$, (MPa)$^{1/2}$		Modification factor (1)/(2)
				Experimental (1)	ACI440.1R-06 prediction (2)	
NC6.3	NC6.3-3.0-350	150	23.8	1.057	0.641	1.650
		350	55.5	0.677	0.471	1.436
	NC6.3-3.0-450	150	23.8	1.147	0.641	1.791
		350	55.5	0.791	0.471	1.680
		450	71.4	0.678	0.443	1.531
	NC6.3-3.0-600	150	23.8	1.129	0.641	1.762
		350	55.5	0.785	0.471	1.666
		450	71.4	0.681	0.458	1.488
		600	95.2	0.577	0.418	1.380
NC9.5	NC9.5-3.0-550	200	21.1	0.922	0.680	1.355
		550	57.9	0.598	0.466	1.282
	NC9.5-3.0-750	200	21.1	0.914	0.680	1.343
		550	57.9	0.696	0.466	1.493
		750	78.9	0.628	0.434	1.449
	NC9.5-3.0-950	200	21.1	0.792	0.680	1.164
		550	57.9	0.512	0.466	1.097
		750	78.9	0.636	0.434	1.467
		950	100.0	0.592	0.415	1.426
NC12.7	NC12.7-3.0-850	200	15.75	1.026	0.792	1.295
		550	43.3	0.844	0.507	1.663
		850	66.9	0.620	0.450	1.378
	NC12.7-3.0-1250	200	15.7	1.074	0.791	1.357
		550	43.3	0.689	0.507	1.359
		850	66.9	0.591	0.450	1.315
		1250	98.4	0.520	0.416	1.250
	NC12.7-3.0-1400	200	15.7	0.818	0.641	1.650
		550	43.3	0.666	0.471	1.436
		850	66.9	0.556	0.641	1.791
		1250	98.4	0.499	0.471	1.680
		1400	110.2	0.477	0.443	1.531
NG12.7	SG12.7-3.0-350	200	15.8	0.80	0.792	1.01
		350	27.6	0.69	0.600	1.15
	SG12.7-3.0-550	200	15.8	0.66	0.792	0.83
		350	27.6	0.58	0.600	0.97
		550	43.3	0.48	0.507	0.95

6.5.2 Bond and development of GFRP and CFRP bars in SCC beams

As presented and discussed in Chapter 4, the bond stress profiles of both GFRP bars and CFRP bars in SCC beams were slightly different than those for bars embedded in NVC beams. The main difference was that SCC showed a larger bond ability within the uncracked zone of the reinforced member, while the bond stress in the cracked zone was lower than that in similar bars in NVC. The average bond stress of FRP bars in SCC was slightly less than that in NVC. The bond stress equations for both GFRP and CFRP bars were formulated in Chapter 4. In this section, comparisons between the bond stresses of these two types of bars are presented and a new development length equation is formulated.

Figure 6.15 shows that the experimental normalized bond stress results were slightly greater than the results predicted by ACI 440.1R-06. The difference between the predicted and measured bond stresses decreased as the embedment length increased. Based on the experimentally measured tensile stresses of the GFRP bars in SCC, the required embedment length based on CAN/CSA-S6-06, Eqn. (1), CAN/CSA-S806-12, Eqn. (3) and ACI 440.1R-06, Eqn. (5) were calculated and are presented in Figure 6.15. The comparison indicates that the prediction based on ACI 440.1R-06 agrees with the experimental results for GFRP bars in SCC; however, there is no clear margin of safety available.

Bond stress prediction based on CSA-S806-12 was assumed to be constant. This assumption led to unconservative results when the embedment-length-to-bar-diameter ratio exceeded 20 for GFRP bars and about 60 for the CFRP bars. Similarly, ISIS Canada had unconservative prediction of bond stress when the embedment length to bar diameter ratio exceeded 10 for the GFRP and 23 for the CFRP bars. Prediction based on these two equations does not capture the trend of the bond stress versus the embedment-length-to-bar-diameter ratio.

The development length equations for CFRP and GFRP bars embedded in SCC can be developed based on a force equilibrium approach using the normalized average bond equations formulated in Chapter 4 as follows.

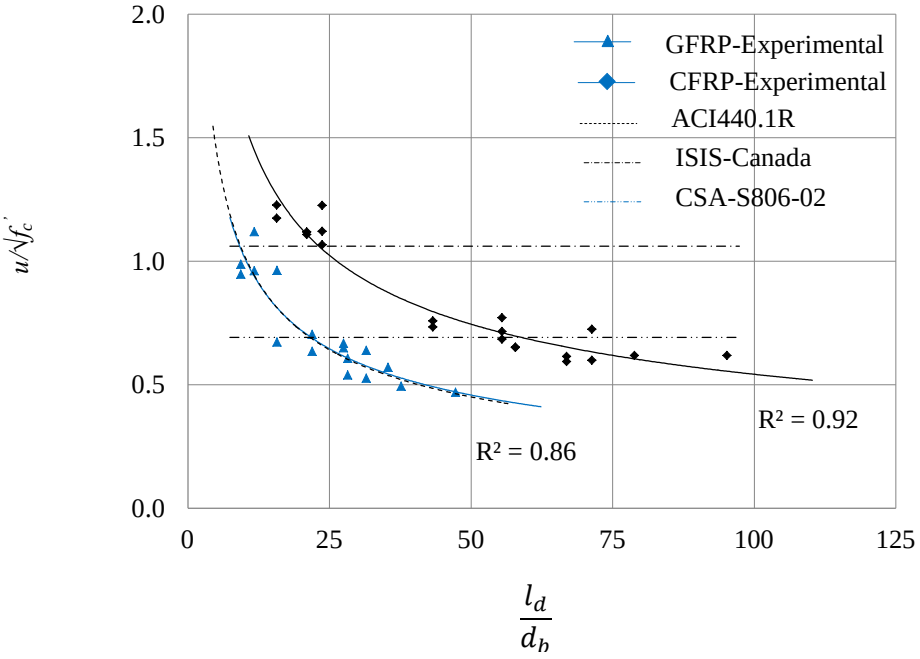

Figure 6.15 Experimental bond stresses of GFRP and CFRP bars in SCC as compared to the available guidelines

6.5.2.1 Development length of GFRP bars in SCC beams

The normalized bond stress equation for GFRP bars in SCC (Eqn. 4.11) is as follows:

$$\frac{\mu}{\sqrt{f_c'}} = 6.479\left(\frac{d_b}{l_e}\right) + 0.072\left(\frac{C}{d_b}\right) + 0.163 \qquad (6.29)$$

Where;

$$1.0 \leq \left(\frac{c}{d_b}\right) \leq 3.0$$

$$10.0 \leq \left(\frac{l_e}{d_b}\right) \leq 50$$

The equilibrium of forces between the beam end and the end of an embedment length (l_e) of a given beam subjected to flexural loading is shown schematically in Figure 6.16 and is given by Eqn. (6.30).

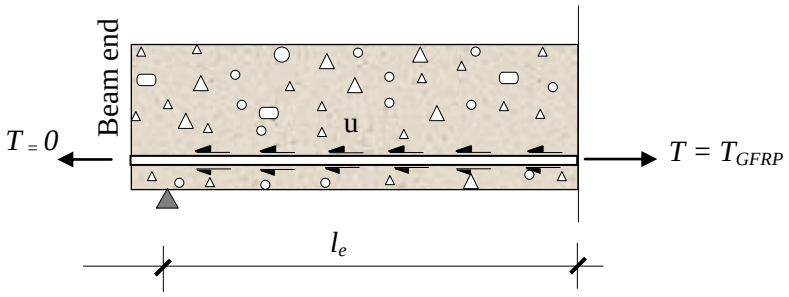

Figure 6.16 Schematic drawing of equilibrium of forces

$$T_{\text{GFRP}} = u_{average}\ \pi\ d_b\ \ l_e \tag{6.30}$$

Equation 6.29 and Equation 6.30 can be solved for the maximum achievable bar stress for a given embedment length l_e as given in Eqn. (6.31).

$$f_{GFRP} = \sqrt{f_c'}\left(0.652\ \frac{l_e}{d_b} + \ 0.288\ \frac{C}{d_b}\ \frac{l_e}{d_b}\ + 25.9\right) \tag{6.31}$$

Equation 6.31 can be rearranged to determine the minimum required embedment length for the GFRP bar embedded in SCC member as follows, Eqn. (6.32).

$$l_e = \left(\frac{\frac{f_{GFRP}}{\sqrt{f_c'}} - \ 25.9}{0.652 + 0.288\ \frac{C}{d_b}}\right) d_b \tag{6.32}$$

Where;

l_e is the embedment length, mm, required for the GFRP bar to develop a tensile stress of f_{GFRP};

f_{GFRP} is the achievable tensile stress in the GFRP bar at the end of the embedment length le, MPa;

$f_c^{'}$ is concrete compressive strength, MPa;

C is the cover thickness to the centre of the GFRP bar, mm; and

d_b is the GFRP bar diameter, mm.

A comparison between the embedment lengths predicted using the proposed model and the experimental data was performed to verify the suitability of the model. Figure 6.17 shows the correlation of the proposed model results and the experimental data. The model fits well with the experimental data with R^2 = 0.84; however, data from others sources are required to verify the applicability of the model under different conditions.

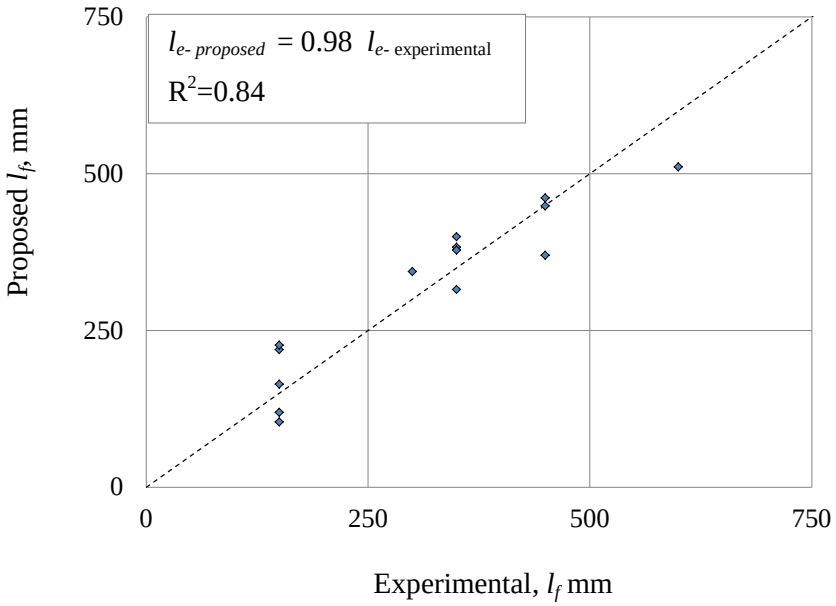

Figure 6.17 Correlation of the proposed vs. experimental flexural bond length of GFRP bars in SCC

6.5.2.2 Development length of the CFRP bars in SCC beams

A similar method was used to develop the development length equation for the CFRP bars in SCC. The bond stress Eqn. (4.14) developed in Chapter 4 is given below.

$$\frac{\mu}{\sqrt{f_c'}} = 13.76\left(\frac{d_b}{l_e}\right) + 0.12\left(\frac{C}{d_b}\right) + 0.09 \qquad (6.33)$$

Equation 6.33 can be used to determine the maximum achievable tensile stress in CFRP bars based on equilibrium Eqn. (6.30) as shown in Eqn. (6.34).

$$f_{CFRP} = \sqrt{f_c'}\left(0.36\,\frac{l_e}{d_b} + 0.48\,\frac{C}{d_b}\,\frac{l_e}{d_b} + 55.04\right) \qquad (6.34)$$

Also, Equation 6.34 can be rearranged to determine the minimum required embedment length, l_e, for a CFRP bar embedded in an SCC member as follows.

$$l_e = \left(\frac{\frac{f_{cfrp}}{\sqrt{f_c'}} - 55.04}{0.36 + 0.48\,\frac{C}{d_b}} \right) d_b \qquad (6.35)$$

Where

l_e is the embedment length, mm, required for the CFRP bar to develop a tensile stress of f_{cfrp}, mm;

f_{cfrp} is the tensile stress in the CFRP bar at the end of the embedment length l_e, MPa;

f_c' is concrete compressive strength, MPa;

C is the cover thickness to the centre of the CFRP bar, mm; and

d_b is the bar diameter, mm.

A comparison between the predictions using the proposed model and the experimental data was performed to verify the suitability of the model. Figure 6.18 shows the correlation between the predicted and the experimental embedment length. It is evident that the model fits well the experimental data with R^2 = 0.97. However, experimental data from others sources are required to verify the applicability of the proposed model under different conditions.

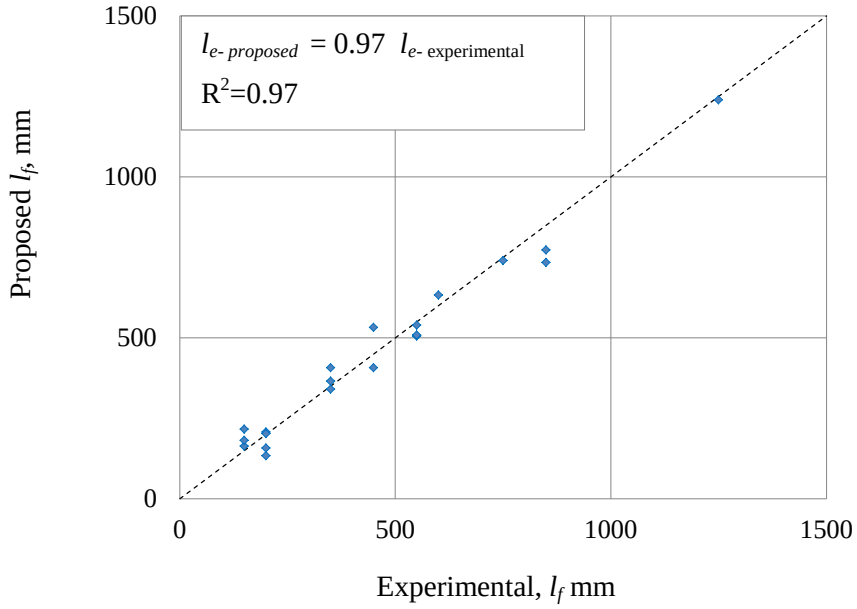

Figure 6.18 Correlation of the proposed vs. experimental flexural bond length of CFRP Bars

Chapter 7 - Analytical Modeling of SCC Beams Prestressed with CFRP Bars

7.1 Introduction

This chapter presents the analytical modeling of the flexural response of SCC beams prestressed with CFRP bars. The main focus is to examine the effect of SCC on the flexural behaviour as compared to that in NVC prestressed beams, using the available prediction models. Models for transfer length and development length of CFRP bars in SCC are formulated and presented. The average bond stress of CFRP bars in the transmission zone due to prestress force release and average bond stress due to flexural loads are analyzed. A new modification factor is applied to exiting code equations to better predict the transfer and development length of CFRP bars in SCC. Results of the transfer length and flexural bond length tests are compared to available design code predictions and to the new models.

7.2 Analytical modeling of FRP prestressed beams

7.2.1 Moment resistance

All of the prestressed beams tested in this program has reinforcement ratios less than the balanced reinforcement ratio. Therefore, the failure mode is expected to be due to rupture of the prestressed CFRP bar. Analysis of the internal forces and prediction of moment resistance is based on tension failure mode as given by ISIS Canada design manual (ISIS M5 - 2008). The analysis is based on strain compatibility and force equilibrium. Constitutive relationships for concrete and CFRP bars were given in Chapter 6. In this analysis, the tensile stress in the concrete after cracking is considered. A schematic of the model is shown in Figure 7.1. The analysis is governed by the following equations.

The compressive force in the concrete as given by Eqn. (7.1)

$$C = \alpha \, \emptyset_c \, f_c' \, \beta \, c \, b \qquad (7.1)$$

Because all the beams were designed to fail due to rupture of the prestressing CFRP bar, the corresponding strain at the extreme compression fibre is less the concrete crushing strain (ε_u). The traditional rectangular stress block distribution cannot be used. The values of β and α used in this analysis account for the strain at the top compression fibre less than ultimate strain of the concrete. The values of β and α used in this analysis were taken from ISIS Design Manual 5.

The tensile force in the CFRP bar as given by Eqn. (7.2)

$$T_{cfrp} = A_{cfrp}\ \emptyset_{cfrp}\ \varepsilon_{cfrp}\ E_{cfrp} \qquad (7.2)$$

The tensile force in the concrete below the neutral axis as given by Eqn. (7.3)

$$T_c = \frac{1}{2}\ \emptyset_c\ \varepsilon_{cx}\ E_c\ x\ b \qquad (7.3)$$

The equilibrium of forces ($C = T_{frp} + T_c$) must be satisfied:

$$\alpha\ \emptyset_c\ f_c'\ \beta\ c\ b = A_{cfrp}\ \emptyset_{cfrp}\ \varepsilon_{cfrp}\ E_{cfrp} + \frac{1}{2}\ \emptyset_c\ \varepsilon_c\ E_c\ x\ b$$

The strain compatibility in the cross section as give in Eqn. (7.3)

$$\frac{c}{d} = \frac{\varepsilon_t}{\varepsilon_t + \left(\varepsilon_{cfrp} - \varepsilon_{pe}\right)} \qquad (7.4)$$

Where

A_{frp} is the cross-sectional area of the FRP bar;

b is the width of the compression face of the member;.

C is the compressive force in the concrete in the compression region;

c is the depth of neutral axis;

d is the depth from the concrete top fibre to the centroid of the prestressing CFRP bar;

f_c' is the specified compressive strength of concrete;

f_{frp} is the tensile stress in the CFRP bar;

T is the tensile force in the FRP bar;

x is the distance from the neutral axis to where the strain in concrete equal to the rupture concrete strain ($\varepsilon_t = f_r/E_c$);

α is the stress factor to calculate the intensity of the compressive stress in concrete;

β is the stress-block factor for concrete;

ε_{cfrp} is the total strain in the CFRP (effective pre-strain and flexural strain);

ε_{pe} is the effective strain in the CFRP bar;

ε_t is the compressive strain at the extreme compression fibre of concrete;

φ_c is the strength reduction factor for concrete taken to be 1.0 in this analysis; and

φ_{frp} is the strength reduction factor for FRP bar taken to be 1.0 in this analysis.

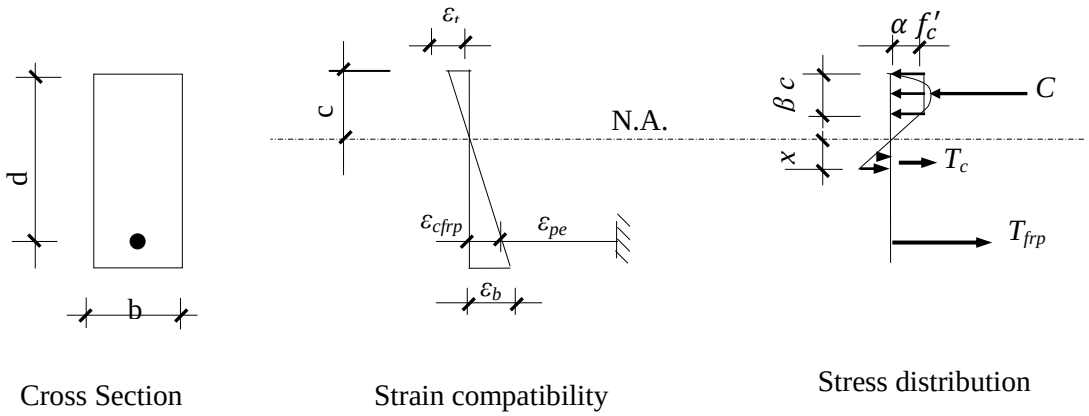

Figure 7.1 Section analysis model

Using an iterative procedure, a solution can be obtained for the two unknowns, c and ε_p, in Eqns. (7.1) and (7.2). A spreadsheet was used to implement the iterative procedure of the model. Then the moment resistance can be calculated using Eqn. (7.5).

$$M_r = T\left(d - \frac{\beta\ c}{2}\right) + Tc\left(\frac{2}{3}\ x + c - \beta\ \frac{c}{2}\right) \qquad (7.5)$$

7.3 Moment deflection response

The moment resistance of CFRP prestressed beams at different loading stages can be calculated using the model presented in Section 2.1. Two methods are used to calculate the midspan deflection in the CFRP prestressed concrete beams. The first method is a simplified method given in ACI440.4 (2004). The deflection is calculated based on the average effective moment of inertia along the beam span. The second method considers two additional parameters not considered in the simplified method. The first parameter is the change in the neutral axis depth in calculating the cracked transformed moment of inertia. As load increases, the neutral axis shifts to the compression side of the cross section, and thus the cracked transformed moment of inertia decreases. The effective moment of inertia used in the detailed model is a function of the cracked transformed moment of inertia. The second parameter reflects the change in the eccentricity in the prestress force as the applied moment increases as proposed by Abdelrahman and Rizkalla (1998). Results of the midspan deflection prediction based on this method had good agreement with independent experimental measurements for NVC beams and prestressed with CFRP bars (Abdelrahman and Rizkalla 1998). The two methods are presented below.

7.3.1 Simplified method for deflection prediction

The midspan deflection is calculated based on the transformed moment of inertia before the concrete is cracked. Basic elastic analysis is used to obtain the midspan deflection at a given applied moment. After cracking, the midspan deflection is calculated based on the effective moment of inertia of the beam. The effective moment of inertia is empirically derived for FRP prestressed concrete flexural members based on the assumption of a uniform moment of inertia along the beam span (ACI 440.4 2004).

$$I_e = \left(\frac{M_{cr}}{M_a}\right)^3 \beta_d I_g + \left(1 - \left(\frac{M_{cr}}{M_a}\right)^3\right) I_{cr} \leq I_g \qquad (7.6)$$

$$\beta_d = 0.5 \left[\frac{E_p}{E_s} + 1\right] \qquad (7.7)$$

$$I_{cr} = \frac{b\,(kd)^3}{3} + n_{frp}\, A_{frp}\, (d - kd)^2 \qquad (7.8)$$

$$n_{frp} = \frac{E_{frp}}{E_c} \qquad (7.9)$$

$$\rho = \frac{A_{frp}}{bd} \qquad (7.10)$$

$$k = \sqrt{\left(\rho n_{frp}\right)^2 + 2\,\rho n_{frp}} - \rho n_{frp} \qquad (7.11)$$

Where;

A_{frp} is the cross sectional area of the FRP bar;

b is the width of the cross section;

d is the depth of the centre of the reinforcing FRP bar;

E_c is the modulus of elasticity of concrete;

E_{frp} is the modulus of elasticity of the FRP bar;

I_{cr} is the moment of inertia of the cracked section;

I_e is the effective moment of inertia;

I_t is the moment of inertia of the uncracked transformed section;

k is a factor given by Eqn (7.11);

M_a is the applied moment;

M_{cr} is the cracked moment;

n_{frp} is the modular ratio; and

ρ is the reinforcement ratio, $\left(\rho = \frac{A_{frp}}{b\,d}\right)$.

The midspan deflections of a symmetrically simply supported CFRP prestressed beam under four-point flexural loading can be calculated based on the basic elastic beam analysis (Eqn. 7.12).

$$\Delta = \frac{P\,a}{24\,E_c\,I_e}\,(3\,l^2 - 4\,a^2) \qquad (7.12)$$

Where

a is the shear span;

l is the total beam span; and

P is applied load.

7.3.2 Detailed method for deflection prediction

Abdelrahman and Rizkalla (1998) proposed a model to calculate the effective centroid (y_e) of the transformed cracked section. This model was based on experimental results of beams prestressed with CFRP bars with measurements taken at various load levels. In this model, the calculated deflection accounts not only for the change in the effective moment of inertia but also the change in the eccentricity ($d_p - y_e$) of the effective prestress force (P_e) after cracking. The procedure is given by the following equations.

The effective moment of inertia is given by Eqn. (7.13).

$$I_e = \Psi^3\,I_g + (1 - \Psi^3)\,I_{cr} \;\leq\; I_g \qquad (7.13)$$

and

$$\Psi = \left(\frac{M_{cr} - M_{dc}}{M_a - M_{dc}}\right), \qquad M_s > M_{cr} \qquad (7.14)$$

Where

I_e is the effective moment of inertia;

I_g is the gross moment of inertia;

I_{cr} is the cracked transformed moment of inertia; and

Ψ is a factor that accounts for the applied moment (M_a), cracking moment (M_{cr}) and decompression moment (M_{dc})

The midspan deflection, including the effect of change in the eccentricity of the prestressing force, of beams prestressed with CFRP bars subjected to four-point flexural loading can be calculated as given in Eqn. (7.15)

$$\Delta = -\frac{1}{8}\frac{P_e\left(d_p - y_e\right)L^2}{E_c\, I_e} + \frac{P\, a}{24\, E_c\, I_e}\left(3\, l^2 - 4\, a^2\right) \tag{7.15}$$

Where

$$y_e = \Psi^2\, y_g + \left(1 - \Psi^2\right)\, y_{cr} \leq y_g \tag{7.16}$$

Where

Δ is the midspan deflection of, mm;

P_e is the effective prestressing force, kN;

I_g is the gross sectional moment of inertia, mm^4;

I_{cr} is the cracked transformed moment of inertia, mm^4;

a is the shear span, mm;

L is the total clear span, mm;

Ψ is a factor that accounts for the applied moment, cracking moment and decompression moment

A sectional analysis is necessary to determine the depth of the neutral axis required for calculation of the I_{cr}.

7.4 Analytical results

The moment versus midspan deflection curves of four CFRP prestressed beams were predicted. Beams that failed by CFRP bar rupture were of interest in this analysis. Two beams were made from SCC: SC-30-1350 and SC-60-1700, and two corresponding beams were made from NVC: NC30-1350 and NC60-1500. These beams provided a wide range of applied moment (above service and up to ultimate) versus midspan deflection for comparison with the predicted responses. The main purpose of the analysis was to assess the applicability of section analysis and deflection prediction models for SCC beams prestressed with CFRP bars as compared to beams made from NVC.

7.4.1 Beams made from SCC

Prediction results of the sectional analysis and midspan deflection of Beam SC30-1350 are given in Table 7.1 and compared graphically in Figures 7.2. The predicted total strain in the prestressed CFRP bar at failure was 10039με, while the measured value was 12530με. The measured CFRP strain was about 20% higher than the predicted value possibly due to the location of the strain gauge with respect to the flexural cracks. The measured compression strain in the concrete at failure was 2160με as compared to the predicted value of 2300με; however, the measured compression strain in the concrete did not include the pretension strain in concrete due to prestressing force.

Since the measured experimental deflection did not include the camber due to prestressing, the camber was removed from the predicted values. Prediction of midspan deflection based on the simplified method had a good agreement with the experimental values at lower load levels; however, the predictions diverged from the measured values as the load increased. At the failure moment (34.3kN.m), the predicted deflection was 42.4mm as compared to the measured value of 50.4mm. Prediction using the detailed method had better agreements with the experimental results at all load levels. At failure moment, the predicted deflection based on this method was 53.1mm versus the measured value of 50.4mm. On average, the detailed method provided closer predictions (less than ±10%) for this beam.

Table 7.1 Analytical sectional analysis and deflection predictions for Beam S30-3

Beam condition	ε_t	ε_{cfrp} (1)	C mm	Curvature ($\times 10^6$) 1/mm	Moment kN.m	Midspan deflection, mm	
						(2)	(3)
					0.0	0.0	0.0
					4.0	1.0	1.0
Zero curvature				0.0	6.2	1.6	1.6
					9.0	2.3	2.3
Bottom concrete crack					10.1	2.6	2.6
	-400	4349.2	149.7	2.7	14.2	8.5	6.5
	-500	4519.7	125.4	4.0	15.1	10.0	8.6
	-1000	5872.2	76.9	13.0	19.6	17.9	19.9
	-1500	7437.5	65.1	23.0	25.1	27.7	33.0
	-2000	9057.1	60.0	33.4	30.8	37.1	44.8
CFRP bar rupture	-2300	10039.8	58.1	39.6	34.3	42.4	53.1

Total strain in CFRP bar (including effective prestress strain of 4200με; (2) deflection based on simplified method and (3) deflection based on detailed method

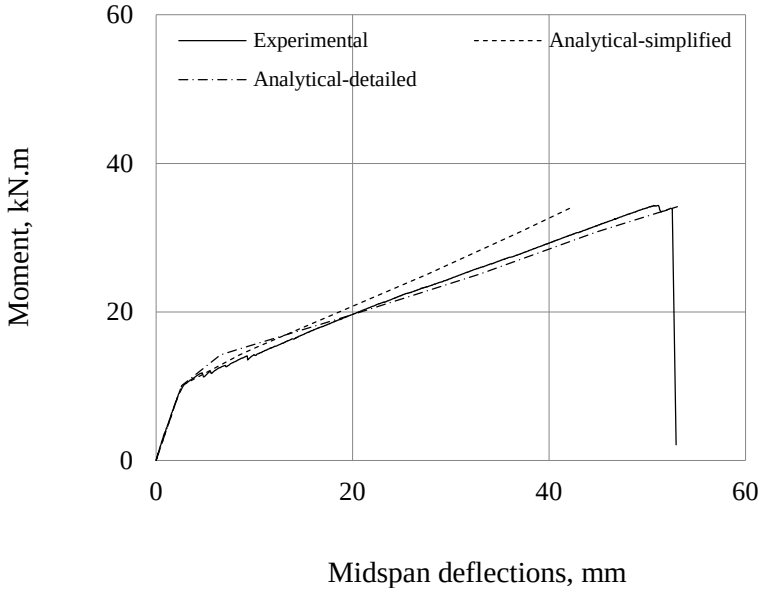

Figure 7.2 Experimental and predicted moment versus midspan deflection for Beam S30-3

Table 7.2 gives the results of sectional analysis for beam S60-4. The predicted strain in the CFRP bar at the failure moment was 12169.6με (corresponding to a tensile stress of 1752MPa). The measured strain was 12039με at the same applied moment, which was in good agreement with the predicted value. The measured strain in the concrete was -2235 με (does not include pretension strain due to prestress force) while the predicted strain (including pre-strain) was -2650με.

The predicted versus measured moment-deflection responses of Beam S60-4 are shown in Figure 7.3. Prediction of the midspan deflection based on the simplified method was unconservative by about 20% throughout the beam response after cracking. Prediction using the detailed method provided better correlation with the measured values. There was a slight underestimation of the midspan deflection after cracking and up to about 60% of the failure moment. This beam experienced stiffness loss as the applied moment exceeded 36.0kN.m. This softening is possibly due to local slip in the CFRP bar within the transfer zone.

Table 7.2 Analytical sectional analysis and deflection predictions for Beam S60-4

Beam status	ε_t	ε_{cfrp}(1)	C mm	Curvature ($\times 10^6$)1/mm	Moment kN.m	Midspan deflection, mm	
						(2)	(3)
					0.0	0.0	0.0
					4.0	0.9	0.9
Zero curvature					6.2	1.3	1.3
					9.0	2.0	2.0
					10.1	2.2	2.2
Bottom concrete crack	-447.0	6763.6	203.9	2.19	20.1	7.1	4.6
	-500.0	6804.3	188.8	2.65	21.3	8.4	5.1
	-750.0	7220.3	127.4	5.89	22.6	9.9	6.0
	-1000.0	7771.4	101.9	9.82	24.9	12.8	7.9
	-1250.0	8423.1	88.2	14.2	27.4	16.1	10.6
	-1500.0	9124.3	79.8	18.8	30.0	19.6	14.2
	-2000.0	10614.1	70.2	28.5	35.4	27.0	20.6
	-2500.0	12169.6	65.0	38.5	40.9	34.2	31.1
Beam failed	-2650.0	12169.6	63.8	41.5	42.5	36.4	33.9

Total strain in CFRP bar (including effective prestress strain of 6760με; (2) deflection based on simplified method and (3) deflection based on detailed method.

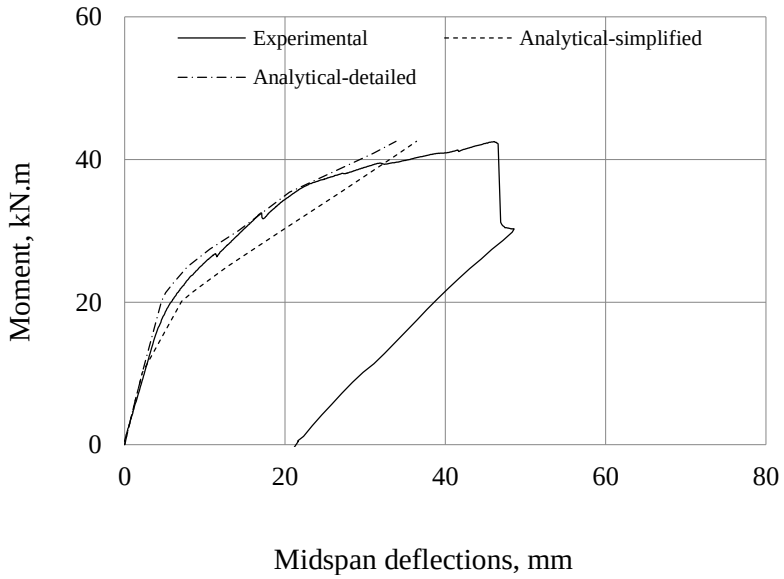

Figure 7.3 Experimental and predicted moment versus of midspan deflection for Beam S60-4

7.4.2 Beams made from NVC

Prediction results of sectional analysis and midspan deflection of Beam N30-1 are given in Table 7.3 and compared graphically in Figures 7.4. Beam N30-1 had a failure moment of 43.6kN.m, a measured total strain in the prestressed CFRP bar of 14100με and a strain in concrete of -3086 με (without the pretension strain). The predicted total strain in the prestressed CFRP bar was 12612.0με (corresponding to a tensile stress of 1816.0MPa), which was 11% lower than the measured value. The predicted compression strain in the concrete was -2680με, which was 13% less than the measured value.

Prediction of the midspan deflection based on the simplified method was unconservative after cracking. The predicted midspan deflection at the failure moment was 51.8mm, and the measured value was 68.1mm or 31% higher than the prediction value. The predicted midspan deflection based on the detailed method had less unconservative predictions with about 10% at the low load levels, and the difference between predicted and measured values decreased to less than 5% at the failure moment. The possible explanation of this trend in the detailed method could be related to the change in eccentricity of the prestressing force due to change in the effective centroid of the cracked transformed section as the flexural cracks propagate in the concrete section. This specimen had a relatively higher stiffness (E_c of 37,400MPa) than the SCC specimens discussed in Section 7.1.2.1. The difference between predicted and measured deflections was less in SCC specimens with small unconservative predictions at low load levels.

Table 7.3 Analytical sectional analysis and deflection predictions for Beam N30-1

Beam condition	ε_t	ε_{cfrp} (1)	C mm	Curvature ($\times 10^6$)1/mm	Moment kN.m	Midspan deflection, mm	
						(2)	(3)
					0	0	0
					4.0	0.70	0.7
Zero curvature					5.7	1.0	1.0
					9.0	1.5	1.5
Bottom concrete crack					10.5	1.8	1.8
	-400.0	4257.9	109.9	3.6	14.2	6.1	4.8
	-500.0	4505.7	93.8	5.3	15.3	7.5	6.2
	-550.0	4658.8	87.0	6.3	15.8	8.2	6.9
	-750.0	5322.1	71.3	10.5	18.0	11.7	11.0
	-1000.0	6218.3	62.1	16.1	21.2	16.9	17.5
	-1500.0	8091.1	54.3	27.6	27.8	28.0	31.9
Beam failed	-2000	10000.2	50.8	39.4	34.5	38.5	45.1
	-2500	11925.7	48.9	51.2	41.2	48.5	60.7
	-2680	12612.3	48.4	55.4	43.6	51.8	65.7

Total strain in CFRP bar (including effective prestress strain of 4200με; (2) deflection based on simplified method and (3) deflection based on detailed method

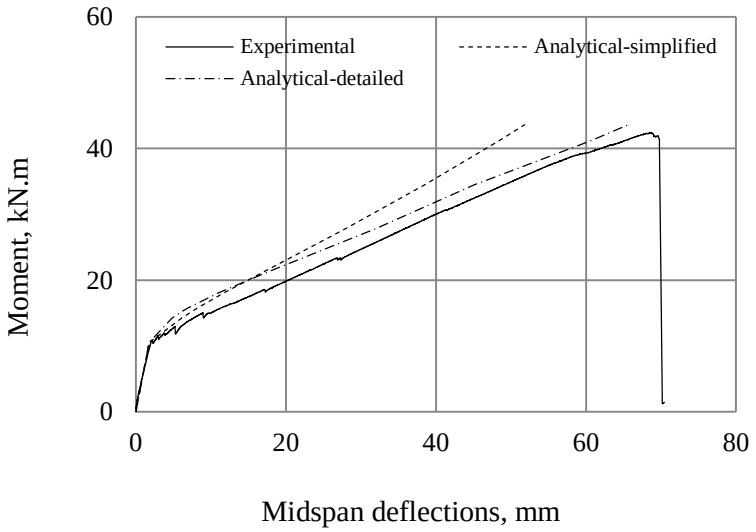

Figure 7.4 Experimental versus predicted moment versus midspan deflection for Beam N30-1

Table 7.4 gives the results of sectional analysis and midspan deflection predictions of Beam N60-4 which had a failure moment of 42.6kN.m, and a measured total strain in the prestressed CFRP bar of 14200με. It is important to note that the strain gauge attached on the prestressed CFRP bars of this beam stopped working at an applied moment of 31.7kN.m and a strain of 12300με. Extrapolation was used to obtain the strain at the failure moment of 42.6kN.m. The strain in the concrete at the failure moment was -2508με (without the pretension strain). The predicted total strain in the prestressed CFRP bar was 12456.0με (corresponding to a tensile stress of 1794.0 MPa) and the compression strain in concrete was -2120με. The predicted values were about 15% less than the measured responses.

Prediction of the midspan deflection based on the simplified method was unconservative after cracking. The predicted midspan deflection at the failure moment (42.3kN.m) was 33.3 mm, and the measured value was 47.6mm; thus the prediction was 30% lower than the measured value. The prediction of midspan deflection based on the detailed method was also unconservative at low load levels. At an applied moment of 22.0kN.m, for example, the predicted midspan deflection was 5.1mm, and the measured value was 8.2mm (unconservative by more than 50%). The difference between the predicted and measured midspan deflection decreased as the applied moment increased. At the failure moment (42.3kN.m), the predicted midspan deflection was 45.2mm and the measured was 47.5mm, i.e. the predicted/ measured ratio was 0.95.

Table 7.4 Analytical sectional analysis and deflection predictions for Beam N60-4

Beam status	ε_t	ε_{cfrp}*(1)*	C Mm	Curvature ($\times 10^6$)1/mm	Moment kN.m	Midspan deflection, mm	
						(2)	(3)
					0	0	0
					4.0	0.9	0.9
Zero curvature					5.7	1.1	1.1
					16.0	2.8	2.8
Bottom concrete crack	-400	7326.6	189.0	2.12	22.2	7.0	5.1
	-500	7454.4	155.1	3.22	23.5	8.3	7.1
	-750	7983.8	106.9	7.02	25.6	10.7	11.4
	-1000	8664.5	86.6	11.50	28.4	14.0	16.6
	-1500	10269.4	68.9	21.80	34.4	22.2	28.8
	-2000	12022.2	61.1	32.70	40.7	31.2	42.0
Beam failed	-2120	12456.4	59.8	35.40	42.3	33.3	45.2

Total strain in CFRP bar (including effective prestress strain of 7290με; (2) deflection based on simplified method and (3) deflection based on detailed method

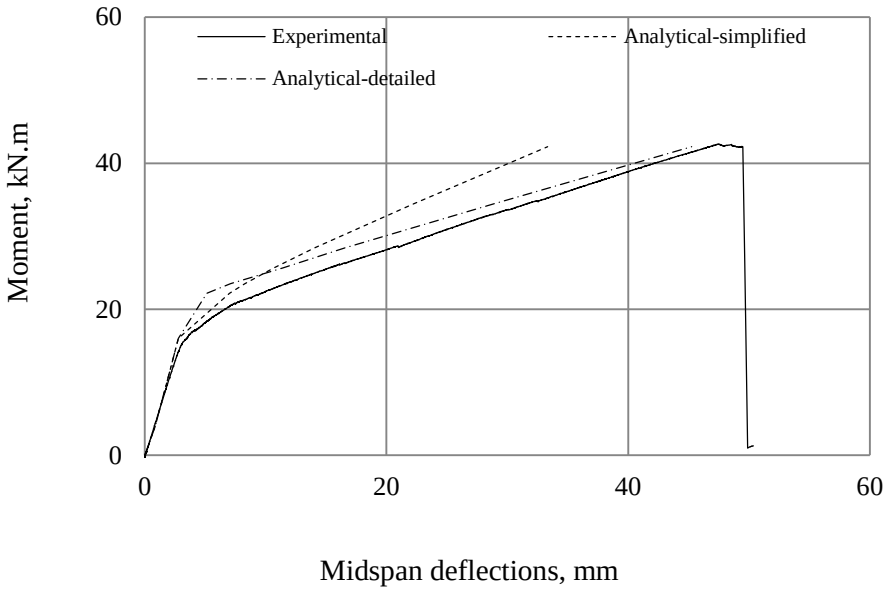

Figure 7.5 Experimental versus predicted moment versus midspan deflection for Beam N60-4

7.5 Transfer length modeling

This section provides a comparison of the experimentally measured transfer length and the predictions using design code equations. Both ISIS Canada M5 (2008) and ACI 440.4R (2004) have the same equation for the transfer length prediction and will be referred to as ACI prediction. The average bond stress within the transmission zone was evaluated using the transfer length results from concrete strain profile and draw-in methods. Then a new bond stress equation was formulated and a modification to the exiting transfer length model was proposed to account for SCC.

7.5.1 Comparison of the transfer length results with design equation predictions

The average measured transfer lengths from both methods (concrete strain profile and draw-in) were compared to the ACI440.4R (2004) prediction, Eqn. (7.17) as given in Table 7.5. The actual values of the prestressing force and concrete compressive strength at transfer for each beam were used to calculate the predicted transfer length values.

$$l_t = \frac{f_{pi}\, d_b}{\propto_t \; f_{ci}^{0.67}} \qquad (7.17)$$

Where

l_t is the transfer length, mm;

f_{pi} is the initial prestress stress in the CFRP bar, MPa;

d_b is the CFRP bar diameter, mm;

α_t is a coefficient that depends on the bar type: 1.9 for Leadline bars and 4.8 for CFCC strand, the value of 1.9 was taken in this comparison analysis; and

f'_{ci} is the concrete compressive strength at transfer, MPa.

The measured transfer length of the 30% prestressed CFRP bars in SCC based on draw-in method was 75% of the predicted value and the transfer length based on the concrete strain profile was 95% of the predicted value. At a 45% prestressing level, the measured transfer lengths from both methods were close to the prediction values. At a 60% prestress level, the ACI prediction underestimated the transfer length; the experimental transfer length was 25% longer than predicted. For NVC specimens, at both 30% and 60% prestress levels, the experimental transfer length based on draw-in method was about 75% of the predicted value and the transfer length based on the concrete strain profile method was 90% of the predicted values.

Table 7.5 Comparison of the average transfer length measured by concrete strain profile and draw-in methods as compared to the ACI440.4 prediction values

Group/ Beam label		f_i, MPa	ACI 440.4 transfer length prediction, mm (1)	Concrete strain profile method		Draw-in method	
				Experimental transfer Length, mm (2)	$\frac{(1)}{(2)}$	Experimental transfer Length, mm (3)	$\frac{(1)}{(3)}$
I	S30-1	568.3	386	-	-	306	0.79
	S30-2	552.5	375	355	0.95	259	0.69
	S30-3	647.2	439	-	-	337	0.77
	S30-4	623.5	423	-	-	320	0.76
II	S45-1	764.1	450	-	-	534	1.19
	S45-2	814.5	479	505	1.05	492	1.03
	S45-3	796.4	469	530	1.13	499	1.06
	S45-4	760.1	447	-	-	487	1.09
III	S60-1	960.5	533	655	1.23	677	1.27
	S60-2	1026.0	570	-	-	733	1.29
	S60-3	954.7	530	695	1.31	629	1.18
	S60-4	1003.2	557	650	1.17	694	1.25
IV	N30-1	582.0	300	300	0.90	250	0.72
	N60-2	1112.9	662	-	-	527	0.80
	N60-3	1060.3	631	580	0.92	511	0.81
	N60-4	1101.3	655	590	0.90	478	0.73

The measured transfer length results from both concrete strain profile and draw-in methods were plotted versus the initial prestressing stress in Figure 7.6. The predictions using ACI 440.4R-04 (Eqn. (7.17)) were also plotted on the same figure. The experimental transfer lengths of the CFRP bars in NVC beams were on the conservative side, ranging between 90% of the prediction at low prestressing level to 75% of the prediction at higher prestressing levels. The experimental transfer lengths of the CFRP bars in SCC deviated to the unconservative side of the ACI prediction when the prestressing stress exceeded 750MPa. The ratio between experimental to predicted values was about 1.25 at a prestressing stress of around 1000MPa. As the prestressing level increased, the transfer length of CFRP bars in SCC showed a slightly nonlinear trend with the prestress level. A possible explanation of this trend is the difference in the stress-strain behaviour of SCC versus NVC at early ages. SCC exhibits higher compressive strain values than NVC at similar prestressing forces (Figures 5.1 and

5.2). The low modulus of elasticity of SCC at early concrete age could be an indication of a slow bond strength development of the SCC mixes. More research is needed to verify this hypothesis.

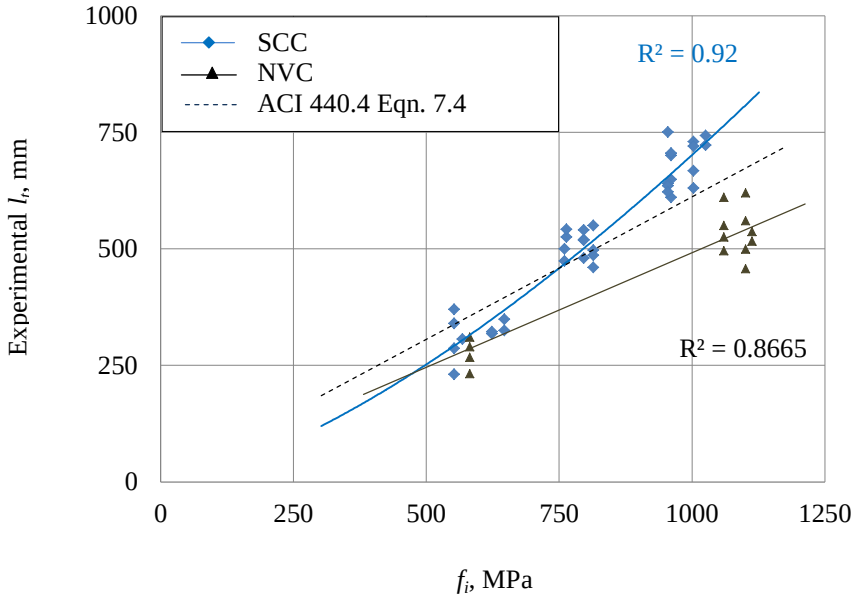

Figure 7.6 Transfer length results compared to ACI 440.4 prediction

7.5.2 Bond stress formulation

Figure 7.7 shows the relationship between the normalized bond stress and initial prestressing stress. The normalized bond stress was taken as the average bond stress divided by $f_{ci}^{0.67}$ to account for differences in the concrete compressive strength at transfer. The data shown in Figure 7.7 includes all transfer length results at the live end and dead end based on the two measurement methods. It is evident from Figure 7.7 that the average bond stress decreased as the prestressing level increased.

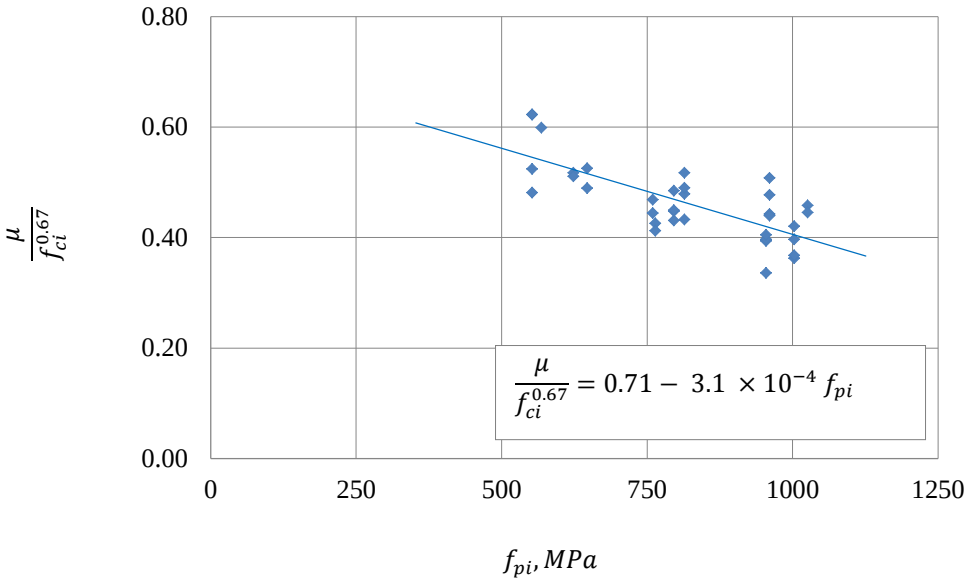

Figure 7.7 Normalized bond stress of CFRP bar in SCC versus initial prestressing stress

A linear relationship was used as the best fit curve for the normalized bond stress data versus the initial prestress in SCC as given in Equation 7.18. This approach is consistent with the bond equation used for NVC specimens. The linear relationship provided an acceptable fit with R^2 of 0.72. It should be noted that there was no improvement for higher degree relationships between the normalized bond stress and the initial prestress of this data. This relationship is valid within the prestressing limits in this study. While this range is the most widely used in construction, this relationship needs to be verified for other prestressing ranges.

$$\frac{\mu_t}{f_{ci}^{0.77}} = 0.71 - 3.1 \times 10^{-4} f_{pi} \qquad (7.18)$$

Where

f_{pi} is the initial prestressing stress, MPa;

μ_t is the average bond stress due to prestress load release, MPa; and

f_{ci} is the concrete compressive strength at release.

7.5.3 Formulation of transfer length equation

The equilibrium of forces between the beam end section, where the bar stress is zero, and at the end of the transfer length section, where the prestressing force is fully transferred, is shown schematically in Figure 7.8 and is given by Eqn. (7.19).

$$T_{pi} = \mu \pi d_b l_t \quad (7.19)$$

Where

T_{pi} is the prestressing force, N;

u is given by Eqn (7.3);

d_b is the prestressing bar diameter, mm; and

l_t is the transfer length.

Solving Eqn. (7.18) and Eqn. (7.19) gives the transfer length l_t in Eqn. (7.20):

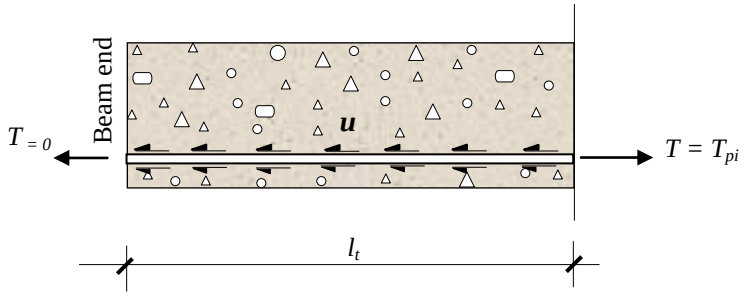

Figure 7.8 Schematic of equilibrium of forces within transfer zone

$$l_t = \frac{f_{pi}\, d_b}{\alpha_t\, f_{ci}^{0.67}} \quad (7.20)$$

Where;

$$\alpha_t = 2.84 - \frac{f_{pi}}{800}$$

The predicted results based on this equation correlated well with the experimental results for the transfer length of a 12.7mm diameter CFRP bar in SCC as shown in Figure 7.9. The CFRP bar used in this study has different mechanical and physical properties than previously available bars. The author expects that the effect of bar diameter would be similar to that previously reported by Mahmoud et al., (1999).

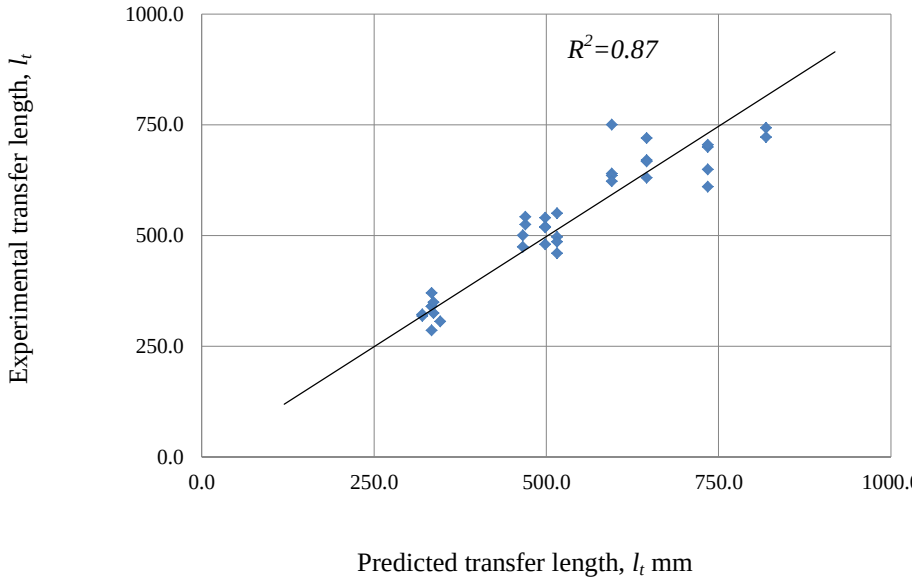

Figure 7.9 Correlation of the predicted vs. experimental transfer length of CFRP bars in SCC

7.5.4 Flexural bond length of SCC beams prestressed with CFRP bars

As a prestressed member is loaded in flexure, additional tensile stresses are developed in the prestressing reinforcement to generate an internal moment to counteract the external applied moment. The minimum embedment length required for a prestressing bar to develop a tensile stress from the effective prestressing stress to the full tensile strength of this prestressing bar is defined as the flexural bond length. The summation of the transfer length and the flexural bond length is defined as the development length. In this section, an analysis of the bond stress within the flexural bond length is carried. Then, a model is formulated that predicts the flexural bond length of the prestressed CFRP bars in SCC.

7.5.4.1 Average bond stress within the flexural bond length

The average bond stresses in the flexural bond region of the beams were calculated based on the measured increase in the tensile stresses in the CFRP bars during the flexural test. Table 7.6 gives the available flexural bond length, the increase in tensile stresses due to flexural load and the calculated average bond stresses. The results indicate that the flexural bond stresses were significantly less than the average bond stress developed within the transfer zone.

Table 7.6 Flexural bond stress of CFRP prestressed beams

Beam	f_e, MPa	l_{tr}, mm	Shear span, mm	Available l_f, mm	Increase in CFRP tensile stress, MPa	Average u_f, MPa	$\frac{u_f}{f_c'^{0.67}}$
S30-1	549.9	306.0	1100	794.0	810.5	3.2	0.19
S30-2	534.8	301.8	1250	943.0	1166.3	3.9	0.24
S30-3	626.4	337.0	1350	1013.0	1215.5	3.8	0.28
S30-4	604.8	320.0	1500	1180	583.0	*	*
S45-1	750.3	533.5	1100	566.5	582.4	3.4	0.19
S45-2	794.3	515.8	1250	751.8	714.7	2.9	0.17
S45-3	776.6	514.5	1350	835.5	635.8	2.7	0.16
S45-4	741.1	487.0	1500	1013.0	927.3	2.9	0.17
S60-1	932.7	668.5	1100	434.0	369.5	2.7	0.16
S60-2	995.3	732.5	1350	617.5	478.6	2.5	0.15
S60-3	920.3	661.8	1500	838.2	611.2	2.3	0.17
S60-4	974.1	671.8	1700	1028.2	813.5	2.5	0.18
N30-1	540.0	274.8	1350	1075.2	1291	3.8	0.23
N60-2	1076.0	526.5	1250	723.5	540.0	2.4	0.15
N60-3	1026.4	545.4	1350	804.6	791.0	3.1	0.19
N60-4	1052.9	534.1	1500	965.9	806.2	2.6	0.16

* This beam failed by premature bar rupture and its test results were excluded from the average bond stress analysis.

The data for normalized bond stress versus the flexural tensile stress of the CFRP bars is shown in Figure 7.10. Only the beams that failed by bond pullout were used. It is evident that the normalized bond stress increases as the flexural tensile stress of the CFRP bar increases. SCC specimens had normalized flexural bond stresses at a given flexural tensile stress similar to those of NVC.

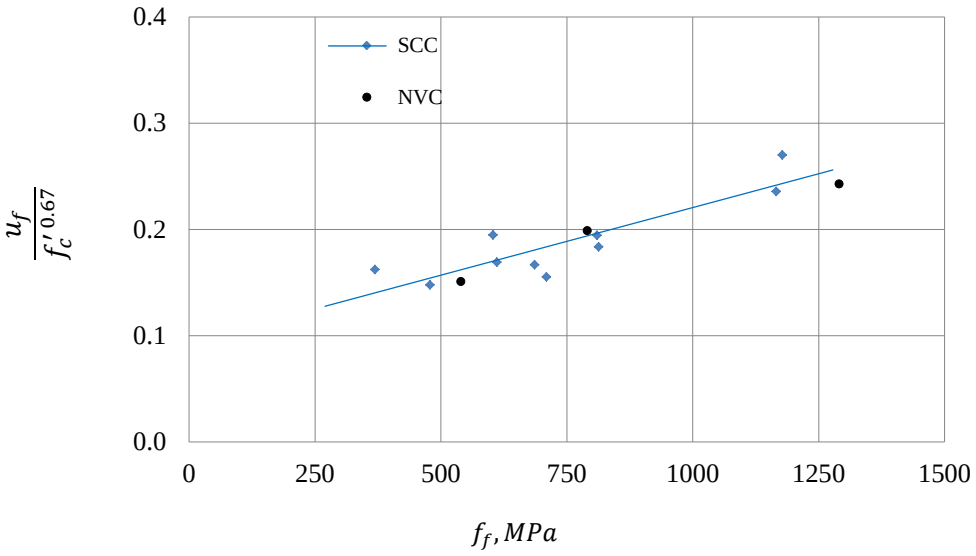

Figure 7.10 Normalized bond stress of CFRP bar in SCC versus flexural tensile stress

7.5.4.2 Formulation of flexural bond length equation

Based on the data shown in Figure 7.10, a linear relationship between the normalized flexural bond stress and flexural tensile stresses in a prestressed CFRP bar in SCC was formulated (Eqn. 7.21). This relationship represents the best fit curve of the data with R^2 of 0.79. The equation is valid for bond pullout failure because a sufficient concrete cover was available to prevent splitting bond failure.

$$\frac{u_f}{f_{ci}^{0.67}} = 1.0 \times 10^{-4} f_f + 0.0934 \qquad (7.21)$$

Where

f_f is the flexural bond stress, MPa;

u_f is the flexural average bond stress, MPa; and

f'_c is the concrete compressive strength, MPa.

The equilibrium of forces between two sections (1) and (2) located within the flexural bond length of a prestressed beam subjected to flexural loading is shown schematically in Figure 7.11 and is given by Eqn. (7.22).

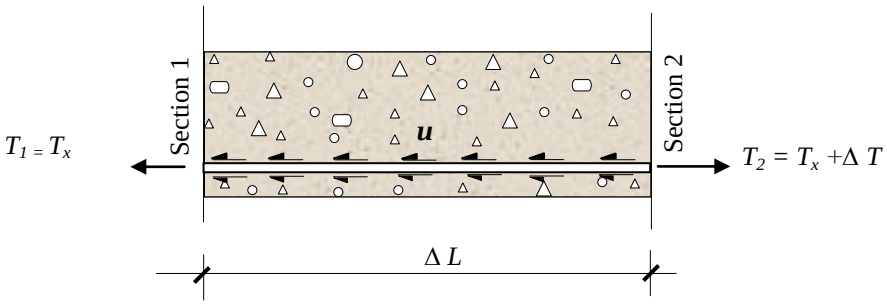

Figure 7.11 Schematic drawing of equilibrium of forces within flexural length, l_f

$$T_2 = T_1 + u_f \; d_b \; \Delta l \qquad (7.22)$$

Substituting the values of the $T_1 = T_x$ and $T_2 = T_x + \Delta T$ yields Eqn (7.23)

$$T_x + \Delta T = T_x + \mu_f \, \pi \, d_b \, \Delta l \qquad (7.23)$$

Simplifying Eqn. (7.23) yields Eqn (7.24)

$$\Delta T = \mu_f \; \pi \; d_b \; \Delta l \qquad (7.24)$$

Where

T_1 and T_2 are the tensile forces in the CFRP bar at Sections 1 and 2, respectively, N;

ΔT is the increase in the tensile force in the CFRP bar over the length of Δl *(mm)*, N;

u_f is the average bond stress between Section 1 and Section 2, MPa; and

d_b is the CFRP bar diameter, mm.

Replacing distance Δl by the available flexural bond length (l_f) of a beam, Eqn (7.24) can be rewritten as shown below:

$$T_f = \mu_f \; \pi \; d_b \; l_f \qquad (7.25)$$

Where

T_f is the additional tensile force in the prestressed CFRP bar at the end of the flexural bond length, N;

u_f is the average flexural bond stress, as given in Eqn (7.21); and

l_f is the available flexural bond length.

Solving Eqn. (7.21) and Eqn. (7.25) for l_f gives a relationship between the flexural tensile stress and the flexural bond length required to accommodate the flexural stress without bond pullout failure (Eqn. 7.26). The equation determines the minimum flexural bond length required for the prestressed CFRP bar to attain rupture tensile stresses, but the equation can also be used to determine the maximum tensile stress of a prestressed CFRP bar for a given flexural bond length.

$$l_f = \frac{(f_{frpu} - f_{pi})\, d_b}{\alpha_f \; f_c^{i\ 0.67}} \qquad (7.26)$$

and

$$\alpha_f = 0.37 + \frac{(f_{frpu} - f_{pi})}{2500}$$

Where

f_{frpu} is tensile rupture stress of the CFRP bar, Mpa;
f_{pi} is the initial prestress, Mpa
α_f is the coefficient of flexural bond length

A comparison between the proposed model predictions (Eqn. 7.26) and the experimental data of the current study was carried out. Figure 7.12 shows the correlation between the prediction results using the proposed model and the experimental data. The model predictions fit well the experimental data of the current study with R^2 = 0.87; however, experimental data from an independent work is required to verify the proposed model.

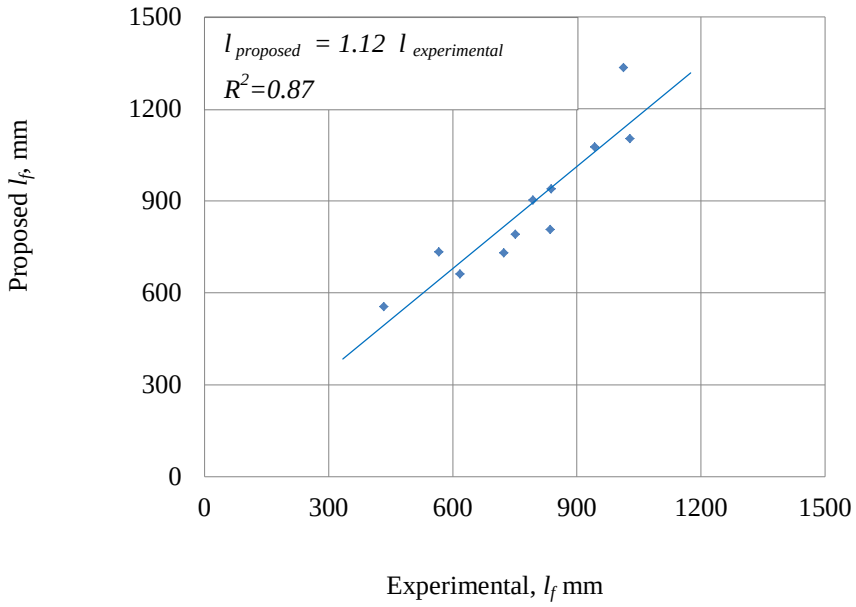

Figure 7.12 Correlation of the proposed vs. experimental flexural bond length of CFRP Bars prestressed in SCC

Table 7.7 compares the experimental flexural bond lengths and the predicted flexural bond lengths by ACI equation and the proposed model (Eqn. 7.26). The ACI prediction values were unconservative by a range of 20% to 40%, possibly because the ACI equation assumes a constant bond stress within the flexural bond length irrespective of the flexural tensile stress in the prestressed bar and the length of the flexural bond. The experimental results in this study showed that the flexural average bond stresses were a function of the additional flexural tensile stresses. It is expected that high values of flexural tensile stress can be achieved when longer flexural bond lengths are available. A longer flexural bond length has an uncracked portion of the beam with no transfer bond stresses. The proposed model was able to account for the change in flexural bond stress by varying the coefficient ($\propto_f$). Predicted results obtained based on the proposed model correlate well with the experimental results with the ratio of proposed to predicted ratio ranging from 0.94 to 1.28 with a mean value of 1.12.

Table 7.7 Comparison between the experimental data, ACI predictions and proposed model predictions for flexural bond length of CFRP bars in SCC specimens

Group/ Beam labels		Experimental results		ACI 440.4 prediction		Proposed model	
		f_f, Mpa	l_f, mm	Pre. L_d, mm	Pre/exp	l_f, mm	Proposed/ Exp
I	S30-1	810.5	794.0	617.4	0.78	884.5	1.11
	S30-2	1166.3	943.3-	889.0	0.94	1057.6	1.12
	S30-3	1215.5	1013.0	1128.7	1.11	1294.2	1.28
	S30-4	-	-	-	-	-	-
II	S45-1	603.7	566.5	441.3	0.78	716.9	1.27
	S45-2	686.7	751.8	501.6	0.67	773.4	1.03
	S45-3	709.8	835.5	518.8	0.62	788.6	0.94
	S45-4	-	-	-	-	-	-
III	S60-1	369.5	434.0	281.6	0.65	539.7	1.24
	S60-2	478.6	617.5	364.8	0.59	645.1	1.04
	S60-3	611.2	838.2	567.6	0.68	917.7	1.09
	S60-4	813.5	1028.2	755.4	0.73	1008.1	1.05

-This beam failed by premature bar rupture and the experimental embedment length was larger than that required for the CFRP bar to reach rupture.

7.5.5 Development length of prestessed CFRP bars in SCC beams

The development length can be calculated by adding the transfer and flexural bond lengths obtained in Section 7.3 and Section 7.4, respectively. Eqn. (7.27) gives the total development length of a prestressed CFRP bar in SCC.

$$l_d = l_t + l_f \tag{7.27}$$

$$l_d = \frac{f_{pi}\, d_b}{\alpha_t\, f_{ci}^{0.67}} + \frac{(f_{frpu} - f_{pi})\, d_b}{\alpha_f\ f_c^{i\ 0.67}} \tag{7.28}$$

Where

$$\alpha_t = 2.84 - \frac{f_{pi}}{800}$$

$$\alpha_f = 0.37 + \frac{(f_{frpu} - f_{pi})}{2500}$$

Table 7.9 gives the development length results as compared to predictions by ACI 440 equation and the proposed model. The comparison showed that the ACI prediction of the development length was in good agreement with specimens when the CFRP bar was prestressed to 30%; however, when the prestress was increased above 45%, the ACI prediction was unconservative on average by up to 25%. Predictions of the development length using the proposed model were in good agreement with the experimental values. The ratio of predicted to experimental development lengths ranged from 0.94 to 1.28. The average predicted to experimental ratio was 1.08, with a standard deviation of 0.078.

Table 7.8 Summary of the development length results and comparison to the ACI440 prediction and the proposed model of SCC beam

	Beam	Experimental results		ACI 440.4 prediction		Proposed model	
		l_e, mm	Total stress, MPa	l_d, mm	ACI/Exp	l_d, mm	Proposed/ Exp
I	S30-1	1100.0	1359.9	1003.0	0.91	1230.6	1.12
	S30-2	1250.0	1701.1	1263.8	1.01	1391.4	1.11
	S30-3	1350.0	1841.9	1488.1	1.10	1630.5	1.21
	S30-4	1500.0	-	-	-	-	-
II	S45-1	1100.0	1354.0	913.0	0.83	1188.1	1.08
	S45-2	1250.0	1480.5	1004.4	0.80	1290.7	1.03
	S45-3	1350.0	1486.4	1010.5	0.75	1289.0	0.95
	S45-4	1500.0	-	-	-	-	-
III	S60-1	1100.0	1302.2	933.3	0.85	1273.8.6	1.16
	S60-2	1350.0	1473.9	1060.9	0.79	1464.1	1.08
	S60-3	1500.0	1531.5	1097.7	0.73	1512.5	1.01
	S60-4	1700.0	1787.6	1312.4	0.77	1725.4	1.01

- This beam failed by bar rupture and the experimental embedment length cannot be correlated to the stresses in the CFRP bar.

Chapter 8 - Conclusions and Recommendations

8.1 Introduction

Fifty-six beam specimens were fabricated and tested. Forty beams were non-prestressed beams reinforced with fibre reinforced polymer (FRP) bars. Twenty-four beams were made from self consolidating concrete (SCC) and sixteen beams were made from normal vibrated concrete (NVC). All the beams were reinforced with a single FRP bar in the tension zone. Steel stirrups were provided to prevent shear failure. The parameters included for the non-prestressed beams were the type of concrete (SCC and NVC), concrete cover thickness, bar diameter and embedment length. Sixteen prestressed beams were included in this research study. Sand coated carbon FRP bars of 12.7mm diameter were used as prestressing reinforcement for the prestressed beams. The beams were grouped based on the prestress level: 30%, 45% and 60% of the guaranteed tensile strength of the CFRP bar.

Analytical modeling for sectional response and midspan deflections was carried out for all non-prestressed beams and selected prestressed beams. Bond models for FRP reinforcement bars in SCC were developed. The proposed models were used to predict the moment-deflection responses of SCC beams reinforced with FRP bars. New development length equations for the GFRP and CFRP bars embedded in SCC members were formulated and modifications to the existing ACI440.4 equations for the transfer, and development lengths were proposed.

The findings of this research study provide a better understanding of SCC structural performance with FRP reinforcement and will be beneficial for the development of design guidelines. The main conclusions and recommendations of this work are as follows.

8.2 SCC material properties

Three SCC mixes and one NVC mix were used in this study. The SCC mixes proved to be easy to cast and finish. The material flowed smoothly into the forms, filled all the voids, and encapsulated the reinforcing bars under its own weight. SCC was able to save time in casting by 50% and in manpower at a similar rate as compared to that needed when the NVC mix was used. Furthermore, reduced construction noise and improved safety, in general, was evident when SCC was used. Based on the material tests, the following conclusions can be drawn.

1) The average modulus of elasticity of SCC mix-1, mix-2 and mix-3 was found to be 78%, 72% and 81% of the ACI 318 Code prediction, respectively. The modulus of elasticity of the NVC mix was slightly higher than ACI 318 code prediction. At similar concrete compressive strengths, the modulus of elasticity of SCC mix-1 and the NVC mix were 30.48GPa and 37.4GPa, respectively. The possible explanation of this trend is due to the decreased coarse aggregate content in SCC which increased the mortar volume fraction in SCC and thus influenced the modulus of elasticity of SCC versus NVC.

2) The SCC mixes had a lower concrete tensile strength to concrete compressive strength ratio than the NVC mix. Based on splitting cylinder tests, the tensile strength to the square root of compressive strength ratio for SCC mix-1, mix-2 and mix-3 was 0.79, 0.76 and 0.82, respectively. The ratio of tensile stress to the square root of the compressive strength for the NVC mix was 0.88. This trend was due to less coarse aggregate content and smaller aggregate size in SCC as compared to the NVC.

3) Material tests showed that SCC had lower tensile strength than the NVC mix. There were no clear differences in the cracking moment of beams made from SCC as compared to beams made from NVC. However, SCC beams showed a larger number of flexural cracks than similar NVC beams.

8.3 Non-prestressed beams

Forty non-prestressed FRP reinforced concrete beams were fabricated and tested in flexure. The main focus of these tests was to examine the flexural responses of FRP reinforced concrete and the bond behaviour of GFRP and CFRP bars in SCC and NVC. When beams were tested at a shear span less than the development length of the FRP reinforcing bar, a bond pullout failure occurred. Based on the analysis of the strain gauge readings and visual inspection, the bond loss was initiated at the peak moment and propagated back to the unloaded end. The interface between the sand coating and FRP fibers of the bar was the critical interface where the bond failure occurred and it was observed as a common failure type for the pullout specimens. Measuring the end slip at the free end did not detect initiation of the bond loss or local slip. In fact, most of the beams that had bond pullout failure failed simultaneously with slippage being recorded at the free end. Beams that failed with bond pullout showed noticeable crack widening and a plastic hinge formation at the end of the shear span where the bond loss initiated. Beam rupture failure was more brittle than bond pullout; however, both cases exhibited high curvature. The main findings of analysis of the results of the non-prestressed beams based on concrete type and FRP bar type are as follows.

8.3.1 NVC beams

1) The normalized average bond stress of CFRP bars embedded in NVC was found to be on average higher than that of GFRP bars in NVC at a similar embedment length to bar diameter ratio. The increase in bond stress for the CFRP bars as compared to the GFRP bars suggest that as the modulus of elasticity of the reinforcing bars increased, the bond strength is increased.

2) The prediction of the development length of both GFRP and CFRP bars based on CAN/CSA-S6-06 and CSA S806-12 did not fit the trend in experimental results. Both of these design guidelines assume constant bond stress for a given concrete strength, which does not captured the actual bond stress behaviour. Thus leading to unconservative predictions.

3) The current ACI 440.1R-06 overestimated the development length of CFRP bars in NVC by about 30%. A modification factor of (1/1.35) was recommended as a material factor to be used with the current ACI400.1R06 equation for the development length of the CFRP bars embedded in NVC.

4) Prediction of deflection in NVC beams reinforced with CFRP bars based on elastic structural analysis and effective moment of inertia over the entire span gave slightly unconservative results. The predicted midspan deflection ranged from 68% to 137%, with a mean value of 97% of the experimental measurements. The simplified method is based on assumption of uniform effective moment of inertia along the beam length. This prediction overestimates the stiffness of beams reinforced with CFRP bars. A model based on a curvature approach and involving a newly developed bond stress model provided an excellent fit with the experimental measurements.

8.3.2 SCC beams

Beams made from SCC and reinforced with FRP bars had a load-deflection similar to those made from NVC. Load-deflection predictions based on effective moment of inertia overestimate the stiffness of beams reinforced with CFRP bars and were conservative with beams reinforced with GFRP bars. The average bond stress of SCC was slightly less than that in beams made from NVC. Bond stresses in uncracked region were higher than those in similar beams made from NVC. This finding is in agreement with literature that showed SCC had higher bond strength than NVC based on pullout specimens. Based on the analysis of the obtained results, the following conclusions can be drawn for SCC beams reinforced with FRP bars.

8.3.2.1 SCC beams reinforced with GFRP bars

1) Flexural responses of beams made from SCC exhibited slightly increased deflection than NVC beams. The increased deflection in SCC beams is related to the lower modulus of elasticity of SCC

as compared to NVC. SCC beams had closer flexural crack spacing associated with fine widths. This observation implies that SCC had better bond strength as compared to SCC; however, when flexural cracks formed, the bond stress dropped significantly.

2) The mode of failure in SCC beams reinforced with GFRP bars changed from a pullout to bond splitting failure when the cover thickness was reduced below twice the bar diameter ($C/d_b < 2.0$). The average bond stress decreased from 4.49 MPa to 3.90 MPa when the cover thickness to the bar diameter ratio decreased from 3.0 to 1.0. This result is limited for beams that had minimum shear reinforcement.

3) The normalized average bond stress profile of GFRP bars in SCC decreased as the embedment length to bar diameter ratio increased. This is mainly due to the fact that the local bond stress in cracked region is less than that in the uncracked region and for long embedment length, the cracked portion contribution is increased. GFRP bars embedded in SCC showed similar normalized average bond stress similar to that of GFRP bars embedded in NVC; however, SCC specimens showed a higher normalized bond stress in the uncracked region and vice versa in the cracked region as compared to NVC specimens.

4) Predictions of the development length of a GFRP bar in SCC using ACI 440.1R-06 were in agreement with the experimental values; however, there was no margin of safety in the predictions as in the case of NVC. Both CAN/CSA-S6-06 and CSA S806-12 yielded unconservative predictions of the development length. The development length based on these equations did not fit the trend of experimental results. Both CAN/CSA-S6-06 and CSA S806-12 assume constant bond stress for a given concrete strength, which does not capture the actual bond stress behaviour.

5) A new model was proposed to predict the development length of GFRP bars embedded in SCC. This model captured the bond stress profiles obtained from the experimental results.

$$l_e = \left(\frac{\frac{f_{GFRP}}{\sqrt{f_c'}} - 25.9}{0.652 + 0.288\,\frac{C}{d_b}} \right) d_b$$

6) Deflection prediction based on elastic structural analysis and effective moment of inertia over the entire span gave conservative deflection values. Predicted to experimental ratios of the midspan deflection ranged from 1.06 to 1.56 with a mean value of 1.19.

8.3.2.2 SCC beams reinforced with CFRP bars

1) Using a concrete cover of $3.0d_b$ was found to be sufficient to prevent bond splitting failure of SCC beams reinforced with CFRP bars. Splitting bond failure of SCC beams reinforced with CFRP bars was recorded at a cover thickness of $2.0d_b$. The normalized average bond stress dropped by 15%, 21%, 25% when the cover thickness was reduced from $3.0d_b$ to $2.0d_b$, $1.5d_b$ and $1.0d_b$, respectively. This result is limited for beams that had minimum of shear reinforcement.

2) The average bond stress of CFRP bars in the cracked region of beams under flexure was about 50% of the average bond stress over the entire embedment length. The bond stress within a cracked beam can be used to assess the development length within a beam span where the applied moment is greater than the cracking moment.

3) The normalized average bond strength of CFRP bars in SCC beams was about 1.5 times that of GFRP bars in SCC at a similar embedment length to bar diameter ratio. The increased modulus of elasticity of the CFRP bars improved the bond strength as compared to the beams reinforced with GFRP bars.

4) Predictions of the development length of a CFRP bar using CAN/CSA-S6-06 were unconservative by about 50%, while ACI 440.1R-06 predictions were conservative by above 30%.

5) A new model was proposed to predict the development length of the CFRP bars embedded in SCC to achieve a given tensile stress in the CFRP. The model correlated well with experimental results.

$$l_e = \left(\frac{\frac{f_{cfrp}}{\sqrt{f_c'}} - 55.04}{0.36 + 0.48\,\frac{C}{d_b}} \right) d_b$$

6) The deflection prediction for SCC beams reinforced with CFRP bars based on elastic structural analysis and effective moment of inertia over the entire span gave unconservative results. This reason was similar to beams made from NVC for which the uniform effective moment of inertia

overestimated the stiffness of beams reinforced with CFRP bars. Predicted midspan deflections ranged from 63% to 90% of the experimental measurements. A model based on the curvature approach, using a newly developed bond stress model of CFRP bars in SCC, provided an excellent fit with the experimental measurements.

8.4 Prestressed beams

Sixteen prestressed beams with CFRP bars were fabricated and tested for transfer length and flexural bond length. The prestressing level was varied from 30% to 60% of the guaranteed rupture stress of CFRP bars as reported by the manufacturer. All beams were tested for the transfer length of the CFRP bars immediately after prestressing load release and were tested in flexure 28 days after. The draw-in method was a simple and quick way to determine the transfer length. However, results based on this method were slightly less than those obtained with the concrete strain profile method. Beams tested for flexural bond length, with a shear span less than their development length, exhibited slippage of the prestressed CFRP bar within the transfer zone. The slip was recorded at the unloaded end but the loads on the beams were maintained. The slip reached up to 15mm without the beams collapsing. This slippage shifted the transmission zone toward the beam midspan. The slippage started when the flexural bond stress front reached the transmission zone. The failure mechanism was bond loss at the transmission zone, which progressed to the beam centre. The beams collapsed when the residual bond stress (mainly due to friction bond) could no longer accommodate the tensile stress in the prestessed bars. The interface between the sand coating and the fiber was proven to be the critical bond interception. Based on the analysis of test results, the following conclusion can be drawn.

1) The average measured transfer length of 12.7mm diameter CFRP bars prestressed to 30%, 45% and 60% were found to be $25d_b$, $40d_b$, $54d_b$, respectively. Predictions of the transfer length of the prestressed 12.7mm CFRP bars in SCC using the ACI 440.4R-04 equation correlated closely with the measured transfer length of CFRP bars at a 30% prestress level but were unconservative for prestress levels beyond 45%. The transfer length of CFRP bars in SCC tended to be nonlinear when the prestress level exceeded 45%.

2) The average bond strength of SCC beams prestressed with CFRP bars within the transfer zone decreased linearly as the prestressing level increased; thus, the transfer length was found to be nonlinear with the prestressing level. The increased fines and lowered modulus of elasticity of SCC might have decreased the Hoyer effect which improves the bond stress with transmission

zone. The ability of SCC to deform reduces the bond strength thus increases the transfer length especially at high prestress level which is associated with less bond strength at transfer.

3) When subjected to flexural tests prestressed beams with shear spans of less than the minimum development length experienced local bar slippage within the transmission zone. When these beams experienced local bond slip, their stiffness was significantly decreased.

4) The ACI440.1R-04 guideline gave close predictions of the development length of the 12.7mm CFRP bars prestressed to 30%, but was unconservative by about 25% and 40% for prestressing levels of 45% and 60%, respectively.

5) A new model based on the prestressing level at transfer was proposed to predict the transfer and development lengths of the CFRP bars in SCC. This model proposes modifications to the constant coefficients ($\propto_t$ and $\propto_f$) in the existing ACI440.4R-04 equations. The model is shown below. The first term represents the transfer length and the second term represents the flexural bond length. Good correlation with the experimental results was demonstrated.

$$l_d = \frac{f_{pi}\, d_b}{\alpha_t\, f_{ci}^{0.67}} + \frac{(f_{frpu} - f_{pi})\, d_b}{\alpha_f\ f_c^{i\ 0.67}}$$

The proposed modifications for the constant coefficients ($\propto_t$ and $\propto_f$) are as follows.

$$\alpha_t = 2.84 - \frac{f_{pi}}{800}$$

$$\alpha_f = 0.37 + \frac{(f_{frpu} - f_{pi})}{2500}$$

8.5 Recommendations for future studies

1) Work should be undertaken to collect a database on the mechanical properties of the SCC mixes. This database can be used to establish a new model for the modulus of elasticity and modulus of rupture of SCC mixes.

2) Further work is recommended to investigate the crack spacing and crack widths of SCC reinforced beams with FRP reinforcement.

3) Further work is recommended to investigate the effect of bar spacing, bar surface configuration, and stirrups confinement on bond stress of FRP bars in SCC beams.
4) Further work is recommended to examine the effect of fatigue loading on SCC beams reinforced with FRP bars, particularly its effects on bond behaviour.

5) While the proposed development length models of the GFRP and CFRP bars embedded in SCC had a good correlation with the experimental results, examination of these models against an independent research work is recommended.

References

Abdelrahman A. and Rizkalla S. (1997), "Serviceability of Concrete Beams Pre-stressed by Carbon-Fiber-Reinforced-Plastic Bars," ACI Structural Journal, Vol. 94, No. 4, pp. 447-457.

Abdelrahman A. and Rizkalla S. (1999), "Deflection Control of Concrete Beams Pretensioned by CFRP Reinforcements," Journal of Composites for Constructions, Vol. 3 No. 2, pp. 55-62.

ACI Committee 237 (2007), "Self-Consolidating Concrete," American Concrete Institute, Farmington Hills, MI, USA.

ACI Committee 318 (2008), "Building Code Requirements for Structural Concrete (ACI 318M-08) and Commentary," American Concrete Institute, Farmington Hills, MI. 48331, USA.

ACI Committee 440 (2003), "Guide for the Design and Construction of Concrete Reinforced with FRP Bars," ACI 440.1R-03, American Concrete Institute, Farmington Hills, MI.

ACI Committee 440 (2004), "Pre-stressing Concrete Structures with FRP Tendons," ACI 440.4R-04, American Concrete Institute, Farmington Hills, MI.

ACI Committee 440 (2006), "Guide for the Design and Construction of Concrete Reinforced with FRP Bars," ACI 440.1R-06, American Concrete Institute, Farmington Hills, MI.

Aly R., Benmokrane B. and Ebead U. (2006), "Tensile Lap Splice of Fiber-Reinforced Polymer Reinforcing Bars in Concrete," ACI Structural Journal, Vol. 103, No. 6, pp. 857-864.

Barnes R. W., Grove J. W. and Burns N. H. (2003), "Experimental Assessment of Factors Affecting Transfer Length," ACI Structural Journal, Vol. 100, No. 6, pp. 740-747.

Burgueno R. and Haq M. (2007), "Effect of SCC Mixture Proportioning on Transfer and Development Length of Prestressing Strand," American Concrete Institute, SP- 247-9, pp. 105-116.

Burns N. W. and Russell, B. W. (1996), "Measured Transfer Length of 0.5 and 0.6 in Strands in Pretensioned Concrete," PCI Journal, Vol. 41. No. 5, pp. 44-65.

Canadian Standards Association (2006), "Canadian Highway Bridge Design Code CAN/CSA-S6-06," A National Standard of Canada, Mississauga, Ontario, Canada.

Canadian Standards Association (2012), "Design and construction of building structures with fibre-reinforced polymers," CSA/S806-12.

Castel A., Vidal T., Viriyametanont K. and Francois R. (2006), "Effect of Reinforcement Bar Orientation and Location on Bond with Self-Consolidating Concrete," ACI Structural Journal, Vol. 103, No. 4, pp. 559-567.

Chen Y. W., Chen Y. S. and Liu Y. S. (2003), "Development of Bond Strength of Reinforcement Steel in Self-Consolidating Concrete," ACI Structural Journal, Vol. 100, No. 4, pp. 490-498.

Collins, M. P., and Mitchell D., (1997) "Prestressed Concrete Structures," Response Publications, Toronto, Canada.

Comite Euro-International Du Beton (CEB), (1993), *CEP-FIP model Code-Design Code*, Thomas Telford, London, UK.

Domenico N. G., Mahmoud Z. I. and Rizkalla S. (1998), "Bond Properties of Carbon Fiber Composite Pre-stressing Strands," ACI Structural Journal, Vol. 95, No. 3, pp. 281-290.

Esfahani M. R., Lachemi M., and Kianoush M. R. (2008), "Top-bar Effect of Steel Bars in Self-Consolidating Concrete (SCC)," Cement and Concrete Composite Vol. 30, pp. 52-60.

Girgis A F. and Tuan C. Y. (2005), "Bond Strength and Transfer Length of Pretensioned Bridge Girders Cast with Self-Consolidating Concrete," PCI Journal Vol. 50, No. 6, pp. 72-87.

Goodier C. I. (2003), "Development of Self-Compacting Concrete," Proceedings of the Institution of Civil Engineers Structures & Buildings, Issue SB4 pp. 405–414.

Hanson N. W. and Kaar P. H. (1959), "Flexural Bond Tests of Pretensioned Prestressed Beams," ACI Journal, Vol. 55, No. 7, pp. 783–802.

Holley J. (2005), "Application of Self-Consolidating Concrete," Second North American Conference on the Design and Use of Self-Consolidating Concrete (SCC) and the Forth International RILEM Symposium on Self-Compacting Concrete, Chicago, Illinois, USA.

Hossain K. and Lachemi M. (2008), "Bond Behavior of Self-Consolidating Concrete with Mineral and Chemical Admixtures," Journal of Materials in Civil Engineering, Vol. 20, No. 9, pp. 608-616.

Hwang S., Khayat K., and Bonneau O. (2006), "Performance-Based Specifications of Self-Consolidating Concrete Used in Structural Applications," ACI Materials Journal, Vol. 103, No. 2, pp 121-129.

ISIS Canada (2007), "Reinforced Concrete Structures with Fiber reinforced Polymers," Design Manual No. 3 Version 2, Winnipeg, Manitoba, Canada.

ISIS Canada (2008), "Prestressing Concrete Structures with Fiber Reinforced Polymers," Design Manual No. 5, Winnipeg, Manitoba, Canada.

Khayat K. (1999), "Workability, Testing and Performance of Self-Consolidating Concrete," ACI Materials Journal, Vol. 96, No. 3, pp. 46-353.

Khayat K. and Guizani Z. (1997), "Use of Viscosity Modifying Admixtures to Enhance Stability of Fluid Concrete," ACI Materials Journal, Vol. 94, No. 4, pp. 332–340.

Khayat K. and Mitchell D. (2009), "Self-Consolidating Concrete for Precast, Prestressed Concrete Bridge Elements," NCHRP report 628, Transportation Research Board, Washington, D.C., USA.

Koch G.H. et al (2002) "Corrosion Costs and Prevention Strategies in the United States," Report No. FHWA-RD-01-156, Federal Highway Administration, Washington, DC., USA.

Larson, K. H, Peterman, R. J., and Esmaeily, A. (2005), "Determining the Time-Dependent and Bond Characteristics of an SCC Mix for Kansas Prestressed Concrete Girders," 2nd North America Conference on the Design and Use of Self-Consolidating Concrete (SCC) and Forth International RILEM Symposium on Self-Consolidating Concrete, Chicago, Illinois, USA.

Logan D. R. (1997), "Acceptance Criteria for Bond Quality of Strand for Pretensioned Prestressed Concrete Applications," PCI Journal, Vol. 42, No. 2, pp. 52-90.

Lu, Z.; Boothby, T. E.; Bakis, C. E.; and Nanni, A. (2000) "Transfer and Development Length of FRP Prestressing Tendons," PCI Journal, Vol. 45, No. 2, pp. 84-95.

Mahmoud Z., Rizkalla S. and Zaghloul E. (1999), "Transfer and Development Lengths of Carbon Fiber Reinforcement Polymers Pre-stressing Reinforcement," ACI Structural Journal, Vol. 96, No. 4, pp. 594-602.

Marti-Vargas J. R., Arbelaez C. A., Serna-Ros P., and Castro-Bugallo C. (2007), "Reliability of Transfer Length Estimation from Strand End Slip," ACI Structural Journal, Vol. 104, No. 4, pp. 487-494.

Mosley C. P., Tureyen A. K. and Forsch R. J. (2008), " Bond Strength of Nonmetallic Reinforcing Bars," ACI Structural Journal, Vol. 105, No. 5, pp. 634-642.

Moustafa, and Saad (1974), "Pull-Out Strength of Strand and Lifting Loops," Concrete Technology Associates Technical Bulletin, Report 74-B5.

Naito C. J., Parent G. and Brunn G. (2006), "Performance of Bulb-Tee Girders Made with Self-Consolidating Concrete," PCI Journal, Vol. 51, No. 6, pp. 72-85.

Newman N., Ayoub A. and Belarbi A. (2009), "Development Length of Straight FRP Composite Bars Embedded in Concrete," Journal of Reinforced Plastics and Composites, Vol. 29, No. 4, pp 571-589.

Okamura H. (*1997),* "*Self*-Compacting High-Performance Concrete", Concrete International, Vol. 19, No. 7, pp. 50-54.

Okamura H. and Ouchi M. (2003), "Self-Compacting Concrete," Japan Concrete Institute, Journal of Advanced Concrete Technology, Vol. 1, No. 1, pp. 5-15.

Petersson S. A. (2000), "Self-Compacting Concrete," State-of-the-Art Report of RILEM Technical Committee 174, RILEM-Report No. 23, Ca-chan Cedex/France.

Rafi M., Nadjai A. and Ali F. (2007), "Experimental Testing of Concrete Beams Reinforced with Carbon FRP Bars**,"** Journal of Composite Materials, Vol. 41, No. 22, pp. 2657-2673.

Stanton, B.W., Do, N.H., Ruiz, E.D., and Hale, W.M. (2006). "Transfer Lengths for Prestressed Concrete Beams Cast with Self-Consolidating Concrete Mixtures," 2006 National Bridge Conference, Grapevine, TX.

Schindler A. K. et al (2007), "Properties of Self-Consolidating Concrete for Prestressed members," ACI Material journal, Vol. 104, No. 1, pp. 53-61.

Sonebi, M.; Tamimi, A. K.; and Bartos, P. J. M., (2003) "Performance and Cracking Behavior of Reinforced Beams Cast with Self-Consolidating Concrete," ACI Materials Journal, Vol. 100, No. 6, pp. 492-500.

Soudki K. A., Green M. F. and Clapp F. (1997), "Transfer Length of Carbon Fiber Rods in Precast Pretensioned Concrete Beams," PCI Journal. Vol. 42, No. 5, pp. 78-87.

Valcuende M. and Parra C. (2008), "Bond Behavior of Reinforcement in Self-Compacting Concretes," Construction and Building Materials, Vol. 23, No. 1, pp. 162-170.

Wambeke B. and Shield C. (2006), "Development Length of Glass Fiber-Reinforced Polymers Bars in Concrete," ACI Structural Journal, Vol. 103, No. 1, pp. 11-17.

Xue W., Wang X. and Zhang S. (2008), "Bond Properties of High-Strength Carbon Fiber-Reinforced Polymer Strands," ACI Materials Journal, Vol. 105, No. 1.

Zou P. (2003), "Long-Term Properties and Transfer Length of Fiber-Reinforced Polymers," ASCE Journal of Composites for Construction, Vol. 7, No. 1, pp. 10-19.

Appendices

Appendix A – Flexural Test Results of Beams Reinforced with GFRP Bars

Appendix B – Flexural Test Results of Beams Reinforced with CFRP Bars

Appendix C – Flexural Test Results of Beams Prestressed with CFRP Bars

Appendix A – Flexural Test Results of Beams Reinforced with GFRP Bars

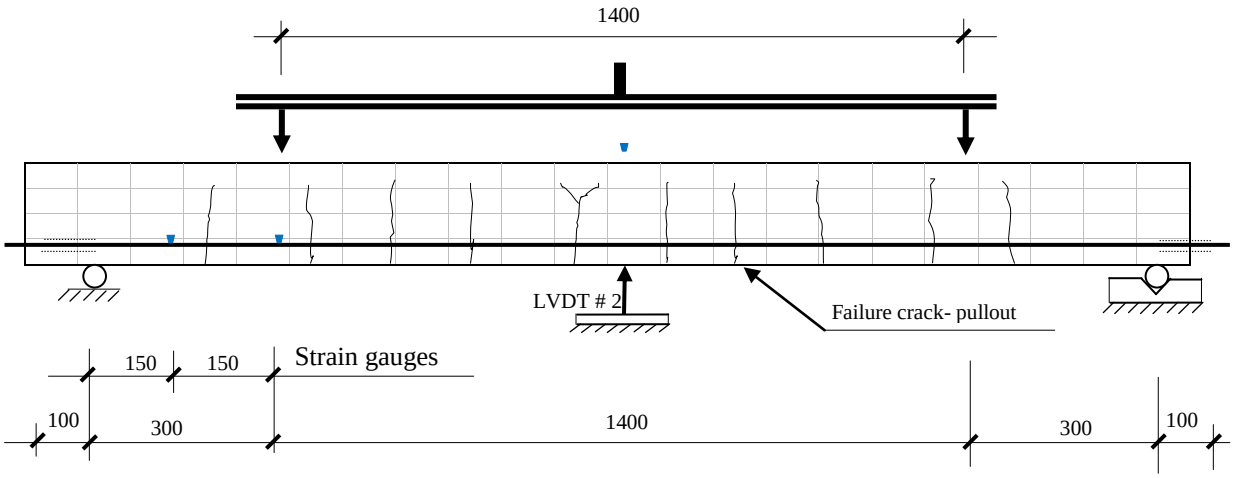

(a) Cracks pattern at failure, bar pullout at f_{frp} of 680.9MPa

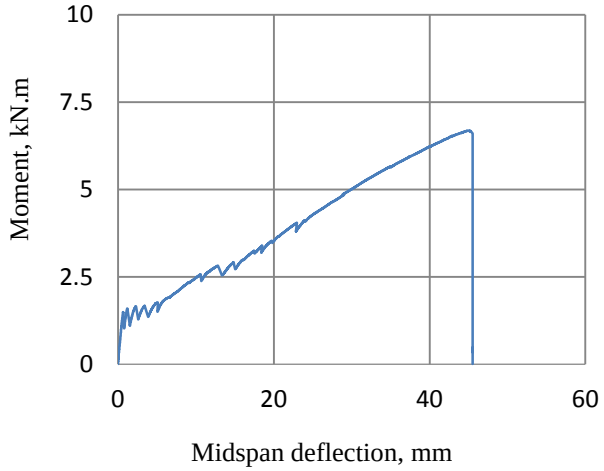

(b) Moment versus midspan deflection responses

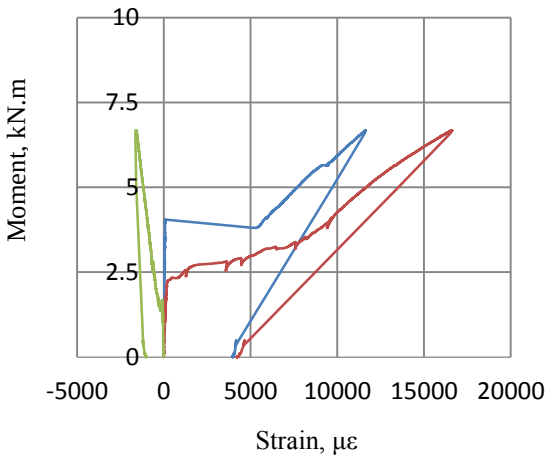

(c) Strain response in the GFRP bar and concrete

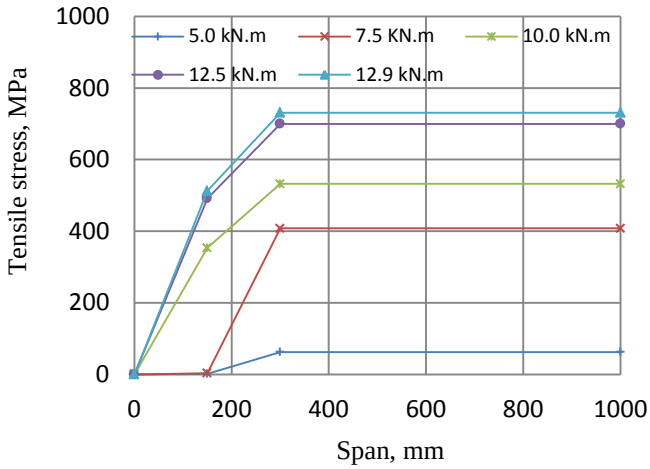

(d) Stress profile in the GFRP bar at varies load levels

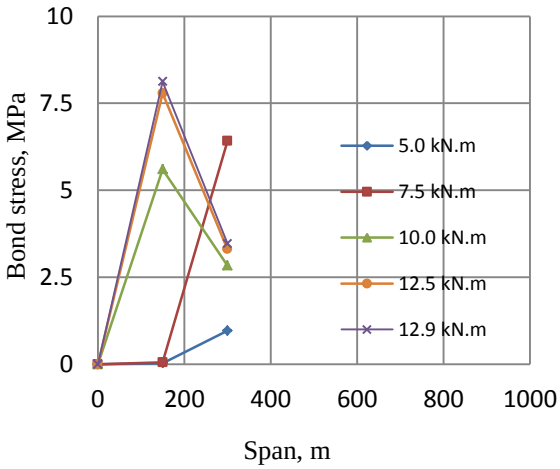

(e) Bond stress profile at various load levels.

Figure A.1 Specimen SG9.5-3.0-300 flexural test results

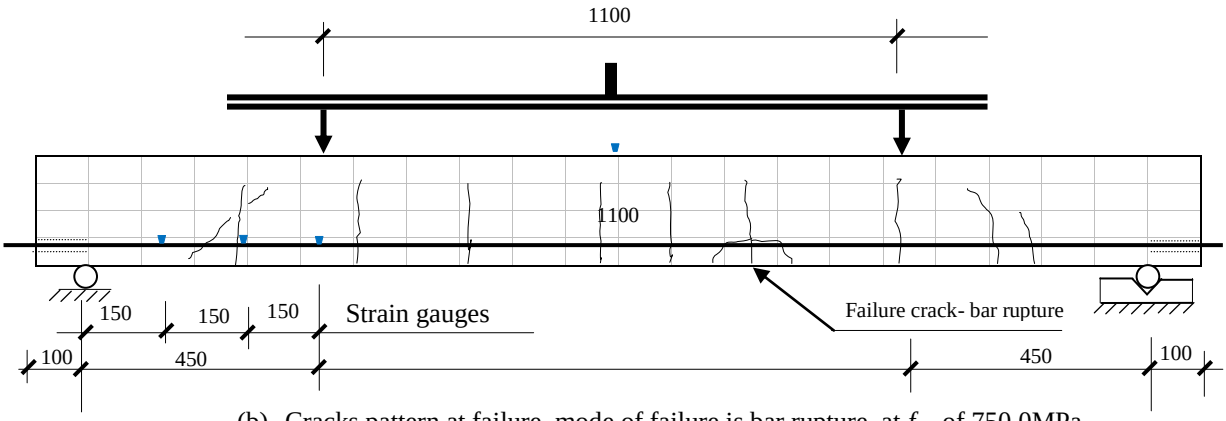

(b) Cracks pattern at failure, mode of failure is bar rupture at f_{frp} of 750.0MPa

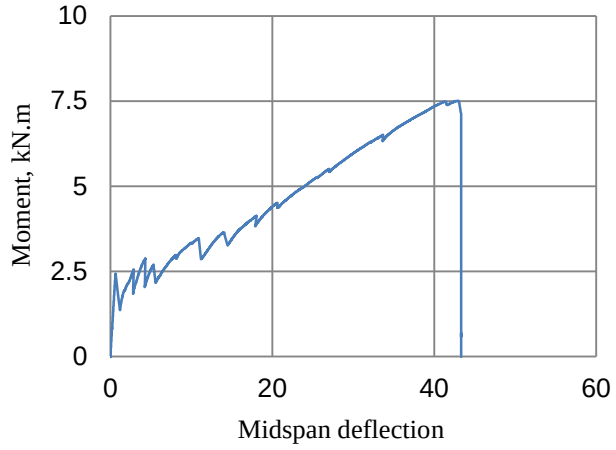

(b) Moment versus midspan deflection responses

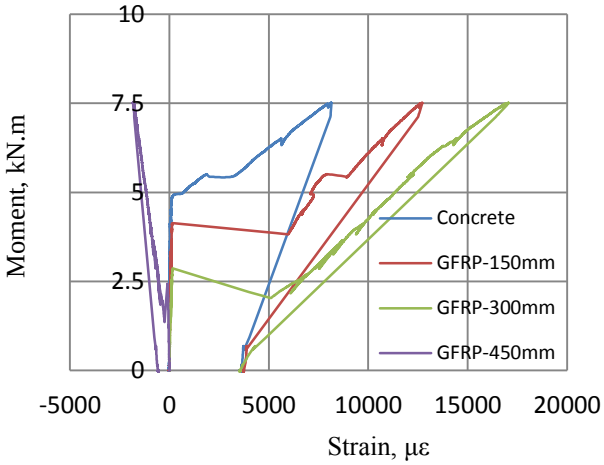

(c) Strain responses in the GFRP bar and concrete

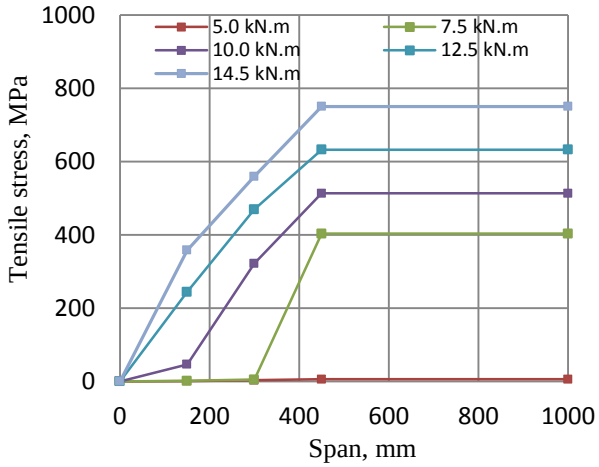

(d) Tensile stress profile in the GFRP bar at various load levels

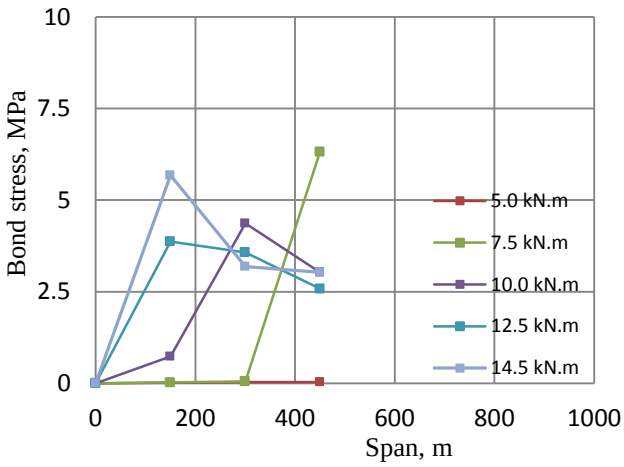

(e) Bond stress profile at various load levels

Figure A.2 Specimen SG9.5-3.0-450

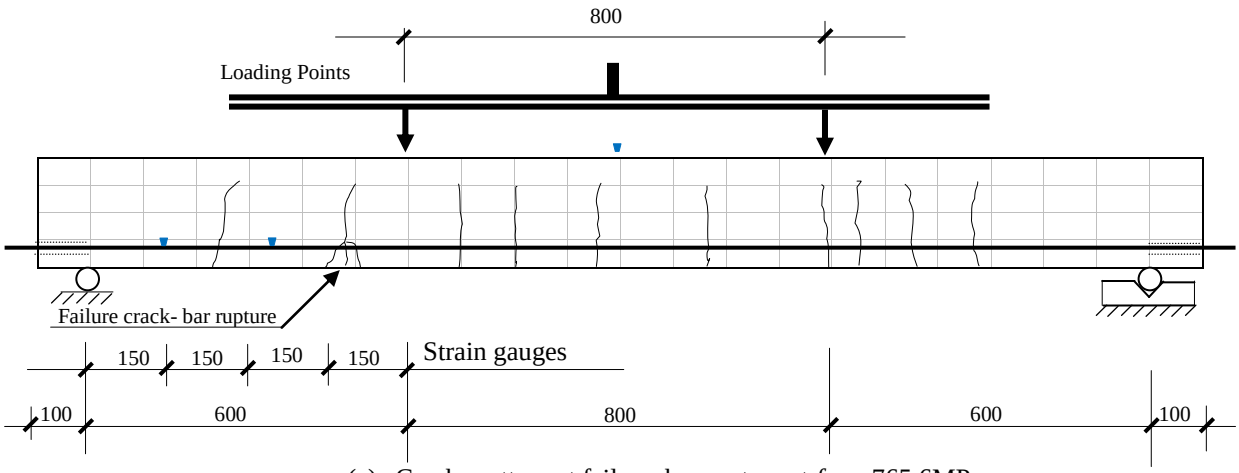

(a) Cracks pattern at failure, bar rupture at f_{frp} = 765.6MPa

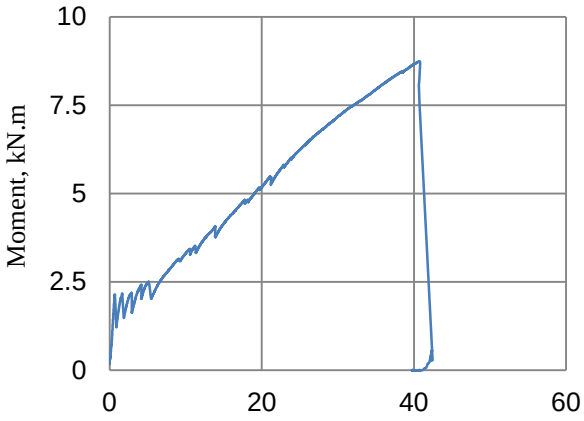

(b) Moment versus midspan deflection responses

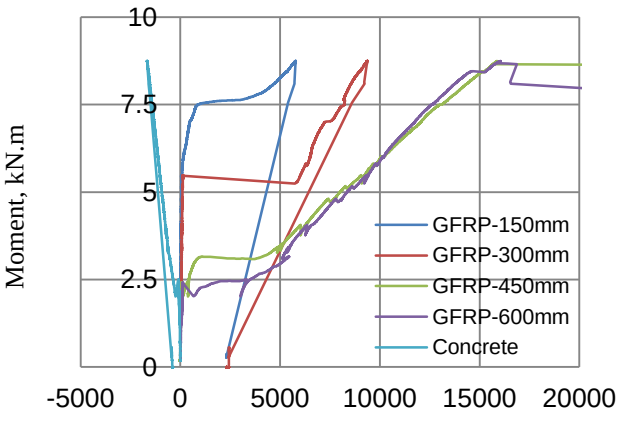

(c) Strain responses in the GFRP bar and concrete

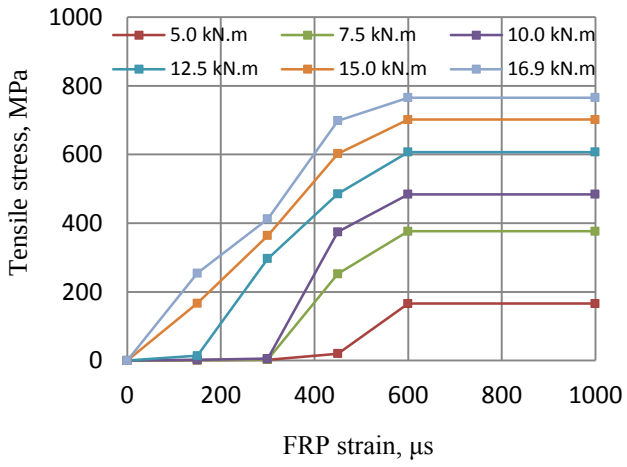

(d) Tensile stress profile in the GFRP bar at varies load levels

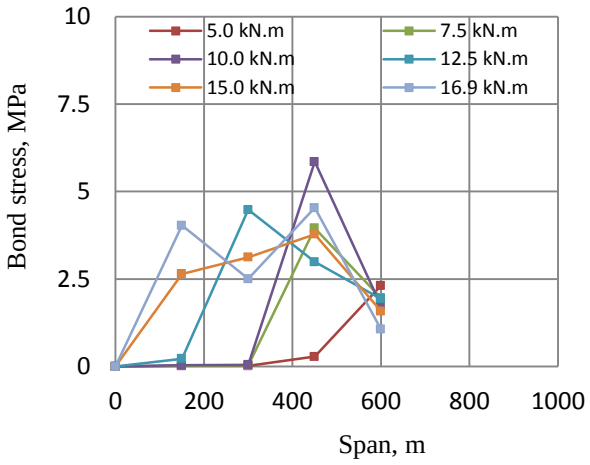

(e) Bond stress profile at various load levels

Figure A.3 Specimen SG9.5-3.0-600

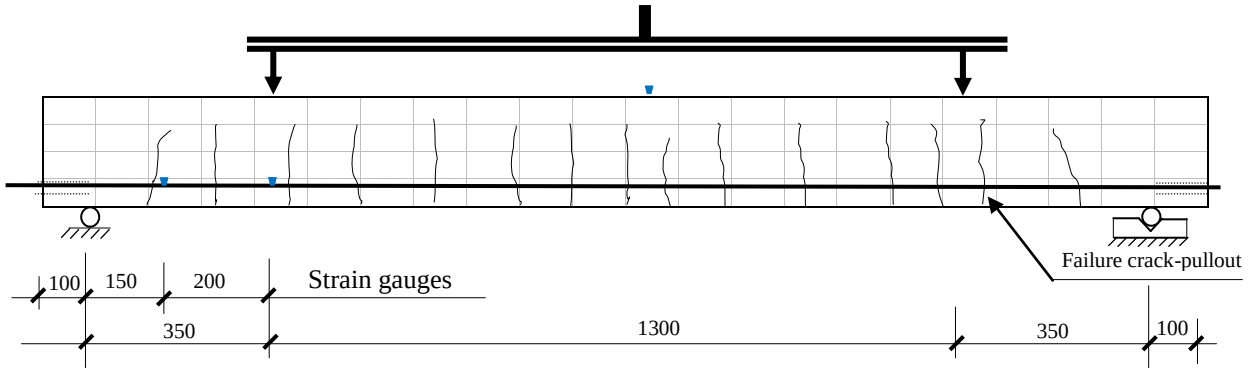

(d) Cracks pattern at failure, pullout at f_{frp} of 518.2 MPa

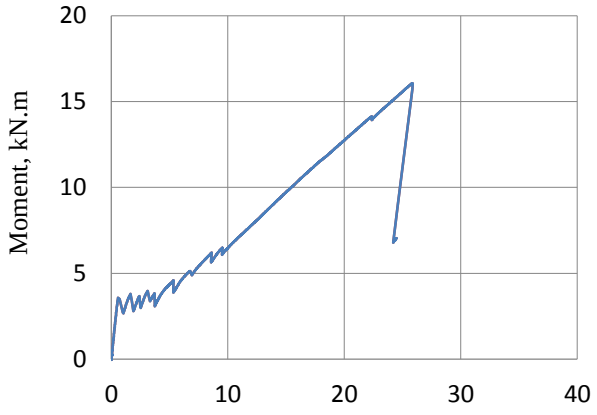

(b) Moment versus midspan deflection responses

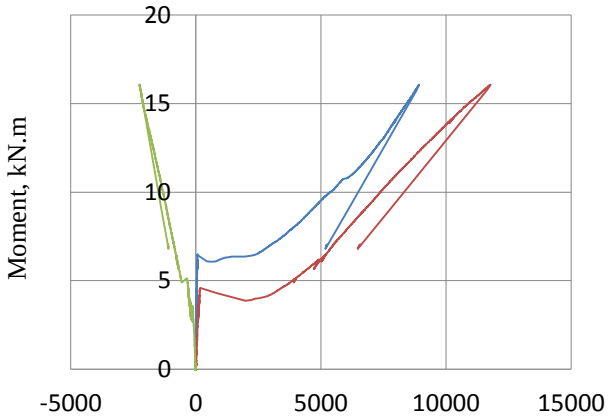

(c) Strain response in the GFRP bar and concrete

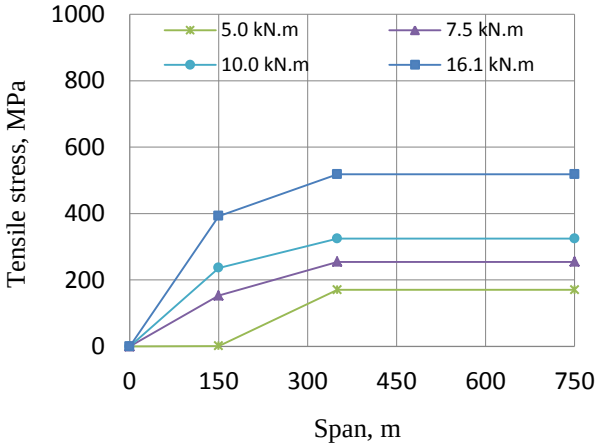

(d) Tensile stress profile in the GFRP bar at varies load levels

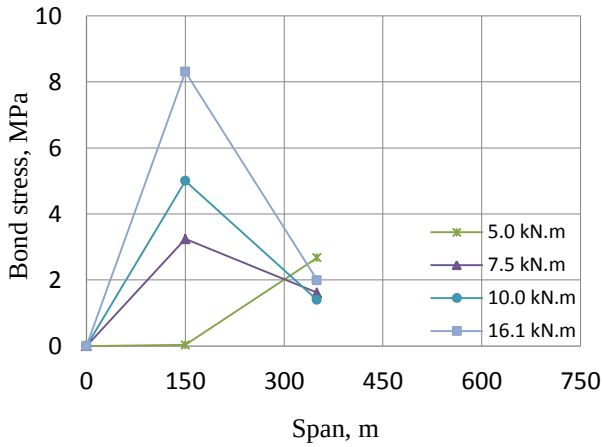

(e) Bond stress profile at various load levels

Figure A.4 Specimen SG12.7-3.0-350 flexural test results

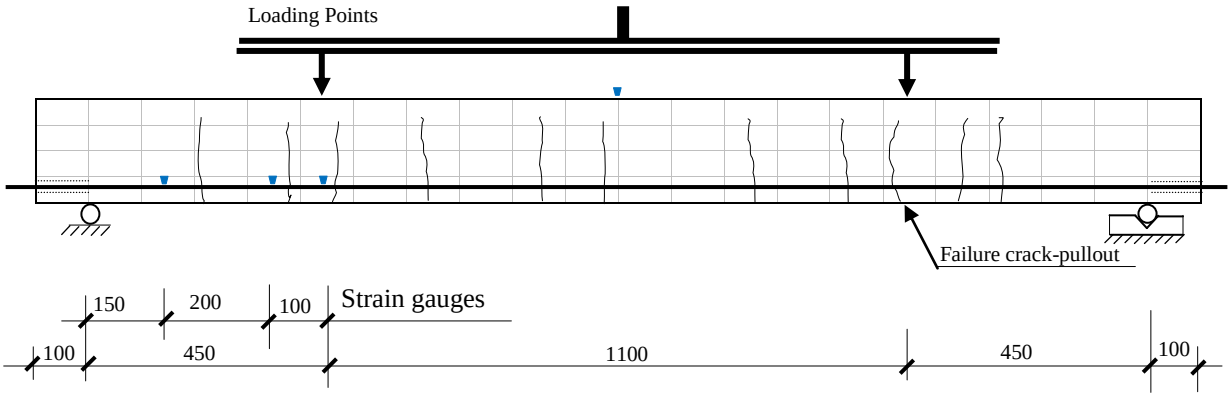

(e) Cracks pattern at failure, pull out at f_{frp} of 569.8 MPa

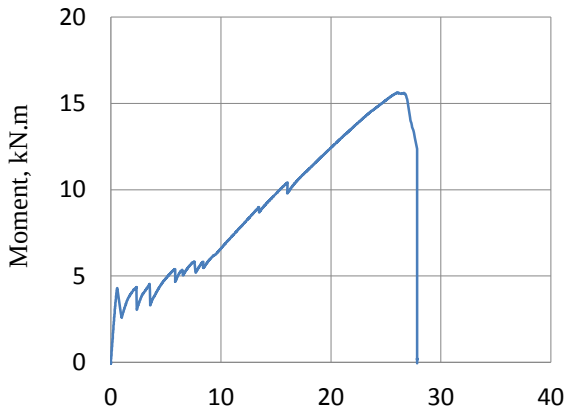

(b) Moment versus midspan deflection responses

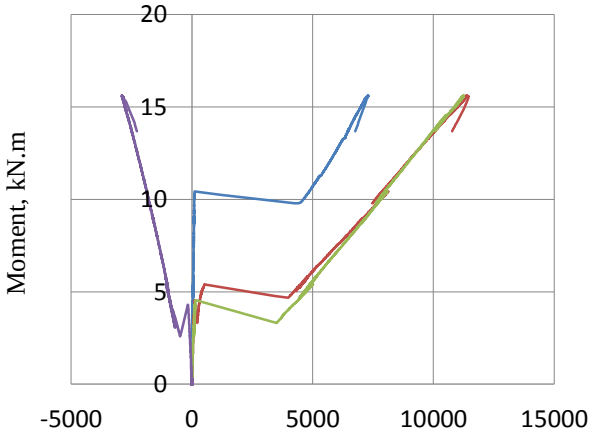

(c) Strain response in the GFRP bar and concrete

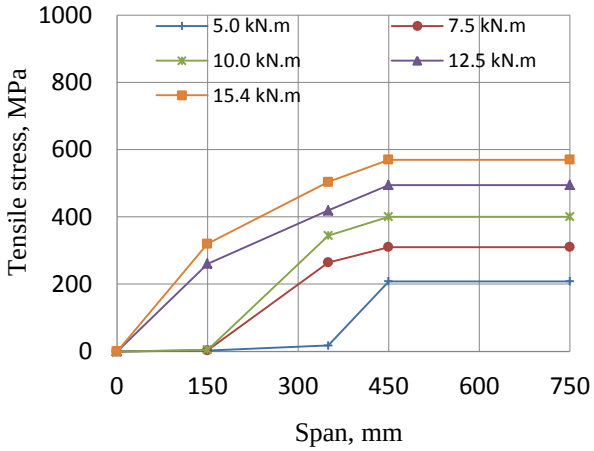

(d) Tensile stress profile in the GFRP bar at varies load levels

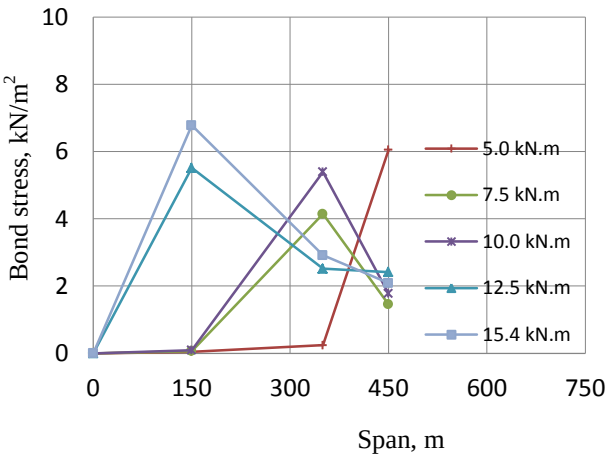

(e) Bond stress profile at various load levels

Figure A.5 Specimen SG12.7-3.0-450 flexural test results

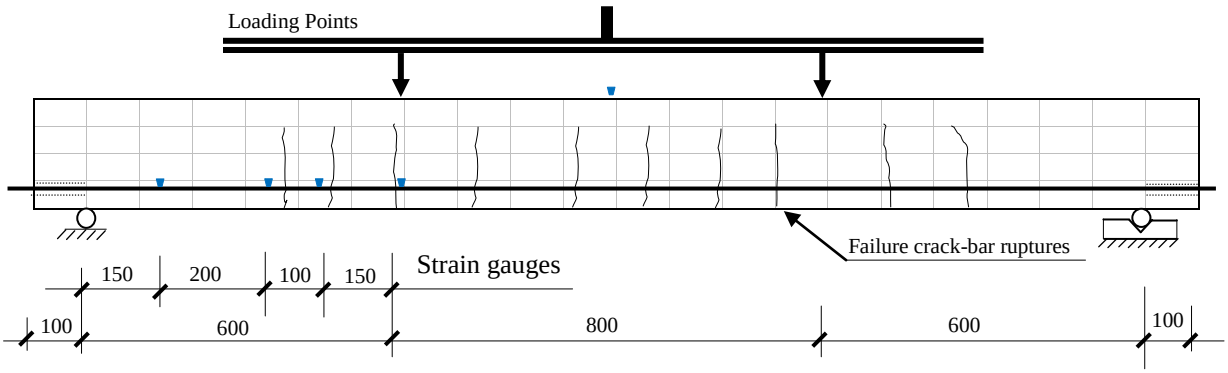

(a) Cracks pattern at failure, bar rupture at f_{frp} of 614.2 MPa

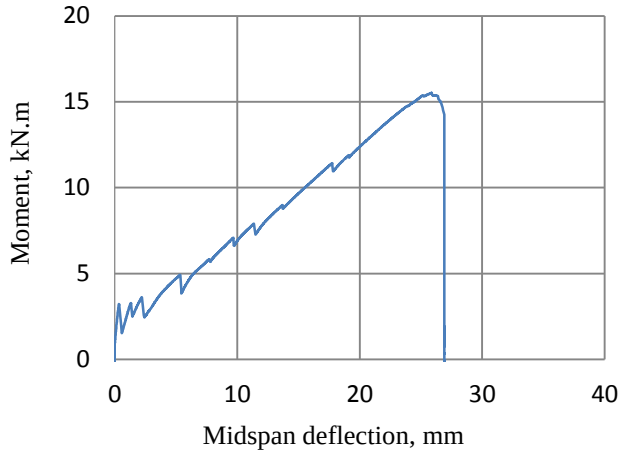

(b) Moment versus midspan deflection responses

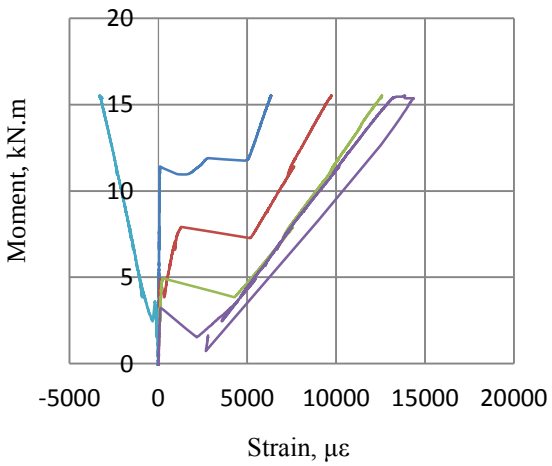

(c) Strain profile in the GFRP bar and concrete

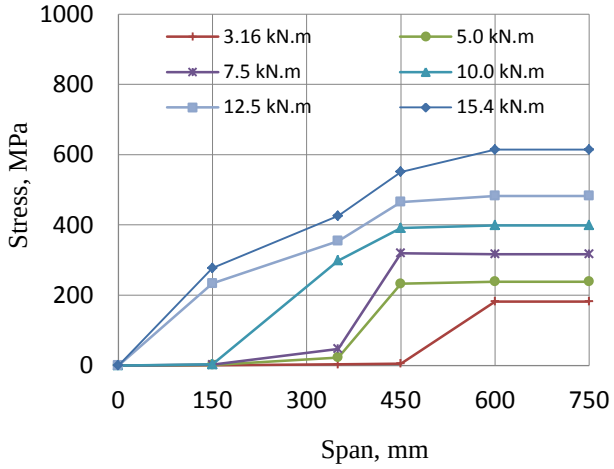

(d) Tensile stress profile in the GFRP bar at varies load levels

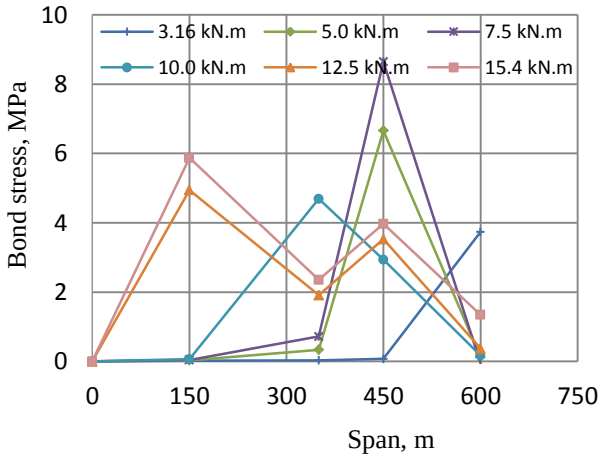

(e) Bond stress profile at various load levels

Figure A.6 Specimen S60-G12.7-3.0-600 flexural test results

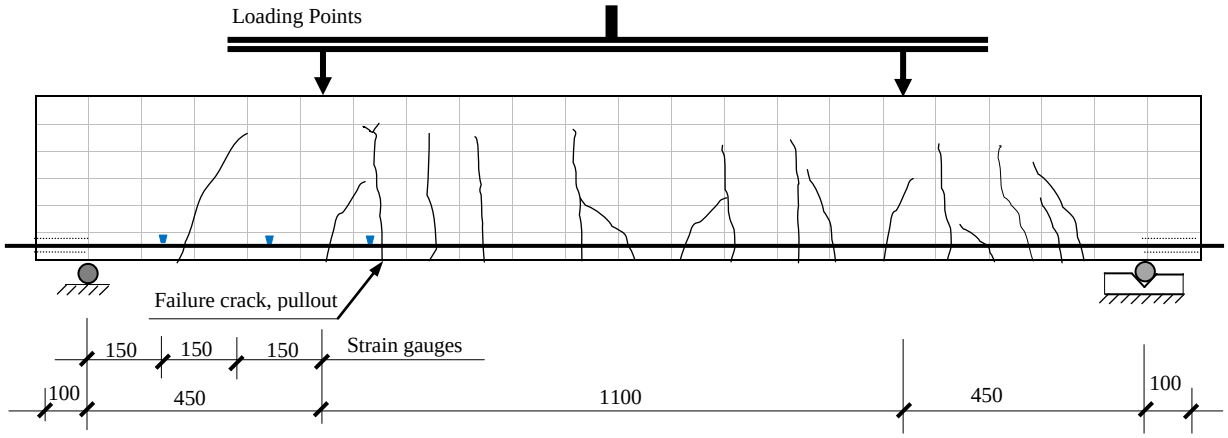

(a) Cracks pattern at failure, pullout at f_{frp} of 514.8 MPa

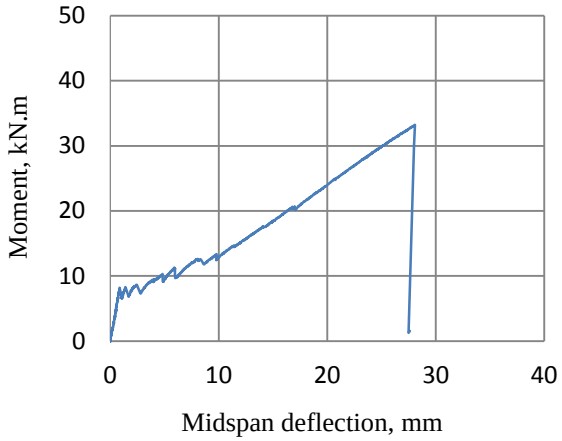

(b) Moment versus midspan deflection responses

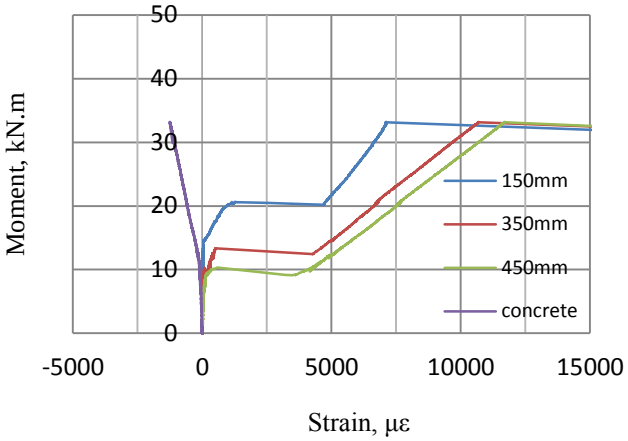

(c) Strain response in the GFRP bar and concrete

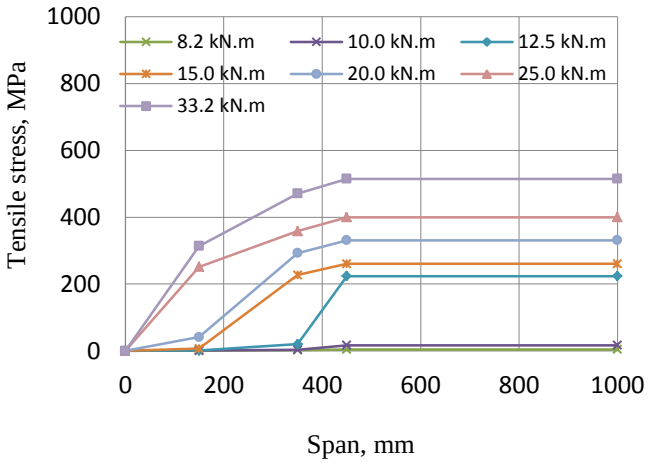

(d) Tensile stress profile in the GFRP bar at varies load levels

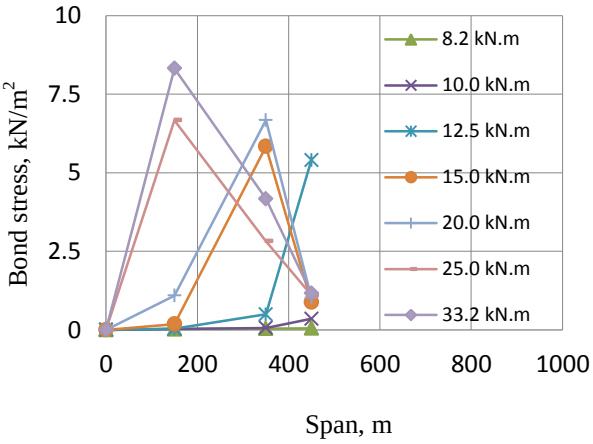

(e) Bond stress profile at varies load levels

Figure A.7 Specimen SG15.9-3.0-450 flexural test results

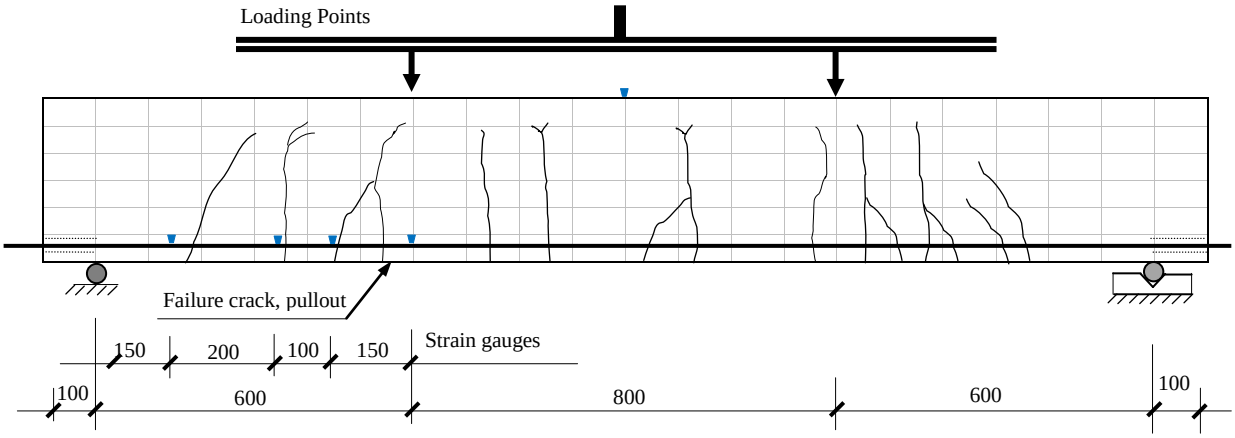

(a) Cracks pattern at failure, pullout at f_{frp} of 627.8 MPa

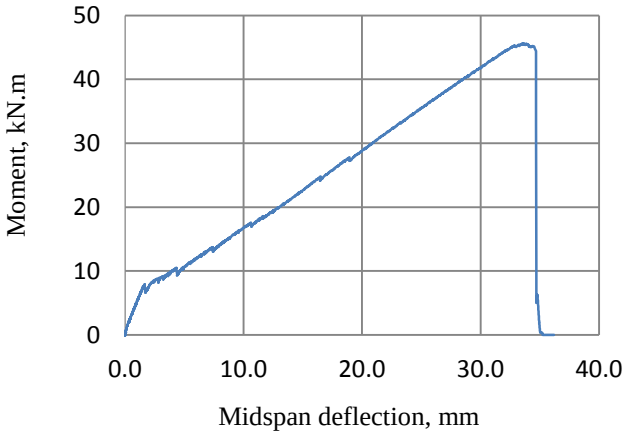

(b) Moment versus midspan deflection responses

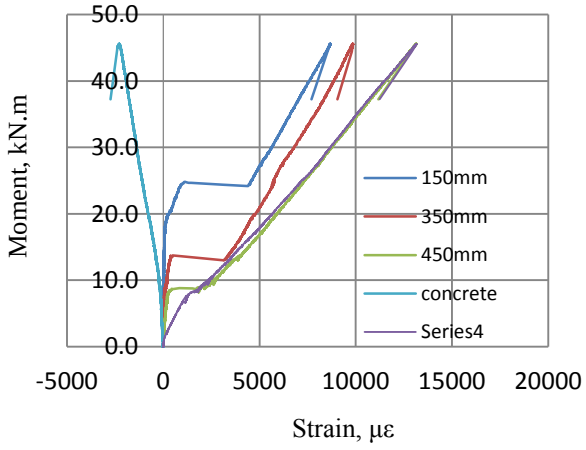

(c) Strain response in the GFRP bar and concrete

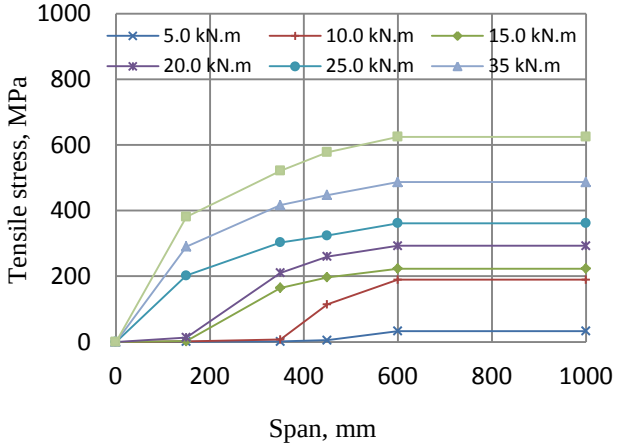

(d) Tensile stress profile in the GFRP bar at varies load levels

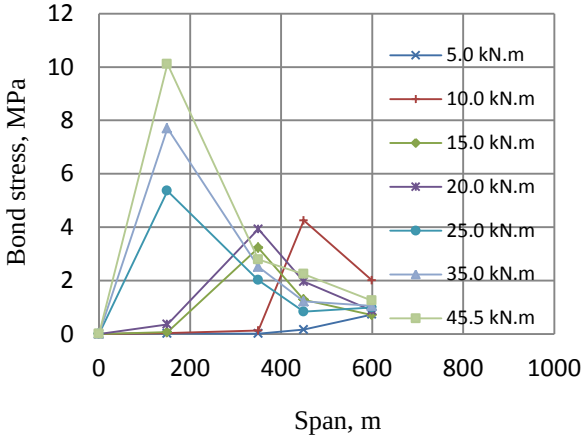

(e) Bond stress profile at varies load levels

Figure A.8 Specimen SG15.9-3.0-600 flexural test results

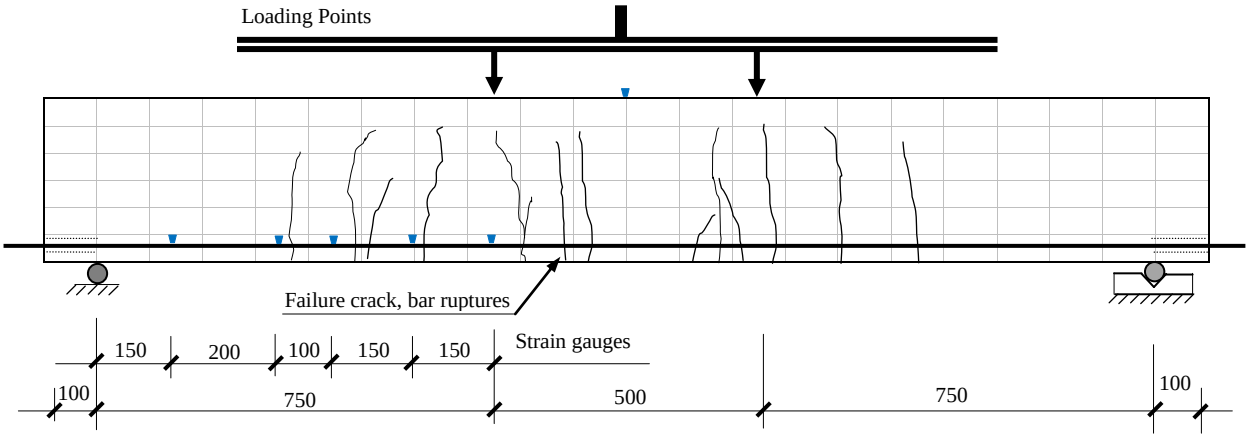

(a) Cracks pattern at failure, bar rupture at f_{frp} of 654.9 MPa

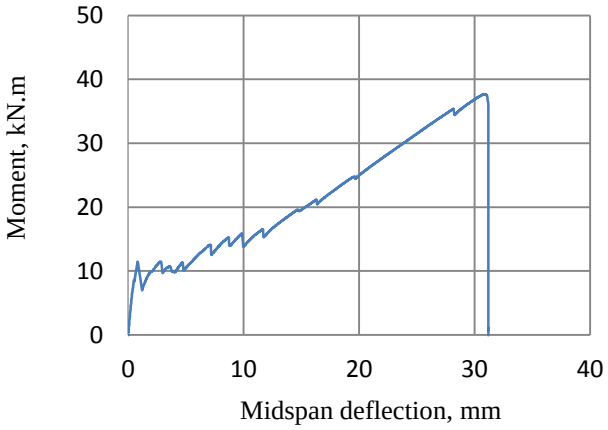

(b) Moment versus midspan deflection responses

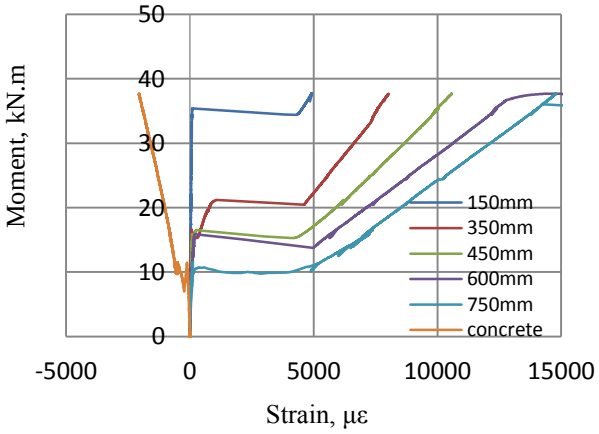

(c) Strain in the GFRP bar and concrete

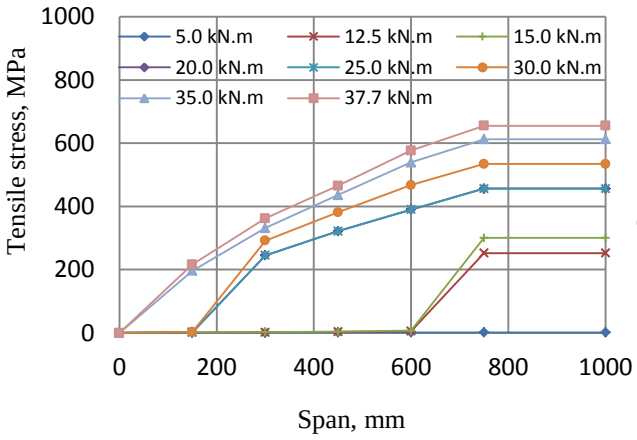

(d) Tensile stress profile in the GFRP bar at varies load levels

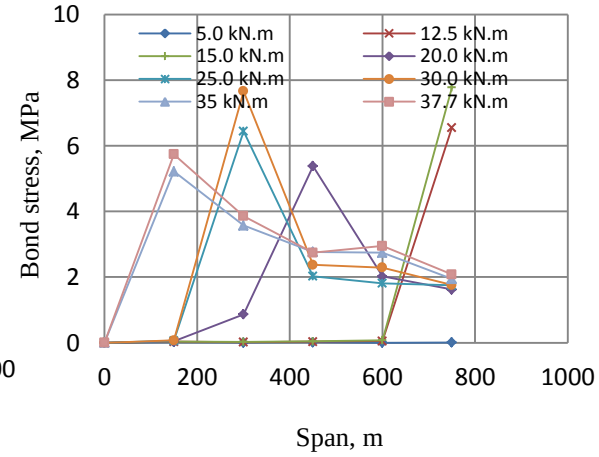

(e) Bond stress profile at varies load levels

Figure A.9 Specimen SG15.9-3.0-750 flexural test results

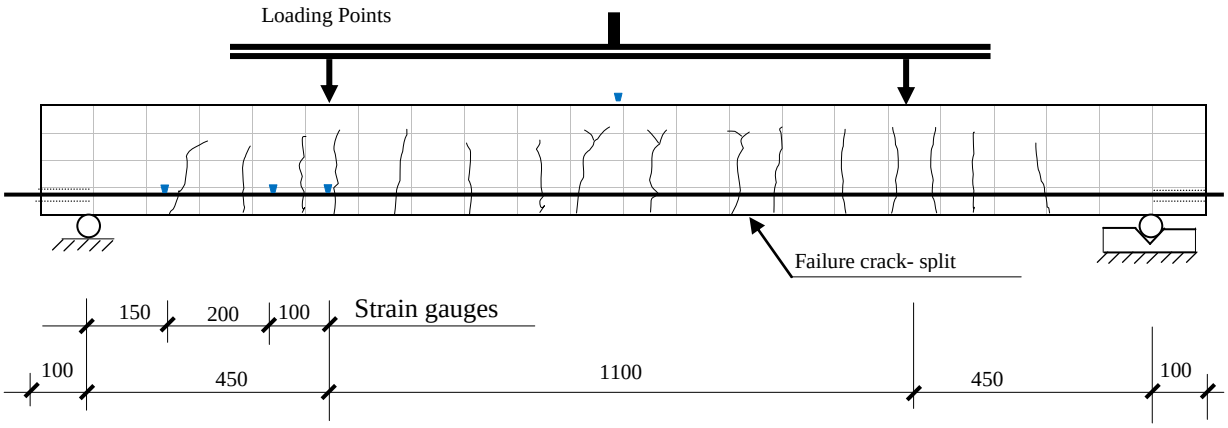

(a) Cracks pattern at failure, bond split failure at f_{frp} of 552.6 MPa

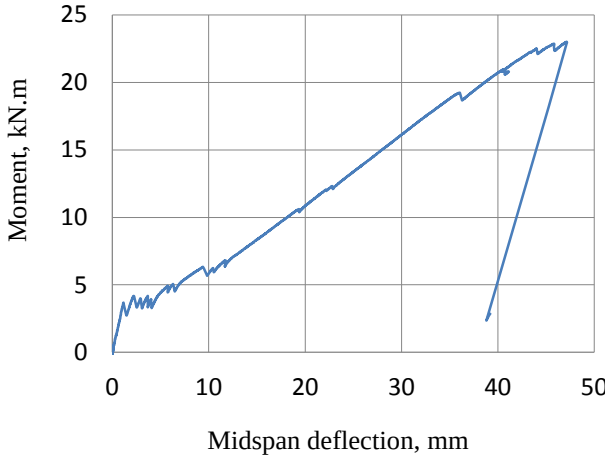

(b) Moment versus midspan deflection responses

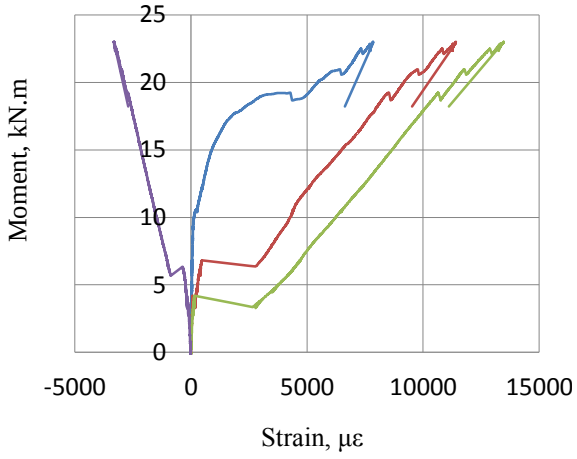

(c) Strain response in the GFRP bar and concrete

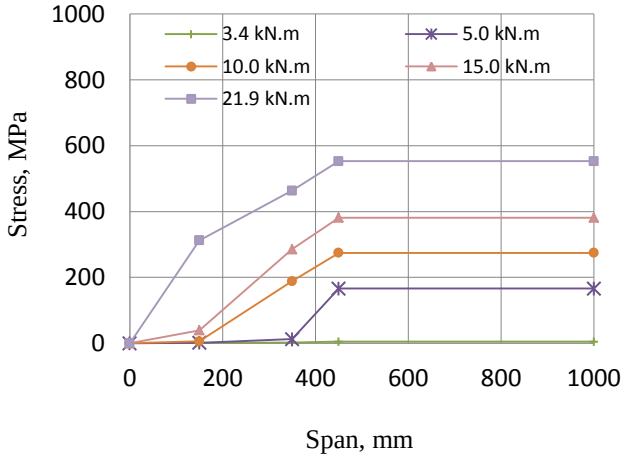

(d) Tensile stress profile in the GFRP bar at various load levels

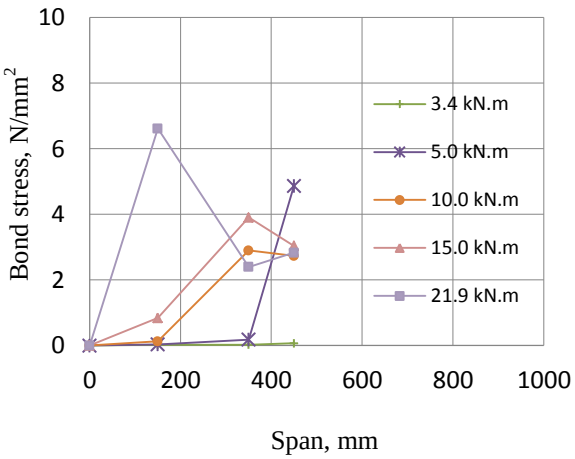

(e) Bond stress profile at various load levels

Figure A.10 Specimen SG12.7-1.0-450 flexural test results

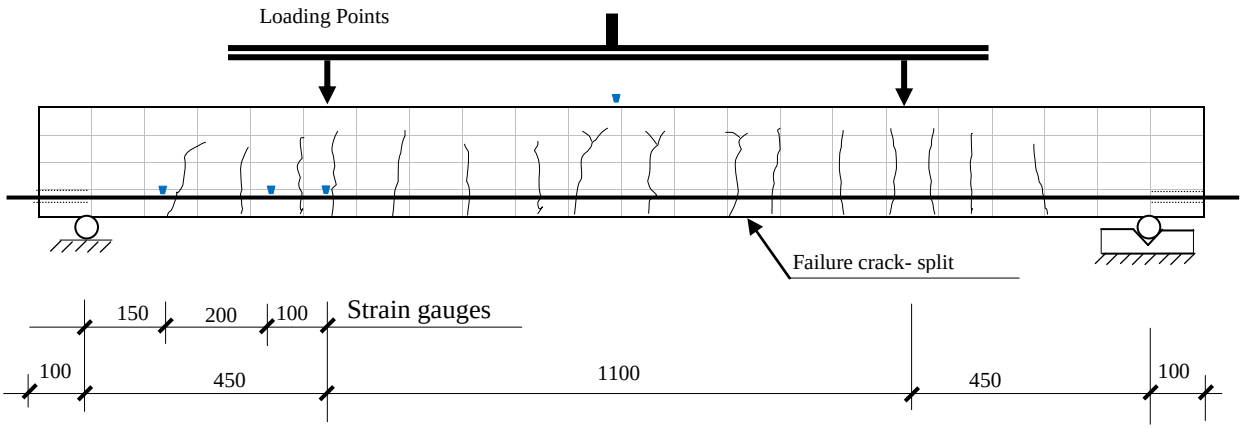

(a) Cracks pattern at failure, bond split failure at f_{frp} of 556.2 MPa

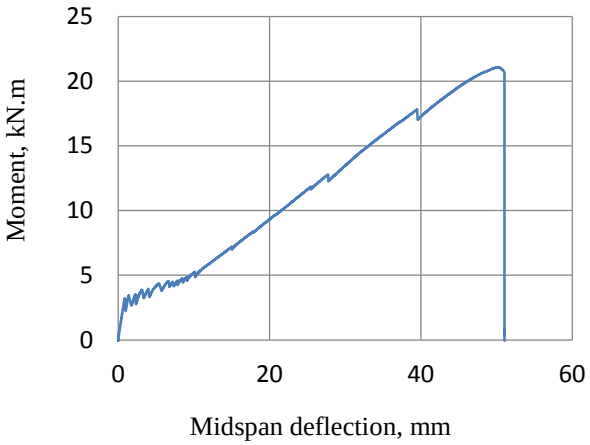

(b) Moment versus midspan deflection responses

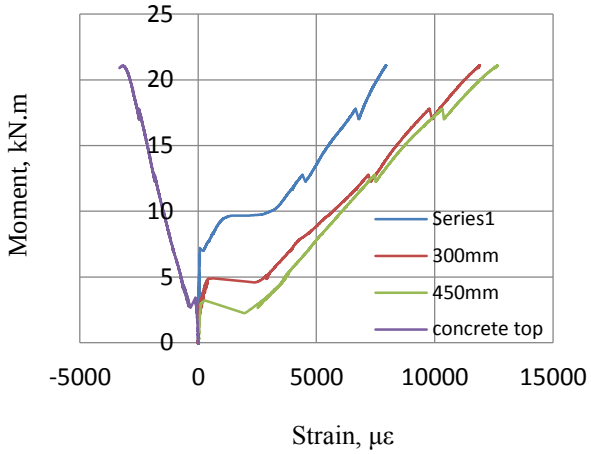

(c) Strain response in the GFRP bar and concrete

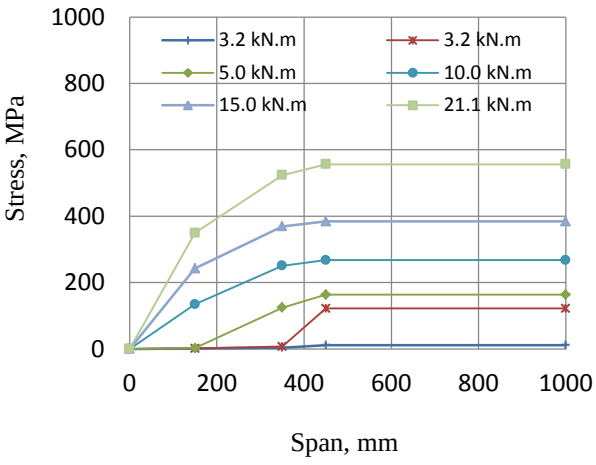

(d) Stress profile in the GFRP bar at various load levels

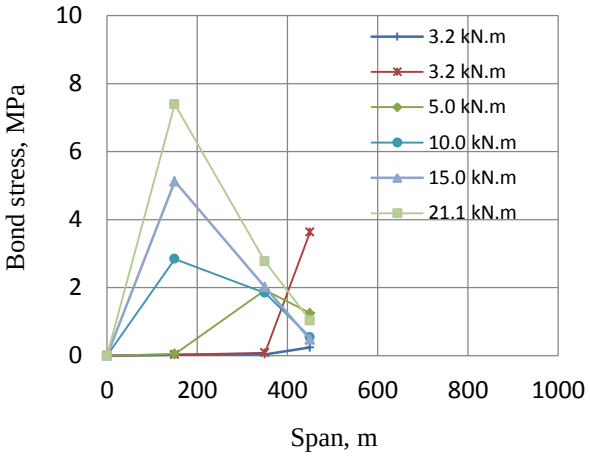

(e) Bond stress profile at various load levels

Figure A.11 Specimen SG12.7-1.5-450 flexural test results

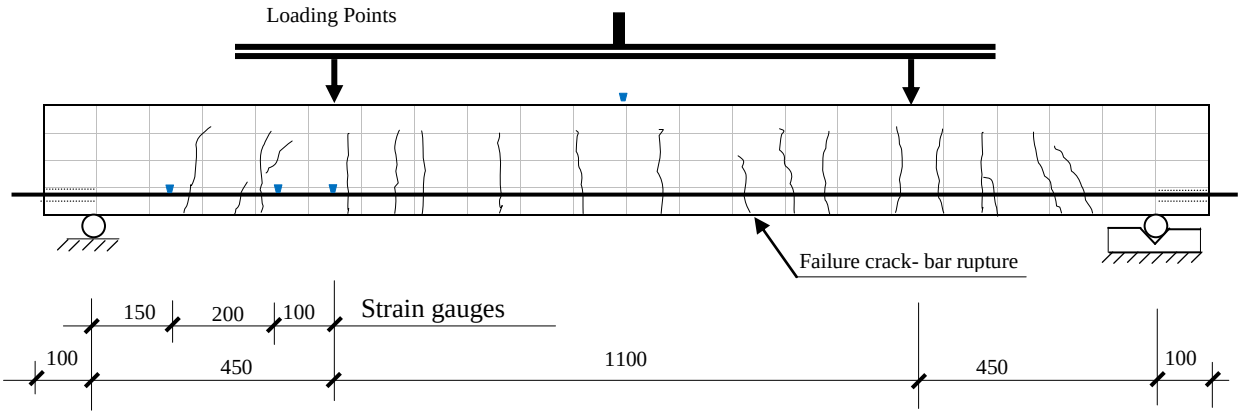

(a) Cracks pattern at failure, bar rupture at f_{frp} of 636.8 MPa

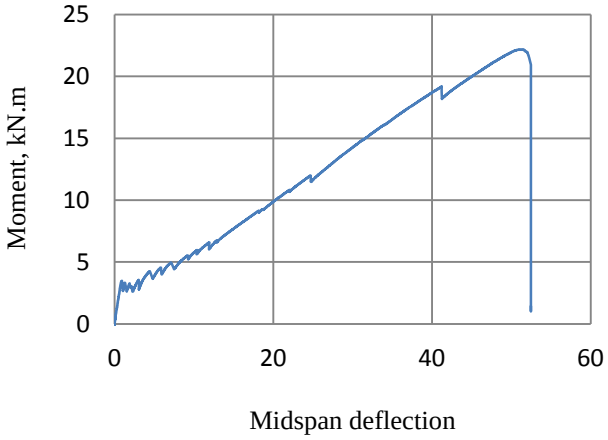

(b) Moment versus midspan deflection responses

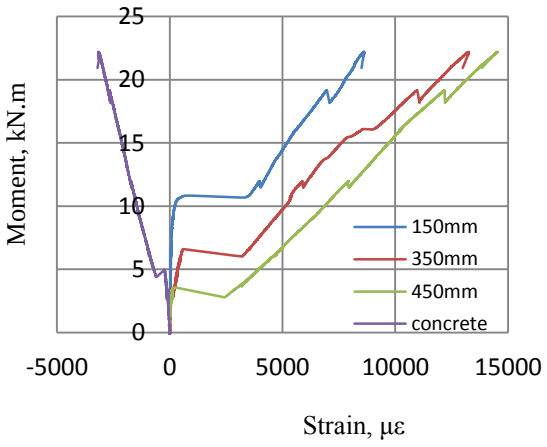

(c) Strain response in the GFRP bar and concrete

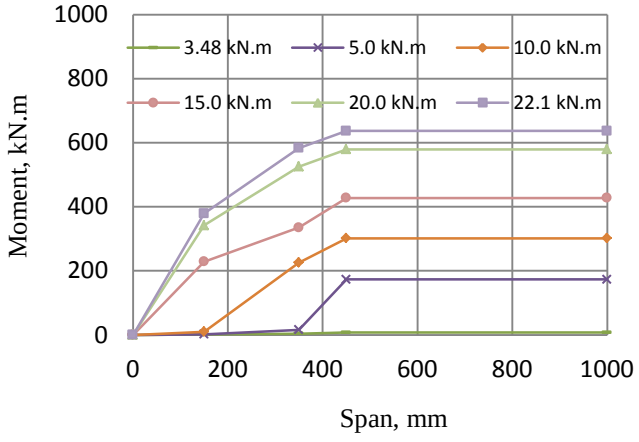

(d) Tensile stress profile in the GFRP bar at various load levels

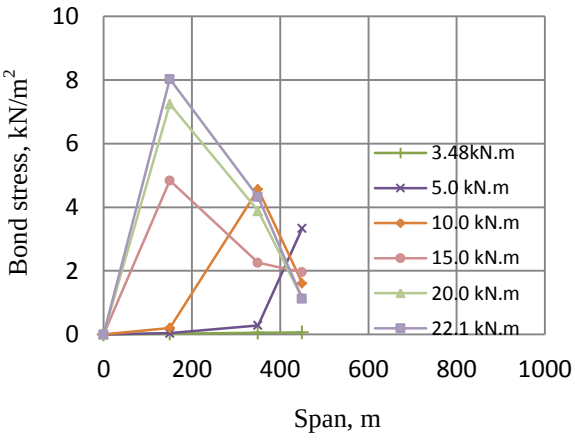

(e) Bond stress profile at various load levels

Figure A.12 Specimen SG12.7-2.0-450 flexural test results

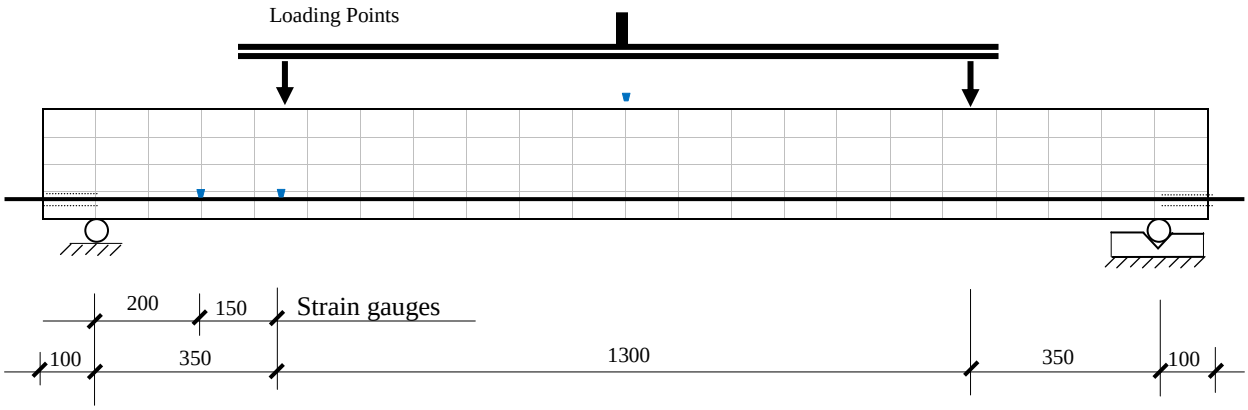

(a) Cracks pattern at failure, bar pullout at f_{frp} of 601.2 MPa

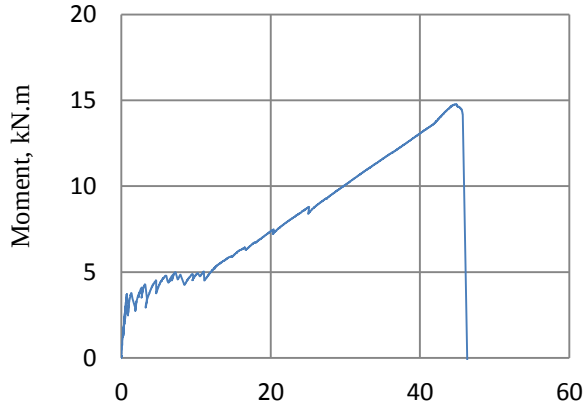

(b) Moment versus midspan deflection responses

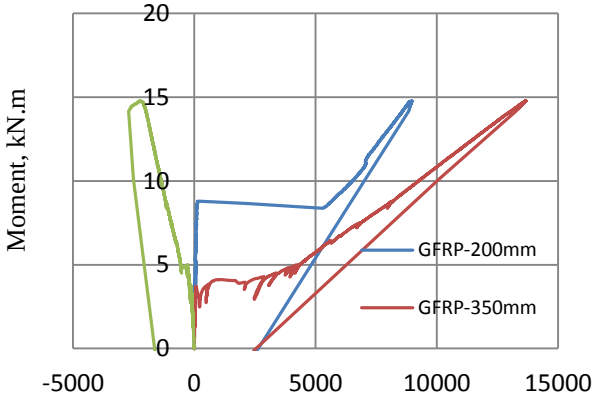

(c) Strain response in the GFRP bar and concrete

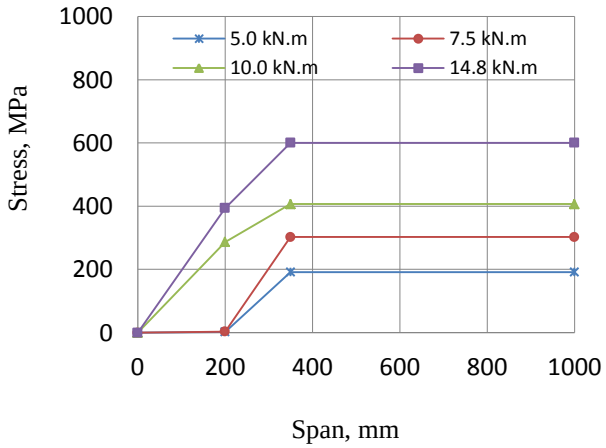

(d) Tensile stress profile in the GFRP bar at various load levels

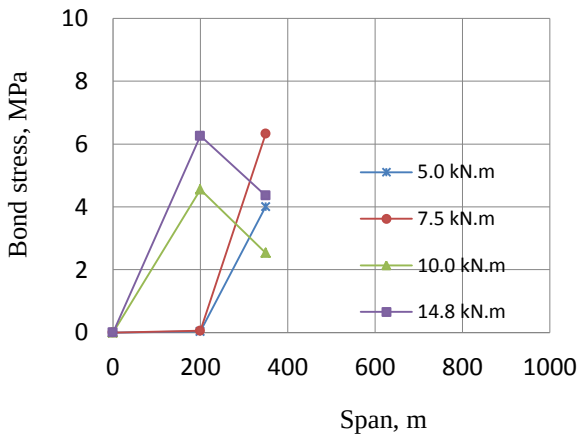

(e) Bond stress profile in GFRP bar at various load levels

Figure A.13 Specimen NG12.7-3.0-350 flexural test results

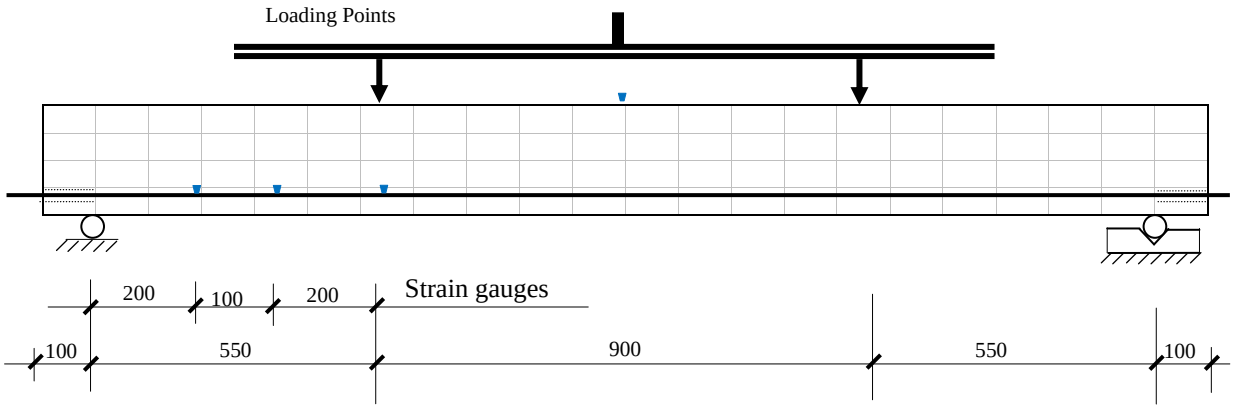

(a) Cracks pattern at failure, bar rupture at f_{frp} of 651.6 MPa

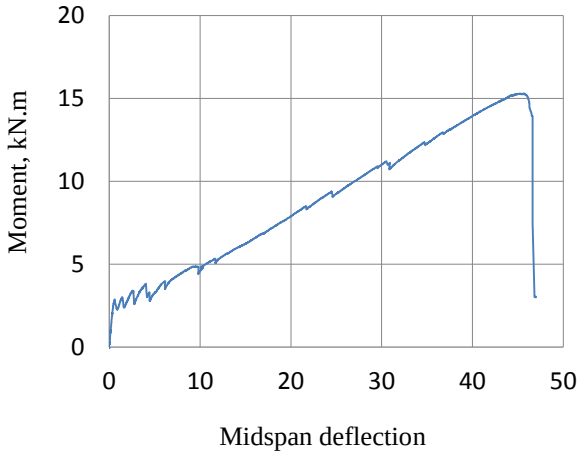

(b) Moment versus midspan deflection responses

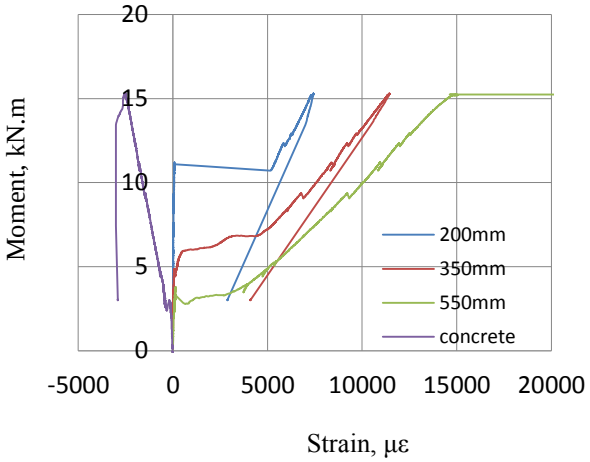

(c) Strain response in the GFRP bar and concrete

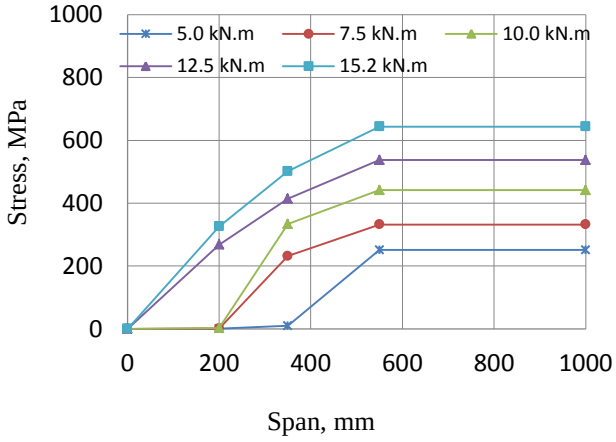

(d) Tensile stress profile in the GFRP bar at various load levels

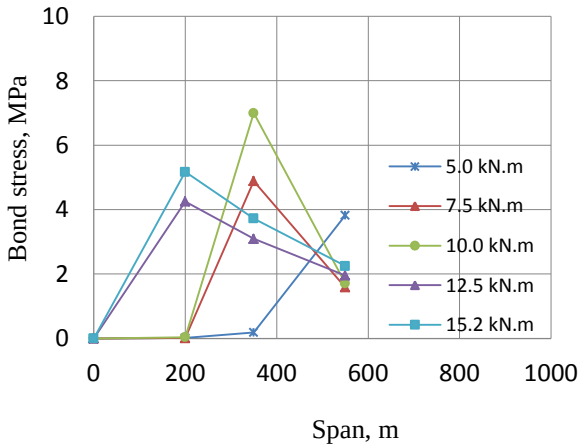

(e) Bond stress profile in GFRP bar at various load levels

Figure A.14 Specimen NG12.7-3.0-550 flexural test results

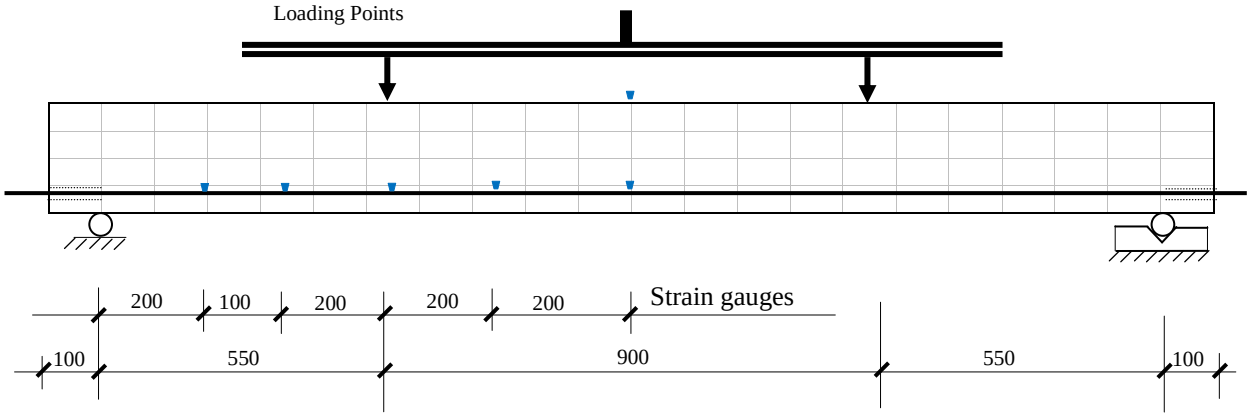

(a) Cracks pattern at failure, bar rupture at f_{frp} of 603.4 MPa

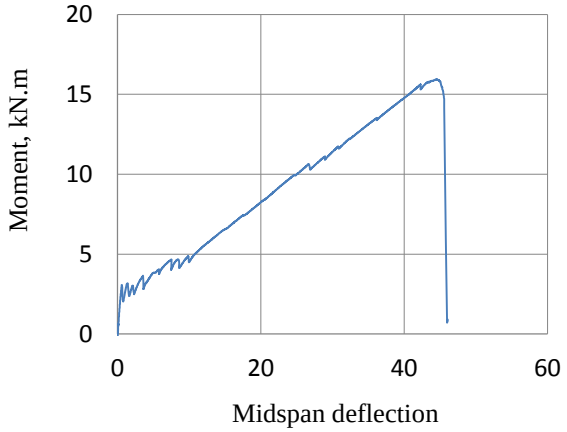

(b) Moment versus midspan deflection responses

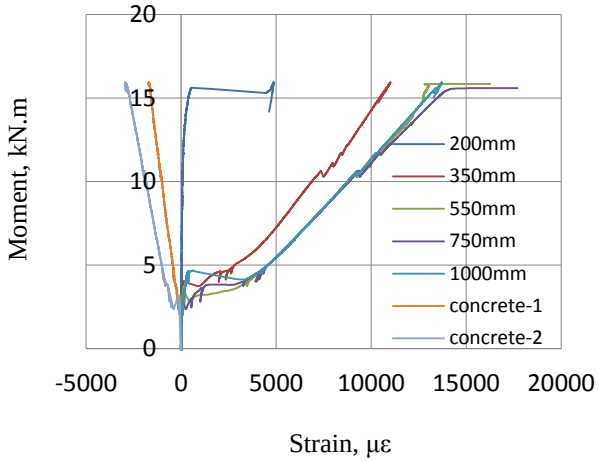

(c) Strain response in the GFRP bar and concrete

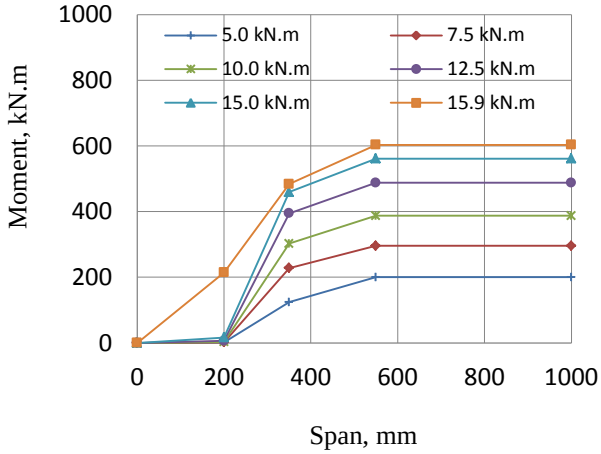

(d) Tensile stress profile in the GFRP bar at various load levels

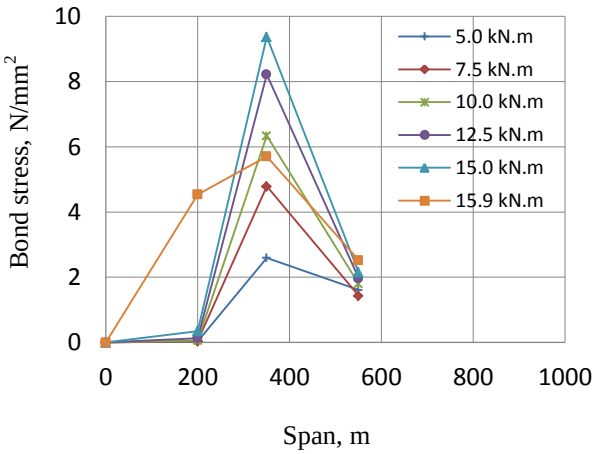

(e) Bond stress profile in GFRP bar at various load levels

Figure A.15 Specimen NG12.7-3.0-550-2 flexural test results

Appendix B - Flexural Test Results of Beams Reinforced with CFRP Bars

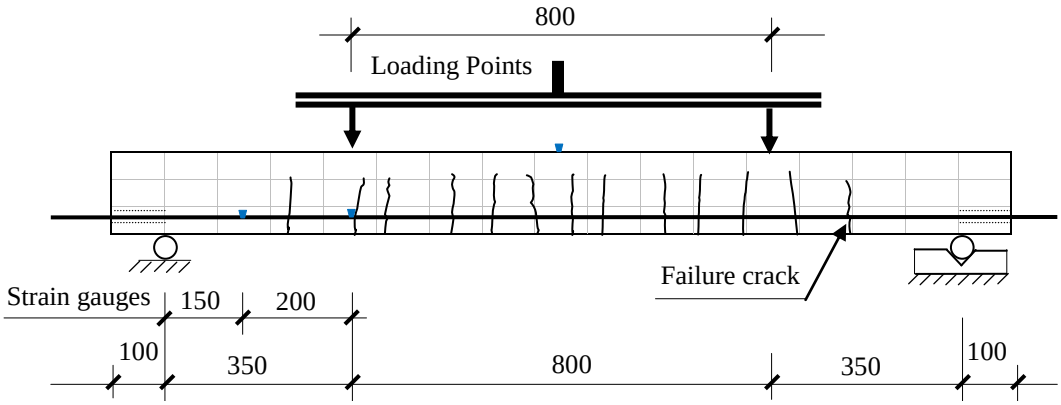

(a) Cracks pattern at failure, average spacing of 80mm, f_{frp} at failure was 971.3MPa

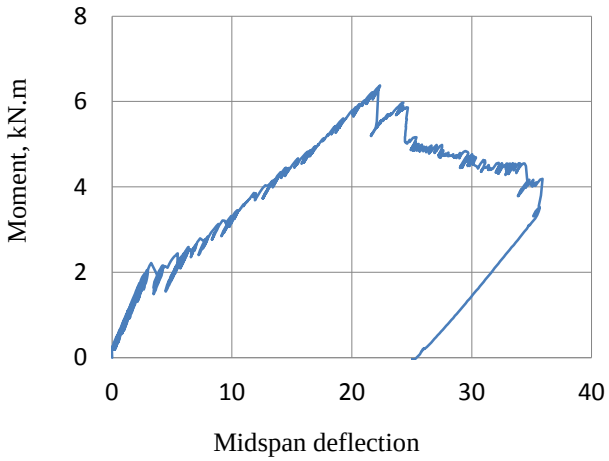

(b) Moment versus midspan deflection responses

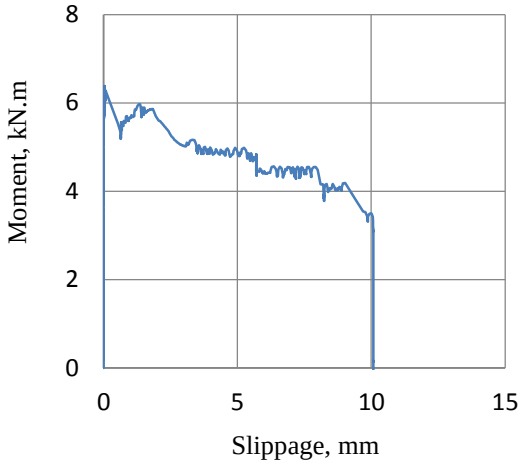

(c) End-slip response

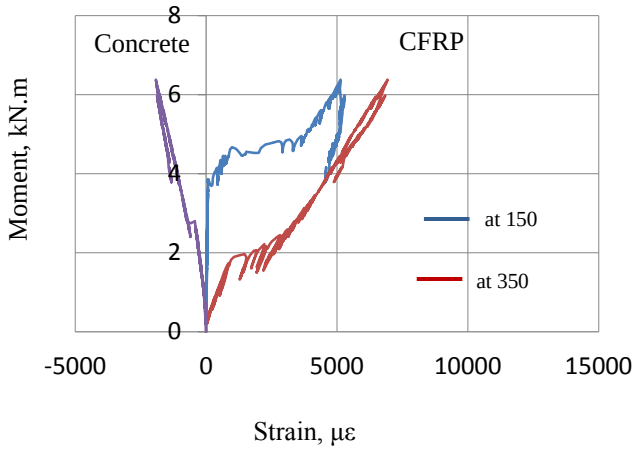

(d) Strain in CFRP bar and concrete at versus load levels

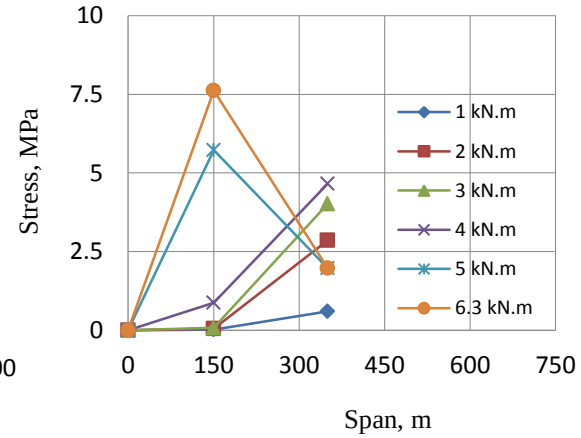

(e) Bond stress profile at various load level

Figure B.1 Specimen SC6.3-3.0-350 flexural test results

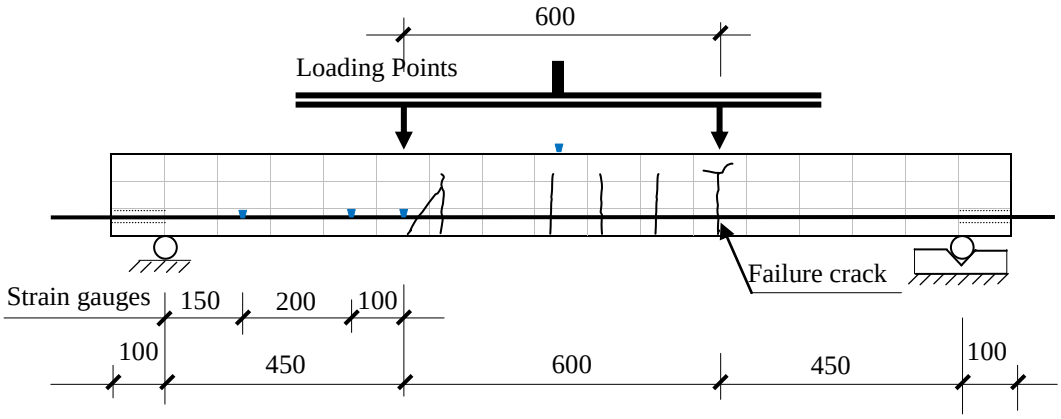

(a) Cracks pattern at failure, average spacing of 125mm, , f_{frp} at failure was 1205.9MPa

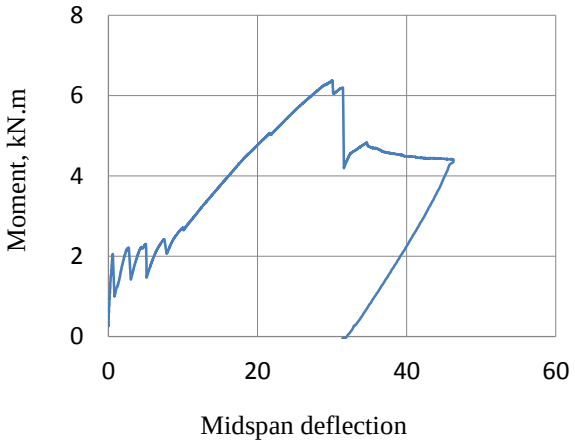

(b) Moment versus midspan deflection response

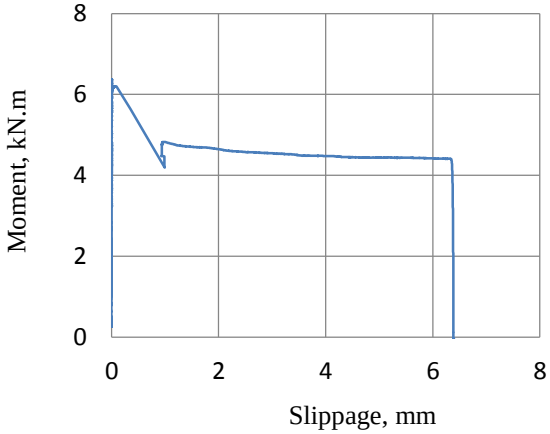

(c) End slip response

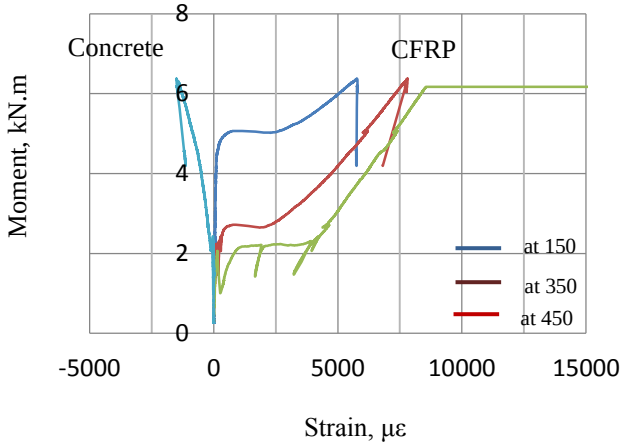

(d) Strain in the CFRP bar and concrete at versus load levels

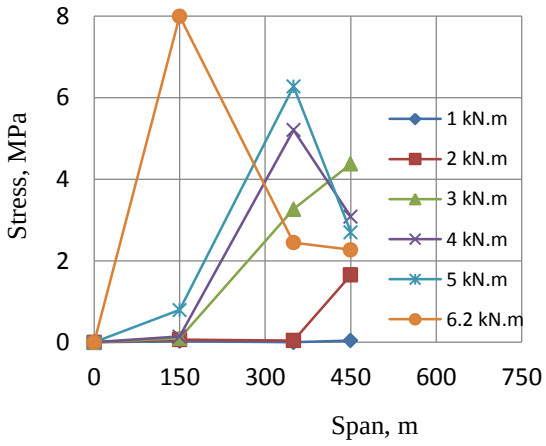

(e) Bond stress profile at various load levels

Figure B.2 Specimen SC6.3-3.0-450 flexural test results

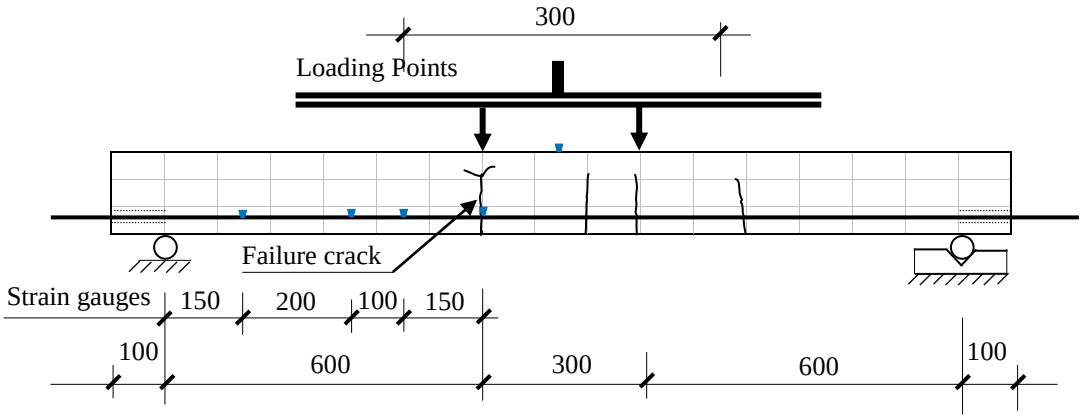

(a) Cracks pattern at failure, average spacing of 135mm, , f_{frp} at failure was 1660.7 MPa

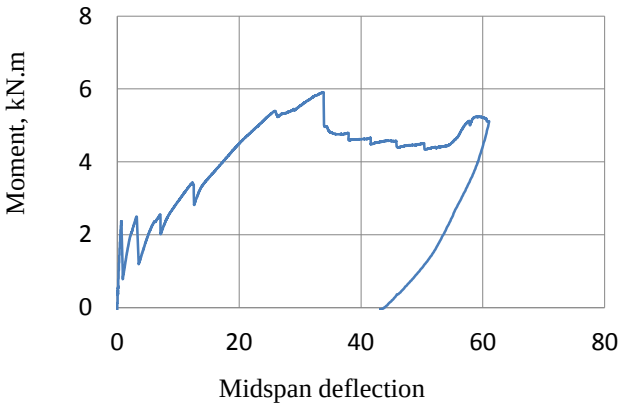

(b) Moment versus midspan deflection responses

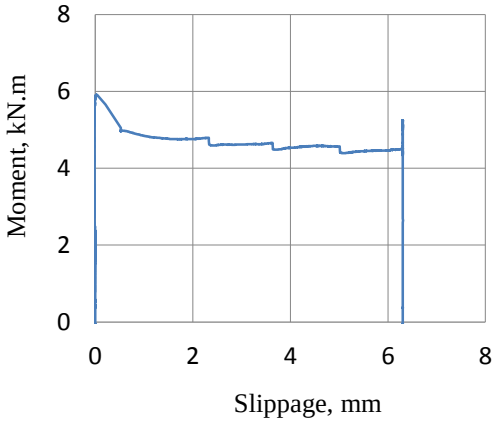

(c) End slip response

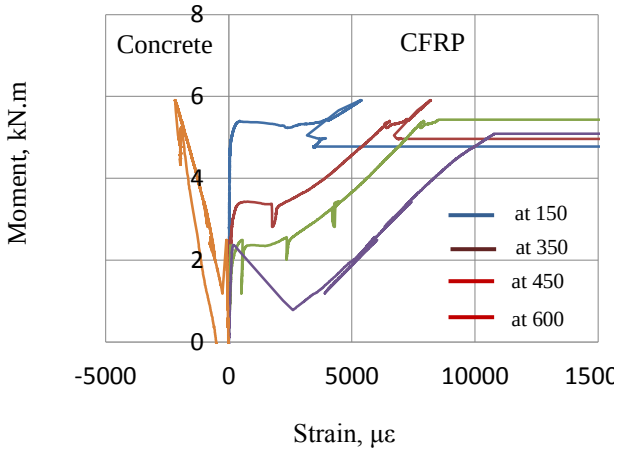

(d) Strain in the CFRP bar and concrete at versus load levels

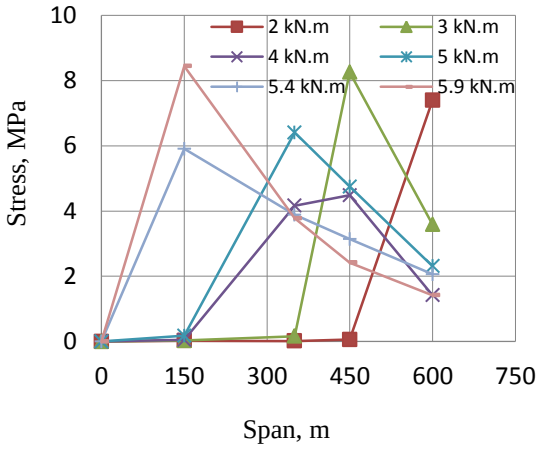

(e) Bond stress profile at various load levels

Figure B.3 Specimen SC6.3-3.0-600 flexural test results

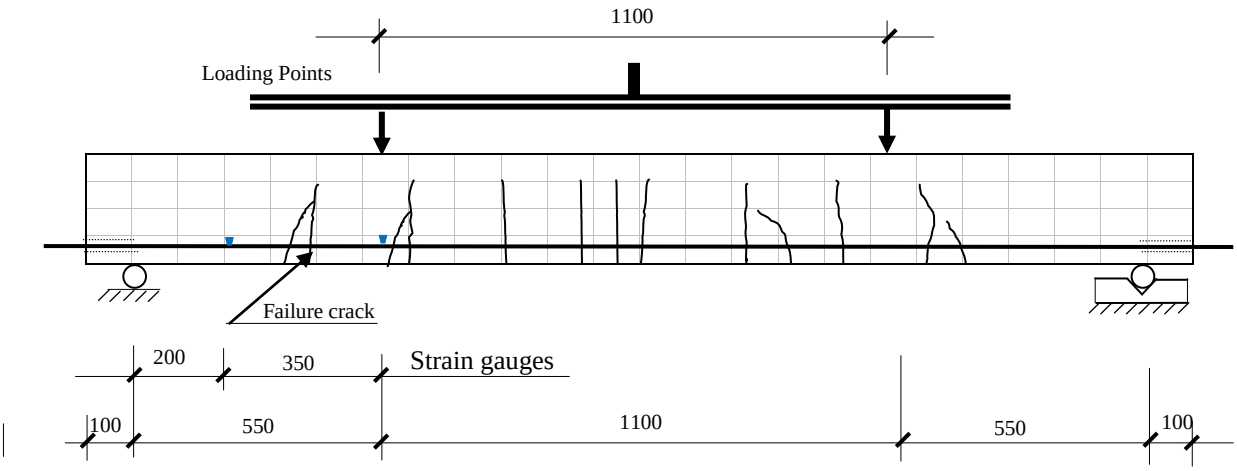

(a) Cracks pattern at failure, average spacing of 175mm, , f_{frp} at failure was 1063.1 MPa

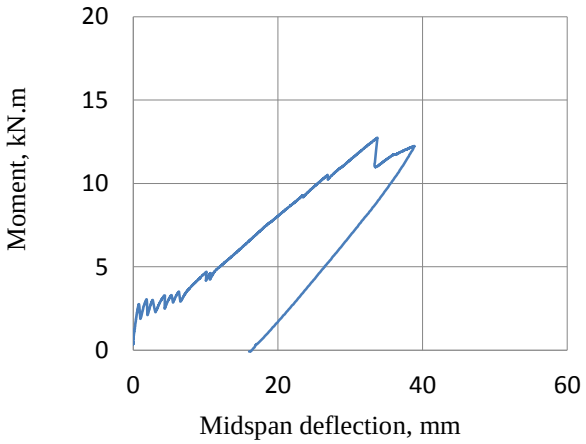

(b) Moment versus midspan deflection responses

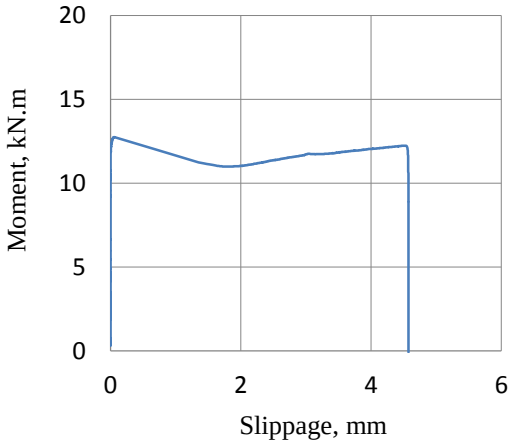

(c) End slip response

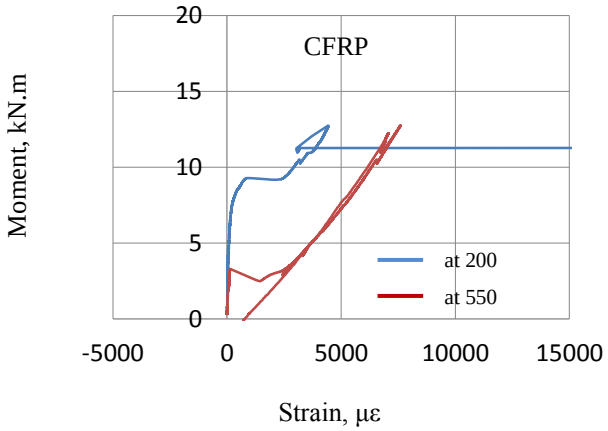

(d) Strain in the CFRP bar and concrete at various load levels

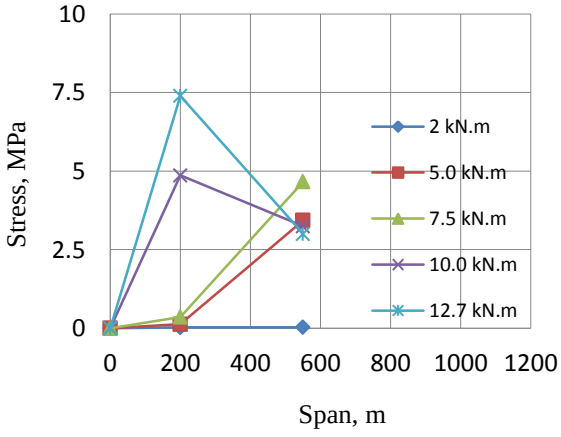

(e) Bond stress profile at various load levels

Figure A.4 Specimen S60-C9.5-3.0-550 flexural test results

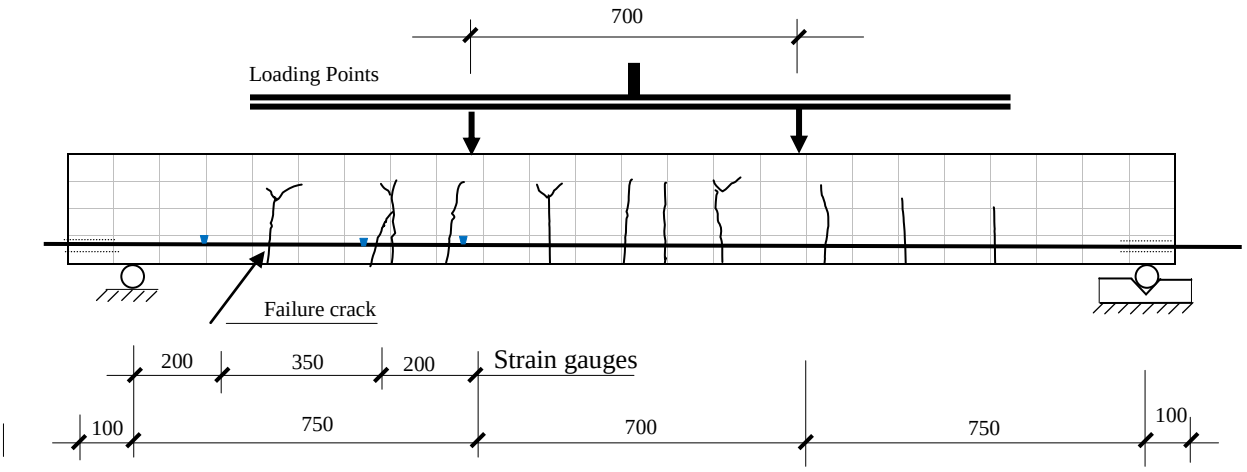

(a) Cracks pattern at failure, average spacing of 170mm, , f_{frp} at failure was 1375.2MPa

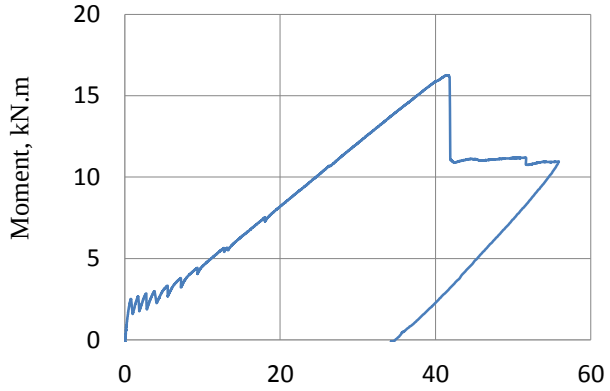

(b) Moment versus midspan deflection responses

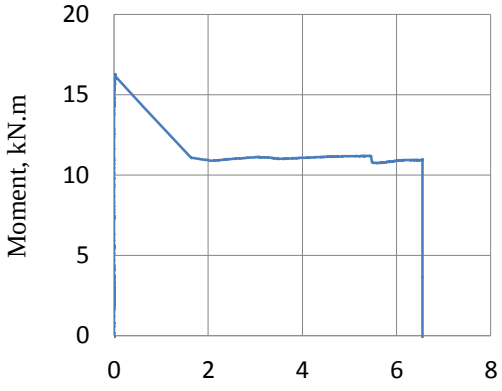

(c) End slip response

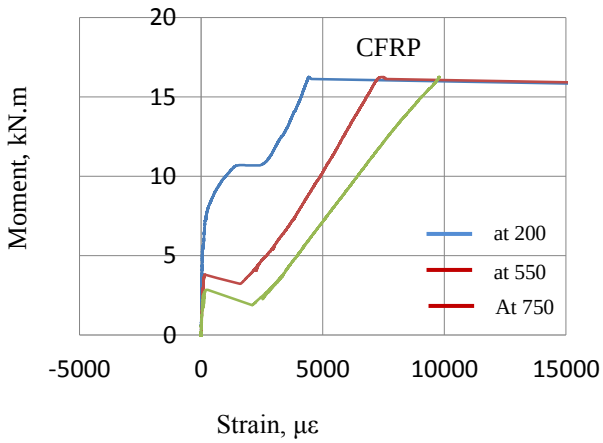

(d) Strain in the CFRP bar and top concrete

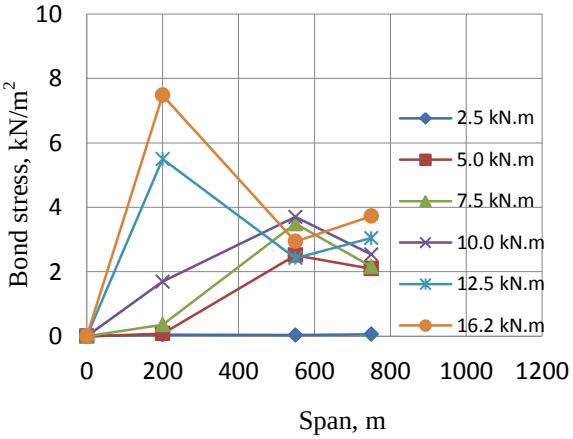

(e) Bond stress profile at various load levels

Figure B.5 Specimen SC9.5-3.0-750 flexural test results

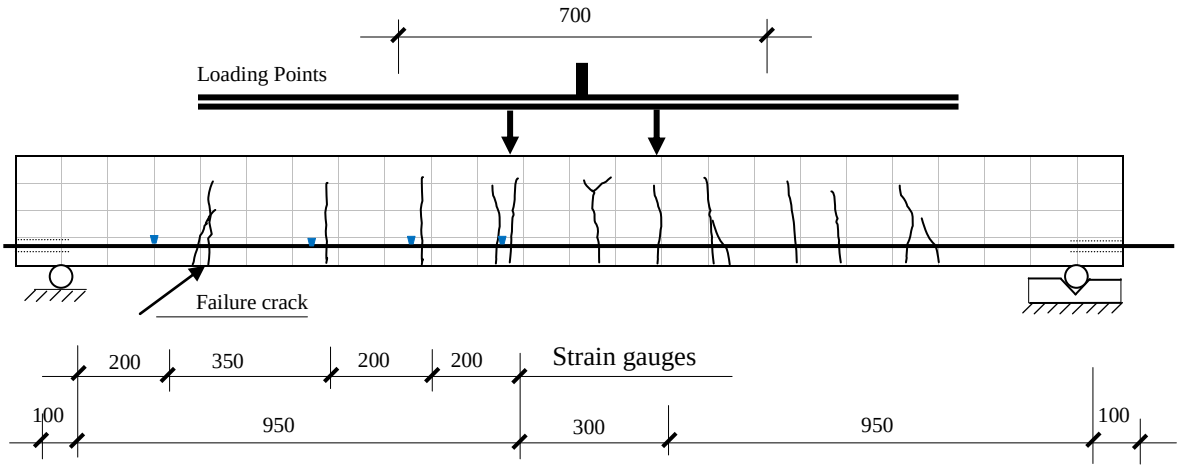

(a) Cracks pattern at failure, average spacing of 160mm, , f_{frp} at failure was 1435.1 MPa

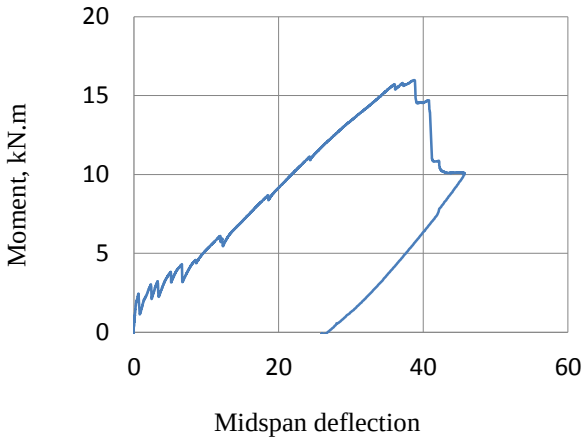

(b) Moment versus midspan deflection responses

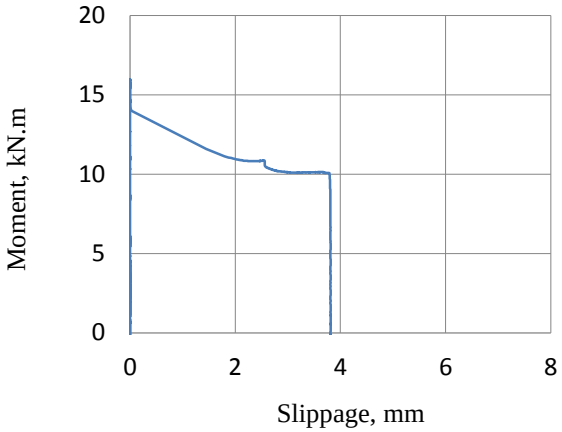

(c) End slip response

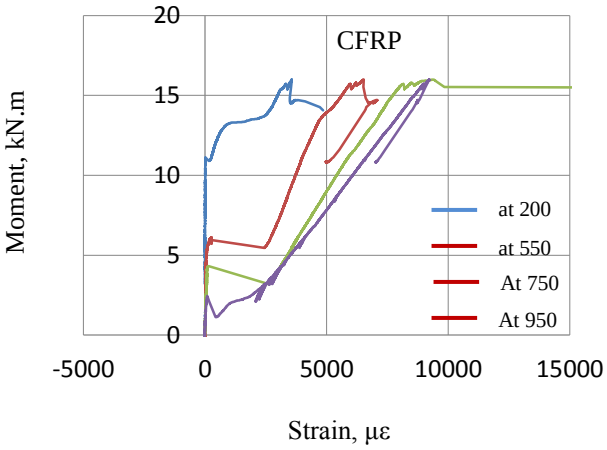

(d) Strain in the CFRP bar and at versus load levels

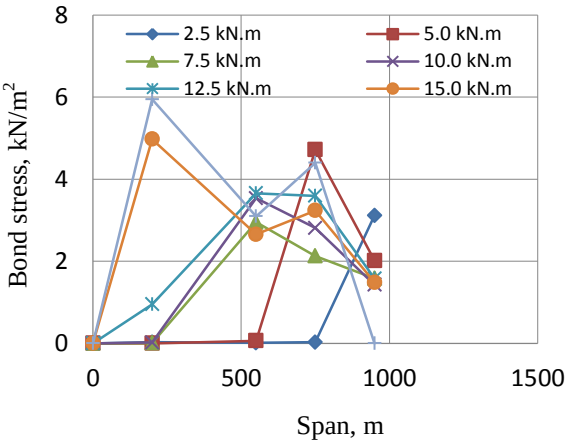

(e) Bond stress profile at various load levels

Figure B.6 Specimen SC9.5-3.0-950 flexural test results

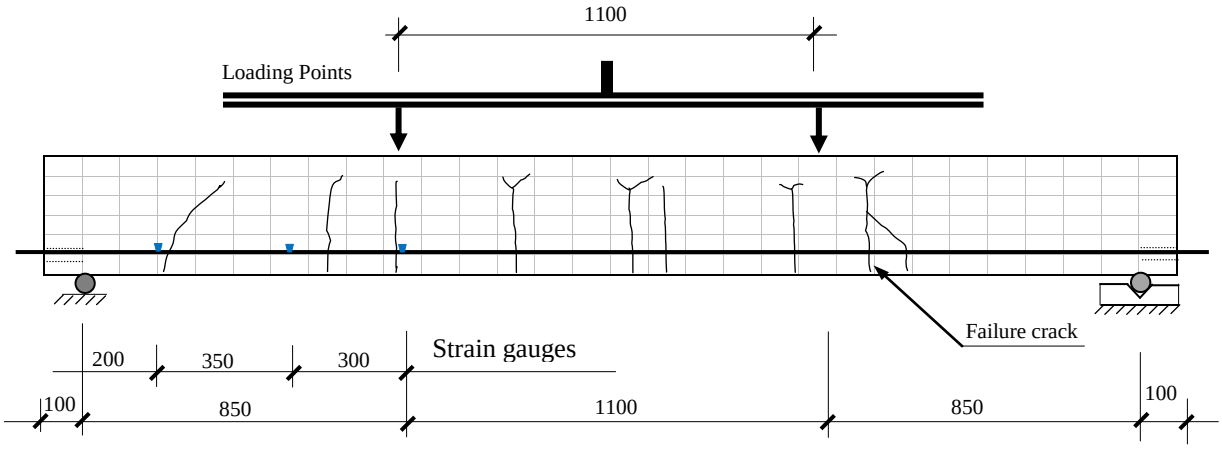

(a) Cracks pattern at failure, average spacing of 280mm, , f_{frp} at failure was 1119.6 MPa

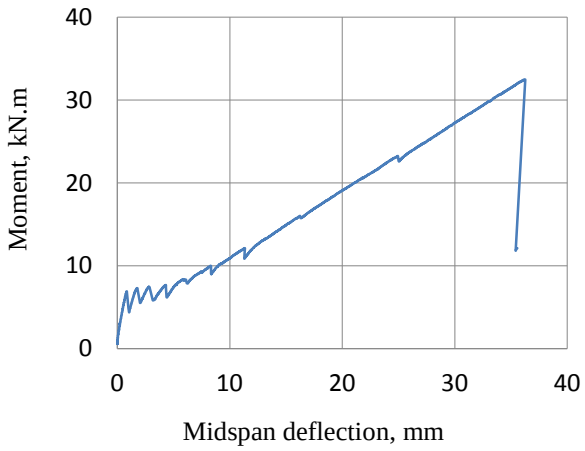

(b) Moment versus midspan deflection responses

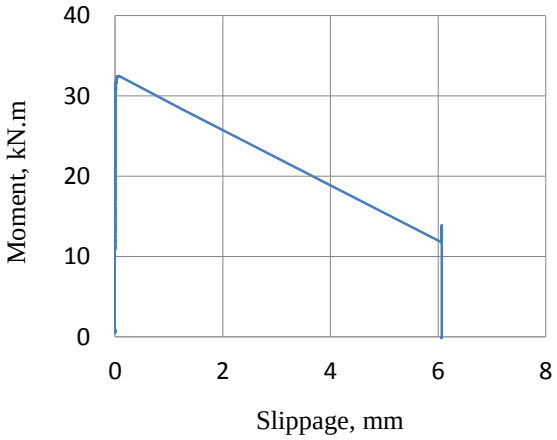

(c) End slip response

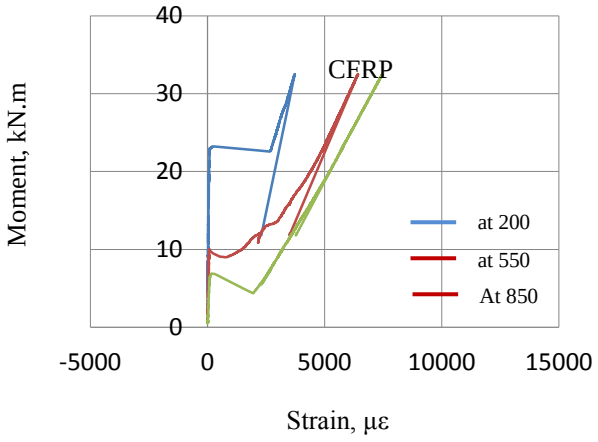

(d) Strain in the CFRP bar at various load levels

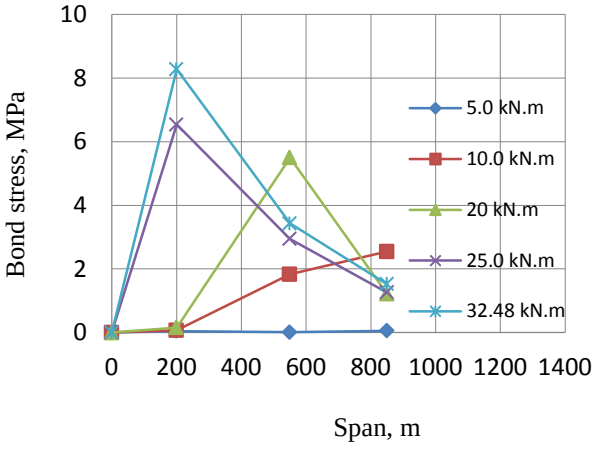

(e) Bond stress profile at various load levels

Figure B.7 Specimen SC12.7-3.0-850 flexural test results

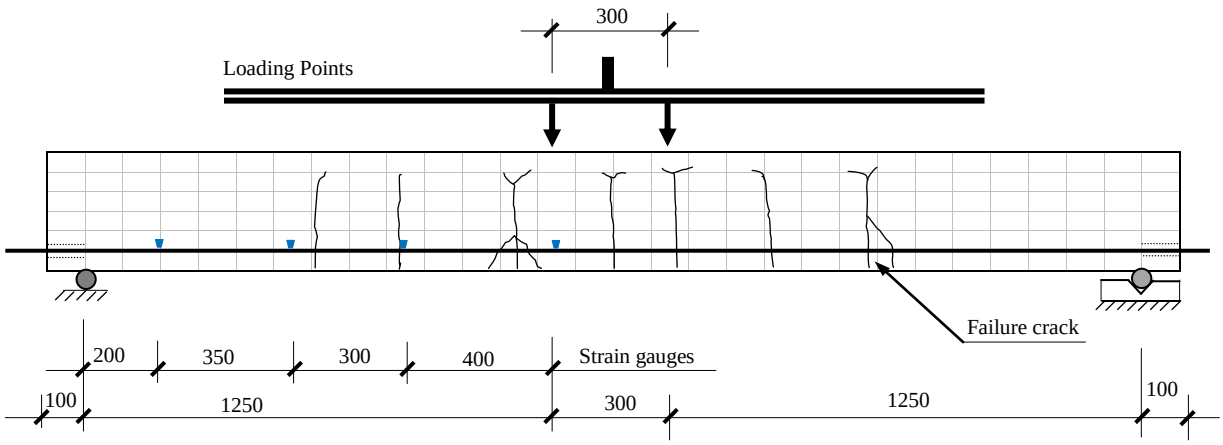

(a) Cracks pattern at failure, average spacing of 250mm, , f_{frp} at failure was 1424.1 MPa

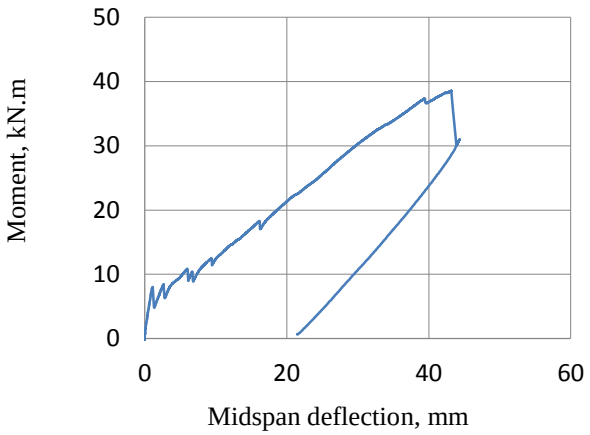

(b) Moment versus midspan deflection responses

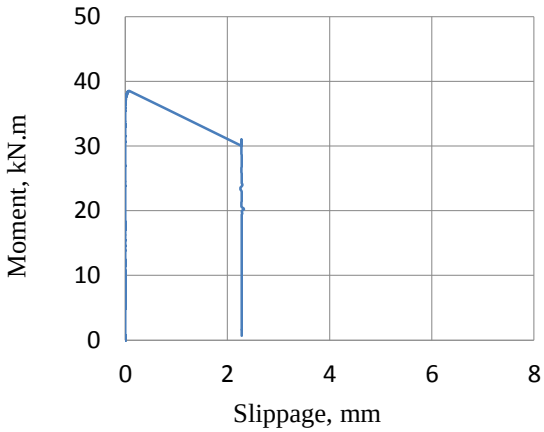

(c) End slip response

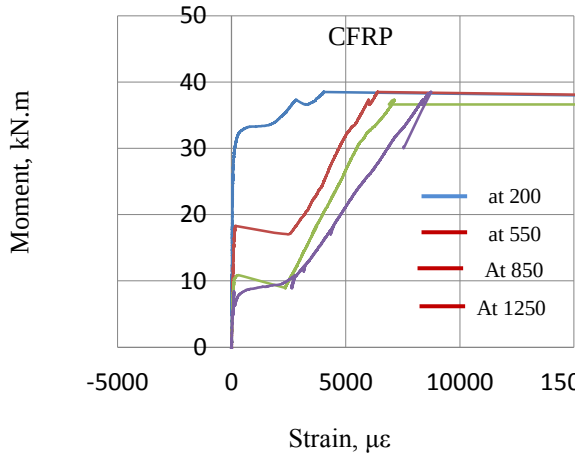

(d) Strain in the CFRP bar response

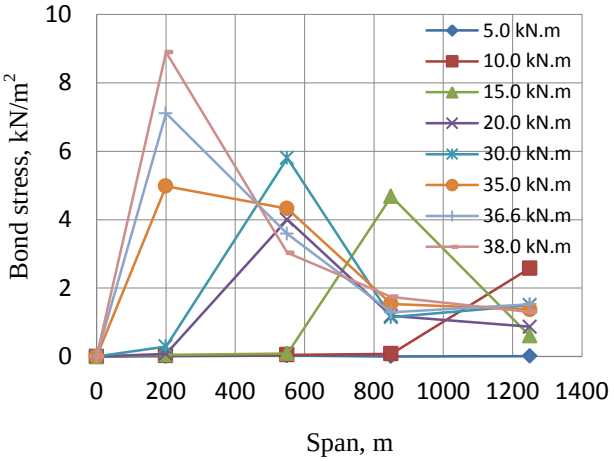

(e) Bond stress profile at various load levels

Figure B.8 Specimen SC12.7-3.0-1250 flexural test results

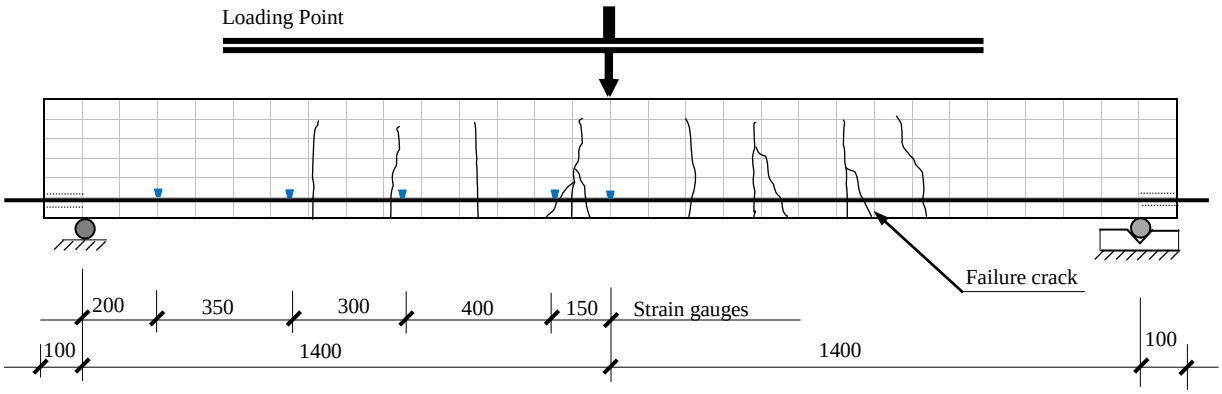

(a) Cracks pattern at failure, average spacing of 240mm, , f_{frp} at failure was 1617.1 MPa

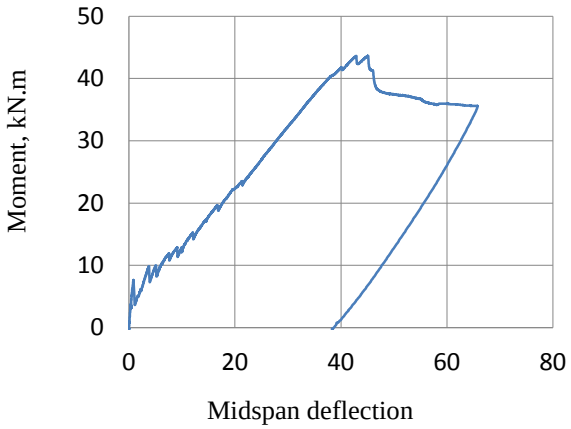

(b) Moment versus midspan deflection responses

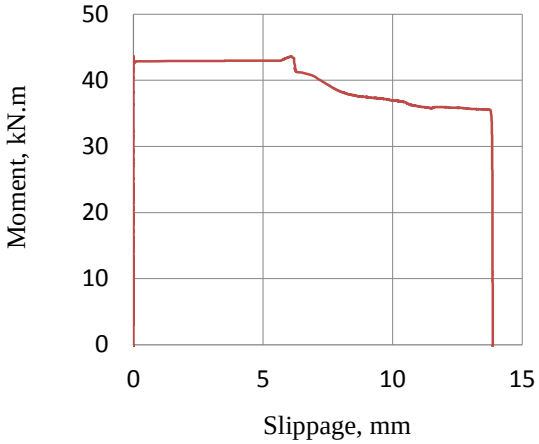

(c) End slip response

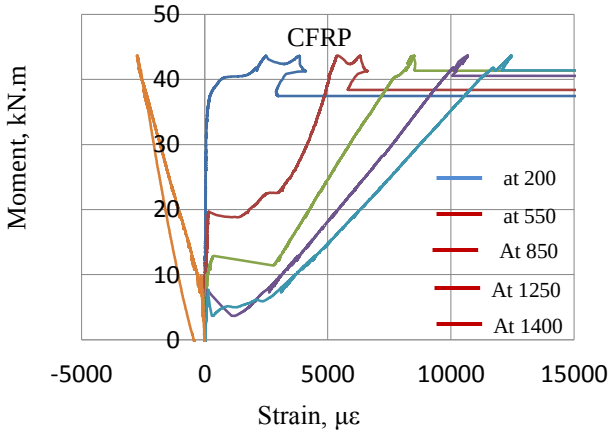

(d) Strain in the CFRP bar response

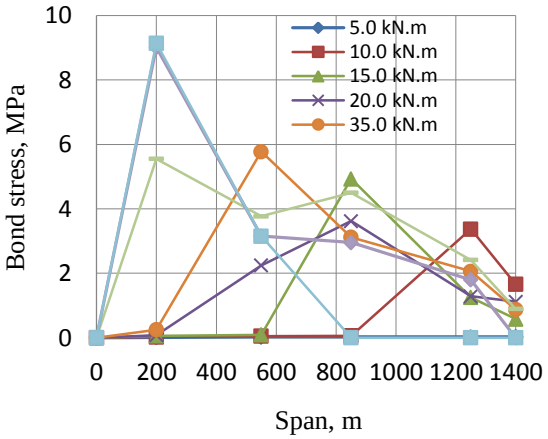

(e) Bond stress profile at various load levels

Figure B.9 Specimen SC12.7-3.0-1400 flexural test results

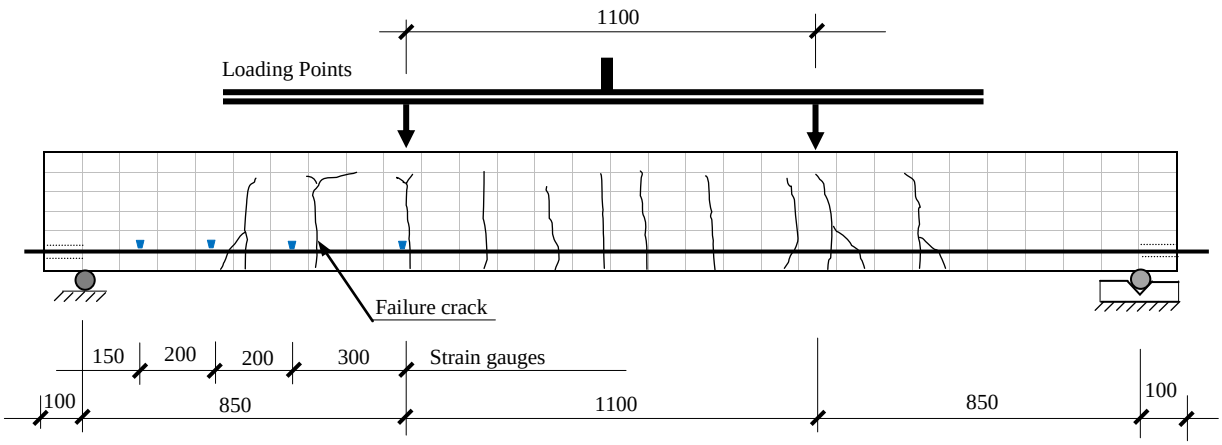

(a) Cracks pattern at failure, average spacing of 180mm, , f_{frp} at failure was 1006.6 MPa

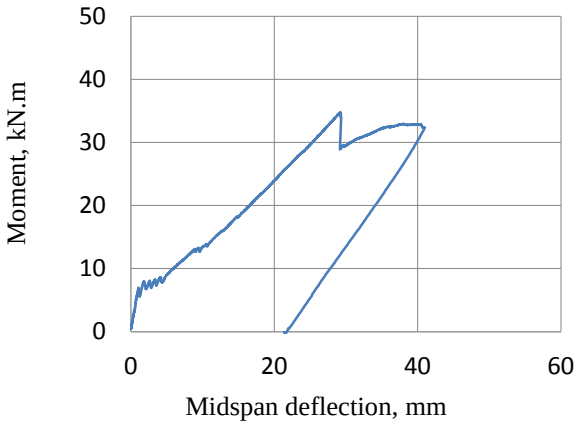

(b) Moment versus midspan deflection responses

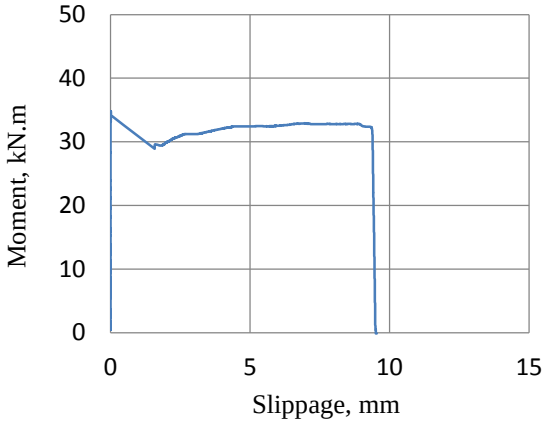

(c) End response

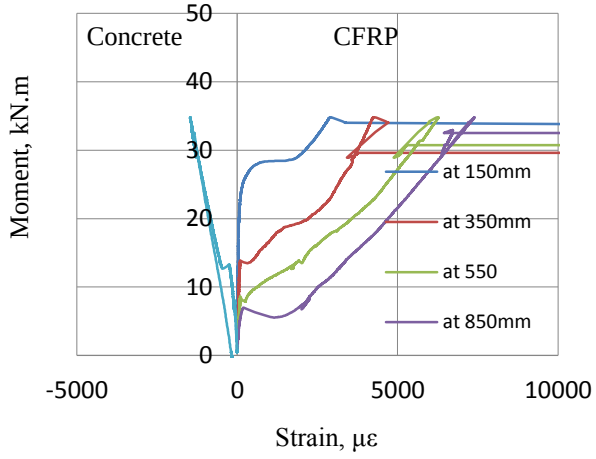

(d) Strain in the CFRP bar and concrete response

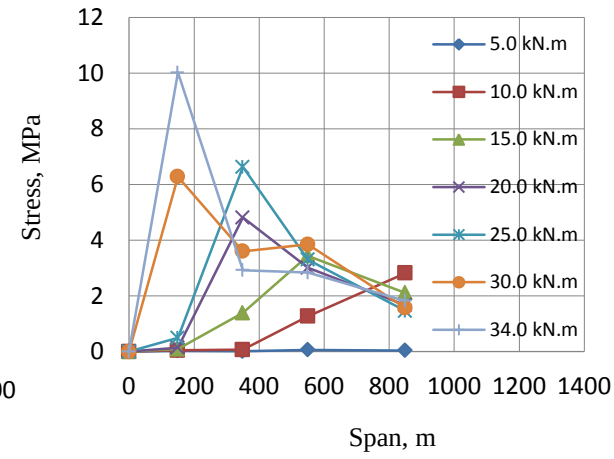

(e) Bond stress profile at various load levels

Figure B.10 Specimen SC12.7-1.0-850 flexural test results

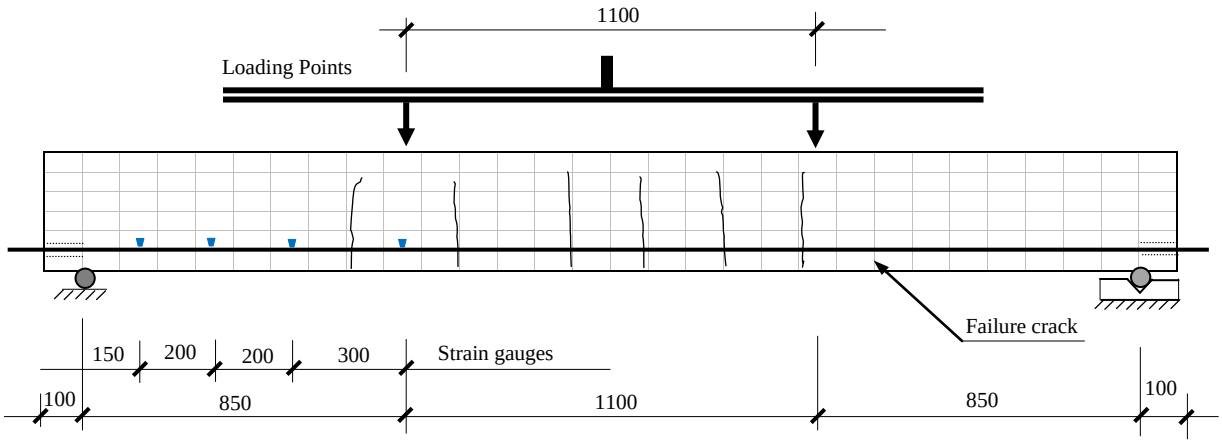

(a) Cracks pattern at failure, average spacing of 240mm, , f_{frp} at failure was 1064.6 MPa

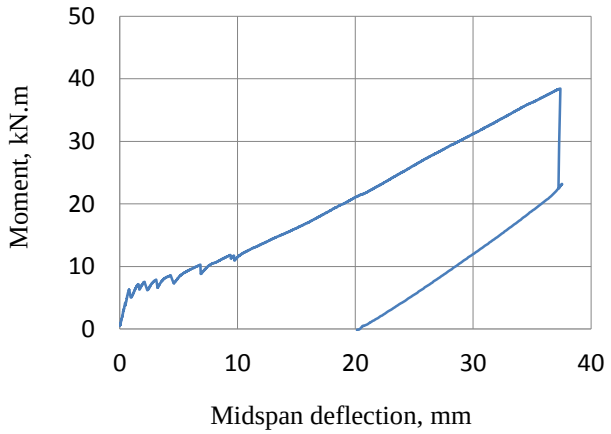

(b) Moment versus midspan deflection responses

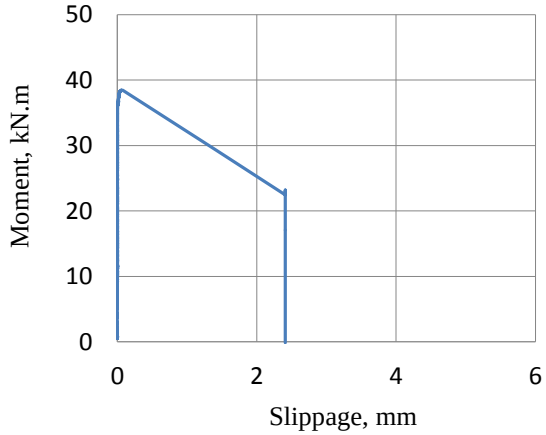

(c) End slip response

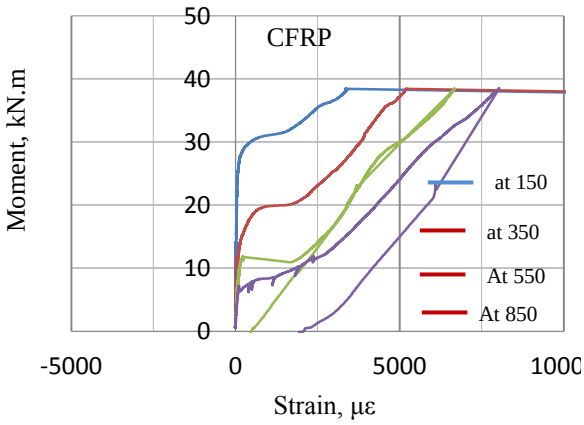

(d) Strain in the CFRP bar response

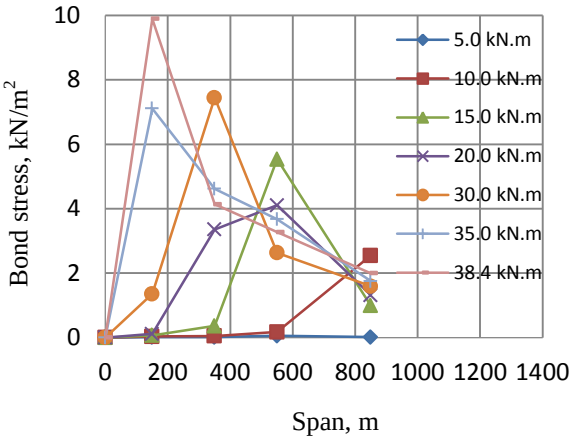

(e) Bond stress profile at various load levels

Figure B.11 Specimen SC12.7-1.5-850 flexural test results

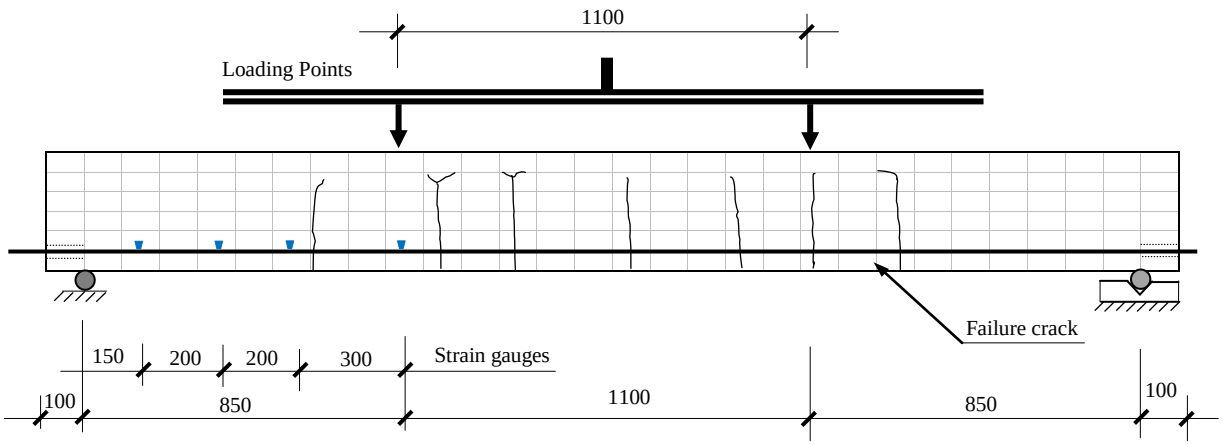

(a) Cracks pattern at failure, with average spacing of 250mm, , f_{frp} at failure was 1142.8 MPa

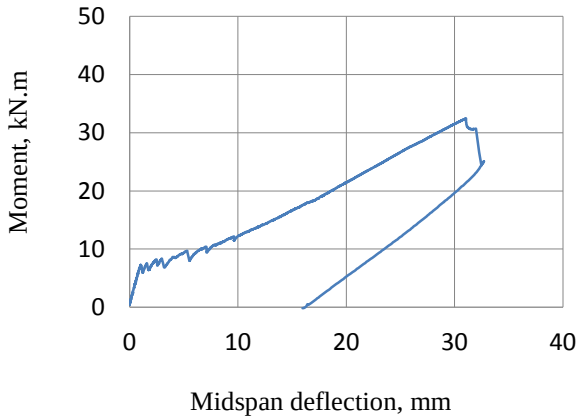

(b) Moment versus midspan deflection responses

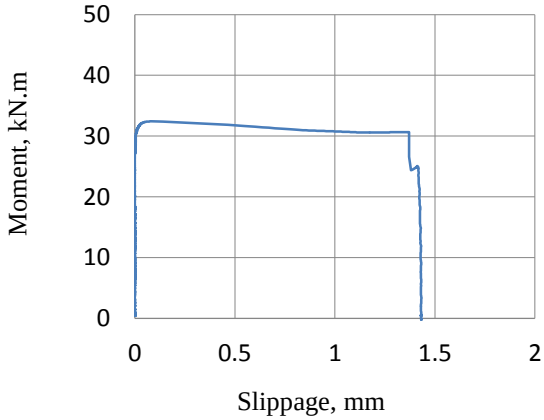

(c) End slip response

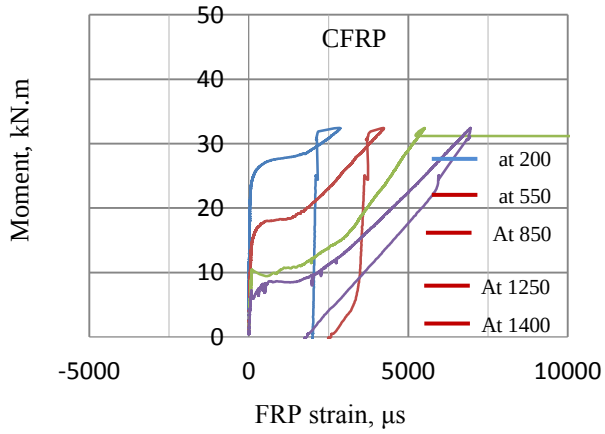

(d) Strain in the CFRP bar response

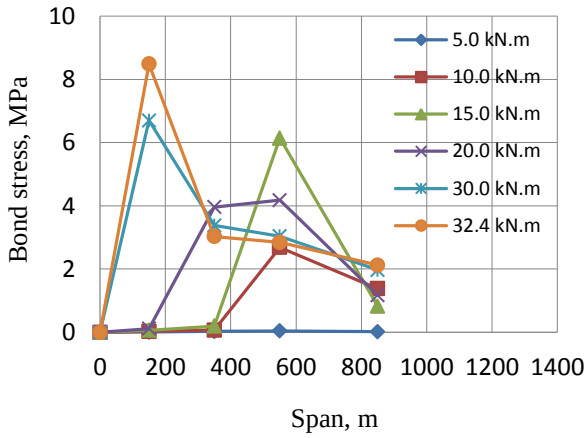

(e) Bond stress profile at various load levels

Figure B.12 Specimen SC12.7-2.0-850 flexural test results

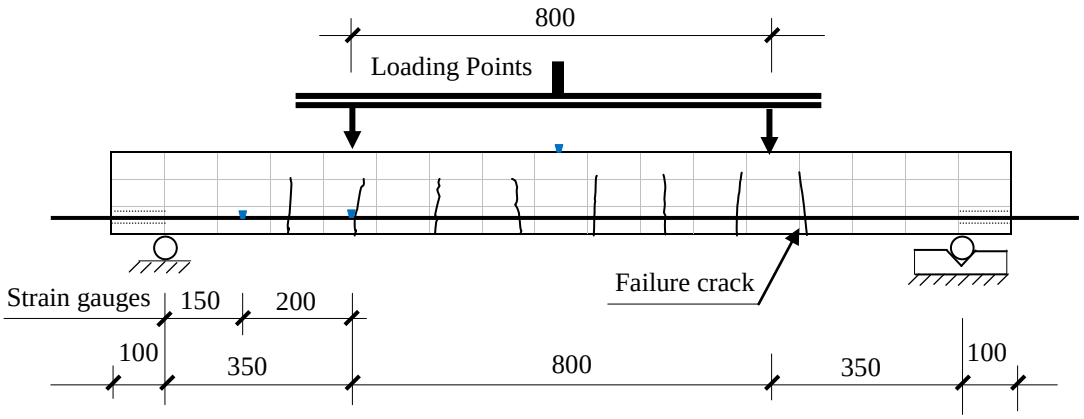

(a) Cracks pattern at failure, average crack spacing was 120mm, tensile stress in the CFRP was 1207.5MPa

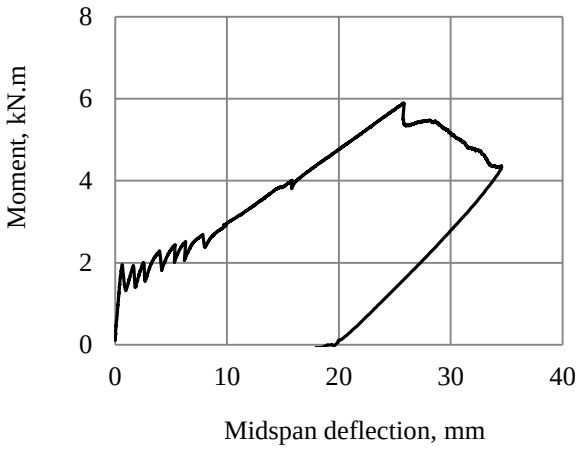

(b) Moment versus midspan deflection responses

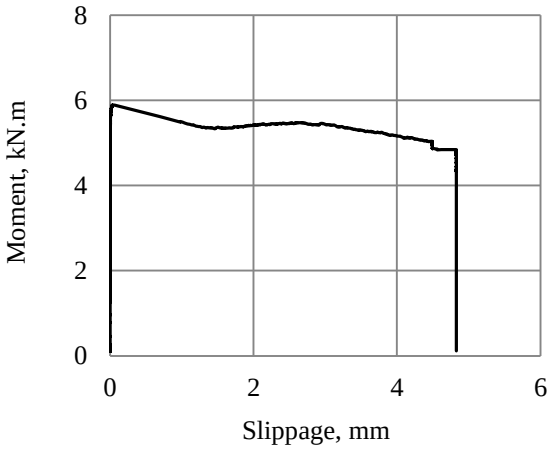

(c) End slip response

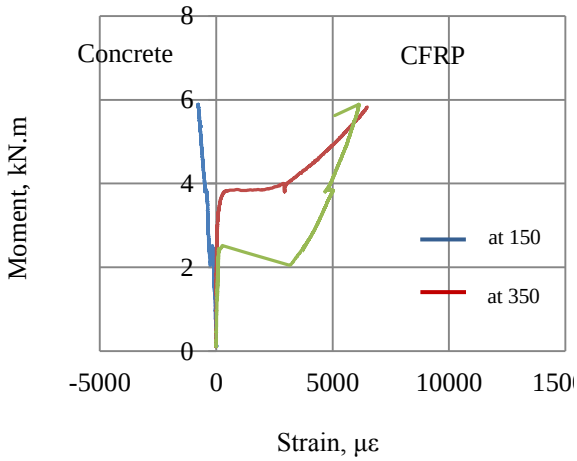

(d) Strain in the CFRP bar and concrete response at various load levels

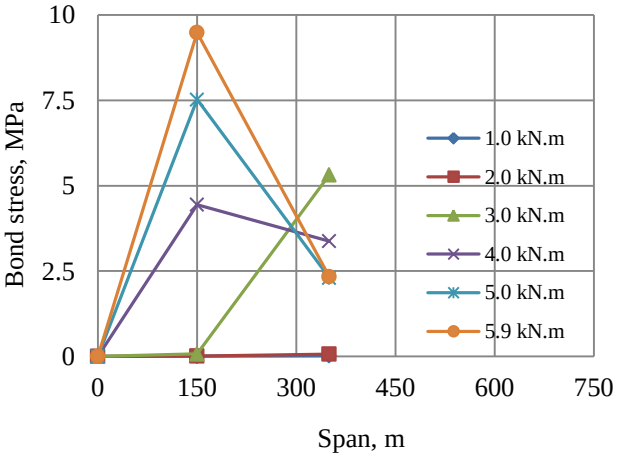

(e) Bond stress profile at various load levels

Figure B.13 Specimen NC6.3-3.0-350 flexural test results

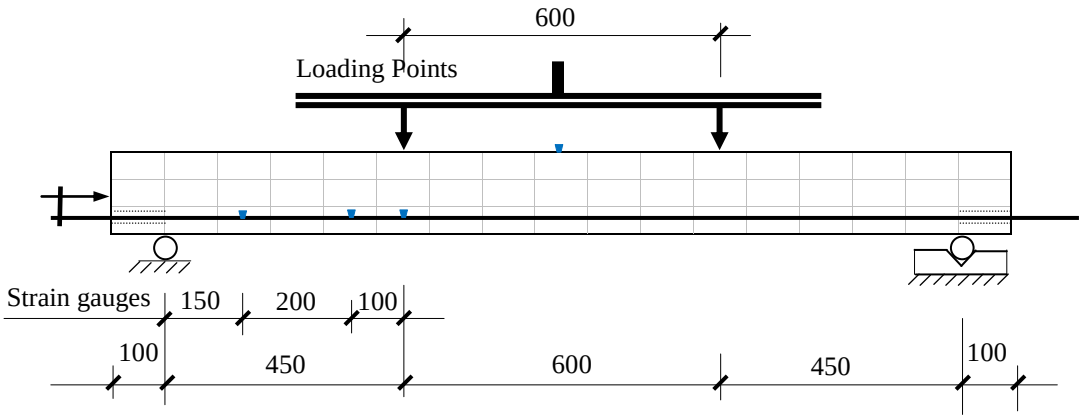

(a) Cracks pattern at failure, average spacing of 125mm, tensile stress in the CFRP bar at failure was 1556.8MPa

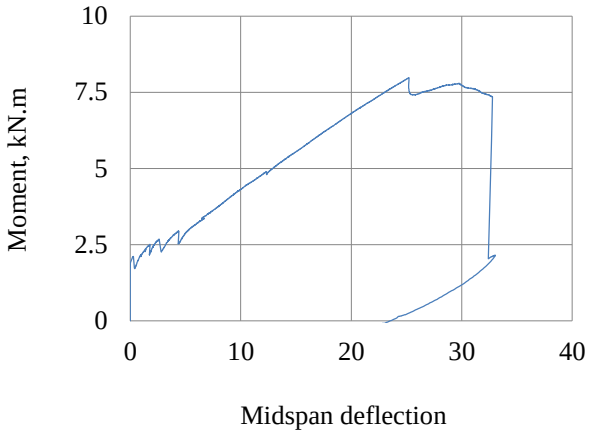

(b) Moment versus midspan deflection responses

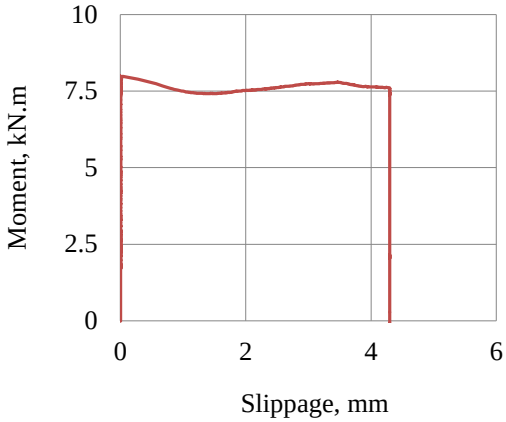

(c) End slip response

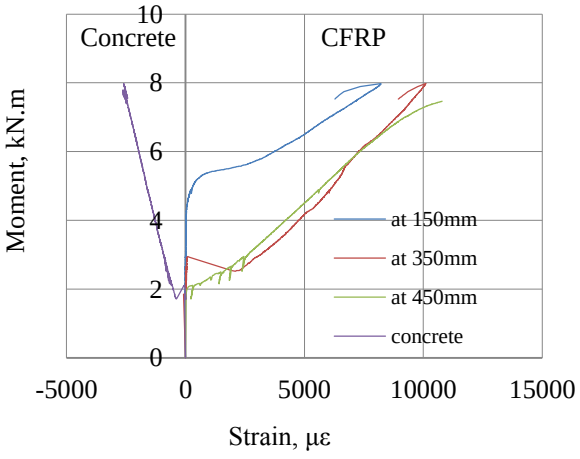

(d) Strain in the CFRP bar and concrete responses

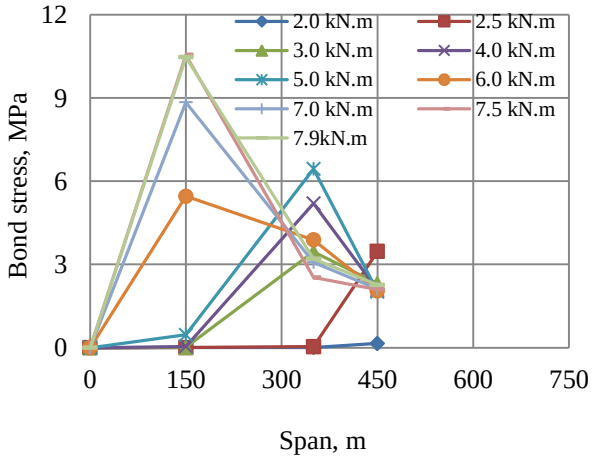

(e) Bond stress profile at various load levels

Figure B.14 Specimen NC6.3-3.0-450 flexural test results

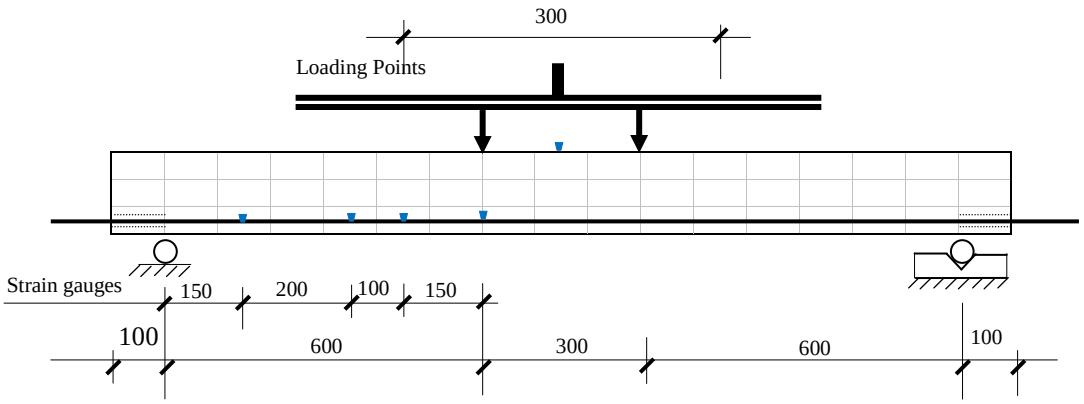

(a) Cracks pattern at failure, tensile stress in the CFRP bar at failure was 1822.0MPa

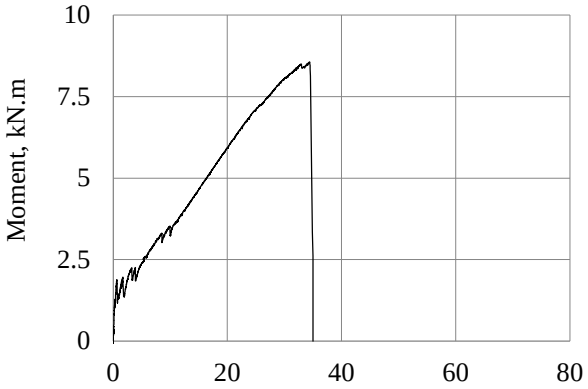

(b) Moment versus midspan deflection responses

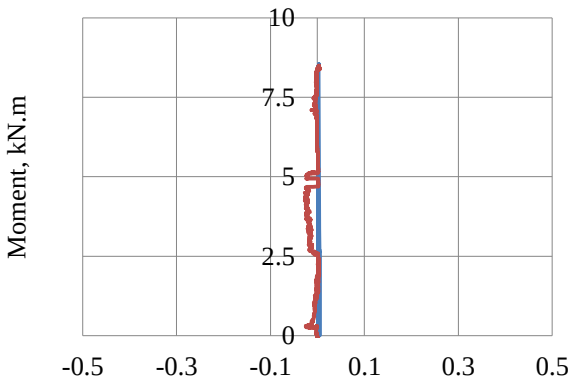

(c) End slip response

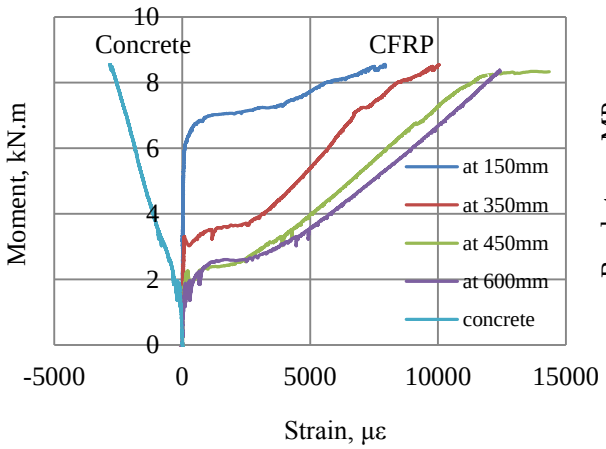

(d) Strain in the CFRP bar and concrete response

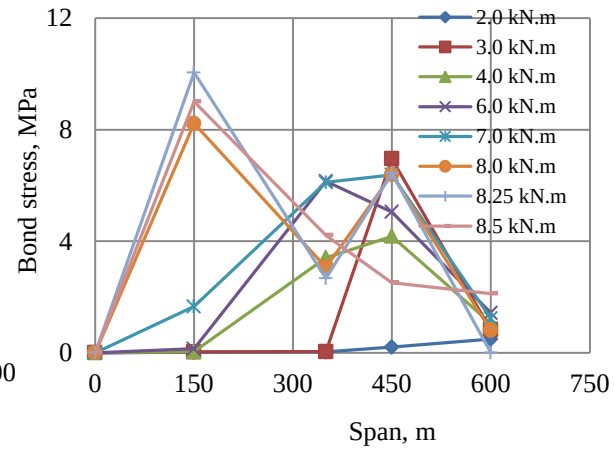

(e) Bond stress profile at various load levels

Figure B.15 Specimen NC6.3-3.0-600 flexural test results

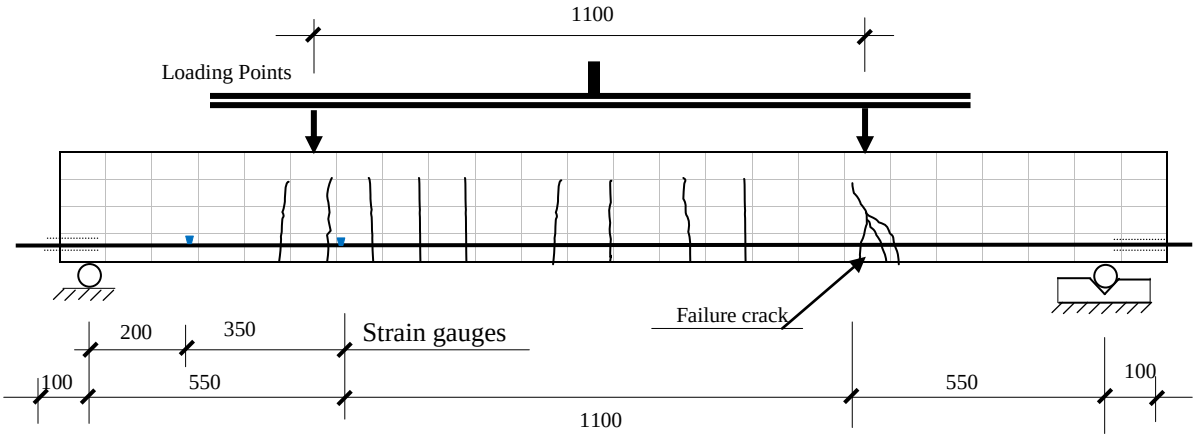

(a) Cracks pattern at failure, average spacing was 130mm, tensile stress in the CFRP bar at failure was 1112.1MPa

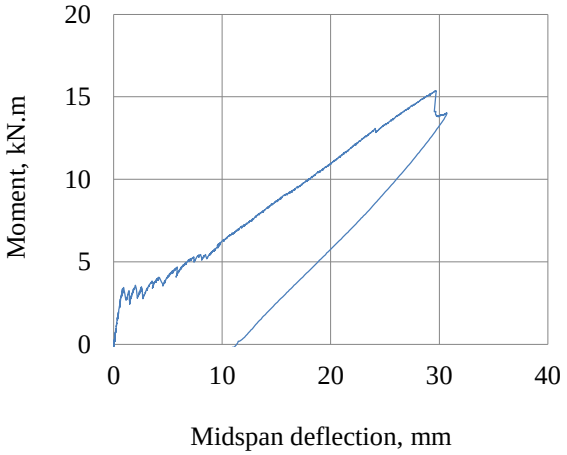

(b) Moment versus midspan deflection responses

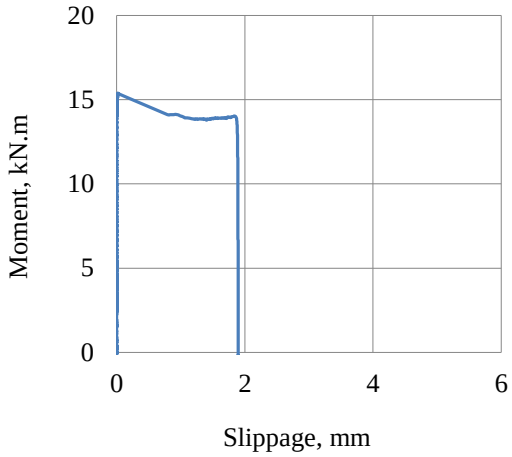

(c) End slip response

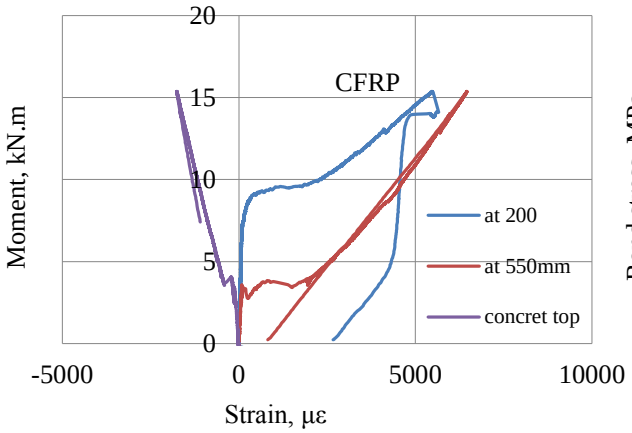

(d) Strain in the CFRP bar and concrete response

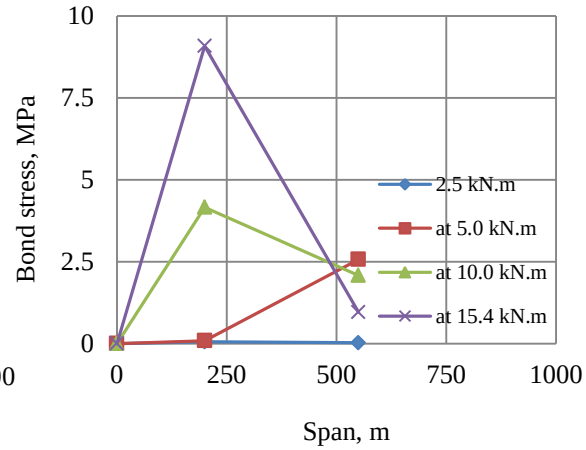

(e) Bond stress profile at various load levels

Figure B.16 Specimen NC9.5-3.0-550 flexural test results

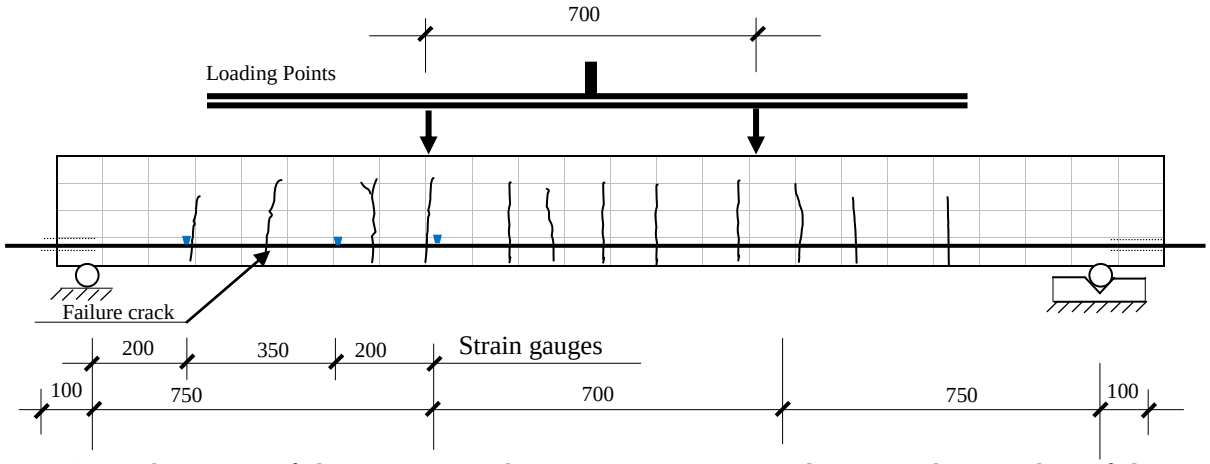

(a) Cracks pattern at failure, average crack spacing was 155mm, tensile stress in the CFRP bar at failure was 1593.6MPa

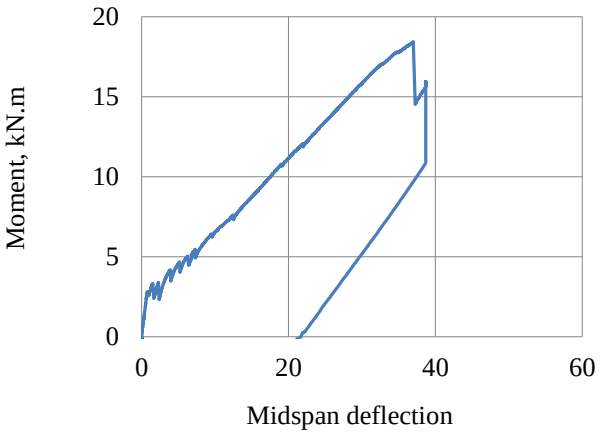

(b) Moment versus midspan deflection responses

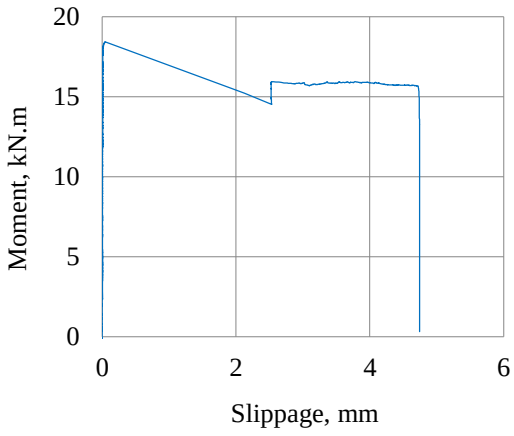

(c) End slip response

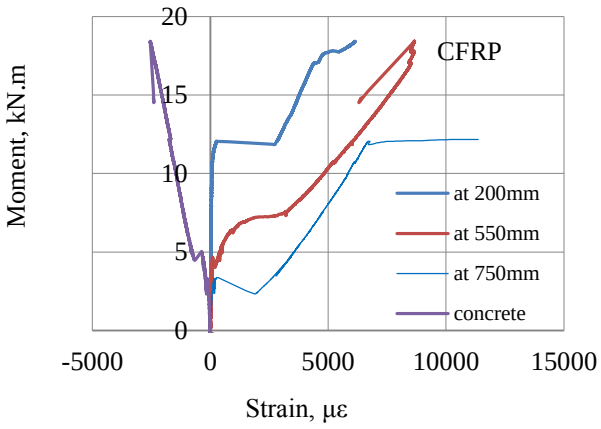

(d) Strain in the CFRP bar and concrete response

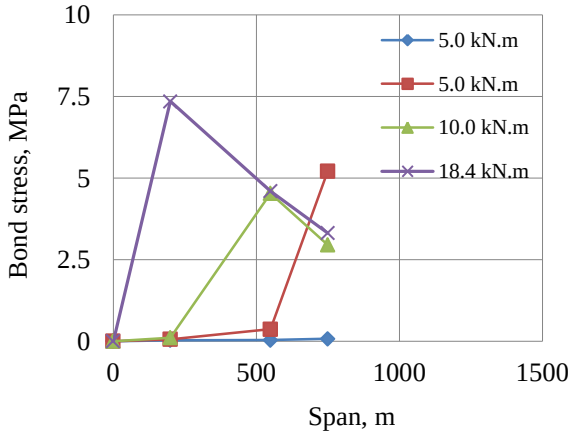

(e) Bond stress at various load levels

Figure B.17 Specimen NC9.5-3.0-750 flexural test results

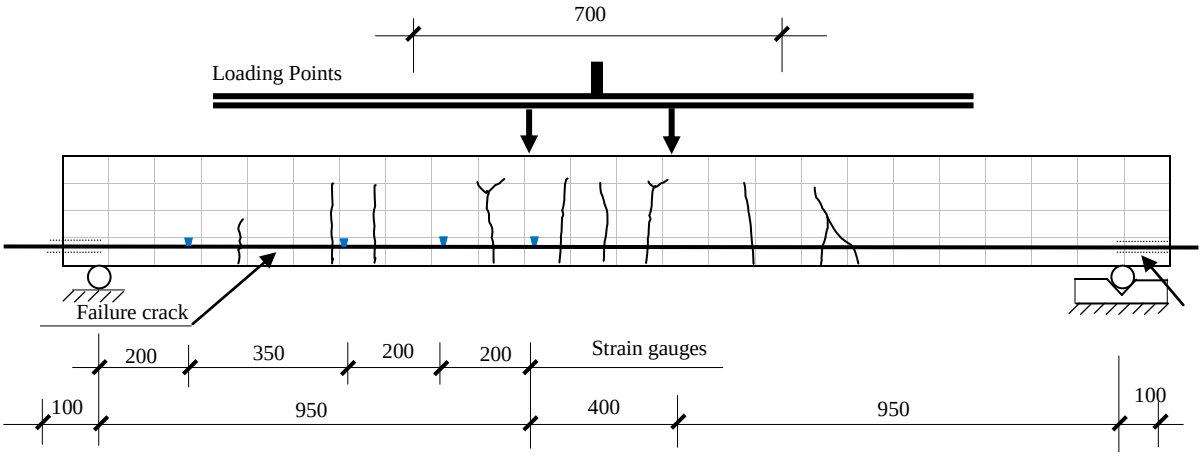

(a) Cracks pattern at failure, average spacing of 175mm, tensile stress in the CFRP bar at failure was 1900.8MPa

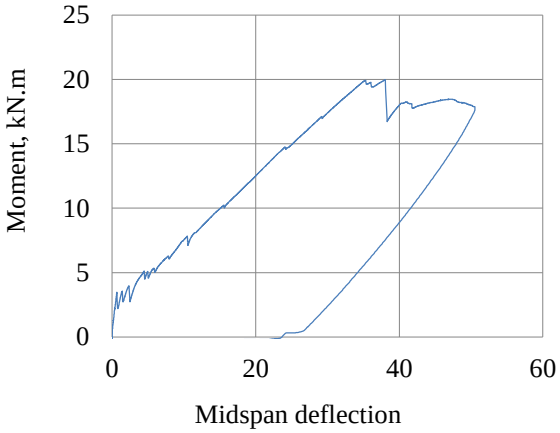

(b) Moment - midspan deflection responses

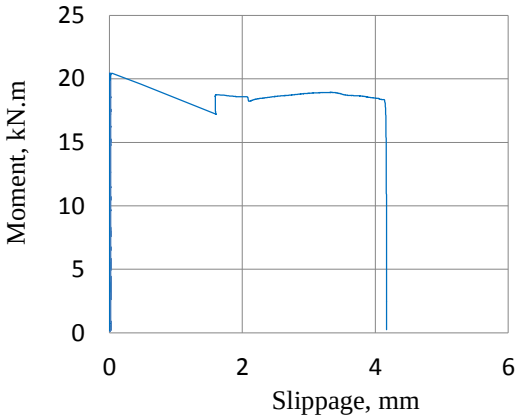

(c) End slip response

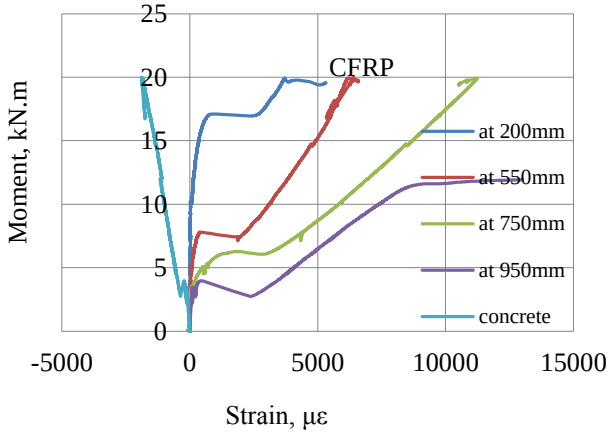

(d) Strain in the CFRP bar and concrete response

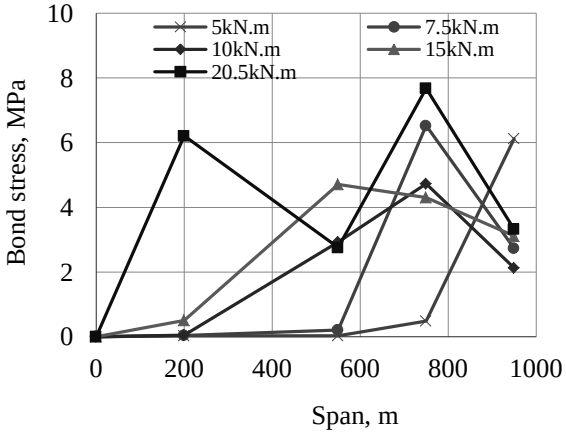

(e) Bond stress profile at various load levels

Figure B.18 Specimen NC9.5-3.0-950 flexural test results

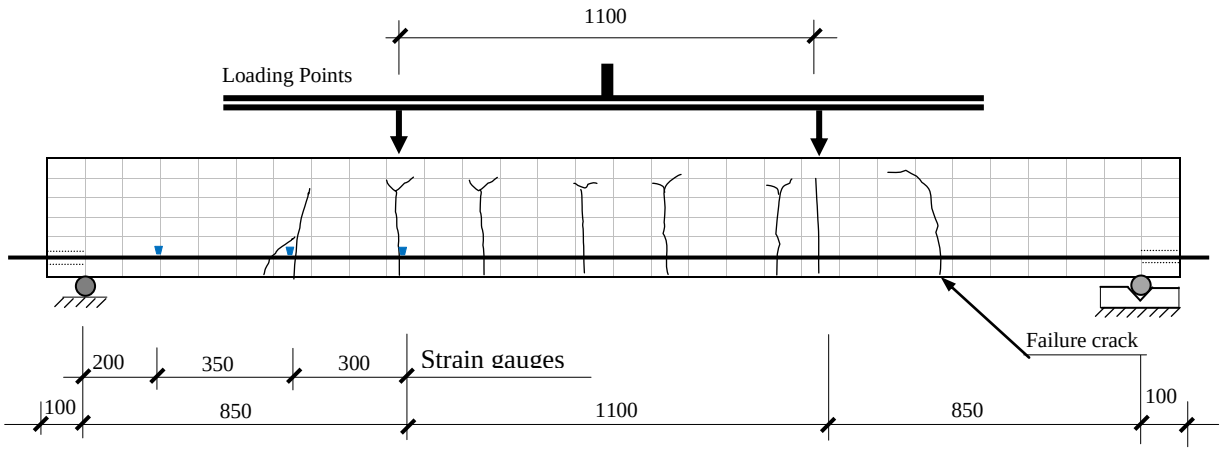

(a) Cracks pattern at failure, average spacing of 240mm, , f_{frp} at failure was 1332.3MPa

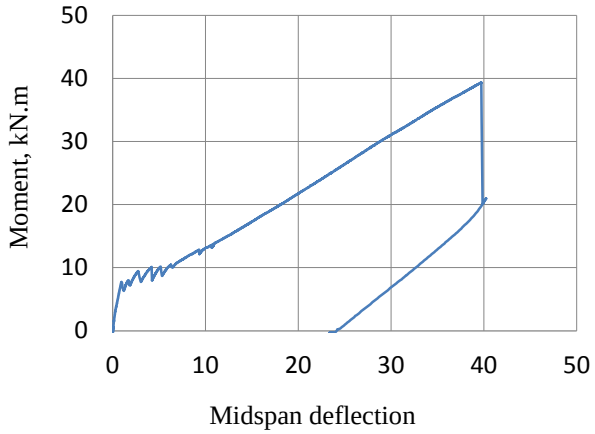

(b) Moment versus midspan deflection responses

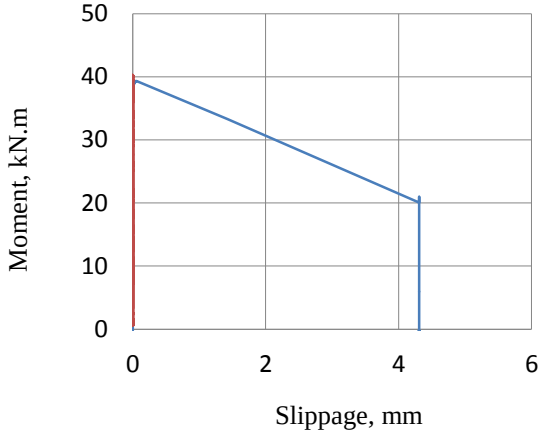

(c) End slip response

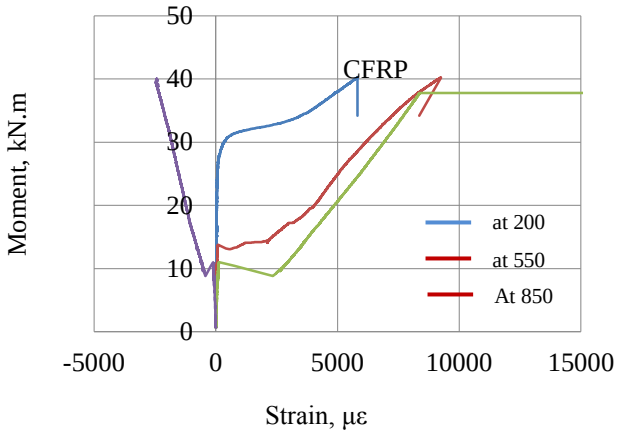

(d) Strain in the CFRP bar and concrete response

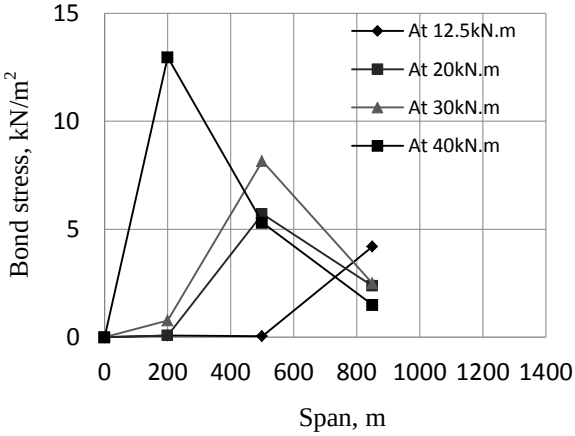

(e) Bond stress profile at various load levels

Figure B.19 Specimen NC12.7-3.0-850 flexural test results

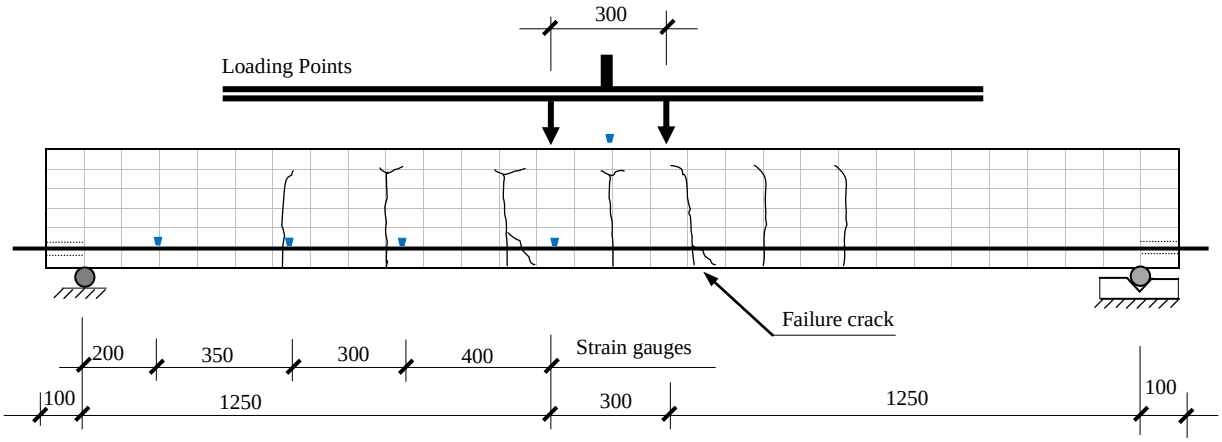

(a) Cracks pattern at failure, average spacing of 270mm, , f_{frp} at failure was 1723.9 MPa

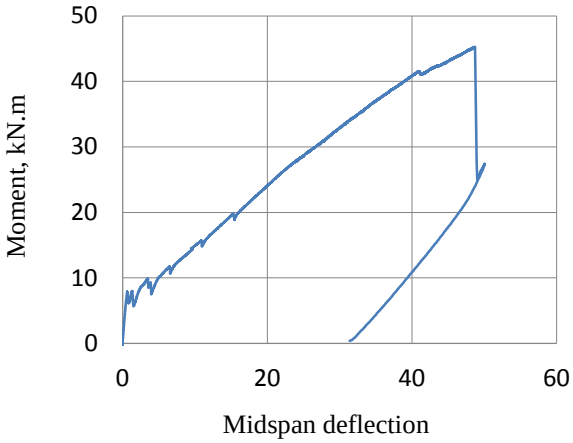

(b) Moment versus midspan deflection responses

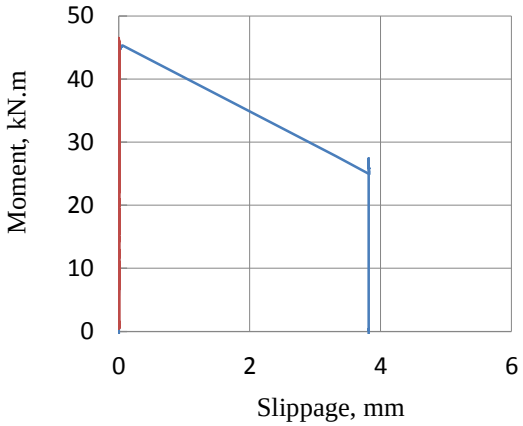

(c) End slip response

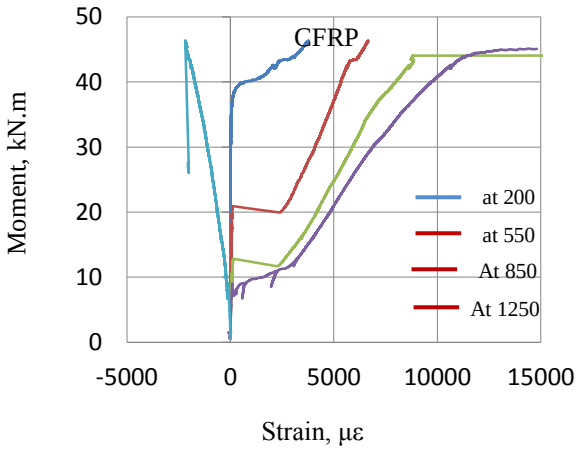

(d) Strain in the CFRP bar and concrete

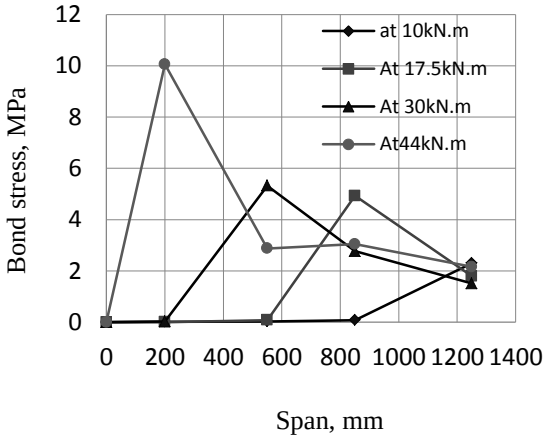

(e) Bond stress profile at various load levels

Figure B.20 Specimen NC12.7-3.0-1250 flexural test results

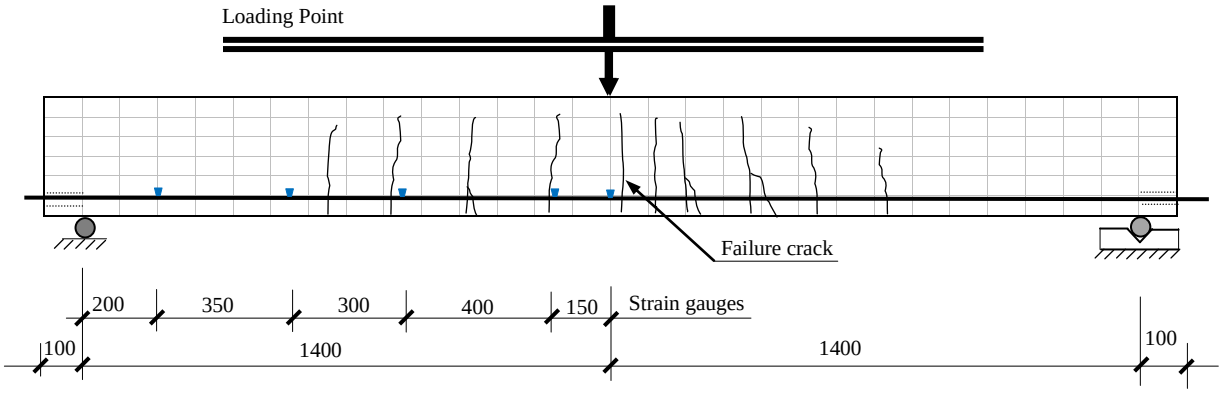

(a) Cracks pattern at failure, average spacing of 180mm, , f_{frp} at failure was 1688.4 MPa

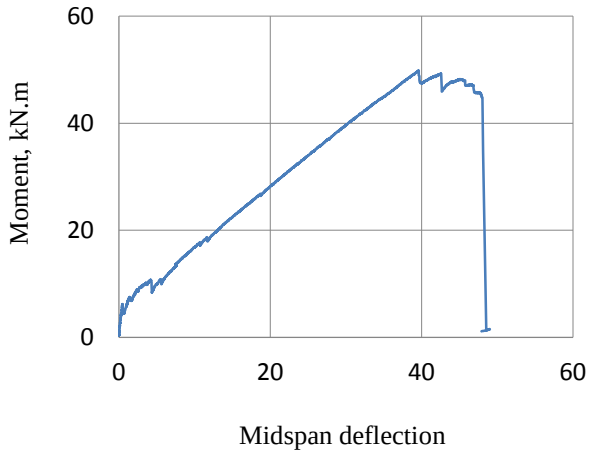

(b) Moment versus midspan deflection responses

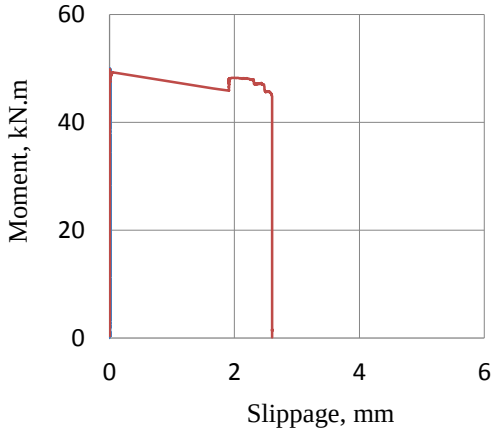

(c) End lip response

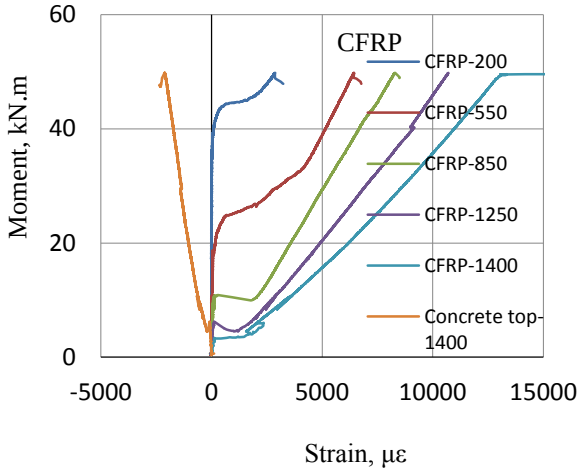

(d) Strain in the CFRP bar and concrete response

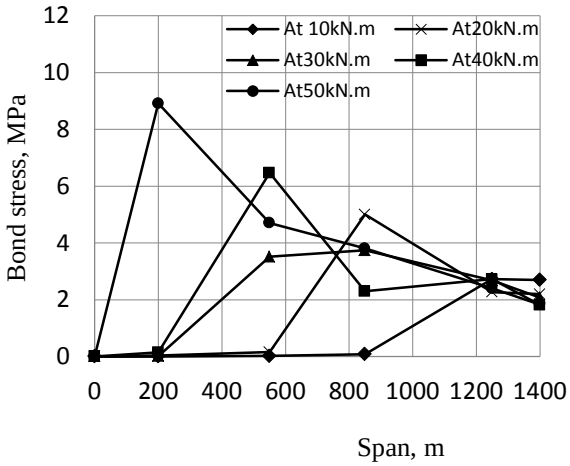

(e) Bond stress profile at various load levels

Figure B.21 Specimen NC12.7-3.0-1400 flexural test results

Appendix C - Flexural Test Results of Beams Prestressed with CFRP Bars

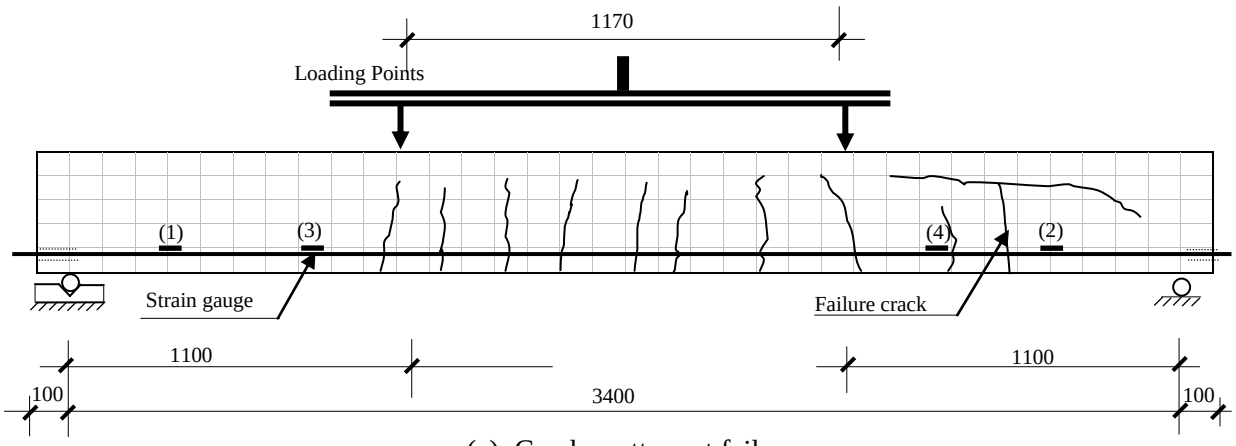

(a) Cracks pattern at failure

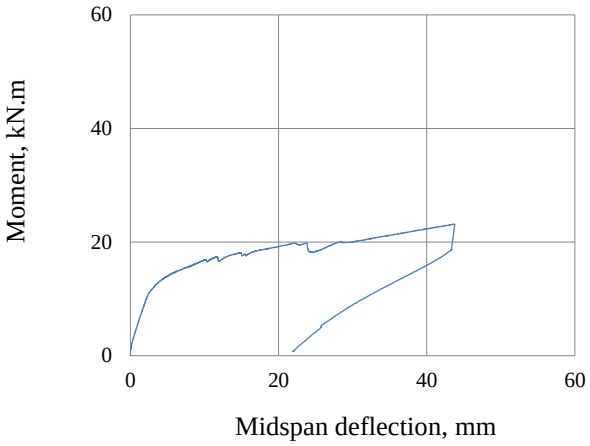

(b) Moment- deflection response

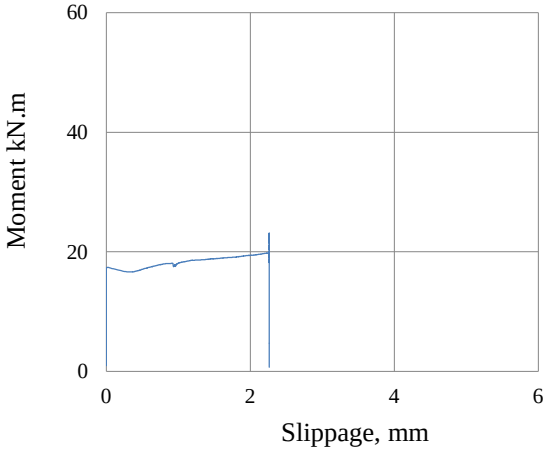

(c) End slip response

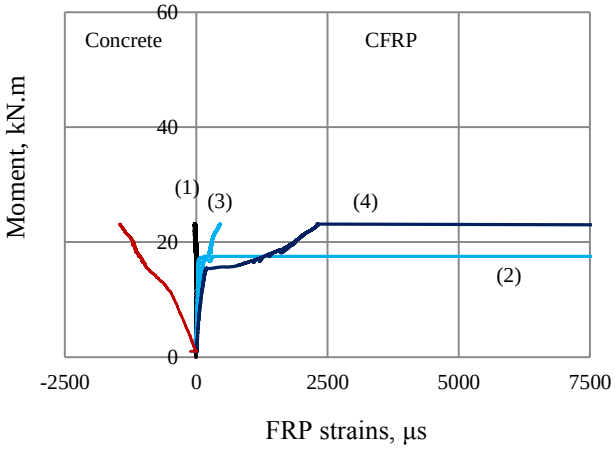

(d) Strains in CFRP bar and concrete (strain due to prestressing is not included)

Figure C.1 Flexural test results of Beam S30-1100

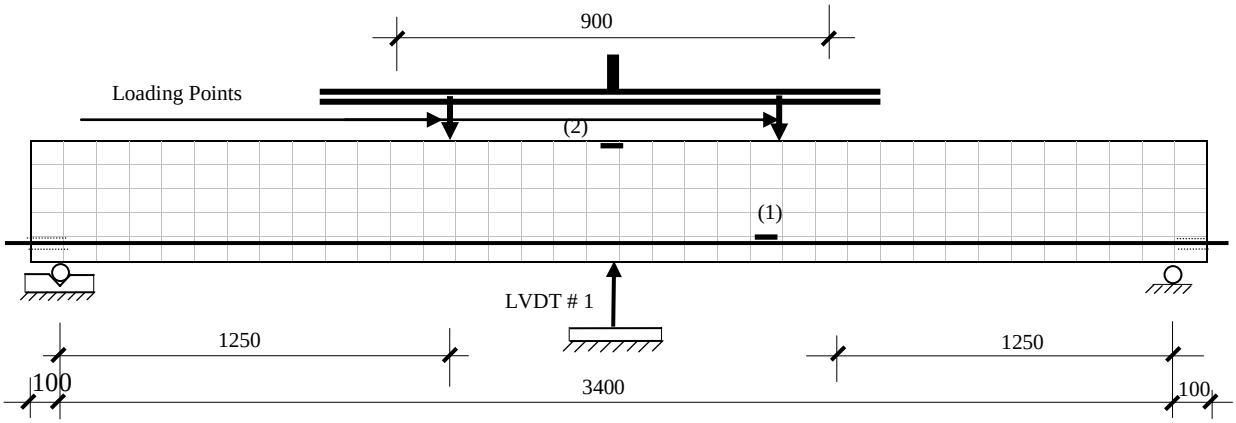

(a) Testing details

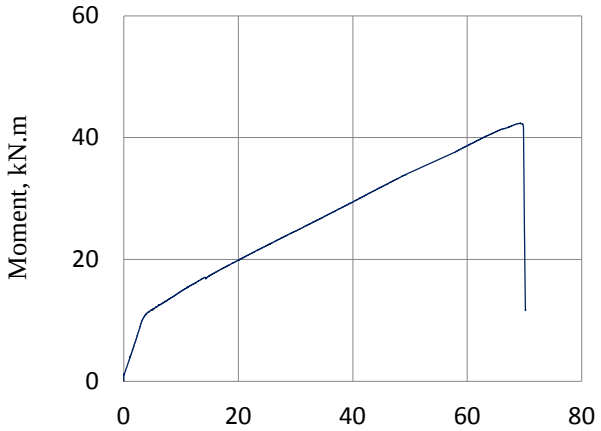

(b) Moment- midspan deflection response

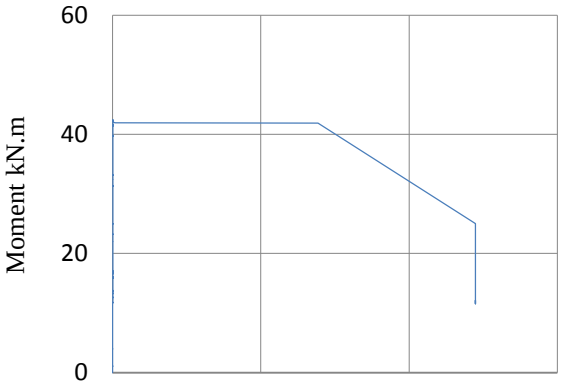

(c) End slip response

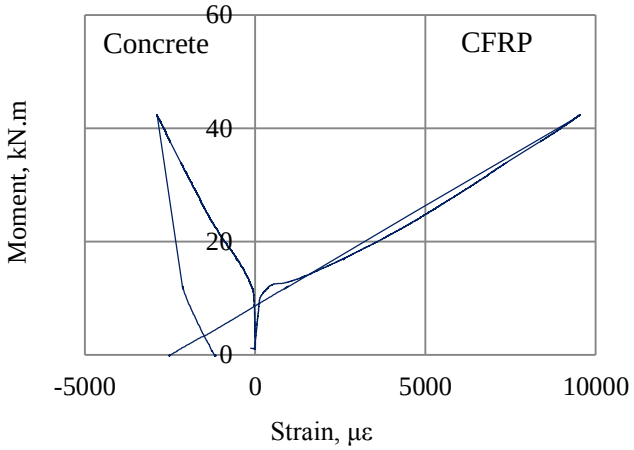

(d) Strains in CFRP bar and concrete (strain due to prestressing is not included)

Figure C.2 Flexural test results of Beam S30-1250

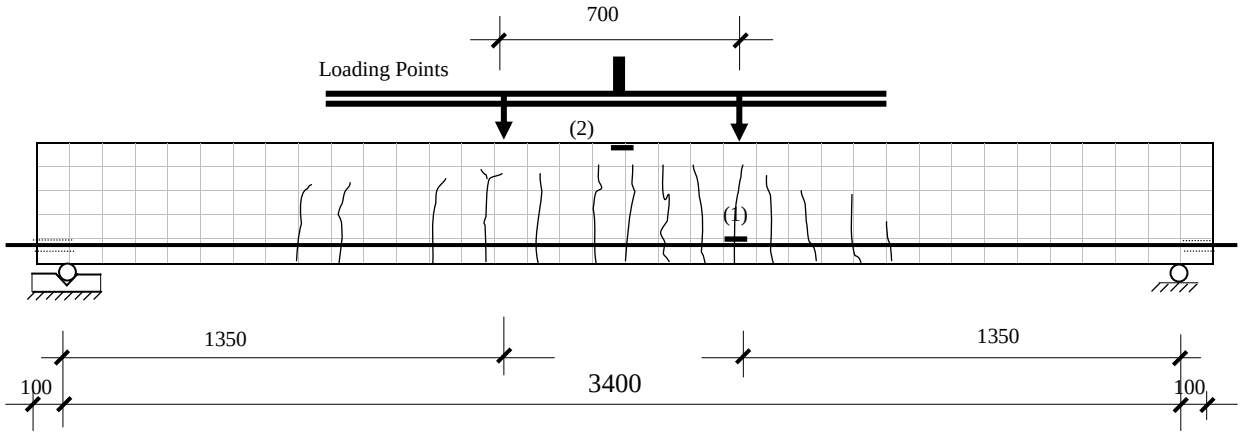

(a) Testing details, average crack spacing 166 mm, bar rupture at 1841.9MPa

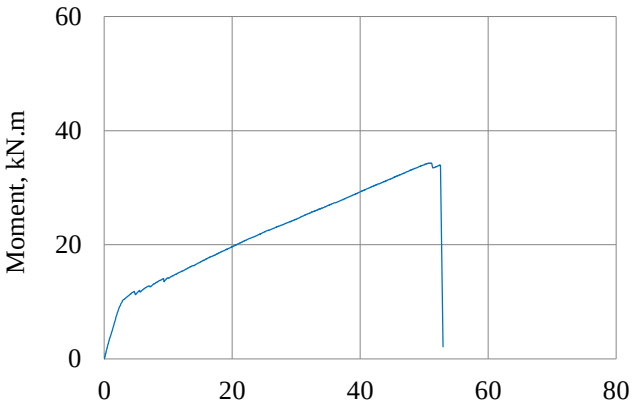

(b) Moment- midspan deflection response

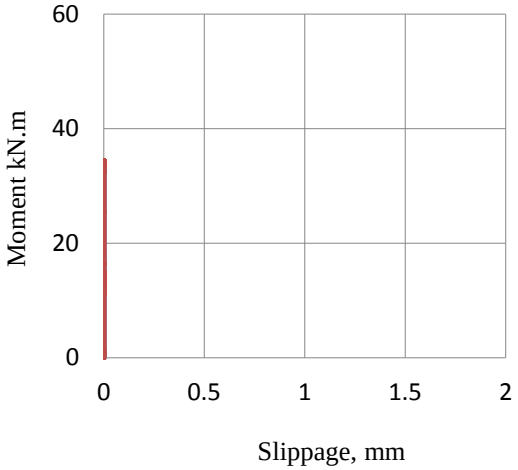

(c) End slip response

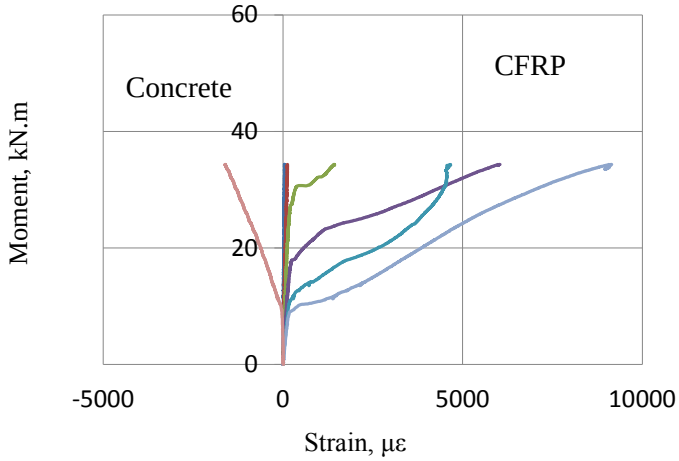

(d) Strains in CFRP bar and concrete (strain due to prestressing is not included)

Figure C.3 Flexural test results of Beam S30-1350

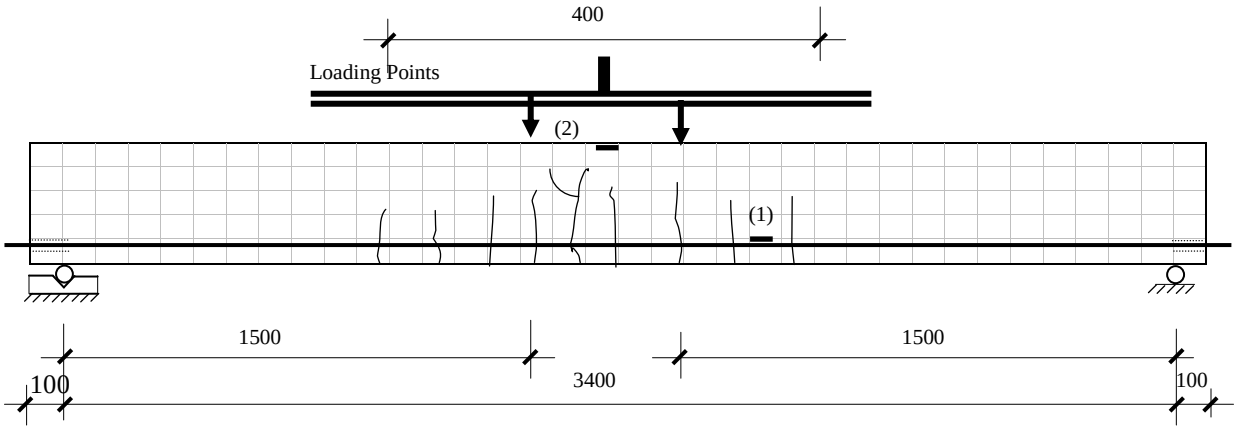

(a) Testing details, average crack spacing 170mm, bar rupture at 1189.0MPa

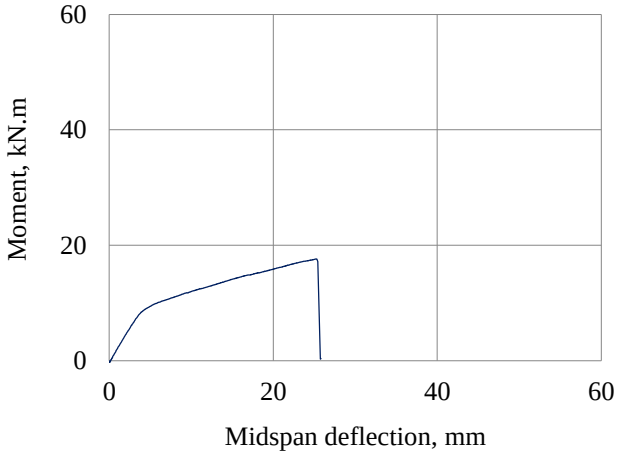

(b) Moment- midspan deflection response

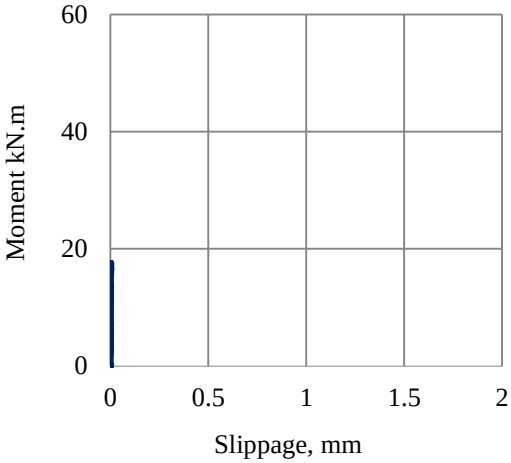

(c) End slip response

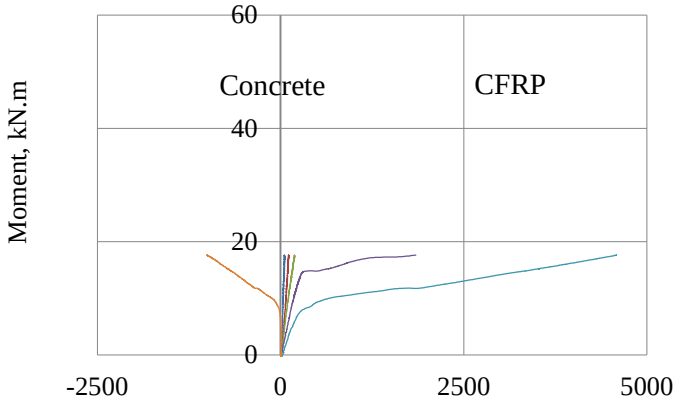

(d) Strains in CFRP bar and concrete (strain due to prestressing is not included)

Figure C.4 Flexural test results of Beam S30-1500

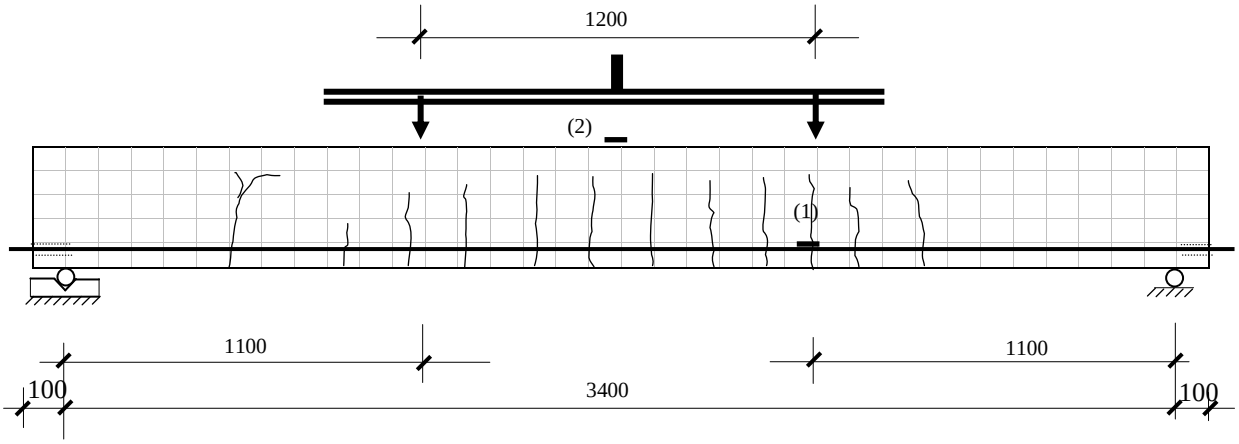

(a) Testing details, average crack spacing 170mm, bond pullout at f_{frp} of 1332.7MPa

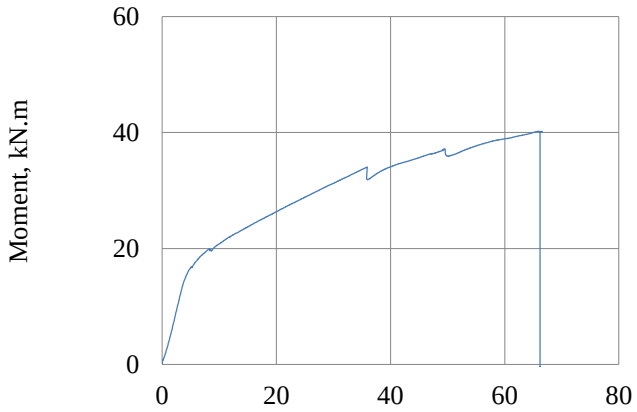

(b) Moment- midspan deflection response

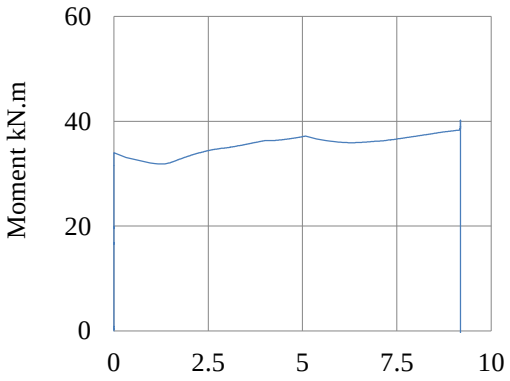

(c) End slip response

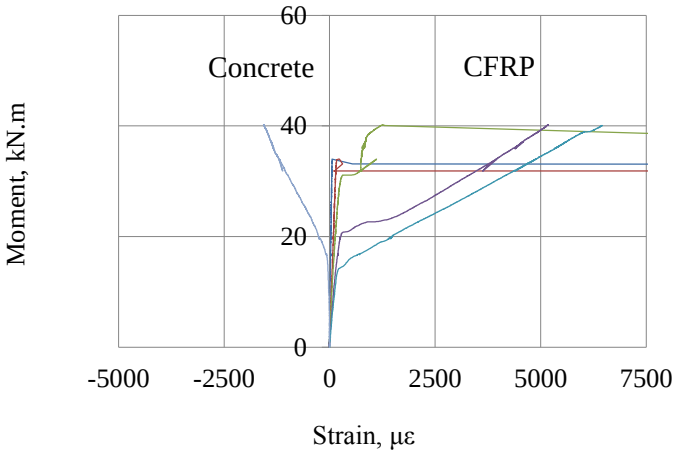

(d) Strains in CFRP bar and concrete (strain due to prestressing is not included)

Figure C.5 Flexural test results of Beam S45-1100

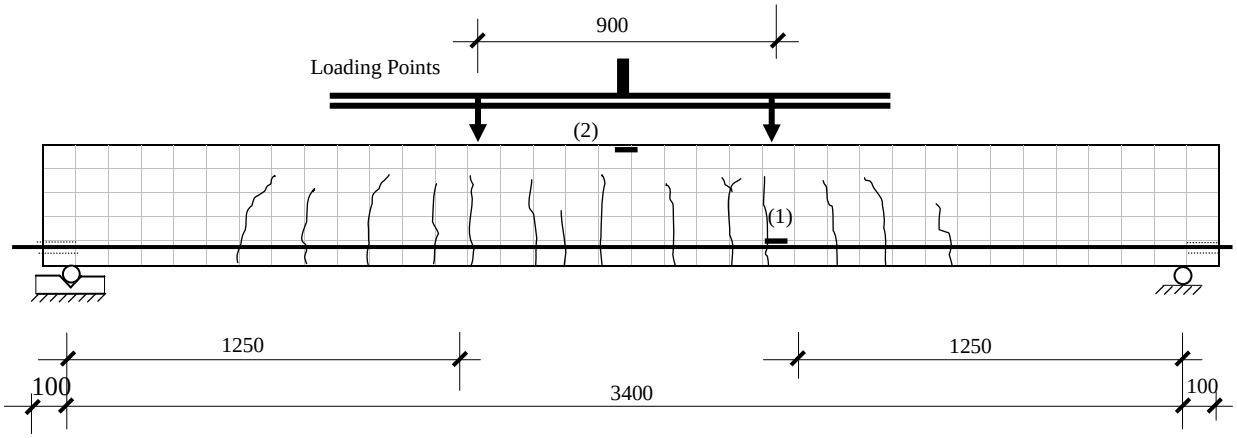

(a) Testing details, average crack spacing 150mm, bond pullout at f_{frp} of 1509.0 MPa

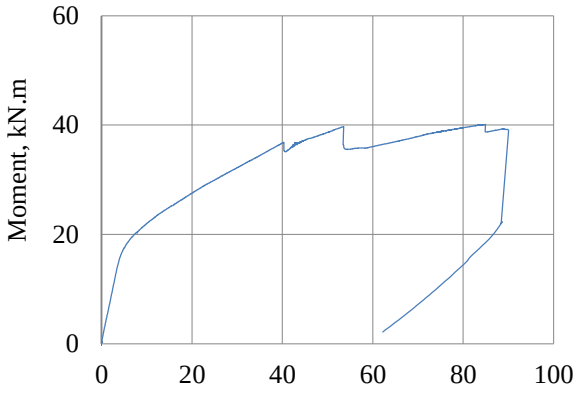

(b) Moment- midspan deflection response

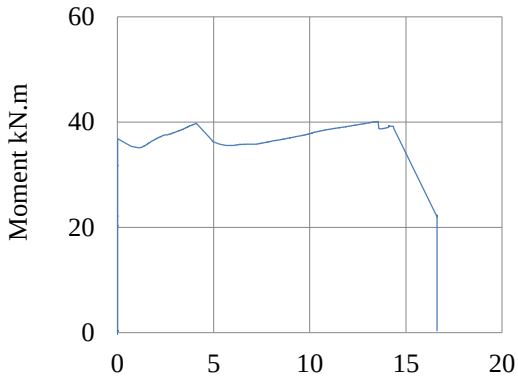

(c) End slip response

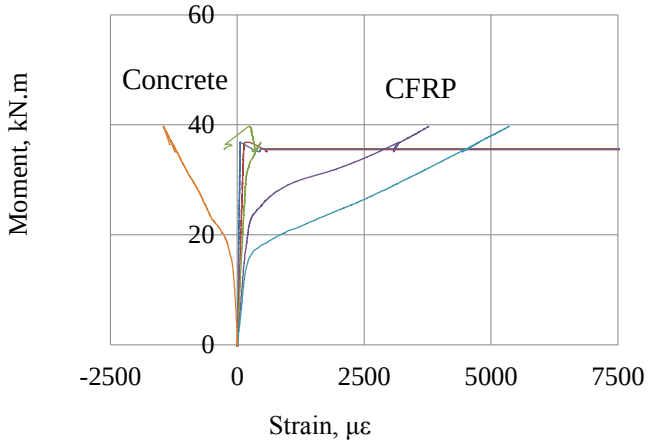

(d) Strains in CFRP bar and concrete (strain due to prestressing is not included)

Figure C.6 Flexural test results of Beam S45-1250

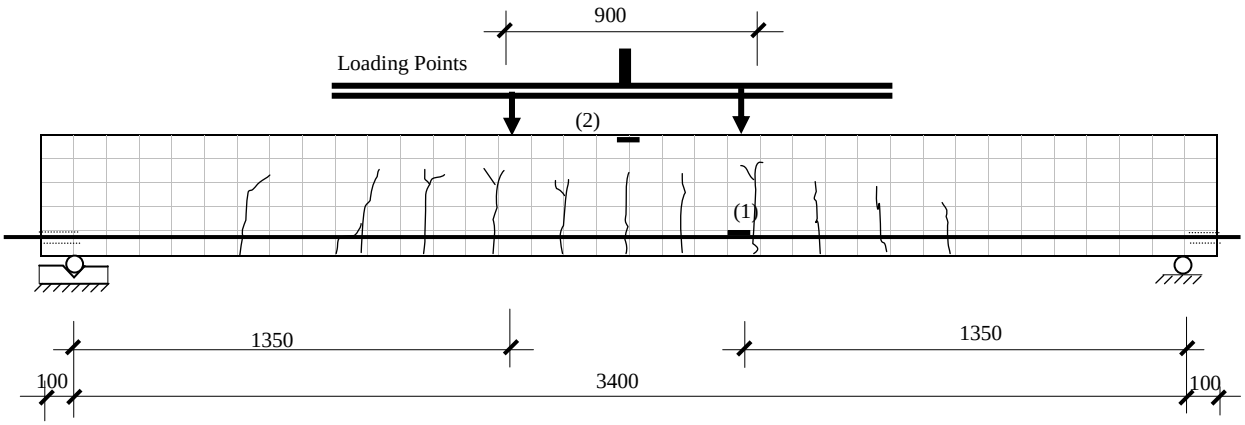

(a) Testing details, average crack spacing was 200mm, bond pullout at f_{frp} of 1412.4 MPa

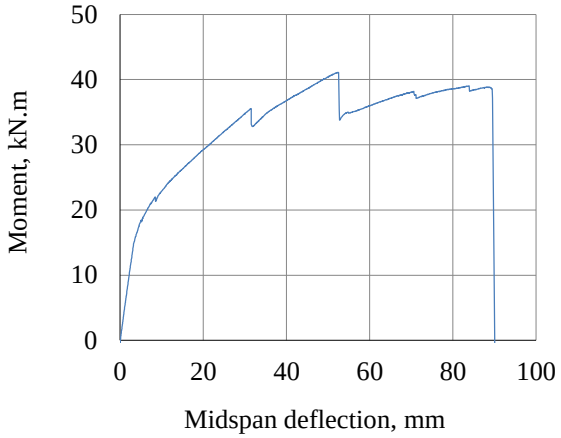

(b) Moment- midspan deflection response

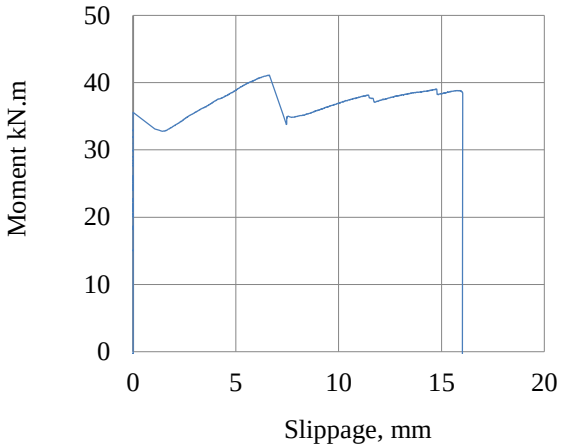

(c) End slip response

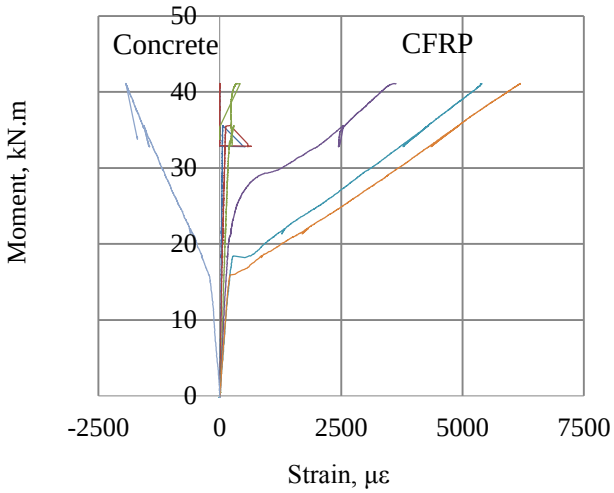

(d) Strains in CFRP bar and concrete (strain due to prestressing is not included)

Figure C.7 Flexural test results of Beam S45-1350

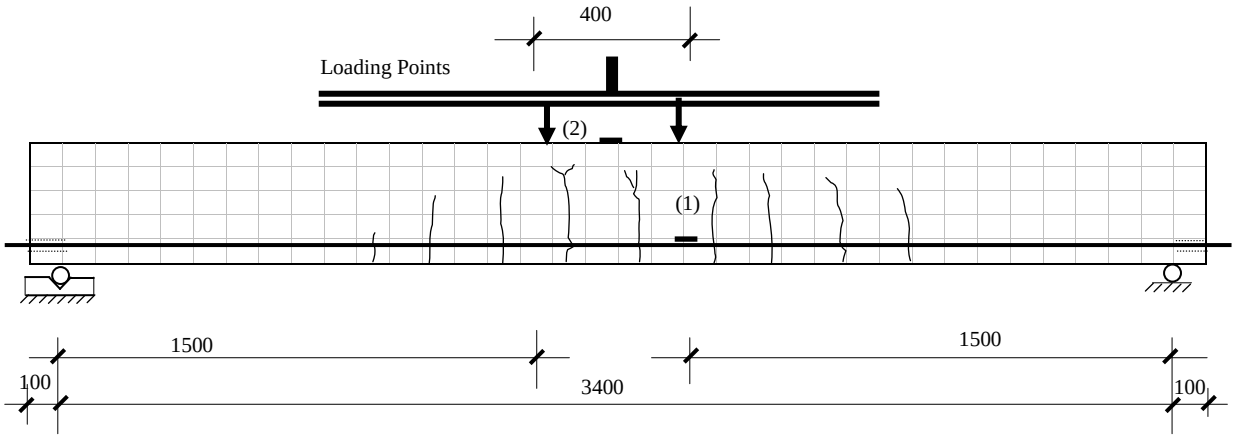

(a) Testing details, average crack spacing is 175nn, bar rupture at tensile stress of 1787.6 MPa

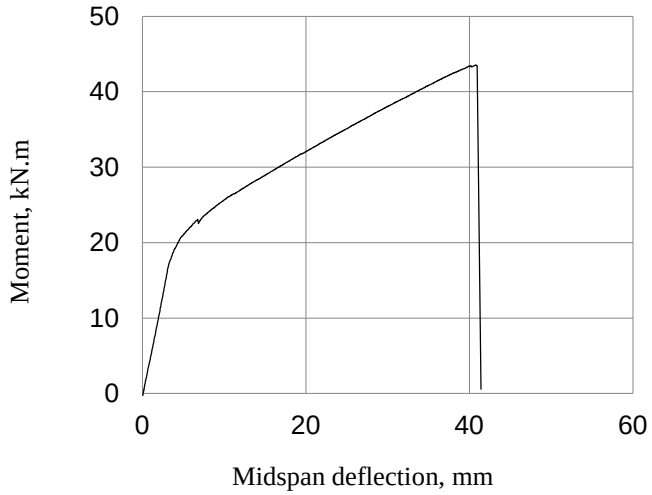

(b) Moment- midspan deflection response

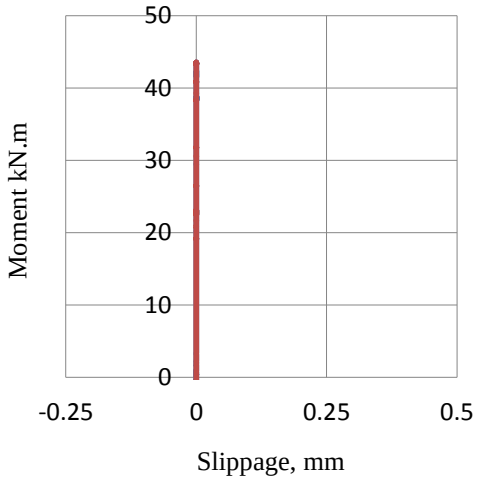

(c) End slip response

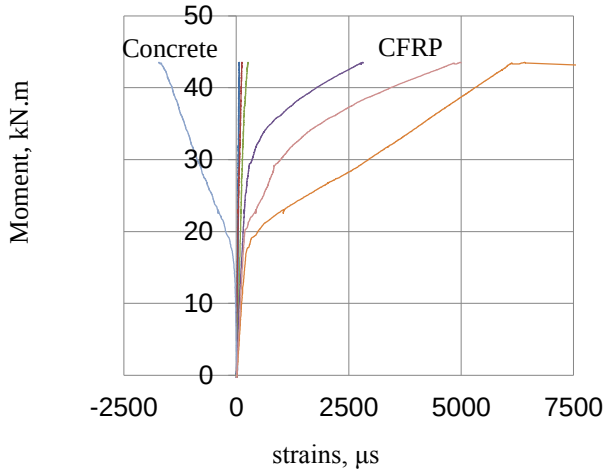

(d) Strains in CFRP bar and concrete

(strain due to prestressing is not

Figure C.8 Flexural test results of Beam S45-1500

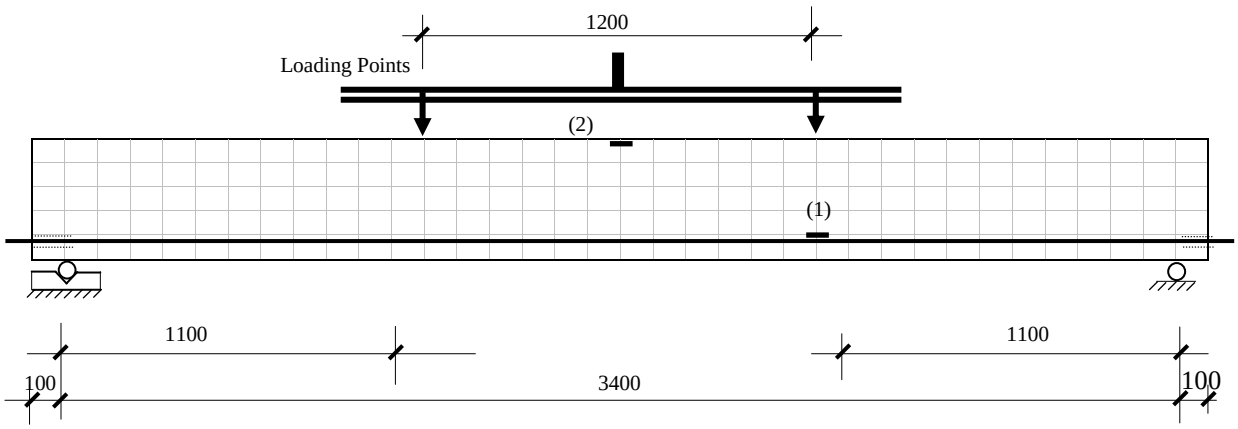

(a) Testing details

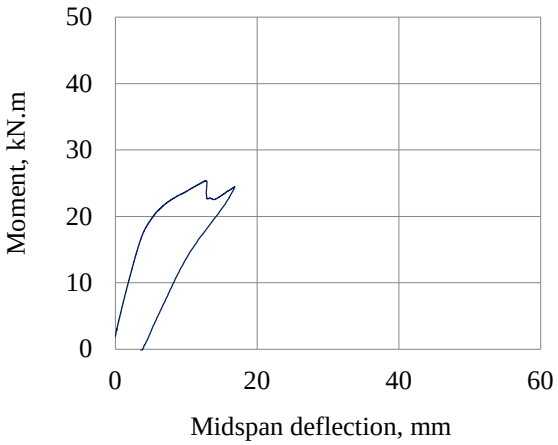

(b) Moment- midspan deflection response

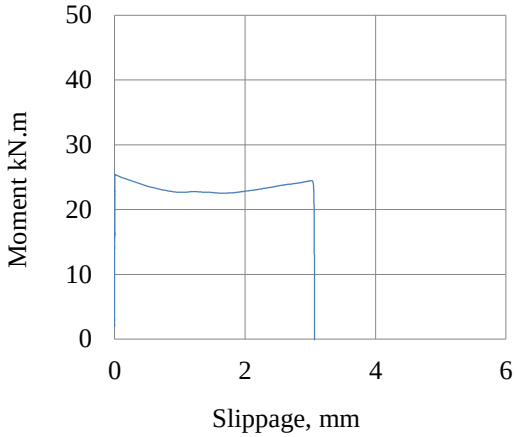

(c) End slip response

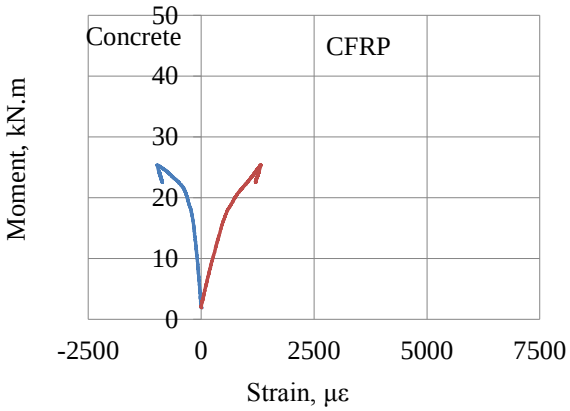

(d) Strains in CFRP bar and concrete (strain due to prestressing is not included)

Figure C.9 Flexural test results of Beam S60-1100

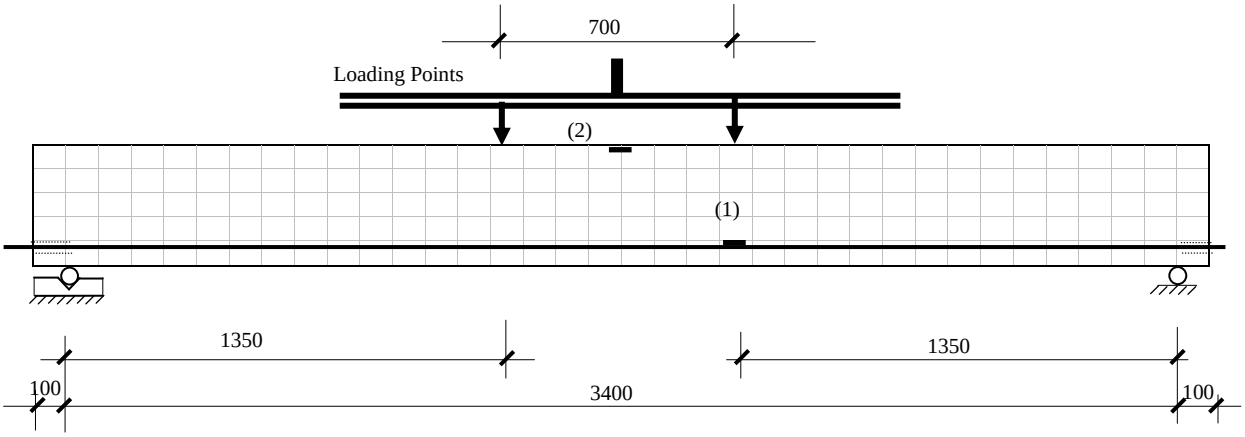

(a) Testing details

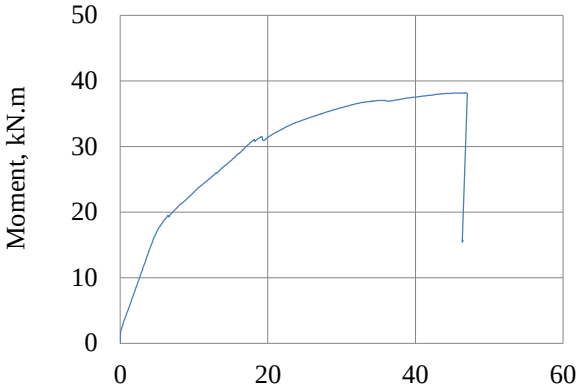

(b) Moment- midspan deflection response

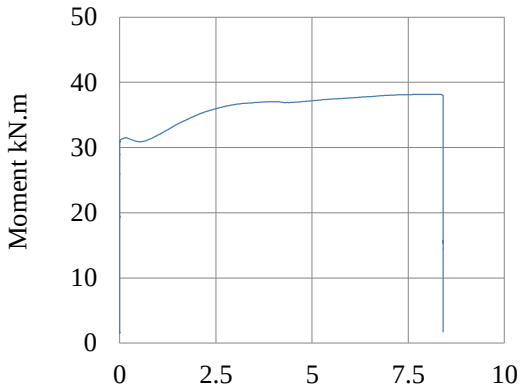

(c) End bar slip response

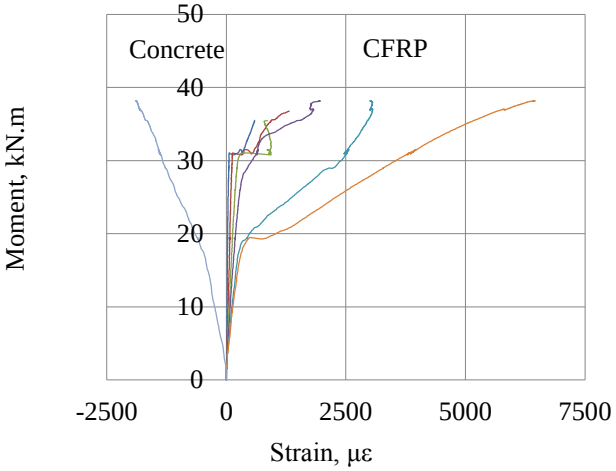

(d) Strains in CFRP bar and concrete (strain due to prestressing is not included)

Figure C.10 Flexural test results of Beam S60-1350

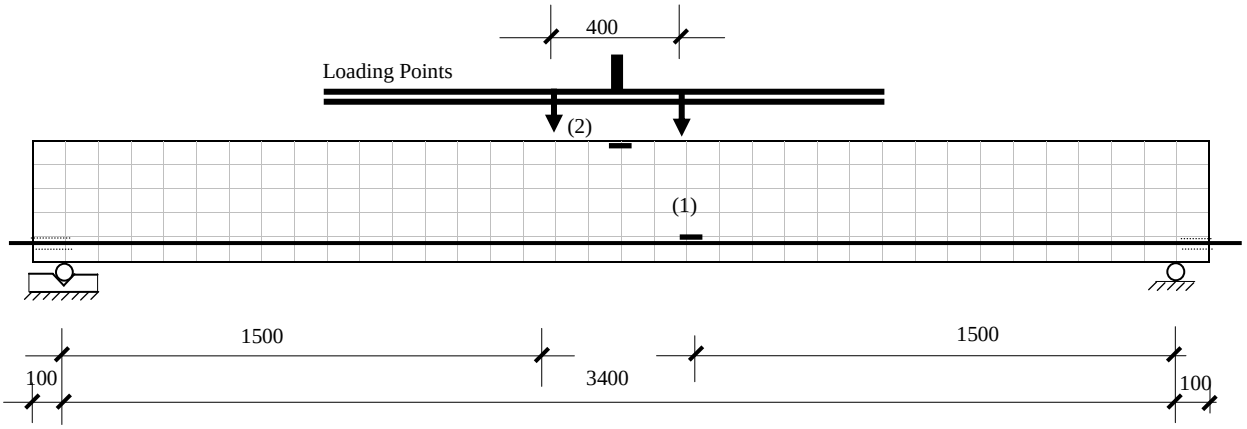

(a) Testing details

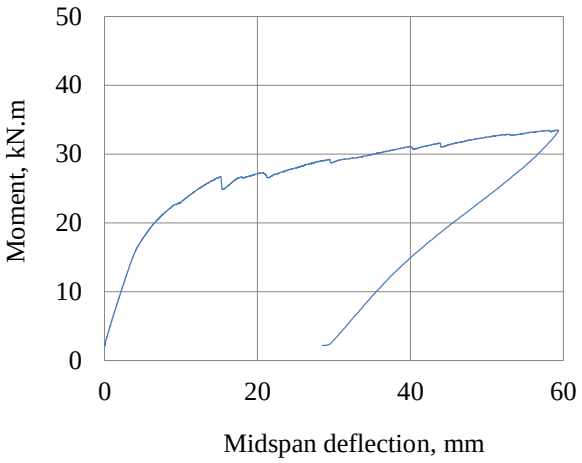

(b) Moment- midspan deflection response

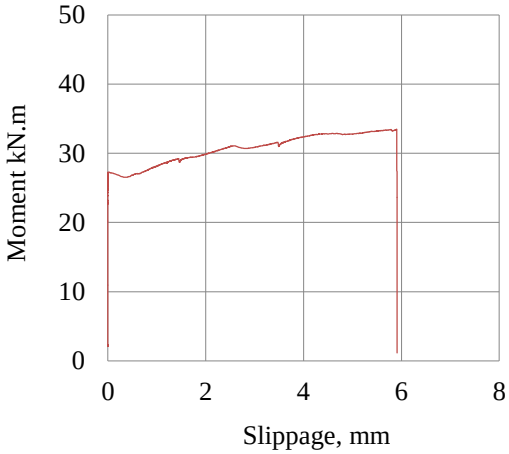

(c) End slip response

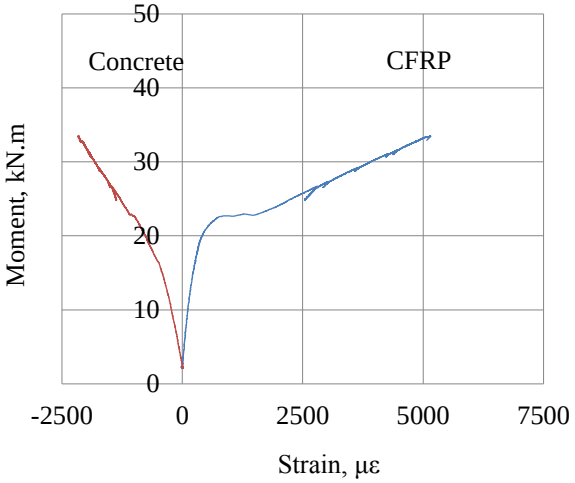

(d) Strains in CFRP bar and concrete (strain due to prestressing is not included)

Figure C.11 Flexural test results of Beam S60-1500

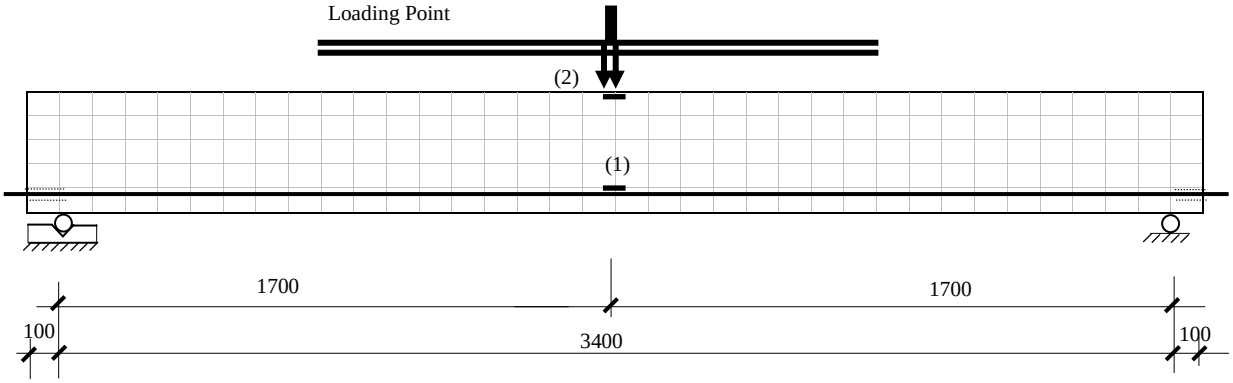

(a) Testing details, bond pullout failure f_{frp} of 1787.6MPa

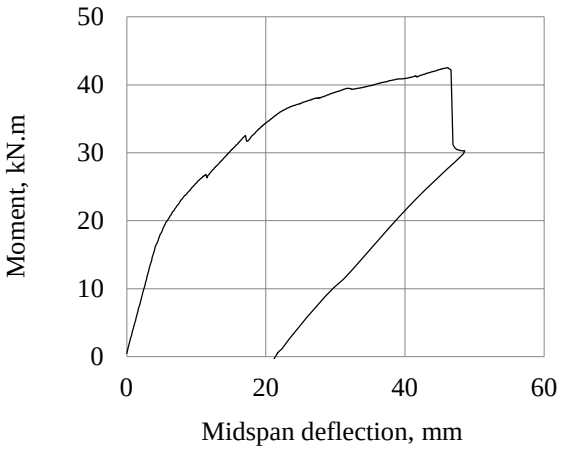

(b) Moment- midspan deflection response

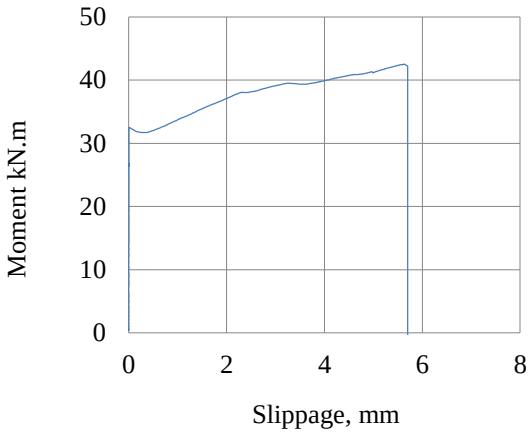

(c) End slip response

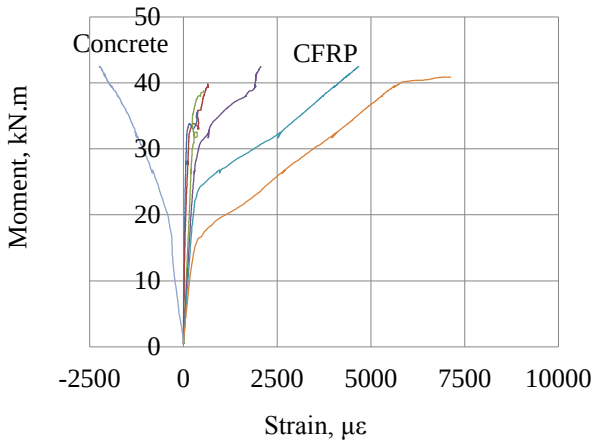

(d) Strains in CFRP bar and concrete (strain due to prestressing is not included)

Figure C.12 Flexural test results of Beam S60-1700

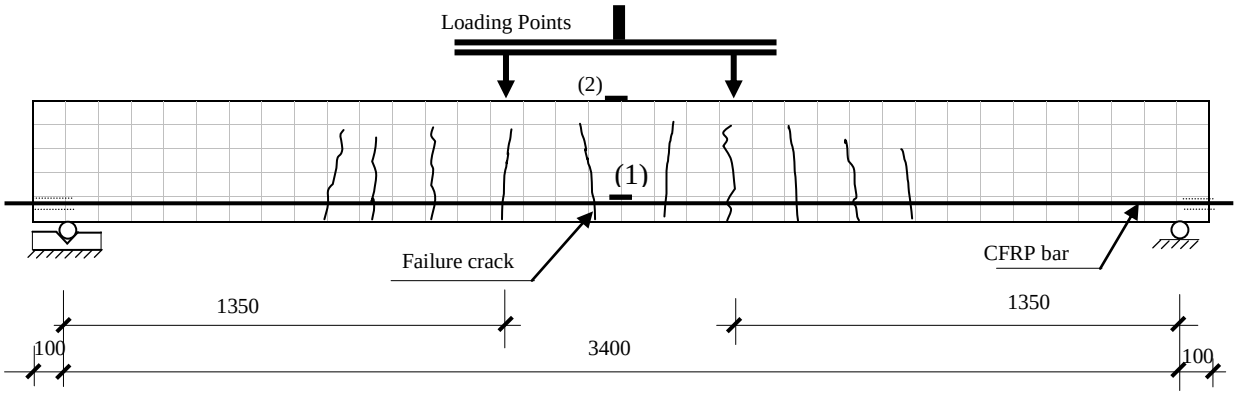

(a) Cracks pattern at failure, total number of cracks at failure is 10 with average spacing of 200mm, bar ruptured at f_{frp} of 1831.0MPa

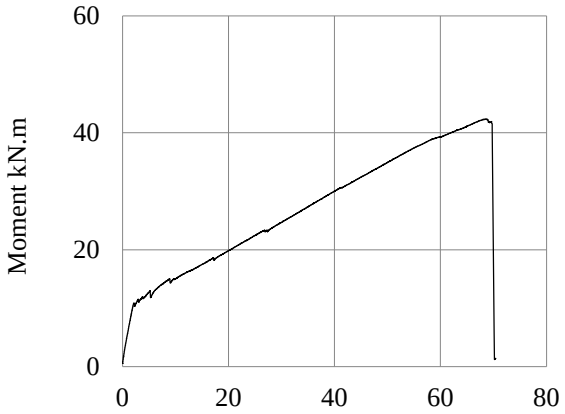

(b) Moment versus midspan deflection response

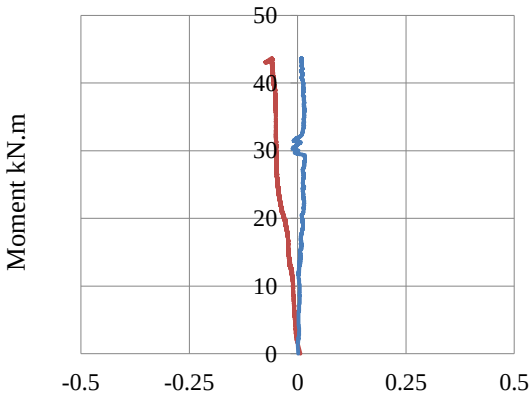

(c) End slip response

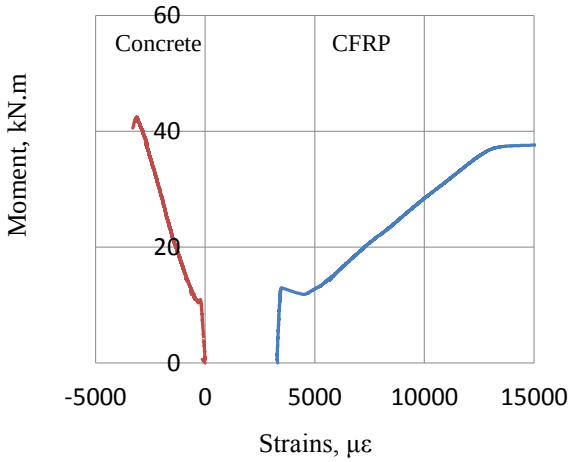

(d) Strains in CFRP bar and concrete, strain in concrete does not include pre-strain

Figure C.13 Flexural test results of beam specimen N30-1350

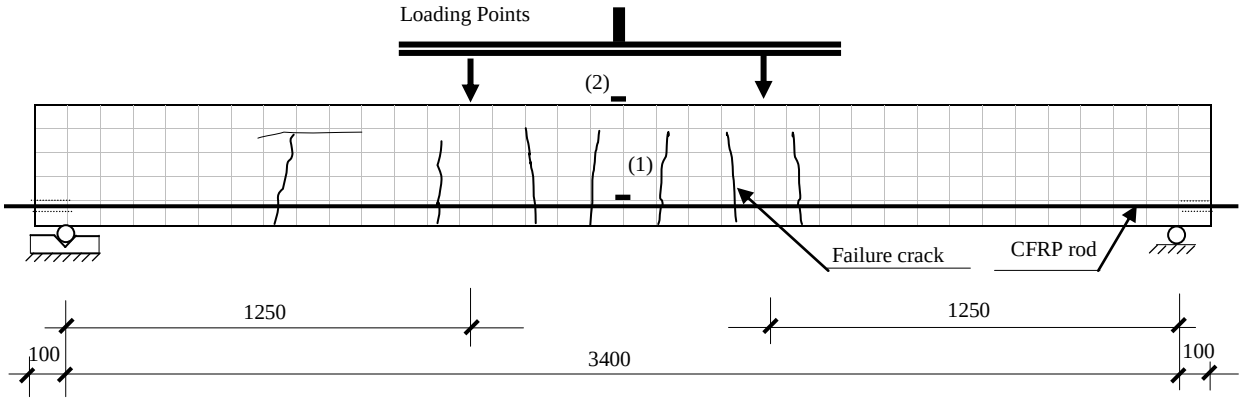

(a) Cracks pattern at failure, average crack spacing 240mm, bond pullout at f_{frp} of 1616.0MPa

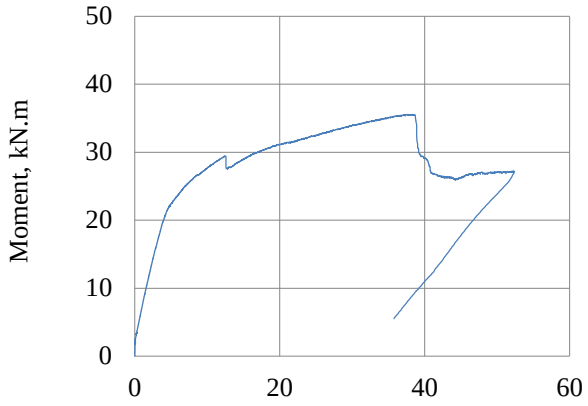

(b) Moment-midspan deflection response

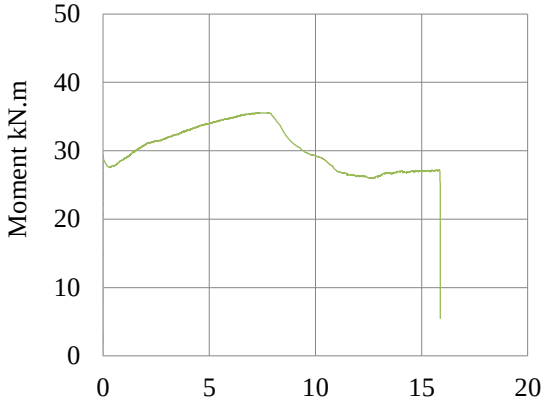

(c) End slip response

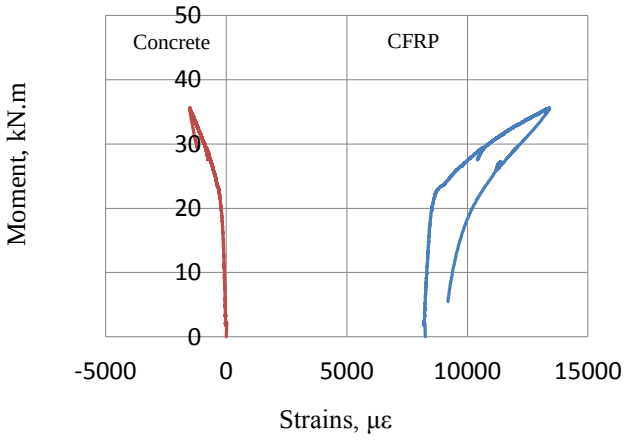

(d) Strains in CFRP bar and concrete, strain in concrete does not include pre-strain

Figure C.14 Flexural test results of beam specimen N60-1250

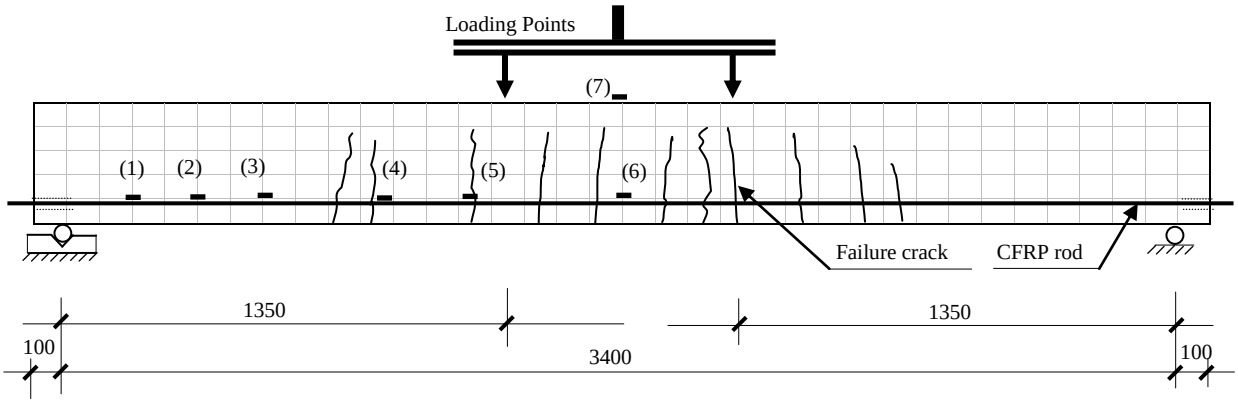

(a) Cracks pattern at failure, average spacing of 175mm (1) - (5) strain gauge locations, bar rupture at 1817.0MPa

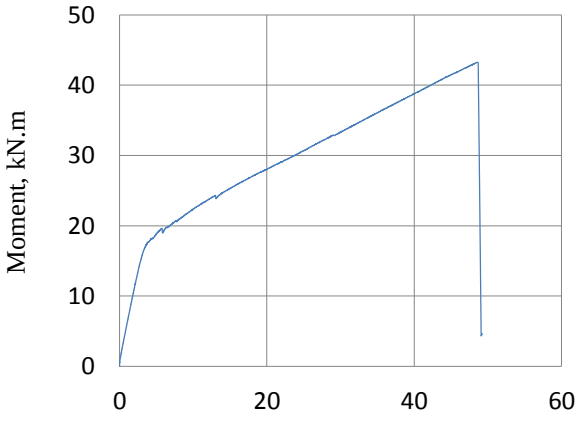

(b) Moment versus midspan deflection response

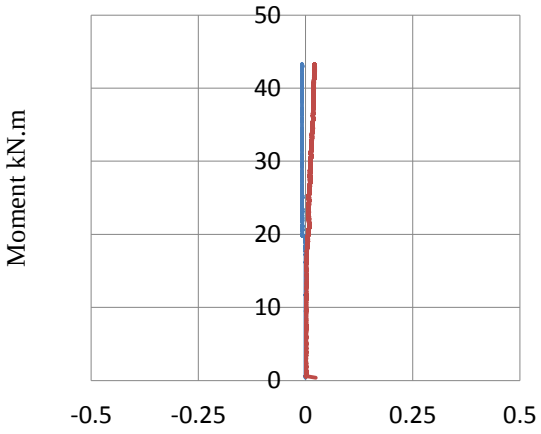

(c) End slip response

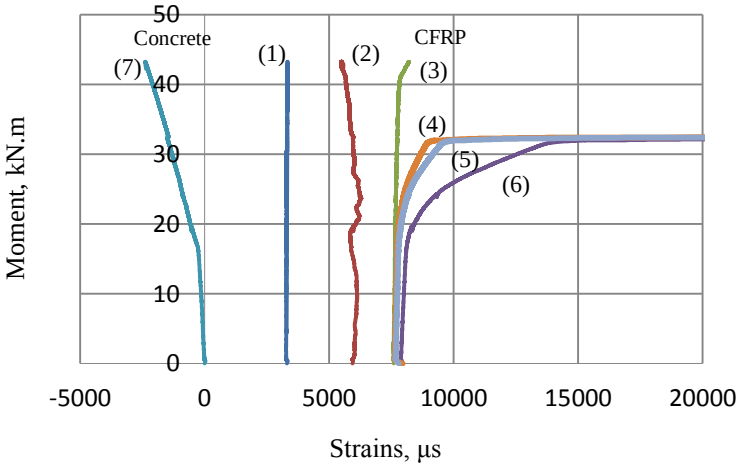

(d) Strains in CFRP bar and concrete

Figure C.15 Flexural test results of prestressed beam N60-1350

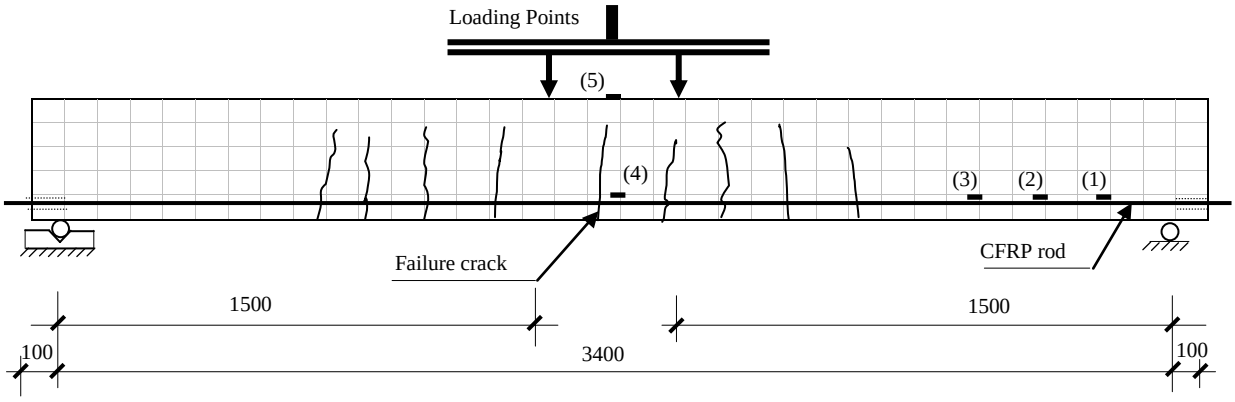

(a) Cracks pattern at failure; average crack spacing of 200mm, bar rupture at 1859.1MPa

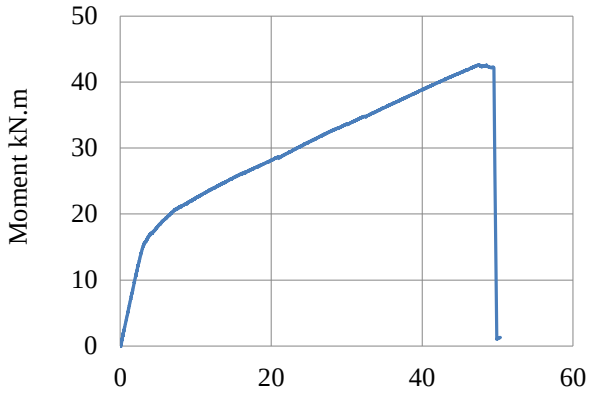

(b) Moment versus midspan deflection response

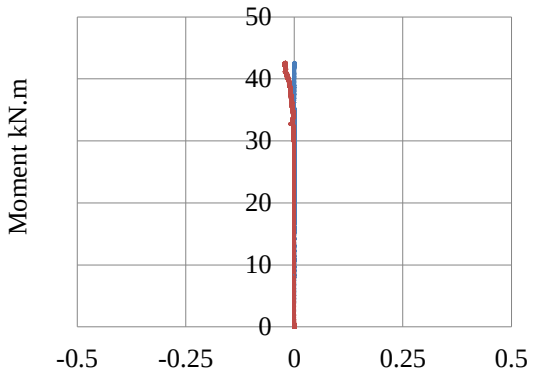

(c) End slip response

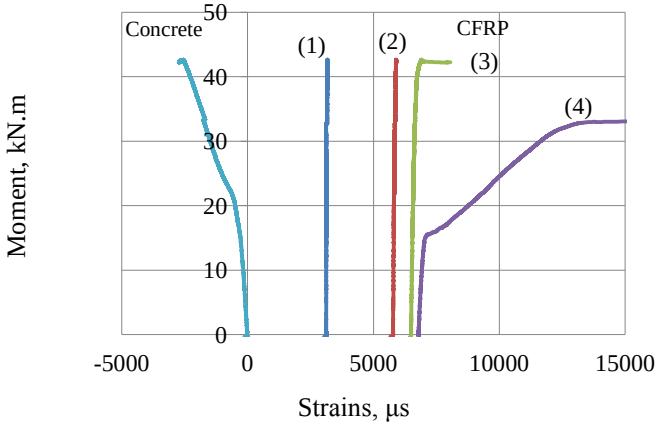

(d) Strains in CFRP bar and concrete, strain in concrete does not include pre-strain

Figure C.16 Flexural test results of beam specimen N60-1500